DEVELOPING AN INSTRUMENT TO QUANTIFY AEROSOL TOXICITY

Inauguraldissertation

zur
Erlangung der Würde eines Doktors der Philosophie

vorgelegt der
Philosophisch-Naturwissenschaftlichen Fakultät
der Universität Basel von

Battist Jeremias Johannes Utinger

2023

Genehmigt von der Philosophisch-Naturwissenschaftlichen Fakultät auf Antrag von:

Prof. Dr. Markus Kalberer (Erstbetreuer)

Prof. Dr. Christine Alewell (Zweitbetreuerin)

Director of Research Dr. Gaëlle Uzu (Externe Expertin)

Basel, 25.04.2023

Prof. Dr. Marcel Mayor (Dekan)

University of Basel

DEVELOPING AN INSTRUMENT TO QUANTIFY AEROSOL TOXICITY

Dissertation submitted for the degree of Doctor in Philosophy

Battist J. J. Utinger

Supervised by Prof. Dr. Markus Kalberer

Co-supervised by Prof. Dr. Christine Alewell

External expert Director of Research Dr. Gaëlle Uzu

2023

mandatory inspirational quote:

"42"

–Douglas Adams

Abstract

Large-scale epidemiological studies have consistently shown that exposure to ambient particulate matter (PM) is responsible for a variety of adverse health effects. However, the specific physical and chemical properties of particles that are responsible for observed health effects, as well as the underlying mechanisms of particle toxicity upon exposure, remain largely uncertain. Studies have widely suggested that the oxidative potential (OP) of aerosol particles is a key metric to quantify particle toxicity. OP is defined as the ability of aerosol particle components to produce reactive oxidative species (ROS) and deplete antioxidants *in vivo*.

Traditional methods for measuring OP using acellular assays largely rely on analyzing PM collected in filters offline. This is labor intensive and involves a substantial time delay between particle collection and OP analysis. It therefore likely underestimates particle OP, because many reactive chemical components which are contributing to OP are short-lived and therefore degrade prior to offline analysis. We investigated these differences in online and offline measurements with different acellular assays and with cellular methods and could show that for biogenic secondary organic aerosol (SOA), a large fraction decays within minutes to hours.

Thus, new techniques are required to provide a robust and rapid quantification of particle OP, capturing the chemistry of oxidizing and short-lived highly reactive aerosol components and their concentration dynamics in the atmosphere. To address these measurement shortcomings, we developed a portable online instrument that directly samples particles into an ascorbic acid-based assay under physiologically relevant conditions of pH 6.8 and 37 °C, providing continuous accurate OP measurements with a high time resolution (5 min). This online oxidative potential ascorbic acid instrument (OOPAAI) runs autonomously for up to three days and has a detection limit of about 5 µg/m^3 in an urban environment, which allows the characterization of particle OP, even in low-pollution areas.

With this novel instrument, we not only measured ambient aerosol, but also conducted various laboratory campaigns where we investigated the toxicity of various aerosol systems. Primary and secondary emissions with different aging times from car exhaust were measured and compared to primary and secondary

aerosols from residential wood combustion, showing a higher toxicity for residential wood combustion for primary and secondary aerosols.
Furthermore, we investigated the influence of transition metals like copper and iron on the OP of secondary organic aerosol. We could show that there is a synergistic effect for biogenic SOA with copper and for anthropogenic SOA with copper and iron, but an antagonistic effect with iron and biogenic SOA measured with the OOPAAI.

Zusammenfassung

Gross angelegte epidemiologische Studien haben durchweg gezeigt, dass die Exposition gegenüber Feinstaub in der Luft für eine Vielzahl gesundheitsschädlicher Auswirkungen verantwortlich ist. Die spezifischen physikalischen und chemischen Eigenschaften der Partikel, die für die beobachteten gesundheitlichen Auswirkungen verantwortlich sind, sowie die zugrundeliegenden Mechanismen der Partikeltoxizität bei Exposition sind jedoch noch weitgehend unklar. In vielen Studien wird das oxidative Potenzial (OP) von Aerosolpartikeln als Schlüsselgrösse für die Quantifizierung der Partikeltoxizität angesehen. Das OP ist definiert als die Fähigkeit von Aerosolpartikeln, reaktive oxidative Spezies (ROS) zu erzeugen und Antioxidantien *in vivo* zu verbrauchen.
Herkömmliche Methoden zur Messung von OP mit azellulären Assays beruhen weitgehend auf der Offline-Analyse von in Filtern gesammeltem Feinstaub. Dies ist arbeitsintensiv und verursacht eine erhebliche Zeitverzögerung zwischen der Partikelsammlung und der OP-Analyse. Daher wird das OP der Partikel wahrscheinlich unterschätzt, da viele reaktive chemische Komponenten, die zum OP beitragen, kurzlebig sind und somit vor der Offline-Analyse abgebaut werden. Wir untersuchten diese Unterschiede zwischen Online- und Offline-Messungen mit verschiedenen azellulären Assays und mit zellulären Methoden. Wir konnten zeigen, dass bei biogenem sekundärem organischem Aerosol (SOA) ein grosser Teil innerhalb von Minuten bis zu Stunden nicht mehr messbar ist.

Daher sind neue Techniken erforderlich, um eine robuste und schnelle Quantifizierung des OP von Aerosolen zu ermöglichen, die die Chemie oxidierender, kurzlebiger und hochreaktiver Aerosolkomponenten und ihre Konzentrationsdynamik in der Atmosphäre erfasst. Um diese Messmängel zu beheben, haben wir ein tragbares Online-Instrument entwickelt, mit dem Partikel unter physiologisch relevanten Bedingungen von pH 6,8 und 37 °C direkt in einen auf Ascorbinsäure basierenden Assay eingespeist werden, der kontinuierliche, genaue OP-Messungen mit hoher zeitlicher Auflösung (5 min) ermöglicht. Dieses Online-Instrument zur Messung des oxidativen Potenzials von Ascorbinsäure (OOPAAI) läuft autonom bis zu drei Tage lang und hat eine Nachweisgrenze von etwa 5 µg/m^3 in einer städtischen Umgebung, was die Charakterisierung von OP auch in Gebieten mit geringer Verschmutzung ermöglicht.

Mit diesem neuartigen Instrument haben wir nicht nur Aerosole in der Aussenluft gemessen, sondern auch verschiedene Laborkampagnen durchgeführt, in denen wir die Toxizität verschiedener Aerosolsysteme untersucht haben. Es wurden primäre und sekundäre Emissionen mit unterschiedlichen Alterungszeiten aus Autoabgasen gemessen und mit primären und sekundären Aerosolen aus der privaten Holzverbrennung verglichen, wobei sich für primäre und sekundäre Aerosole eine höhere Toxizität bei der privaten Holzverbrennung zeigte.
Darüber hinaus untersuchten wir den Einfluss von Übergangsmetallen wie Kupfer und Eisen auf das OP von sekundären organischen Aerosolen. Wir konnten zeigen, dass es einen synergistischen Effekt für biogenes SOA mit Kupfer und für anthropogenes SOA mit Kupfer und Eisen gibt, aber einen antagonistischen Effekt mit Eisen und biogenem SOA, gemessen mit dem OOPAAI.

Contents

Acknowledgements

The completion of this thesis would not have been possible without the support of many people who supported me and my science in many different ways.
First and foremost, I would like to say a big thank you to my supervisor Markus Kalberer for giving me the opportunity to conduct my Ph.D. in his group and providing me with everything that was necessary. From a well-equipped lab, over numerous meetings to discuss challenges, to a very nice working atmosphere. His positive attitude and humorous approach to science made this Ph.D. very educational, instructive, and most of the time also good fun.

I also want to thank Christine Alewell for being my second supervisor and Gaëlle Uzu for being my external supervisor, reading my thesis and finding time to travel to Switzerland for the PhD defense. I also want to thank for chairing my defense.

Moreover, I want to thank the whole atmospheric science group on the fourth floor at the University of Basel (and also at the beginning of my Ph.D. the fourth floor of the University of Cambridge). Without the help of these people, I would not have managed to do my Ph.D. and it would also be much less fun. Special thanks should be given to Steven Campbell, with whom I worked on multiple projects, and it was always a great pleasure to work with him, and his deep insight in science solved a lot of my problems, either directly or by giving me new ideas.

I also thank my Ph.D. peers, with whom I spent a lot of time in the lab. Especially Alexandre Barth, with whom I did multiple campaigns together where we could profit a lot from each other's expertise thanks to the very similar topic we were working on. Moreover, I would like to thank Benjamin Gfeller who worked on his Master Thesis with me and Fabian Wyss and Felix Erb who did a project with me. Also, I am very grateful to Rita Manohar and Yvonne Gilgen for their help with all the administrative stuff. Science is unfortunately always a lot of this, but with their great help I could reduce it to a minimum.

Furthermore, I want to thank Nicolas Bukowiecki for his help with the automation of the online oxidative potential ascorbic acid instrument and various other software tasks. An acknowledgment should also be given to Ray Freshwater,

Hans-Rudolf Rüegg, and Alois Schäuble for their help with the electronic parts and mechanical pieces and various exotic wishes I had during my Ph.D.
Another thanks should be given to all my co-authors from various campaigns.

Special thanks should also be given to my friends in and out of academia who supported me all the time. When things did not go as planned, it was always very important to me to see that other people were also struggling but still managed it in the end. Furthermore, it was also always very important to do other things to maintain balance and remain motivated.

Last but not least I want to thank my family that supported me a lot and raised me with great curiosity that gave me the perseverance to continue to do science even when not everything was always super exciting. I also want to thank them for their financial support during my undergraduate studies, without that I would not have managed to even start a Ph.D. A very big thanks should also be given to my girlfriend who endured me during this time and always provided me with delicious food, when I did not have time to cook and was understanding towards me when I had to invest my time in research instead of cleaning the apartment.

1 Introduction

Aerosols play an important role in the atmosphere of the Earth. They have an impact on climate, visibility, air quality, and thus on human health. Therefore, aerosols are one of the greatest challenges in modern environmental research. For climate, aerosols have a great impact due to the scattering and absorption of sun light. Furthermore, aerosols act as cloud condensation nuclei and therefore have an impact on precipitation and thus on the climate and the weather. Moreover, aerosols also have an impact on the amount of trace gas species in the atmosphere via the gas-phase to particle transition. All these different processes occur through complex, multiphase and heterogeneous processes.[1]

For climate change models, the contribution from aerosols to radiative forcing particles plays an important role in cooling the climate, although it is not well understood and has a high uncertainty. In the most recent IPCC report, the contribution from aerosols to the overall uncertainty of anthropogenic radiative forcing is much greater compared to, for example, greenhouse gases such as CO_2 or CH_4.[2]

Aerosols have an impact not only on the physical properties of the climate and weather, but also have a direct adverse impact on human health. Pollen and other allergens can travel as aerosols over long distances in the atmosphere and can have adverse effects on human health. The resulting allergic reactions, for example hay fever, are widespread diseases that affect a large part of the population.[3] Water droplets can also act as transport vehicles for pathogens like bacteria or viruses. In the last three years, severe acute respiratory syndrome coronavirus 2 (SARS-CoV-2) showed in a drastic way how important aerosols can be for the spread of pathogen.[4, 5, 6] But there are many more pathogens that can be transmitted by aerosols and contribute to infections leading to various diseases.[7, 8]

In addition to pathogens such as pollen or viruses, a wide range of other aerosol particles are also considered harmful, such as particles derived from combustion processes or atmospheric oxidation of volatile organic precursors (VOC). These components that originate from various sources are also a harmful part of air pollution and are very complex in composition. An important aspect of aerosols related to human health are reactive oxygen species (ROS) and thus the oxidative potential (OP) that contributes directly or indirectly to various diseases such as chronic obstructive pulmonary disease (COPD), asthma, heart attack or lung cancer.[9, 10, 11, 12]

Despite the various important contributions aerosols have to climate and human health, there are still many uncertainties about the sources, mechanisms of formation, transport, aging, distribution, and chemical composition of aerosols. Therefore, a better understanding of the properties of aerosols and the toxicological mechanism that leads to these adverse effects on human health would be beneficial in identifying efficient mitigation strategies.
In this Introduction, a general overview of aerosols and especially their health effects will be discussed, and the current state of research will be summarized. In particular, different chemical assays will be presented to determine reactive oxygen species and their advantages and disadvantages in determining the toxicity of aerosols. Moreover, a justification why it is important to measure online, meaning continuously, and an overview of existing online ROS and OP instruments will be given.

1.1 Composition, Size and Source of Atmospheric Aerosols

The term aerosol refers to solid or liquid particles suspended in a gas phase. The term particulate matter (PM) or just particle is often used interchangeably. The term PM also often refers only to the solid or aqueous component exclusively, whereas the term aerosol also includes the gas phase. Typically, PM range from a few nanometers to hundreds of micrometers in size. Aerosols can be classified in various ways, either by their composition, origin, formation process, or physical properties.
To classify aerosols according to their physical properties, size is the most used metric because it is relevant to human health when it comes to penetration depth into the lung. Especially when it comes to policies regarding particle matter (PM) uptake, aerosols are categorized into different size bins. Above an aerodynamic diameter of 10 µm they are called coarse mode. The particle mass below 10 µm is classified as PM_{10}. The particle mass below an aerodynamic diameter of 2.5 µm is called $PM_{2.5}$ and the particle mass with diameters smaller than 1 µm are called PM1. The smallest fraction is ultrafine particles with an aerodynamic diameter less than 0.1 µm.
The two main compositional categories are inorganic aerosols and organic aerosols. In the group of inorganic aerosols, sulfate, nitrate, ammonium, transition metals and elemental black carbon (soot) are the most abundant components in the ambient air. Organic aerosols are all other aerosols that include carbon-containing compounds. Organic aerosols are defined as aerosols that contain carbon analogues

of the definition in organic chemistry. Excluded from that definition are elemental carbon/black carbon (i.e., soot) and any kind of carbonate that can be found in mineral dust and are classified as inorganic aerosols. It is estimated that there are between 10'000-100'000 different organic compounds in the atmosphere and that most of them are in the particle phase.[13]
Aerosols can also be classified by their origin. The two main groups are biogenic and anthropogenic aerosols. Towards anthropogenic aerosols count all aerosols that are produced as a result of human activities. Biogenic aerosols are all aerosols that have a natural origin from the biosphere, meaning coming from living organisms, mostly plants.
Additionally, aerosols can be defined according to their source and formation. They are distinguished into primary aerosols (PA) and secondary aerosols (SA). PAs are emitted directly into the atmosphere, whereas SAs are formed by gas-to-particle conversion mechanisms from volatile organic precursors that can condense to a particle, are absorbed onto an existing aerosol particle, or form a new particle (a process defined as nucleation).
In the literature, these previously described classification schemes are often mixed to describe an aerosol, and overlapping subcategories are introduced. Organic aerosols can be divided into two large subgroups: primary organic aerosol (POA) and secondary organic aerosol (SOA). Examples of anthropogenic aerosols are SOAs from anthropogenic sources, such as industry, transportation, or biomass burning. Examples for biogenic POA are pollen, bacteria and viruses and for anthropogenic are primary particles from combustion processes. POAs are released in the particle phase into the atmosphere and usually stay in the particle phase because of their low volatility. In contrast, SOAs are formed in the atmosphere from volatile organic compounds with sufficiently low volatility that are released in the atmosphere in the gas phase.

1.2 Oxidation Mechanisms Leading to SOA Formation

One of the most significant processes for SOA formation in the lower atmosphere is the oxidation of VOCs in the gas phase. This process has a huge impact on global climate, visibility, and photochemical smog. Most notably, isoprene, monoterpenes (such as α-pinene, β-pinene, limonene, etc.), highly reactive sesquiterpenes such as β-caryophyllene, long-chain alkanes and aromatic chemicals are believed to dominate SOA production in the troposphere (lowest 0-15 km from the Earth's surface).[14] SOA contributes to a large fraction of the total aerosol budget.

Depending on season, location, and climate, it can vary from 20 % up to 80 % of the total aerosol mass.[15, 16, 17] The most abundant oxidation agents in the atmosphere are hydroxyl radicals ($^{\bullet}OH$), ozone (O_3), nitrate radicals ($^{\bullet}NO_3$), and chlorine radicals ($^{\bullet}Cl$).[18] In polluted areas (i.e. areas with a lot of emissions sources like industry or cities), where there are high levels of NO_x and sunlight, and therefore also O_3 and hydroxyl radicals, VOC can also be oxidized by the following simplified mechanism:[19]

$$O_3 + h\nu \rightarrow O(^1D) + O_2 \qquad \lambda \leq 310\,\text{nm} \tag{1}$$

$$O(^1D) + H_2O \rightarrow 2 \times OH \tag{2}$$

The OH radical produced in Equation 2 is a highly reactive species that can oxidize other atmospheric compounds, such as carbon monoxide (CO), methane (CH_4) or other organic compounds. This process results in the production of other atmospheric radicals such as HO_2 or RO_2, where R is any organic compound.

$$HO_2(\text{or } RO_2) + NO \rightarrow OH(\text{or } RH) + NO_2 \qquad \lambda \leq 398\,\text{nm} \tag{3}$$

$$NO_2 + h\nu \rightarrow OH + O(^3P) \tag{4}$$

$$O(^3P) + O_2 + M \rightarrow O_3 + M \tag{5}$$

In Equation 5, "M" is a third species, which most of the time is N_2 because it is the most abundant molecule in the atmosphere. O_3, the OH radical, RO_2 and HO_2 are all very good oxidizing agents and can therefore oxidize in highly polluted environments gaseous VOCs with functional groups, such as ketones (RR'-C = O), aldehydes (HR-C = O), alcohols (R-OH), carboxylic acids (R-C(=O)-OH), and hydroperoxides (R-C-OOH). VOCs that are functionalized have a lower vapor pressure compared to those of their non-oxidized analogues, and therefore,

partitioning in the particle phase becomes more likely. This suggests that a large fraction of the compounds found in SOA are likely highly oxidized.[1]

1.3 Health Effects of Atmospheric Aerosols

Epidemiological studies have provided ample evidence of the harmful effects of exposure to ambient particulate matter (PM), and *in vivo* and *in vitro* cell culture experiments have provided additional evidence. Effects to increased exposure to ambient PM is commonly recognized as an increase in hospital admissions, as well as overall mortality from cancer, cardiovascular disease, and respiratory diseases.[9, 11, 12, 20, 21, 22, 23, 24]

The World Health Organization (WHO) estimates that air pollution is associated with 6.7 million premature deaths annually.[25] Furthermore, 99% of the world's population breathe air that is above the levels of the air quality guidelines recommended as save and, therefore, air pollution is the largest single environmental health risk.[25]

Despite these evidences, the precise toxicological pathways that cause the reported negative impacts on human health are only poorly understood. However, some parameters have been studied quite well, such as the efficiency of the deposition of different particle sizes in the nasal airway, the bronchial and the alveolar.[26] In Figure 1 an overview of the human respiratory tract is shown indicating where the different particle sizes are deposited mainly. The human respiratory tract can be divided into three main regions: the nasal cavity, the tracheabronchial region, and the alveolar part. The nasal airway has as the first defense line nasal hairs for large particles and mucosa, and further down fine cilia hairs to collect particles, and a mucociliary system to direct particles toward the mouth for expulsion from the body. The tracheobronchial area also contains a mucociliary system to remove particles. The alveolar area is where oxygen and CO_2 exchange between the circulatory system and the atmosphere. Because the alveolar area lacks mucociliary or fibrous defense, it may be more vulnerable to the toxic effects of PM. Furthermore, the lung contains the lung lining fluid, which consists, among other things, of antioxidants such as AA which are a first chemical defense against oxidative aerosols.

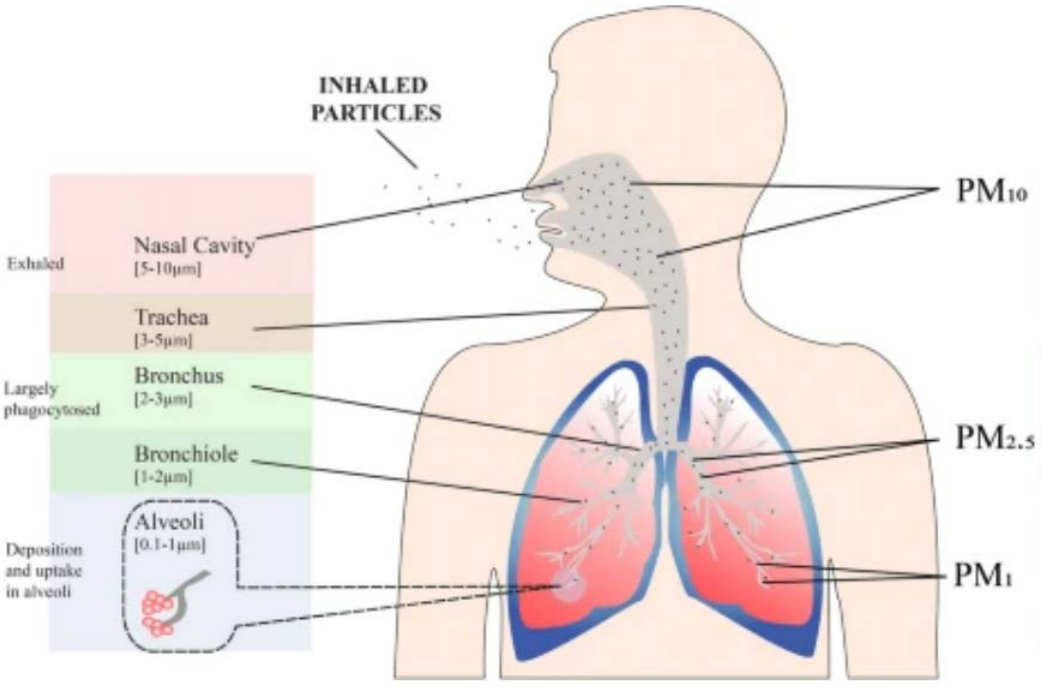

Figure 1: The bigger the particles, the higher they deposit in the respiratory system. Only small PM_1 reaches the alveolar part of the lung. Figure from Poh et al., 2018.[27]

The following sections will discuss the current understanding of the physical and chemical properties that affect the toxicological effects of PM.

1.3.1 Health Relevant Physical Properties of Aerosols

The physical deposition efficiency of different particle sizes is illustrated in Figure 2 where the particle size is plotted against the deposited particle fraction. Very small aerosols, also called ultra fine particles, have the highest deposition fraction in the alveolar region. This behavior makes ultrafine particles potentially so dangerous, because they can enter the deepest part of the lung, where they can also cross the lung blood barrier.[28] Although very fine particles ($\leq 0.01\,\mu m$) already get deposited also early in the nasal region, because diffusional deposition is very efficient for these very small particles. Particle deposition also depends on the particle density. The higher the density, the larger the fraction of deposition in all parts of the respiratory tract (see Figure 2).

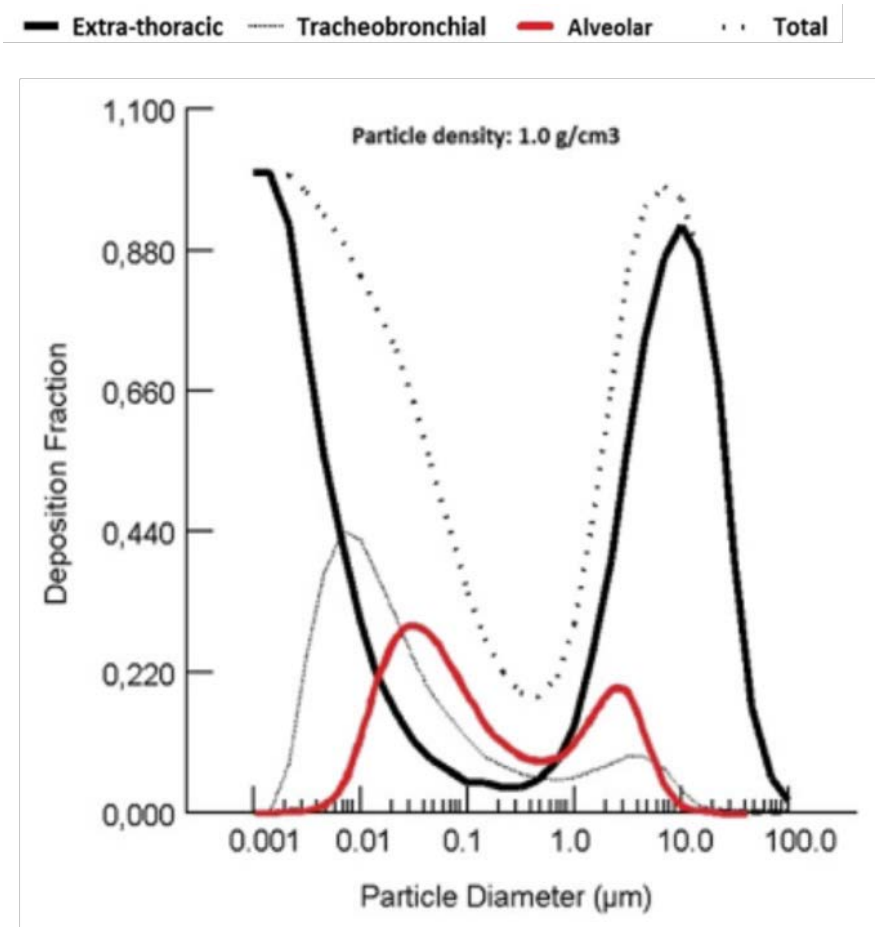

Figure 2: Inhaled particle deposition of aerosols of different sizes in the extrathoracic / nasal region (black line), tracheobronchial (grey line) and alveolar (red line). The deposition of PM between 10 nm and 100 nm is strongest in the alveolar area. The bigger particles are deposited further up in the respiratory system. Figure from Braakhuis et al., 2014.[29]

1.3.2 Health Relevant Chemical Properties of Aerosols

In general there are two different approaches for measuring the toxicity of an aerosol for human health: a bottom-up or a top-down approach. For a bottom-up approach, the negative health effects of aerosols are attributed to the chemical composition of single elements, molecules, or compounds in the aerosol and their chemical pathways that lead to these negative health effects. For these types of measurement, all different compounds of an aerosol need to be analyzed with techniques such as mass spectrometry (MS).[30] Because aerosols are a very complex mixture and especially SOA can consist of thousands of different compounds, with this method it it very difficult to allocate toxicity to single compounds, specific pathways, and to individual particle sources. In contrast, for a top-down approach, the exact composition of an aerosol and the toxicity

pathway do not need to be known, and only a proxy or a biological endpoint is investigated to determine the toxicity of the aerosol.

A specific class of substances, known as particle-bound reactive oxygen species (ROS), is commonly believed to be a good proxy for the negative effects on human health from aerosols, because they contribute significantly to these effects.[31, 32] The term ROS often refers to ionic species such as free radicals, H_2O_2 OH radical, superoxide and organic peroxides).[31, 33, 34, 35, 36, 37, 38] In recent years, not only have particle-bound ROS has been suggested as a more appropriate indicator of the toxicological effect of PM, but also the term oxidative potential (OP) appeared in the literature as a potentially useful metric to quantify the toxicity. OP is the capacity of PM to oxidize target compounds of biological significance. It also includes catalytically generated ROS *in situ* when particles are deposited on epithelial surfaces after inhalation.[31, 33, 39]

Particle-bound ROS can contribute significantly to the reported oxidative potential of PM as well as transition metals and quinones. The concentration of naturally existing antioxidants in the lung can be decreased by exogenous delivery and deposition of particle-bound ROS or endogenous formation of ROS (and OP) in the lung lining fluid. The lung lining fluid is an aqueous layer on epithelial cells with different antioxidants and proteins, which help cells to cope with oxidative stress.[40] Without any external oxidative stress, induced by aerosols, the body is in a redox equilibrium.[33]

The lung lining fluid, the first chemical defense line of antioxidants present in the lung, consists of ascorbic acid (vitamin C), gluthation, uric acid, among many other substances, as well as anti-oxidant proteins.[41, 42] Oxidative stress is the result of an imbalance between the concentration of antioxidants and exogeneous oxidants in the lung resulting in the depletion of these antioxidants.

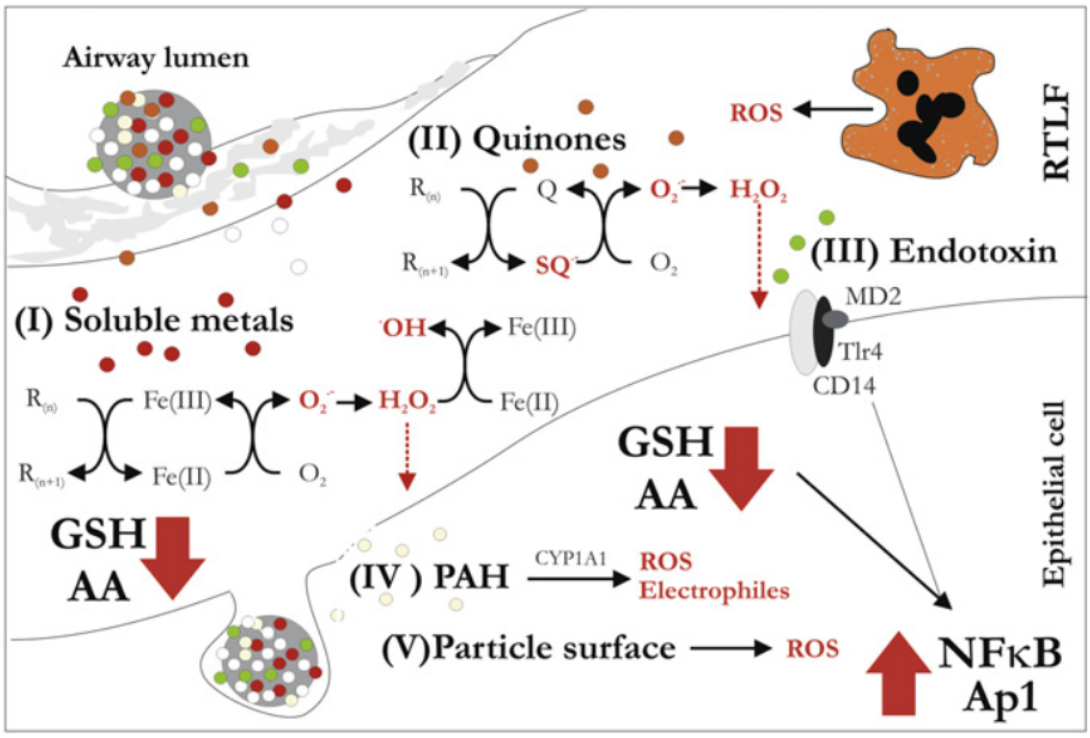

Figure 3: At the airway/lung interface, inhaled particles can induce different toxicity pathways. There are four chemically interconnected processes through which particles cause oxidative stress: (I) By introducing redox-active metals into the lung, such as iron, which undergo a redox cycle in the presence of oxygen, to produce harmful hydroxyl radical ($^{\cdot}OH$), hydrogen peroxide (H_2O_2), and superoxide radical (O_2^-). On the surface of the particle, (II) quinones undergo a redox cycle in the presence of biological reductants to generate the semiquinone radical (SQ), which also produces oxygen and hydrogen peroxide. (III) Through its interaction with the TLr4/CD14/MD2 receptor, the bacterial endotoxin attached to the surface of the particle can cause inflammation. (IV) Although polyaromatic hydrocarbons (PAHs) lack intrinsic oxidative activity, this action can cause them to biotransform *in vivo* into quinone species. (V) Furthermore, they can also produce ROS via a physical pathway from the particle surface. Figure from Kelly., 2012.[22]

1.4 Methods to Quantify Aerosol Toxicity

Measuring OP and/or ROS is crucial to understanding the toxicity of aerosols. There are many different approaches measuring aerosol toxicity, all of which have advantages and disadvantages. It is always a trade-off between being as close to the actual system that should be measured, in this case the human body, and the complexity of the system and practicability of the respective chemical analysis. In epidemiology, the great advantage is that the study subject is directly human and that there are no artifacts of translating results from different species to humans or inferring in *vitro* experimental results to human health effects. However, the drawback is that the human body is a very complex system that is highly variable and has many processes ongoing, which are currently poorly understood and

therefore it is very difficult to identify the most toxic components in PM via epidemiological studies.
As with epidemiology, also with chemical assays, the main advantages are simultaneously also the main disadvantages. With more confined systems such as chemical assays, the advantage is that it is easier to understand a single chemical process very well, due to the simplification of the system, but the measured quantity is further away from the study subject, i.e. the human body. A simplified system has the disadvantages that study results are more difficult to interpret with respect to human health. In between epidemiology and chemical assays, there are cell culture studies, or studies with animals, where the complexity is higher than with acellular chemical assays, but the understanding of fundamental processes is already more complex.
There are many epidemiological studies that have correlated toxicity of aerosols to human health [12, 20, 43] but in this work the focus is more on understanding basic processes at the chemical level with acellular chemical assays and some cell experiments. As mentioned above, the advantage of chemical assays is that it is possible to better understand a complex system. Moreover, it is easier to achieve constant conditions for experiments, the costs are considerably lower, mostly due to reduced workload, and therefore the results are achieved faster.

1.4.1 Epidemiological Methods to Study Aerosol Toxicity

One of the first and well-documented correlations of the toxicity of aerosols on human health, which even found its way into popular fiction, is the great smog event of London in 1952. London at that time was already extremely polluted, but an extraordinary strong episode of air pollution due to cold weather and an temperature inversion of the temperature led to excess mortality. In Figure 4 a strong correlation is shown between the observed concentration of SO_2 and the increase in mortality in Greater London. SO_2 can be considered a good proxy of general air pollution in these times when coal burning was a major air pollution source emitting high amounts of SO_2. Although not an aerosol component in itself, the SO_2 forms quickly to H_2SO_4 particles through reaction with O_3 and H_2O_2, particularly during cloudy conditions. In recent decades, there have been less severe smog events due to stronger regulations for biomass burning, coal burning, better insulation, and regulations for particulate filters for vehicles. Despite all these improvements, only less than 1 in 10 people worldwide breathe clean air according to the World Health Organization (WHO) guidelines.[25, 44]

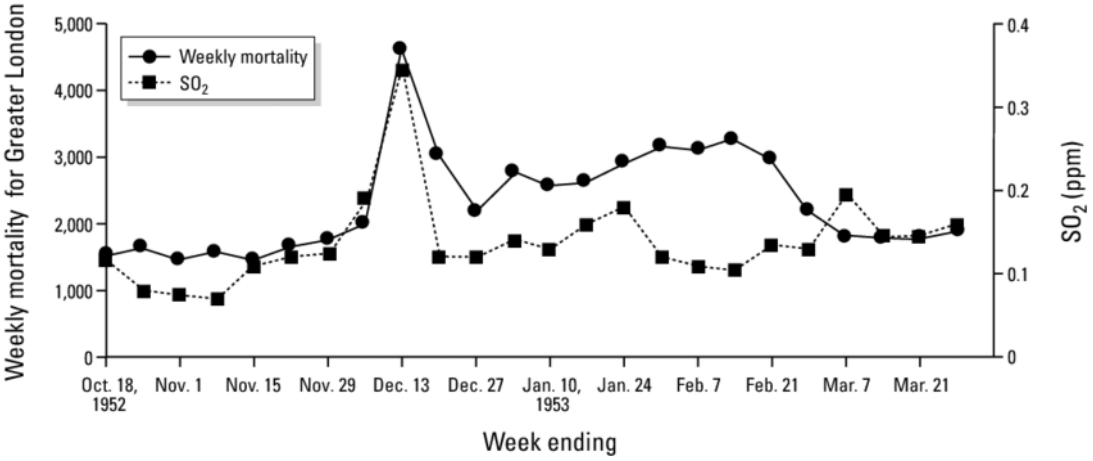

Figure 4: The weekly mortality rate and observed SO_2 concentrations in Greater London from October 1952 to March 1953 are shown. Following the major London smog incident in December 1952, death rates were much higher, increasing by an average of 50% over the next two months compared to the weekly average between 1947 and 1952. Figure from Bell and Davis (2001).[45]

The probably most well-known and cited study showing that air pollution is bad for human health is the so-called six-city studies by Dockery et al. from 1993.[9] In Figure 5 this study is combined with a follow-up study by Laden et al., 2006 [46], where the clear correlation between mortality rate and PM concentration$_{2.5}$ is shown. Lepeule et al., 2012 [47] extended the data set to 2009 and performed further data analysis. They noted that the relationship between $PM_{2.5}$ concentration and the mortality response was linear up to a lower limit of $8\,\mu g/m^3$ and that each increase of $10\,\mu g/m^3$ in $PM_{2.5}$ (based on a moving average of 1-3 years) was found to be associated with an adjusted increase in all-cause mortality, cardiovascular mortality and lung cancer mortality, of 14%, 26%, and 37%, respectively.[47]

A similar study was also conducted in Europe in the late 1990s, where 29 European cities with a combined population of more than 43 million were included in the APHEA-2 (Air Pollution and Health: a European Approach) studies. This study also showed a correlation between PM_{10} levels and hospital admissions for asthma, COPD, and cardiovascular disease.[12] Many more cohort studies were conducted after these initial studies to investigate the cause of increased mortality from air pollution, as demonstrated in the review by Colonna et al., 2022.[48]

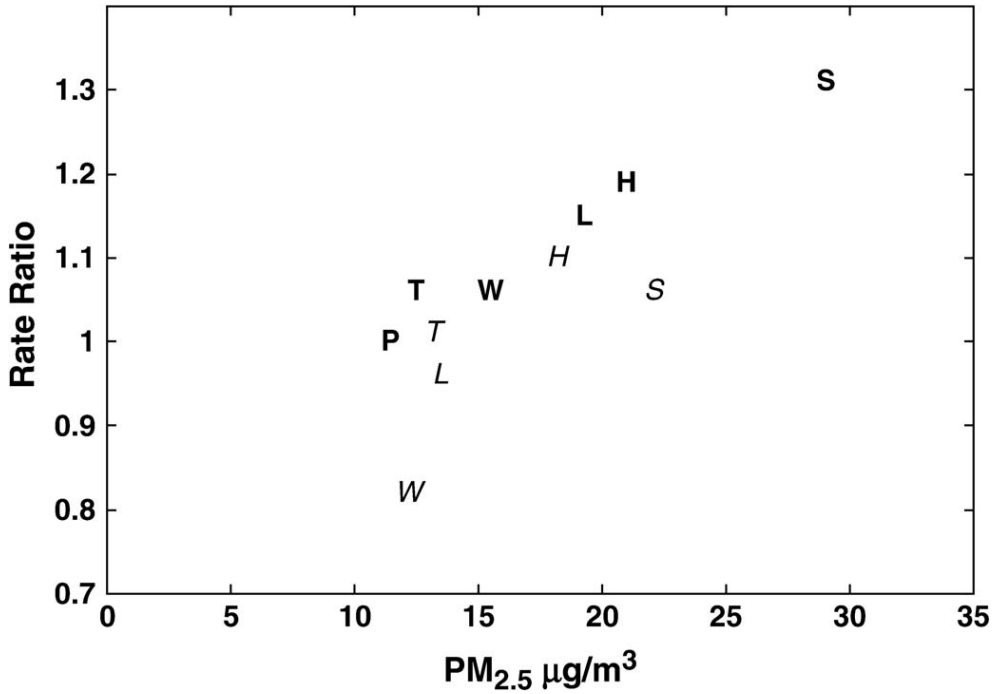

Figure 5: Comparison of mean $PM_{2.5}$ city exposure levels and mean city mortality rate for two periods within the six-city study and follow-up. For each of the six cities, bold letters imply mean values from 1980 to 1985, and italicized letters denote mean values from 1990 to 1998. Note that the city denoted by P is used as a reference city for both time periods.[24] Figure from Laden et al., 2006.

All of these studies unequivocally show a link between increased levels of exposure to ambient particulate matter and higher rates of respiratory disease, cardiovascular disease, and total mortality. Gaining a solid understanding of the underlying physical and chemical characteristics of PM that are responsible for documented detrimental impacts on human health would help to better understand this link. But the composition of the ambient PM changes throughout time and space. It is difficult to pinpoint the precise physical and/or chemical characteristics of PM that cause the toxicological reaction shown in epidemiological investigations due to its complexity. The size of the particles, the content of transition metals, and the oxidative potential (OP) of the aerosol have been found to be more reliable indicators of PM toxicity than the total particle mass.[49]

Epidemiological studies have also been conducted in which OP metrics (see Subsection 1.4.4 have been measured.[31] There are multiple studies showing correlations for different health endpoints in respiratory diseases such as asthma [50, 51, 52], exhaled nitric oxide test [53, 54, 55, 56] and lung cancer [57] but also in cardiovascular diseases[50, 51] or in general correlations of respiratory health markers.[51, 58] In other studies, no association was found between OP and health endpoints.[57, 59, 60]

1.4.2 Animal Models to Study Aerosol Toxicity

In vivo studies are often used to study complex systems and systemic interactions. There are many different studies investigating the toxic effects of aerosols using animal models. Most of the time, mice or rats were used to study the systemic effects of PM *in vivo*. For occupational exposure limits (OEL), animal studies are often used to test the limit of a compound before it leads to negative health effects. An example would be the compound peracetic acid, also called peroxyacetic acid, which is known to be highly reactive and present in ambient aerosols.[61] This compound is also used in hand sanitizers and therefore can also occur in quite high concentrations indoors.[62] Therefore, *in vivo* studies were conducted to derive occupational exposure limits, summarized in the review by Pechacek et al., 2015.[62] With animal studies not only OELs are tested, but they are also used for exposure studies for traffic [63] or electronic cigarettes.[64] These are just a few examples of studies that could be conducted with animals, but there are many more research fields where animal exposures were conducted, often also combined with *in vitro* studies and chemical analysis.[28, 65, 66, 67]

1.4.3 Cellular Experiments to Study Aerosol Toxicity

Because in vivo animal models are very expensive, time-consuming, and ethically debatable, most biological experiments are conducted *in vitro* with human lung cells, immortalized cell lines such as A549 or Beas-2B [68] or primary cells from donors.[69] The advantage of *in vitro* cell exposures with aerosols is that by using human cell lines, aspects of translating findings in animal models to humans do not need to be considered. Human epithelial lung cells can be cultured in systems that provide an air-to-liquid interface. This has the great advantage that epithelial cells are as in the lung, i.e., on one side exposed to air and on the other sitting in the nutrient medium.[68, 70, 71]

1.4.4 Acellular Assays to Study Aerosol Toxicity

There are also disadvantages for cellular studies, such as that there is no possibility of studying systemic effects or that they are still very time-consuming and expensive, and therefore it is difficult to obtain enough statistical power to derive robust information about which particle components and sources are especially toxic. Therefore, there are also various acellular assays and methods for measuring ROS and OP at the chemical level. Their advantage is that they have a high throughput ,i.e. many 100s of samples can be characterized and they are very

cheap and fast compared to animal models or cell assays. Furthermore, they are rather simple experimental requirements and it is easier to achieve constant conditions for experiments, which allows performing these analyses in a wide range of study designs (e.g., at locations without high-end laboratory infrastructure). These advantages are also the disadvantage of acellular assays because they lack a direct biological response, so they are further from the study subject, the human body, compared to *in vivo* or *in vitro* studies.
In addition, different acellular assays have their advantages and disadvantages, and not all of them are useful to measure the same type of aerosol properties[31] Because some of the assays measure different proxies, sometimes they even give contradictory results.[31, 72] Therefore, it is very important to measure with as many assays as possible to obtain a more complete picture of the components and pathways that actually contribute to the toxicity of aerosols in human health.[33]

Dithiothreitol (DTT)

Nowadays, the dithiothreitol assay is the most widely used assay to measure OP in aerosols.[31, 39, 52, 73, 74, 75] DTT is a surrogate for cellular NADPH. In this process, oxygen is reduced to superoxide anion (O_2^-). The total rate of O_2^- generation by the measured aerosols is determined by the rate of consumption of DTT. The consumption rate is proportional to the concentration of redox-active species in the aerosol sample. Filter samples are extracted in a solvent (water or methanol) and incubated with DTT for varying times, between (0 min and (90 min depending on the protocol and analyzed.[73, 76, 77]

Ascorbic Acid (AA)

Most people measure ascorbic acid (AA), a naturally occurring anti-oxidant in the lung, similar to DTT where the rate of AA consumption is determined by aerosol extracts.[78, 79, 80] Filters are extracted and then AA is added to the extract, incubated, and aliquots are taken at different time points to quantify the AA decay. Some measurements are also made with a fluorescent AA assay.[33, 81] These fluorescent assays follow the protocol described by Campbell et al., 2019 [38] that is described here in Section 1.6.

Glutathione (GSH)

Gluthatione, also an naturally occurring antioxdant in the lung, is measured in the same way as AA and DTT by observing its depletion over time. The GSH

assay is often performed in surrogate lung fluid (SLF), which contains not only glutathione but also AA and uric acid in most methods.[31, 82]

Hydroxyl Radical (OH)

Also more specific assays exist that measure one single ROS components like the terephthalate probe that can quantifiy the OH production via producing the highly fluorescent product 2-hydroxyterepthalate.[83]

DCFH

Filter samples are extracted as for the other assays, and then dichlorofluorescin (DCFH) is added to the aliquot. DCFH is a non fluorescent reagent, which is reactive mainly to towards inorganic and organic peroxides and that, when oxidized in the presence of ROS, reacts to the fluorescent dye DCF. Before analysis, DCFH and horseradish peroxidase (HRP) are combined in sodium phosphate buffer to catalyze the reactions.[33, 84, 85]

Electro Paramagnetic Resonance (EPR)

EPR measures the generation of radicals e.g., hydroxyl radicals through electron spin resonance. Therefore, EPR is mainly applied to quantify particle-bound radical species.[86, 87, 88, 89] or for radicals that are formed when an aerosol is suspended in an aqueous solution.[90, 91] EPR can also be performed if the filter is extracted directly into SLF [92] or to quantify environmentally persistent free radicals (EPFR).[93]

1.5 Why Measuring Online?

Traditional offline aerosol sampling techniques rely on the collection of particles on filters or occasionally impacters. The time between the collection and the start of the analytical processes is in the best case some hours, but more typically days. Often, filters from campaigns are stored for weeks or even months before they are analyzed. However, because ROS are reactive by nature and therefore unlikely to be stable or long-lived (see Chapter 3), such slow and time-consuming techniques may not be appropriate for their detection.[94, 95, 96, 97]
The lack of temporal resolution in the data obtained and the labor- and resource-intensive nature of conventional offline analyses are further drawbacks of offline approaches. The advantage of offline methods is that they are relatively easy to

conduct, there is a no need for a specialized instrument, and they are nowadays widely used, so inter-comparison with other studies is better. Furthermore, because collecting filters does not need special equipment, getting a spatially well-resolved data set within a study area is relatively easy. Online methods have the drawback that they usually require are quite complex instruments and are therefore more expensive, which in the end results in a harder to achieve spacial resolution. Moreover, online instruments struggle in very low polluted areas because they have no up-concentrating effect like in a filter sampling method. The online instruments have the advantage that they are in general less time consuming to operate and give a much higher time-resolution. However, the biggest advantage of these fast online techniques is that they are more suitable for measuring these highly reactive species. Due to their nature of being reactive, it is crucial to reduce the time between particle collection and analysis to not heavily underestimate the toxicity or even measure artifacts from storage.[98]

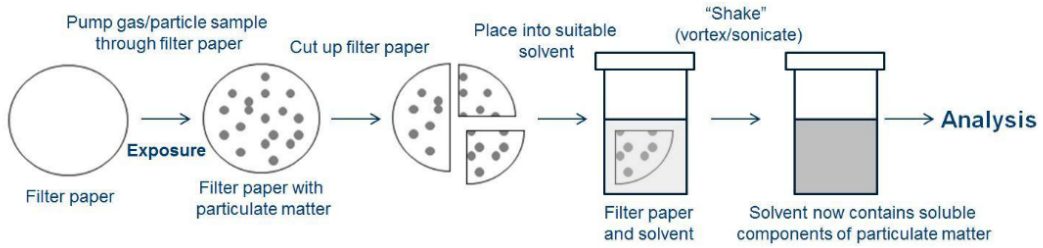

Figure 6: A flow diagram of a typical procedure for the collection of classical offline filters that enables the chemical analysis of sampled particulate matter.[99] Figure adapted from the Ph.D. thesis of Francis Wragg.

1.6 Previous Methods for Online Detection of ROS and OP

Online instrument that measure ROS content or OP with filters by simply automating the offline analysis are not considered here as real online methods. Only online methods that extract the aerosol directly and continuously into a liquid and quantify ROS or OP automatically and automated offline instruments are described here, only briefly. Some semi-online instruments are also discussed, where the collection is done in a batch mode and which are considered here as not fully online.

In recent years there are many online instruments developed to measure the oxidative potential and particle-bound ROS of aerosols.[100] The first online instrument to measure particle-bound ROS by the DCFH assay was developed

by Wang et al., in 2011.[101] Shortly after King and Weber 2013 [102] and Fuller et al., 2014 [94] published methods for an online DCFH assay. Wragg et al., 2016 [95] further developed the online method of Fuller et al., 2014 as an automated field portable instrument. A similar instrument was developped by Zhou et al., 2018.[103] Huang et al., 2016 developed another method that could simultaneously measure the gas phase and the particle in parallel.[104] The King and Weber 2013 [102] method used a mist chamber for aerosol collection, whereas Wang et al., 2011 used a particle into liquid sampler. Fuller et al., 2014 and Wragg et al., 2016 used a home-built particle collector, which has the advantage that it is compact, fully online and runs at room temperature.

So far, online OP measurements have been made with either the DTT assay or AA assay. With both of these assays, online or semi-online instruments were developed. The first online system that measured OP with the DTT assay was introduced by Sameenoi et al., 2012.[105] In this method, they used a particle-into-liquid sampler combined with a cobalt (II) phthalocyanine electrode, which measured the decay of DTT over time. Eiguren-Fernadez et al., 2017 [106] took another approach with a semi-online DTT instrument. This setup uses an automated batch mode with a time resolution of 3 h and the standard DTT assay. Puthussery et al., 2018 [107] build another DTT instrument that had a better time resolution of 1 h. In addition, some automated systems have been developed for the DTT assay to parallelize the analysis of samples.[75, 80, 108, 109] These methods are not considered online, because the crucial step of analyzing the aerosol as quickly as possible is not fulfilled due to the classic filter collection method.

Campbell et al., 2019 [38] developed a fully online setup to measure aerosol OP by oxidating AA with continuously extracted aerosol and fluorescence detection. This method has a very high time resolution of around 15 min and uses a home-built particle collector. Because the online oxidative potential ascorbic acid instrument (OOPAAI) described by Campbell et al., 2019, was an important starting part of this thesis, this instrument is discussed in more detail. Most offline AA assays use absorbance to quantify OP by measuring the decay rate of AA. The measurement of decay rates is not possible with online instruments because, due to the nature of online measurement, they can only measure the sample at one point in time. Furthermore, all kinds of organic compounds also absorb near UV where AA absorbs (265 nm) as well, and therefore for a real online instrument, an AA absorbance measurement is not suitable. Therefore, Campbell et al., 2019 [38] used a fluorescence approach that does not suffer from the self-absorbance problem because fluorescence spectra are usually much more specific. Instead of

AA decay, the formation of the first stable oxidation product, dehydroascorbic acid, is measured. For this, a condensation reaction of dehydroascorbic acid with ortho-phenylenediamine (OPDA) is performed under acidic conditions that form the fluorophor (1,2-dihydroxyethyl)-fluoro[3,4-b]quinoxaline-1-one(DFQ).[110] As an aerosol collection unit, the design of Wragg et al., 2016 [95] was modified to meet the needs of the AA assay.

1.7 The Interaction between Aerosol Components and Ascorbic Acid

Ascorbic acid is a water-soluble vitamin and is also known as vitamin C. It is an essential nutrient for humans. Ascorbic acid is involved in many biochemical reactions in the body and is required for the synthesis of collagen, a protein that forms connective tissue. It also plays a role in immune function and wound healing. The lack of AA can cause scurvy, a condition characterized by fatigue, muscle weakness, and joint pain.[111] Ascorbic acid also plays a key role in antioxidant defense against oxidative stress in the human lung.[112] If an aerosol enters the lung (see Subsection 1.3.1) it first comes into contact with the respiratory tract lining fluids (RTLF) also called lung lining fluid (LLF) which is the first defense line against any object that enters the lung. RTLF has many different antioxidants such as mucin, uric acid, proteins, glutathione, and ascorbic acid.[40, 113]

In Figure 7A the pathways are shown that AA can undergo when it reacts with ROS compounds and the transition metals Cu and Fe. In the human lung with a pH value of around 7, the AA molecule with a pKa of 4.1 is present in its deprotonated form, which is the ascorbate anion (HA-) (see reaction 1, Figure 7). When HA- interacts with any active OP substance, it can subsequently lose electrons (by oxidation) and form the ascorbyl radical (see reaction 6), which can then undergo disproportionation to form the first metastable product, dehydroascorbic acid (DHA) (see reactions 10 and 11). AA can also be converted directly to the ascorbate radical via superoxide reaction or the hydroperoxyl radical reaction (see reaction 2). Furthermore, HA- can be oxidized with transition metals directly to DHA (see reaction 8). DHA can undergo an irreversible opening of the ring to the stable 2,3-diketogulonic acid (see reaction 12).[81, 114, 115]

In Figure 7B the condensation product 3-(1,2-dihydroxyethyl)fluoro[3,4-b]quinoxaline-1-one (DFQ) is shown that can be detected by fluorescence spectroscopy. DFQ is formed when DHA reacts with o-phenylenediamine (OPDA) in

an acidic environment. Because DHA and OPDA have a 1:1 reaction stoichiometry, measuring the change in DFQ concentration can be used to determine how much AA has been oxidized and to quantify the aerosol OP.[110, 116]

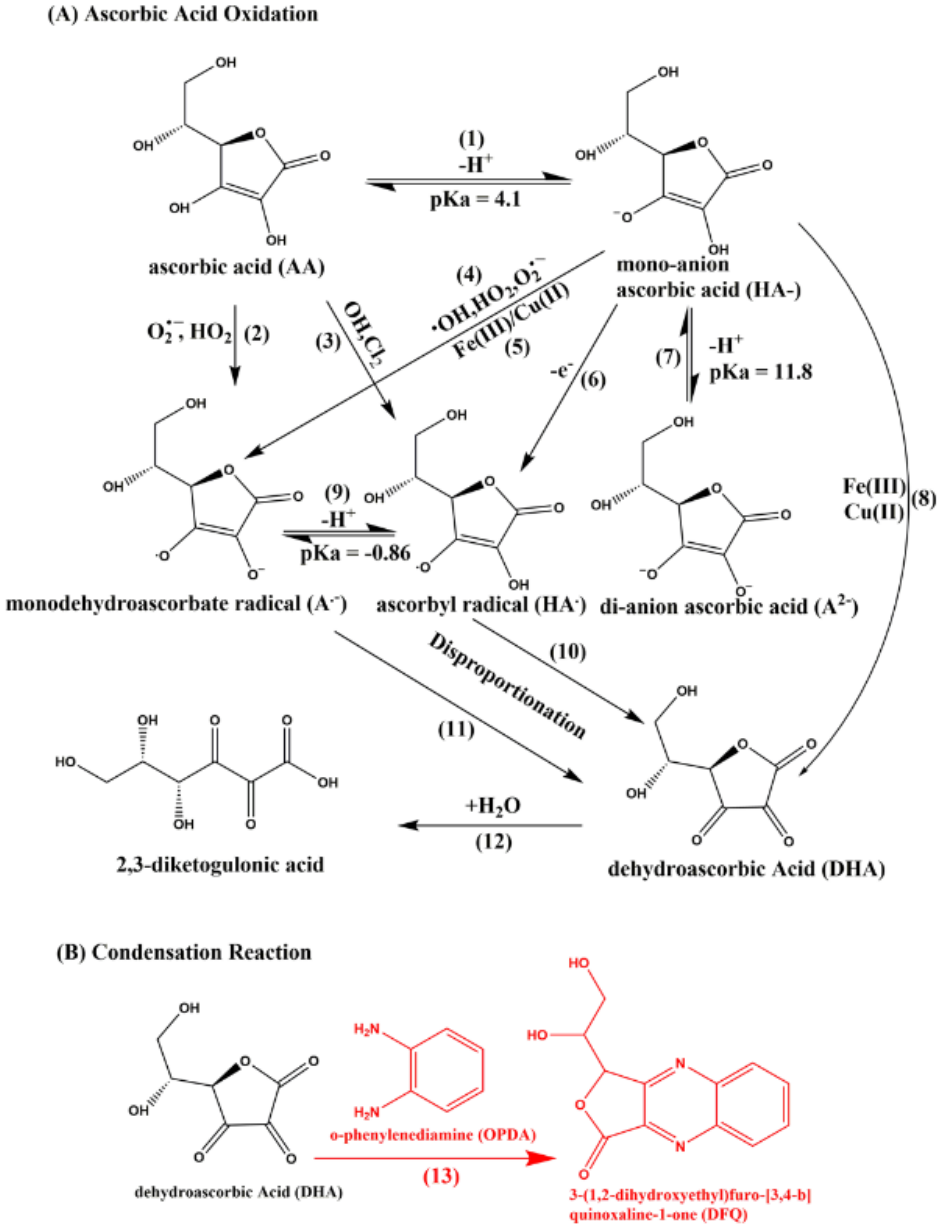

Figure 7: (A) Reaction schematic showing the AA oxidation pathways and (B), the condensation reaction of DHA and OPDA. Figure from Campbell et al. 2019 [38]

1.8 Aim of this Thesis

There are many epidemiological studies that have correlated toxicity of aerosols to human health.[12, 20, 43] Although this evidence linking air pollution to different health effects, it is still very unclear which compounds (and therefore particle sources) actually cause these diseases and, moreover, which pathways should be taken into account. There are numerous methods to estimate the toxicity of aerosols and to quantify and correlate the effect of different compounds in the aerosol. Three main categories of methods for measuring the effects of aerosols on human health can be distinguished: epidemiology, cellular/animal experiments, and chemical analysis.
In epidemiology, frequency and patterns are studied with big data sets to determine the causes and risk factors of diseases in certain populations. In animal or cell experiments, toxicity is measured by exposing cells or animals to certain compounds or emissions and measuring the biological response. With non-cellular methods, fundamental chemical reactions are studied to gain an understanding of the effects that lead to various diseases caused by air pollution. As a result of the high complexity of aerosols, it is very challenging to measure, characterize, and quantify overall toxicity. Therefore, it is crucial to investigate this topic more thoroughly and to find new methods to investigate the toxicity of aerosols.
Recognizing the difficulty to quantify OP in aerosol particles accurately due to the highly complex nature of aerosol particle and the short lifetime of many particle-bound redox-active compounds, this PhD thesis aims to characterize the temporal stability (i.e. lifetime) of OP in various aerosol types and to develop an instrument which is capable of capturing and quantifying also the very short-lived OP-active aerosol components and then quantify the OP in various types of aerosols with that instrument.

In Chapter 2 the design and characterization of a novel, field-portable online instrument (OOPAAI) is described that quantifies the toxicity of aerosol particles through their oxidative potential measured through AA oxidation. In a proof-of-concept field campaign the OP of ambient urban particles was quantified at a moderately polluted urban site in the city center of Basel, Switzerland (Section 2.5), demonstrating that the instrument designed, built and characterized in this study is capable of monitoring the OP of ambient aerosols for a long time.

In Chapter 3 the decay of OP is measured in different SOA systems and with different assays. Furthermore, some ambient data is analyzed with the offline AA assay, and the offline measurement method is compared with the online instrument. The comparison between online and offline measurements is made not only with the acellular AA assay but also with human epithelial lung cells to investigate if a difference in exposure methods can also be seen for cellular systems.

In Chapter 4 experiments are described in which this novel instrument was used to quantify the OP characteristics of real-world emissions from car exhaust and residential wood combustion. These aerosols were not only analyzed as primary, fresh aerosols, but also as secondary, aged aerosols and the difference in aging times were characterized.

In Chapter 5 the OOPAAI was used to measure together with other assays (DCFH, OH) more mechanistic effects of OP-active substances like transition metals and SOA and their synergistic and antagonistic effects. Moreover these measurements were compared to a model.

2 Development of the Online Oxidative Potenial Ascorbic Acid Instrument (OOPAAI)

This chapter is based on work published in Utinger et al., 2023 submitted in Atmospheric Measurement Techniques.[97] The paper Utinger et al., 2023 [97] is a condensed version of this chapter and can be found in Figure D.5. This thesis chapter focusses more on the technical parts and the instrument development process. Some of the preliminary results were also already published in the paper by Campbell et al., 2019.[38]

Author Contribution

Battist Utinger wrote this manuscript and conducted all experiments shown in this chapter, unless otherwise noted. Hardware parts were manufactured by the machine shop of the Chemistry Department at the University of Cambridge and by Hans-Ruedi Rüegg and Alois Schäuble at the University of Basel. The electronic components were designed by Ray Freshwater and the software was written by Nicholas Bukowiecki. Matthias Oscity conducted the intensity modeling for the flow cell. Benjamin Gfeller conducted the experiments for the absorption during his M.Sc. project under the supervision of Battist Utinger, and Alexandre Barth assisted with various experiments. Markus Kalberer supervised the experiments and contributed to the manuscript.

Abstract

Large-scale epidemiological studies have consistently shown that exposure to ambient particulate matter (PM) is responsible for a variety of adverse health effects. However, the specific physical and chemical properties of particles that are responsible for observed health effects, as well as the underlying mechanisms of particle toxicity upon exposure, remain largely uncertain. Studies have widely suggested that the oxidative potential (OP) of aerosol particles is a key metric to quantify particle toxicity. OP is defined as the ability of aerosol particle components to produce reactive oxidative species (ROS) and deplete antioxidants *in vivo*. Traditional methods to measure OP using acellular assays rely largely on the analysis of PM collected in filters offline. This is labor intensive and involves a substantial time delay between particle collection and OP analysis. Therefore, it likely underestimates particle OP because many reactive chemical components that contribute to OP are short-lived and therefore degrade prior to offline analysis.

Thus, new techniques are required to provide a robust and rapid quantification of particle OP, capturing the chemistry of oxidizing and short-lived highly reactive aerosol components and their concentration dynamics in the atmosphere. To address these measurement shortcomings, we developed a portable online instrument that directly samples particles into an ascorbic acid-based assay under physiologically relevant conditions of pH 6.8 and 37 °C, providing continuous accurate OP measurements with a high time resolution (5 min). The instrument runs autonomously for up to three days and has a detection limit of about 5 µg/m^3 in an urban environment, which allows the characterization of particle OP even in areas with low pollution.

2.1 Introduction

Numerous epidemiological studies have linked anthropogenic air pollution with adverse health effects.[20, 24, 47] They demonstrate that exposure to elevated levels of ambient aerosol particles is linked to increased hospital admissions and premature death from various diseases such as cancer, respiratory and cardiovascular diseases.[12, 23] The World Health Organization estimates in a recent report [25] that 1 in 8 deaths worldwide are related to air pollution. Despite compelling epidemiological evidence, the chemical and physical properties of aerosol particles, and detailed pathways of particle toxicity, that cause these negative health effects are largely unknown.[31]

Many countries adopted limit values for the total particle mass as an indicator of particle toxicity. However, several studies have shown that composition, for example elemental black carbon or transition metal levels, are better proxies for particle toxicity than particle mass concentrations alone.[26, 82, 117] Moreover, studies have demonstrated that the oxidative stress resulting from exposure to $PM_{2.5}$ could be a key mechanism to explain the health effects observed after exposure to particles. Oxidative stress occurs when an imbalance develops in cells and tissues between reactive oxygen species (ROS) and natural antioxidant defense mechanisms. This imbalance could lead to oxidative stress and therefore trigger various biological effects, such as inflammation, alteration of DNA/proteins, cell damage and death.[68, 118, 119, 120, 121] ROS (i.e., inorganic and organic radicals and peroxides such as hydroxyl radical ($^{\cdot}OH$), hydrogen peroxide (H_2O_2), and superoxide radical (O_2^{-}), in some cases including organic peroxides) can be delivered exogenously by inhalation of PM into the lung. ROS can also be generated in vivo through redox chemistry initiated by aerosol components such as redox-active transition metals and quinones. This ability of PM components to produce ROS, possibly catalytically, through redox chemistry and subsequent antioxidant depletion in biological cells or tissue is defined as the oxidative potential (OP).[31]

Measurement methods have been developed to quantify OP using cellular assays [122] or acellular assays.[33] In epidemiological studies, cellular and acellular assays have shown a correlation between the overall oxidative capacity of PM and its negative effects on human health.[50, 51, 85, 123, 124] In recent years, several acellular assays have been developed. The advantages of acellular assays are that they are usually cheaper and less time-consuming. The most commonly used assays are the dithiothreitol (DTT), ascorbic acid (AA), glutathione (GHS), and 2,7-dichlorofluorescin/Horseradish Peroxidase (DCFH) assay.[31, 33]

Traditionally, acelluar ROS and OP measurement methods are based on the collection of PM filters, with quantification of OP taking place days, weeks or even months later.[84, 85, 125, 126] This results most likely in an underestimation of PM OP because many highly reactive aerosol components, including particle-bound ROS (e.g. ROOH, $R\cdot$, $ROx\cdot$ species in particular) are short-lived and unstable.[85, 94] In a recent study we showed that only a very small fraction (<10%) of particle-bound ROS in organic aerosol collected on filters is stable when compared to *in situ* online DCFH measurements, [85] emphasizing the need for the rapid collection of particles to capture the chemistry of highly reactive aerosol components. Other studies, which measured the decay rate of organic

radicals, [89] peroxy pinic acid, [127] or hydrolysis of organic hydroperoxides in particles, [128] also show half-live time from minutes to hours of these unstable compounds.
Therefore, new direct online measurement methods are required with direct-to-assay particle collection and rapid quantification of OP to accurately assess the influence of highly reactive components on total OP. Providing robust OP measurements is a key step in achieving a more realistic assessment of the link between particle OP and particle toxicity.[94] Offline methods are also very labor intensive, and the data in most cases have poor temporal resolution. Thus, various attempts have been made to build online methods and instruments to obtain faster measurements with a higher temporal resolution.[75, 80, 95, 129, 130]
The OP measurement depends not only on the aerosol composition, but also on the assay used. The human lung lining layer contains, in addition to AA, other components such as glutathione, uric acid, and many more antioxidants. Calas et al., 2017 [131]showed that a simulated/epithelium lung lining to mimic the lung conditions might be favorable. However, Pietrogrande et al., 2019 [132] demonstrated that when assessing the OP with a mixture of antioxidants, the absolute signal of each antioxidant is lower, because OP is reduced by different antioxidants, resulting in higher detection limits.

In this study, we present the development, characterization, and first field deployment of a new online instrument that continuously quantifies OP in aerosol particles based on AA oxidation with a high time resolution (approx. 5 min). The online oxidative potential ascorbic acid instrument (OOPAAI) is the first instrument that provides rapid, highly time-resolved OP quantification based on the oxidation of ascorbic acid. We run the OOPAAI using an AA-only-based assay to achieve as low a detection limit as possible, allowing quantification of OP in a range of polluted and moderate-pollution environments. The OOPAAI is an instrument with a vastly improved performance, for example, a better detection limit and functionality compared to the method presented by Campbell et al., 2019 [38], now running under physiologically relevant conditions, and including improved hardware components compared to the instrument developed by Wragg et al., 2016.[95]
Because building the instrument is the result of this thesis, there is no separated method or result section, like it would be in a paper. The chapter is divided into a first part, where the chemical assay is described (Section 2.2), in a second part where the hardware of the instrument is discussed (Section 2.3), in a third

part where various calibrations were performed with the instrument (Section 2.4) and in a forth part where the implementation of the instrument for ambient measurement is shown (Section 2.5).

2.2 Ascorbic Acid Assay Chemistry

In this section everything that is related to the chemistry of ascorbic acid used for the OOPAAI is presented. Furthermore, the condensation reaction between OPDA and DHA, the buffer, and the stability of the assay is discussed.

2.2.1 Ascorbic Acid Chemistry

Ascorbic acid (AA) also known as vitamin C is a water-soluble vitamin that is necessary for many different biochemical processes in the body. AA plays a role in the formation of collagen, a protein that helps support skin, bones, and blood vessels.[133] Furthermore, ascorbic acid plays a vital role in the immune system and helps the body fight infection. It is also involved in iron absorption from the diet and proper functioning of the nervous system.[134] Ascorbic acid also acts as a first defense line in the lung against any oxidative stress that can occur from inhaled aerosols. The lung is a particularly vulnerable organ to oxidative stress due to its constant exposure to environmental pollutants and toxins. Oxidative stress can cause inflammation and damage to lung tissue, leading to respiratory diseases such as asthma, chronic obstructive pulmonary disease (COPD), and many more diseases.

Because ascorbic acid is an abundant antioxidant in the human lung and has strong reducing capabilities and because the chemistry is well known, especially from decades of food chemistry research, we chose it as a proxy to measure the oxidative potential of aerosols. AA can be oxidized through several pathways. A graph with the most important pathways and products of AA oxidation is shown in Figure 8. AA has a pKa of around 4.1 and therefore at pH 6.8 in an aqueous environment, AA is present mostly as the ascorbate anion (AH^-). AH^- can be directly oxidized by metals such as Fe(III) or Cu(II) to DHA, or it can be oxidized over intermediate monodehydroascorbate radical $AH^{\cdot -}$ and further react with disproportionation to dehydroascorbic acid (DHA). The DHA reacts then under a condensation reaction with ortho-phenylendiamine (OPDA) to the fluorophor (1,2-dihydroxyethyl)-fluoro[3,4-b]quinoxaline-1-one (DFQ), which is ultimately used in the OOPAAI to quantify the OP of aerosol particles.[38, 81]

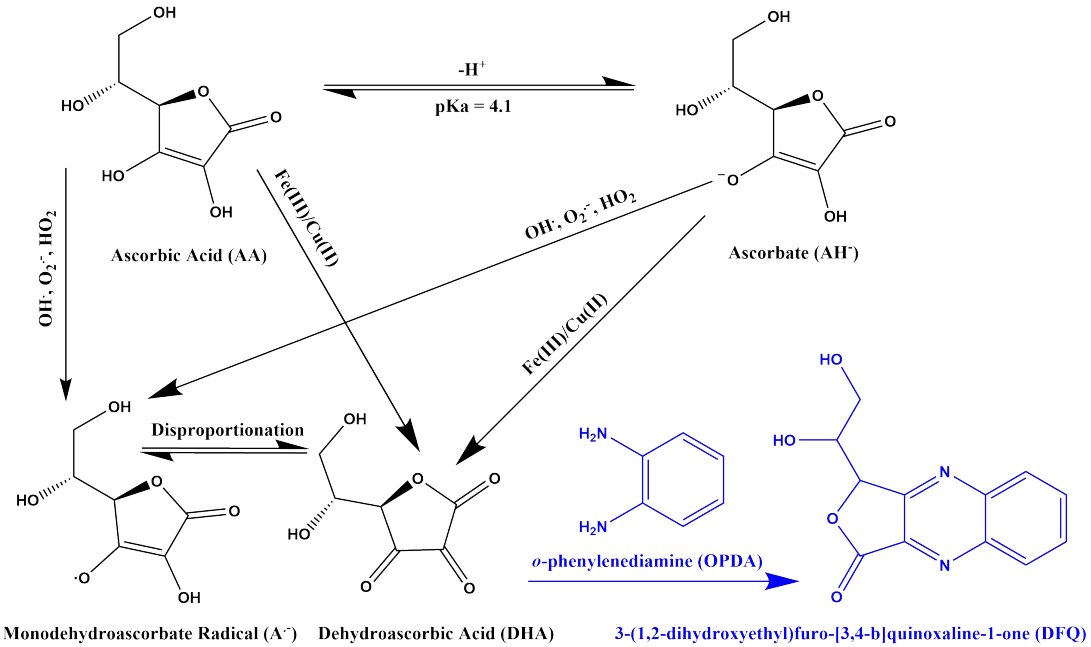

Figure 8: A simplified scheme of the ascorbic acid pathway and the condensation reaction with *o*-phenylendiamine (OPDA) to the fluorophor (1,2-dihydroxyethyl)-fluoro[3,4-b]quinoxaline-1-one (DFQ)

The fluorescence detection approach (i.e. reaction of DHA with OPDA) was selected over a direct UV-vis absorption measurement of AA because fluorescence spectra are often more specific for an individual compound than UV-vis absorption although the fluoresce detection approach needs an additional condensation step (see Figure 8). AA has a broad UV absorption peak at a wavelength of 265 nm. Many other organic compounds present in aerosol extracts also have strong absorption in the UV (see Subsection 2.3.8).[135, 136] Therefore, it is not feasible to develop an instrument for continuous online operation using absorption detection. A decrease in AA would need to be quantified in the presence of a larger background that potentially varies substantially with changes in the organic aerosol composition.

2.2.2 Condensation Reaction of DHA and OPDA

The condensation reaction of DHA and OPDA is well known and was first published by Deutsch and Weeks, 1965.[110] Since then many more studies have used this assay to quantify ascorbic acid, especially in food chemistry.[137, 138, 139] Although the assay is widely used, not too much of the exact mechanistic is known. The condensation reaction is favorable to take place under acidic conditions around pH 2. Wu et al., 2003 show that the keto-form of AA can react with OPDA in an alkaline medium to form DFQ.[138] Under neutral or acidic

conditions, this reaction cannot occur because ascorbic acid is in its enol-form where there are not two ketone groups present in an ortho configuration. The condensation can only take place if there are two ortho-amine groups of OPDA and two ortho-ketone groups of the DHA. In Figure 9 a spectrum of 200 µM DHA with 20 mM OPDA is shown. The spectrum was taken with the fluorescence spectrometer (QePro-UV-VIS, Ocean insight) with the same settings as described in the offline setup (see Subsection 3.2.2). The DFQ peak is at 430 nm and the small scattering peak from the LED is at 365 nm. Note that this is a relative spectrum measured with the settings used in this experiment and that the absolute peak shape could slightly change depending on the exact spectrometer type and settings.

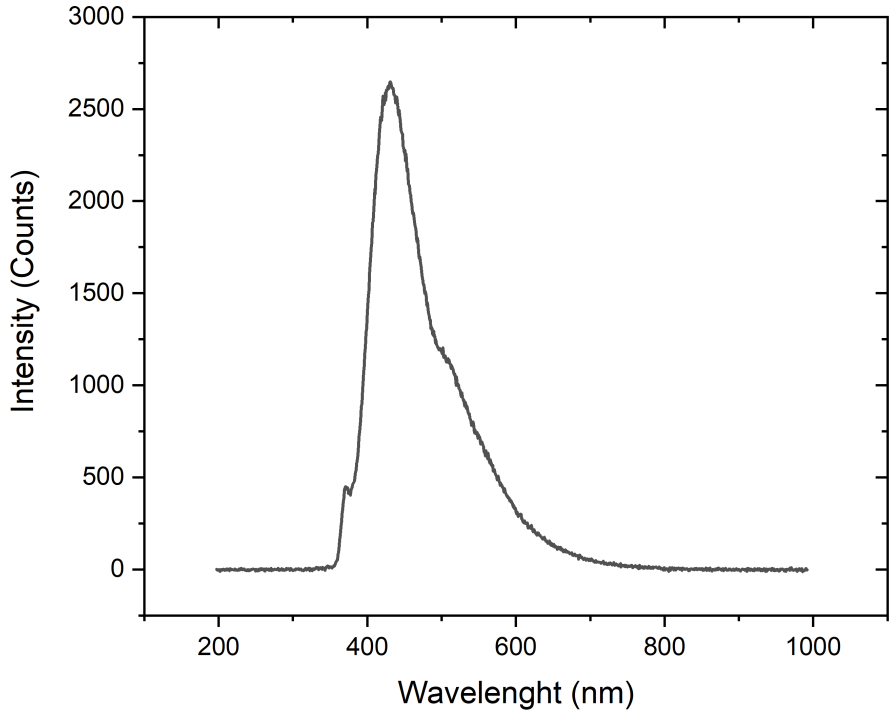

Figure 9: A relative spectrum of DFQ. The small peak at 365 nm is the scattering of the LED, and the large peak at 430 nm is the fluorescent emission of the DFQ.

2.2.3 Reagents

All chemicals were obtained from Sigma-Aldrich and all gases from Carbagas unless otherwise indicated and were used without further purification unless otherwise indicated: ascorbic acid (99%), Dehydroascorbic acid (99%), 0.1 M HCl solution, 0.1 M NaOH solution, Chelex 100 sodium form, $CuSO_4$ (99%),

$FeSO_4$ (99%), $Fe_2(SO_4)_3$ (98%), o-phenylenediamine (≥99.5%), HEPES (4-(2-hydroxyethyl)-1-piperazineethanesulfonic acid, ≥99%), α-pinene (≥98%) β-pinene (≥98%), naphthalene (≥99%), zero grade air, N_2 gas (purity 99.999%). The H_2O used to prepare the solutions was purified with an ultra high purification water unit (resistivity 18.2 MΩ/cm).

2.2.4 Preparation of Chemicals

All chemicals used in this study were made immediately before a measurement, except where otherwise specified. Pure water was additionally prepared using a fritted column and filled with 100 g Chelex®100 resin. The valve was adjusted to a flow of one drop per minute through the resin. The treatment was used to remove trace metals (i.e. copper and iron) from the water and ensure a stable and low transition-metal-free background. Otherwise, there could have been an unwanted interference with AA oxidation from the sample. AA solutions were prepared the evening before the experiment in an effort to stabilize the background drift caused by the autooxidation of AA. A 200 mM HEPES stock solution was prepared monthly using chelexed water and stored in a glass bottle (Duran, Schott) at 4 °C. 8.8 mg of AA were dissolved in 25 mL HEPES stock solution and 225 mL chelexed water to form a 200 mM AA working solution. OPDA was prepared by dissolving 0.54 g in 250 mL of 0.1 M hydrochloric acid to form a 20 mM working solution. The working solutions were stored in brown HDPE bottles (250 ml Nalgene, Merck) that were rinsed with aqueous hydrochloric acid (0.1 M) to remove trace amounts of metals.

2.2.5 Physiological Relevant Conditions

For measuring the oxidative potential in aerosols, it is very important to have an assay that is as physiologically relevant as possible. The further away the assay is from the chemical conditions occurring in the human lung, the greater the chance that measurement artifacts can occur. Therefore, we tried to stay as close to the conditions in the human body as possible. With AA, the assay uses a chemical that is a naturally occurring antioxidant in the human lung. Furthermore, we try to mimic the human body by having the reaction chamber at 37 °C and the pH at a physiologically relevant value around 7.

Buffer

To ensure pH stability, ascorbic acid must be buffered. One of the most commonly used buffers for ROS and OP assays [72, 75, 95, 126, 132, 140] and general in biology [68, 71] is phosphate buffer saline (PBS). This buffer is commonly used because it is inexpensive, well-established, and has a good range of physiological relevance. Therefore, we also used this buffer at the beginning.
Unfortunately, PBS is a very good chelating agent for metals.[141] The ascorbic acid assay is very sensitive to metals and therefore measuring OP with PBS buffer is not suitable. Due to this reason, we tested a different buffer from the Goods buffer family. 4-(2-hydroxyethyl)-1-piperazineethanesulfonic acid (HEPES). HEPES was used because it generally does not form strong complexes with metals.[141, 142, 143, 144]
For several highly OP-active metals, such as iron or copper, the speciation of soluble complexes and the distribution between their soluble form and precipitates, is strongly pH dependent. Therefore, maintaining a physiologically relevant pH is crucial to avoid changing the soluble fraction of metals and their speciation because the reactivity of AA (or any antioxidant) with metals will change significantly depending on the metal speciation and soluble/insoluble fractions.

To show the different effects that buffer can have on metal, we modeled a transition metal (Fe(III)) with two different buffer as shown in Figure 10. To model the different buffer conditions, Visual MINTEQ was used. Visual MINTEQ is a chemical equilibrium model for the calculation of metal speciation, solubility equilibria, sorption, and some other quantities in aqueous solutions. A sweep from pH 2-9 with an increment of 0.1 was calculated. The initial concentrations for the buffer were set to the concentrations we were using in the experiments. The input temperature was set at room temperature (25 °C) and the ionic strength was calculated using Visual MINTEQ.
Furthermore, solid phase reactions were excluded because the model works only on a thermodynamic basis and the times we used in this study (20 min reaction time) are too low to take these processes into account without having any information about the kinetics. In Figure 10 only species that are important for the reaction and present in a sufficient concentration are shown.
In Figure 10A the speciation of Fe(III) is shown when buffered with HEPES and most iron is present as ($Fe(OH)^{2+}$) at pH 7. In contrast, when the system is buffered with phosphate (Figure 10B), a substantial part is also present as iron

phosphate ($FeHPO_4^{2+}$). These findings indicate that phosphate buffer is not a suitable buffer for measuring metal ions as a result of chelation effects. Note that other metals might form other complexes, but HEPES is considered to be a buffer that generally does not form strong metal complexes so it should not make a big difference.

Moreover we tested the different buffers also with human epithelial cells that were exposed to iron sulphate particles and the particles extracted in PBS showed less cytotoxicity than the ones that were extracted with HEPES. This result is shown in Figure 51 and described there in more detail.

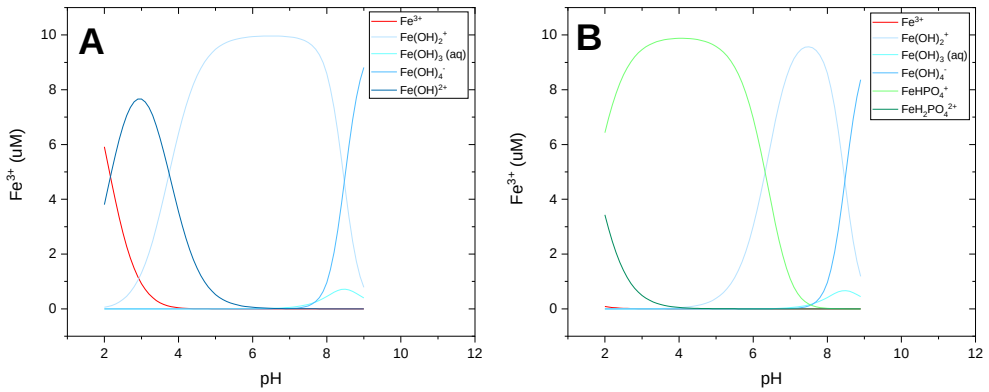

Figure 10: Modeling Fe3+ speciation with different buffers using Visual MINTEQ. (A) HEPES buffer does not chelate metals and at pH 7 iron is almost entirely present as $Fe(OH)_2^+$. When iron is buffered with phosphate (B), a substantial fraction of the total Fe(III) at pH 7 is present as iron phosphate ($FeHPO_4^{2+}$)

Temperature

Temperature is a very important parameter for the ascorbic acid assay, because the assay is very sensitive to temperature changes. The main reaction, in which ascorbic acid is oxidized by aerosol in the heating bath, is at 37 °C to mimic the body temperature of the human lung. The reagents, pump, filter, bubble traps, particle-into-liquid sampler (PILS, model 4001, Brechtel), impaction plate, spectrometer, flow cell, and all connected tubing are in a temperature controlled compartment with insulation to keep temperature as stable as possible (see Figure 17 for details).

This is done using a TECooler set in a temperature range, with a hysteresis of 1 °C. This insulated compartment works quite well, but has some minor issues. The hysteresis is too high, and therefore there is still some wobbliness from the temperature that can be detected in the signal. The temperature gradient in

the compartment is also too large because the mixing is too slow inside the temperature controlled compartment.
The TECooler is on top of the insulated compartment and blows to the side, which does not lead to a perfect distribution of the cooled or heated air. To achieve a more uniform temperature and a smaller hysteresis, an additional fan was placed in the temperature controlled area to better mix the air. This decreased hysteresis and gave a more stable signal. The placement of the temperature sensor in the compartment is also very important in minimizing hysteresis. If the sensor is too far away from the TECooler, it reacts to slow and the temperature changes to slowly and the hysteresis is bigger and, therefore, the signal variability higher.
A higher variability then ultimately leads to a worse detection limit. If the sensor is too close, it only measures the temperature of the TECooler, not the compartment, which is useless for regulation. The set temperature of the TECooler depends on the ambient temperature and the variability present during the measurement. For the solutions, the colder the temperature, the better it would be for their stability.
For the reaction coil of DHA with OPDA, it would be better to have a higher temperature so that the condensation reaction is faster. The compromise is what is feasible so that the TECooler can still cool it but is not so warm that the solutions are not stable anymore. So, in the end we decided to set the TECooler to a one-point regulation at 30 °C where the compartment is heated and not cooled if the room temperature is not too low.

In Figure 11 the hysteresis of the TECooler is shown in black, and the signal of the OOPAAI is shown in red. Both measurements are averaged to a one minute interval. The OOPAAI signal follows exactly the temperature, leading to the assumption that these small variations in the OOPAAI signal come from temperature drifts. The hysteresis of the TECooler is around 1 °C and leads to less than 100 counts, which is an equivalent of around 2 nmol DHA/m^3.
In the ambient measurement 2 nmol DHA/m^3 (see Figure 40) corresponds to less than 2 µg/m^3. So small temperature drifts are not a big problem, especially when they are logged and a post-data correction for the drift can be applied. But when trying to reduce the LOD to be able to measure in very clean environments, the temperature stability has to be optimized.

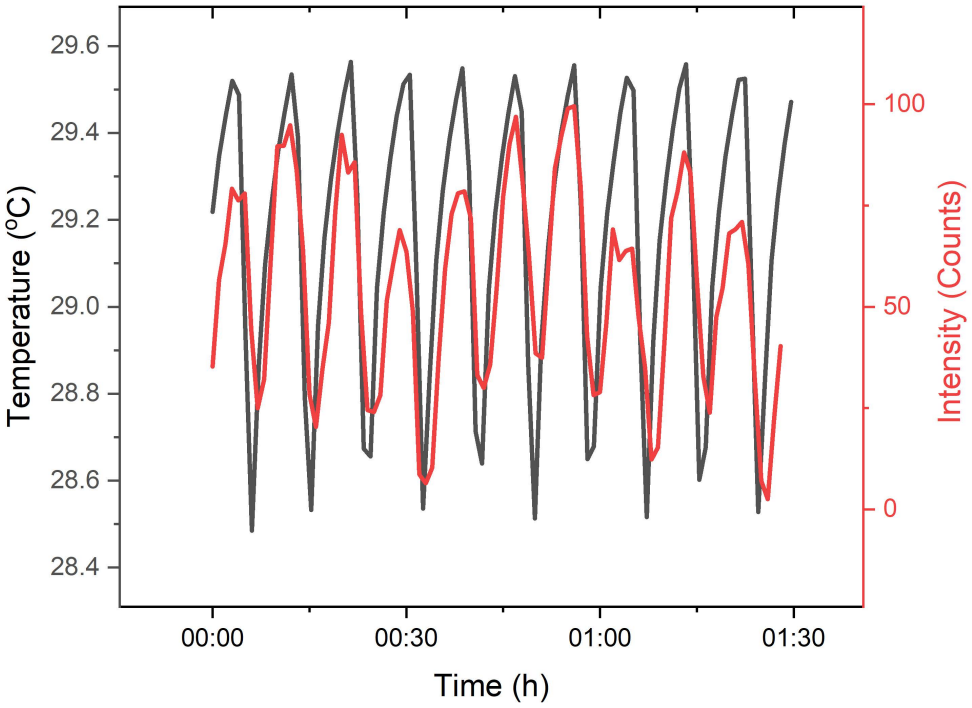

Figure 11: Variability of the blank. In black is the temperature measured inside the temperature-controlled compartment and in red is the signal of the OOPAAI. Both values are averaged at one minute. The periodicity of the signal is the same as the periodicity of the temperature.

2.2.6 OPDA Stability

AA respectively, DHA condenses under acidic conditions with OPDA to the fluorophor DFQ that emits light at 430 nm (see Subsection 2.2.1) However, OPDA can be oxidized with Cu(II) to 2,3-diaminophenazine (DAP) (in Figure 12 called OPD_{ox}).[145] DAP can also further oxidize and react with another DAP to form microfibrils.[146] These microfibrils structures could be observed in the waste of OOPAAI. This side pathway of OPDA reduces the total amount of OPDA that is available for the condensation reaction with DHA and reduces the amounts of photons that are available to react with the DFQ. Therefore, it is important to reduce this effect. With debubbling of the OPDA solution, the dimerization of OPDA could be reduced in the storage vial. The time when OPDA is in contact with the AA solution and therefore also with the oxidizing parts of the aerosol is rather short (3 min), therefore it should not be a significant a problem. In Figure 12 the peak values differ slightly from what we measured and what is stated elsewhere, [110, 116, 147] but this could just be because in this

study it is not published as an absolute spectrum, but just a relative spectrum of their spectrometer.

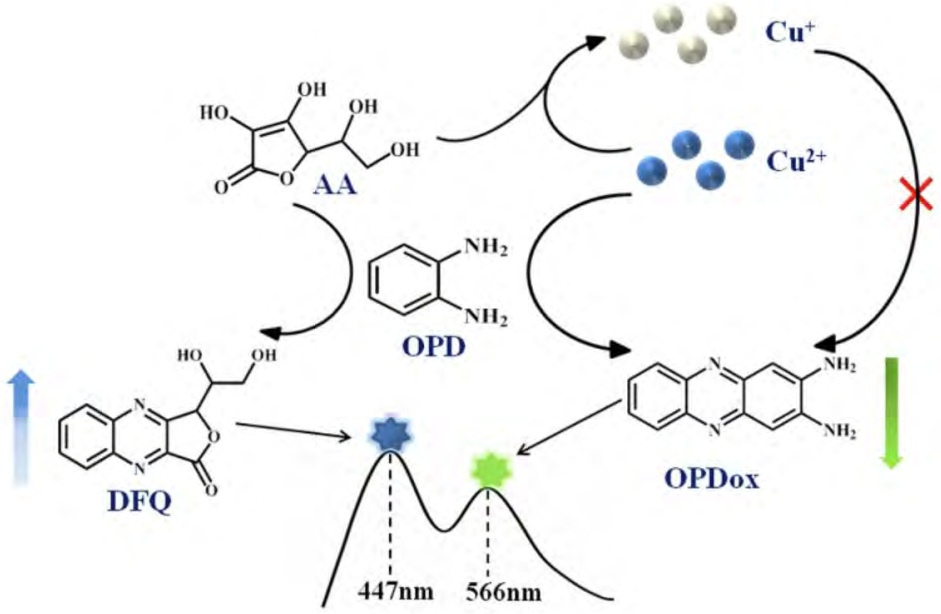

Figure 12: Condensation reaction of AA respectively DHA with OPDA (here called OPD) and the oxidation of OPDA and condensation with itself to $_{ox}$ (also called DAP). Figure adapted from Ding et al., 2022.[145]

We also tested if we could see DAP in an old (three day) OPDA solution that was just sitting at room temperature in a Falcon tube (see Figure 13). It is only a fluorescence measurement without any further analysis, so it can not fully be determined if it is actually this compound, but because the peak looks quite similar and there is nothing else in the solution that could be fluorescent at this intensity, it is very likely that DAP is formed. In Figure 13 it can be seen that the fresh OPDA has no peak for the DAP, which is good because all OPDA is still left for the condensation reaction with DHA to DFQ. The old OPDA is an order of magnitude higher concentrated than the DAP, so even after 3 days, there is only approximately 10% converted to DAP.

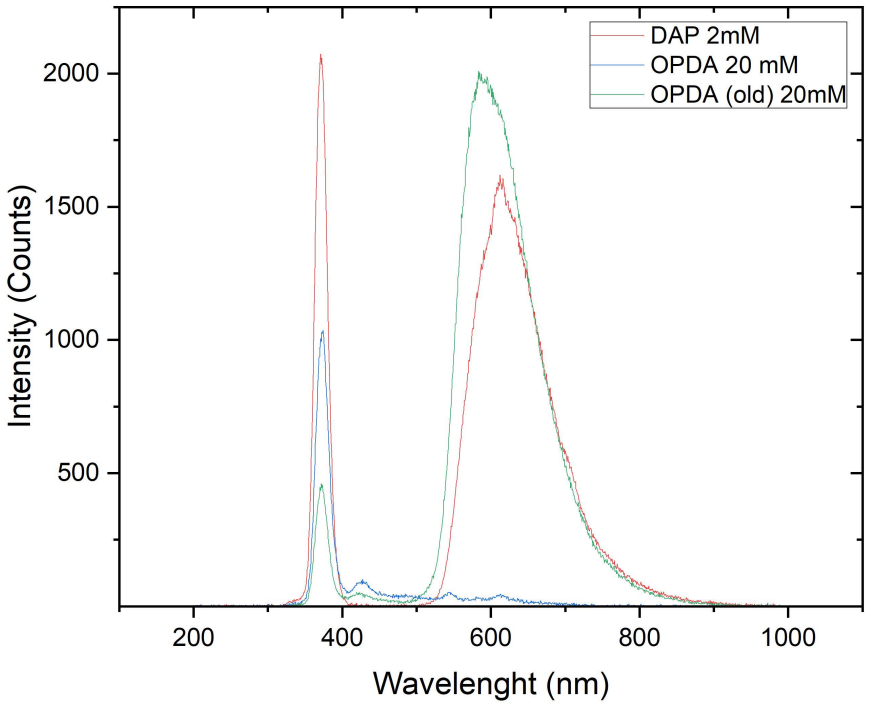

Figure 13: Fluorescence spectra of OPDA, OPDA that was stored for three days at room temperature, and DAP. All of them show a scattering peak at 365 nm, but only DAP and the old OPDA show a peak around 580 nm.

2.2.7 DFQ Stability and Photosensitivity

DFQ, the fluorescent compound used for detection (see Figure 8) is not stable under high-intensity UV light emitted by the 365 nm LED, as can be seen in Figure 14. In the first few seconds after the signal is visible (adding the sample around 00:09), the signal drops very fast by almost a quarter of the original value. After around 30 sec the signal starts to stabilize again and even increases. This effect can be seen for all experiments conducted with DFQ, although the effect at lower concentrations is not that strong and at very low concentrations is not detectable. When the cuvette sits for a couple of minutes in the light, a compound starts to form, which can be seen by the eye as a yellow point where the LED hits the liquid. We have not investigated what DFQ could degenerate under UV light, and to the authors' knowledge, there is also no literature on this topic. It could be that there are actually two different processes, the decay of DFQ, and that the increase could be the formation of another product such as DAP as described in Subsection 2.2.6. For the online instrument, all these effects

do not matter, because at constant flow rates the signal is just a little bit lower, but not unstable. Although it reduces the signal-to noise ratio a little bit.

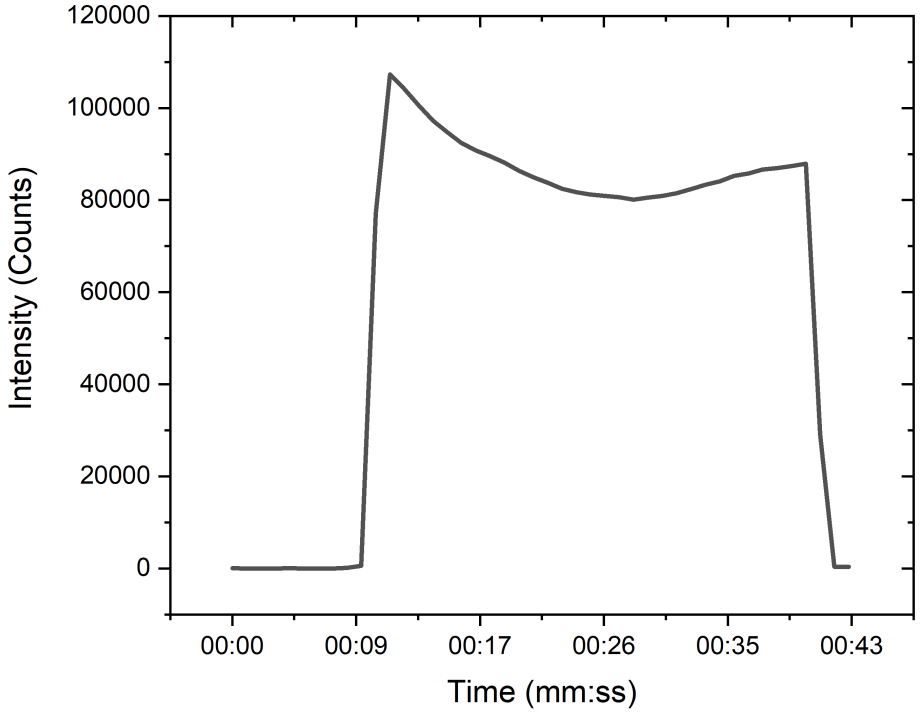

Figure 14: Offline measurement of 200 µM DHA. At 00:09 the cuvette is inserted and the signal rises immediately to its maximum. But after that the signal drops fast and starts to increase again after 00:30 sec.

2.2.8 Reaction Time

Ascorbic Acid and OP-active Compounds.

The reaction time is very important for any chemical reaction. Depending on the reaction and what should be observed, it might be beneficial for the reaction to have longer or shorter reaction times. For the oxidation of AA, a shorter reaction time favors ROS and other short-lived compounds, such as radicals over metals.[81] This is because DHA is not stable (see Table 1) and a longer reaction time will only lead to less signal and therefore to an underestimation of the total ROS concentration. On the other hand, for other OP active substances like metals that react catalytically, it is exactly the opposite. Longer reaction times will lead to more signal (as long as the concentration is high enough to produce more DHA than the DHA that is decomposed). Transition metals can react catalytically to produce ROS via Fenton-type reactions, they can not only react

directly with AA.[81, 148] Analogously, there are also organic compounds that have slow reaction kinetics. So depending on the reaction time the sensitivity for the assay can also be shifted to one or the other group of compounds.
To test the different reaction times we took aliquotes every 10 min from a AA and $CuSO_2$ solution as well as from blank solution with only AA and measured the increase in signal. The data in Figure 15 is done with the setup descibed in Subsection 3.2.2 and under acidic conditions. The blank is stable, but the longer the reaction time for the AA and $CuSO_2$ solution is, the higher the signal gets. For organic components this process is not so easily possible to show, because there is at the same time a decay of the components in the SOA (Chapter 3) which would interfere with the measurement.

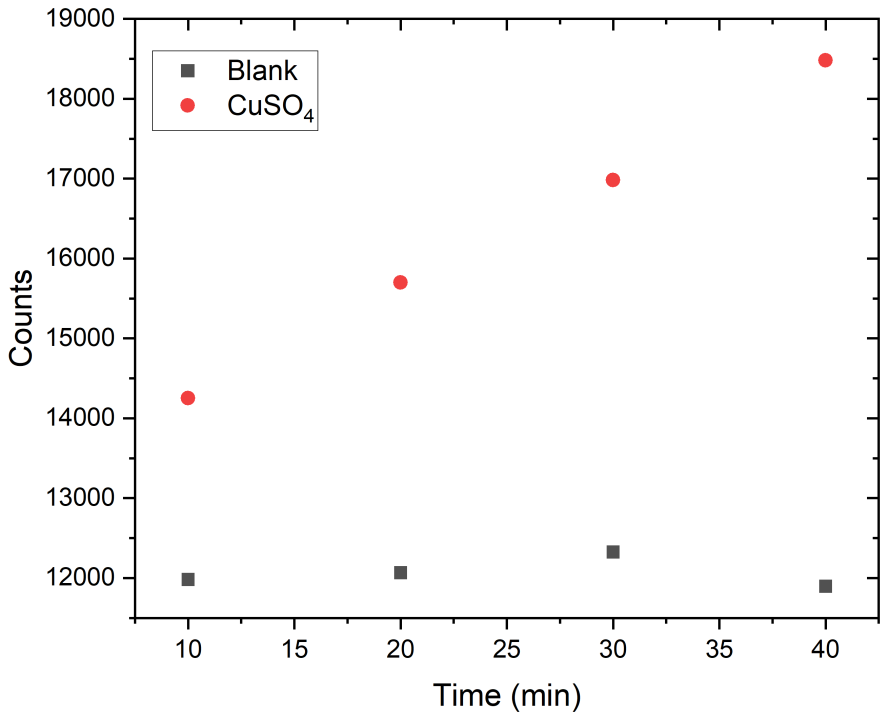

Figure 15: Raw counts of the AA assay with metals and at different times. The longer the metal has time to react, the higher the signal will be.

All of these different reactions, which favor contradictory reaction times, make it very challenging to choose the appropriate reaction time. Furthermore, the reaction time also correlates with mixing (the longer the reaction time is, the better the mixing (Subsection 2.3.3)) and with the smear out (the shorter the reaction time is the smaller is the smear-out effect (Subsection 2.3.5)) Taking all these into account and also due to practical reasons we decided to take a reaction

time of around 20 min. To avoid all these considerations, it would be better to measure the oxidative potential per time as many other offline analysis methods do.[31, 72, 85] Unfortunately, for an online instrument, this is not really possible, because to measure a slope (OP/min) multiply time points have to be measured from the same aerosol. That would only work by running the same analysis in parallel, hence having more than one OOPAAI measuring at the same time, but with different reaction times. Another possibility would be to not measure really online, but to analyze batchwise (see for details Subsection 2.3.8).

DHA and OPDA

The reaction kinetics of the condensation reaction between OPDA and DHA to form DFQ was determined. DHA and OPDA were mixed in a vial at concentrations used in the OOPAAI and every 5 min an aliquot was measured with the same setup that was used for all offline measurements. Campbell et al., 2019 [38] and Vislisel et al., 2007 [149] assumed pseudo first-order kinetics for this reaction and estimated that using the conditions of the OOPAAI, the reaction should be completed within minutes. However, the experiments conducted in this study (see Figure 16) showed that the reaction is much slower and that it takes about 10 min for 50% DHA to react. This agrees with the kinetics described in Deutsch and Weeks, 1965.[110]
In the actual design of the OOPAAI a short reaction time was chosen (around 3 min) to minimize potential artifact that could occur due to the lower pH of the DHA-OPDA condensation reaction. When the OPDA is mixed with the AA and the aerosol solution, the already converted DHA reacts with OPDA to DFQ, but there is no quenching, so the unreacted AA can get oxidized further and also react with OPDA to produce more DFQ. The reaction time in the coil where the aerosol reacts with the AA at pH 6.8 is almost an order of magnitude longer than the time at pH 2 for the condensation reaction. This reduces the signal-to-noise ratio and therefore the sensitivity of the instrument compared to a reaction time of more than 30 min, but it has the important advantage that the OOPAAI measures most of the time under physiologically relevant conditions.

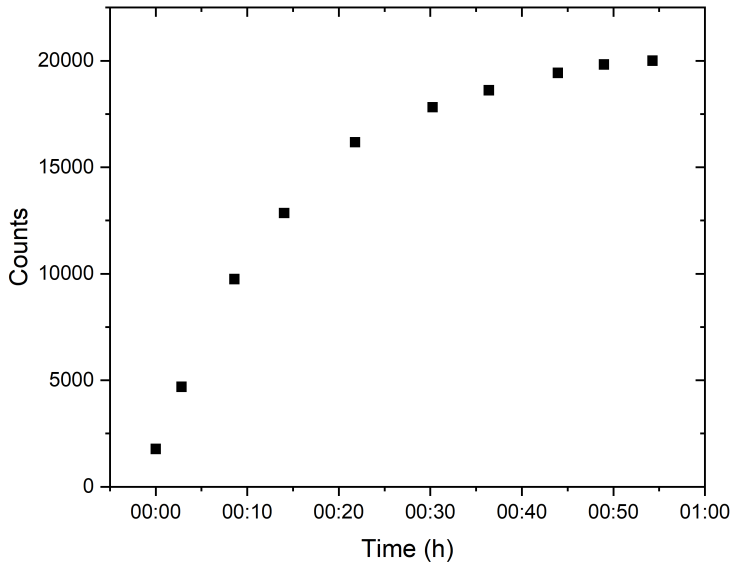

Figure 16: Reaction rate of DHA and OPDA to form DFQ.

2.2.9 Memory Effect of Metal Salts

All tested metal salts (i.e. Cu(II), Fe(II), Fe(III)) cause memory effects at neutral pH in the OOPAAI. The higher the metal concentration of a tested solution, the longer it takes the signal to return to the original blank level. If the solution is at an acidic pH, this effect cannot be observed. In Figure 36B this can be seen that the signal plateaus not as nicely off than as in Figure 36A under acidic conditions. The effect, especially for copper, seems very strong. We could not show exactly what led to that memory effect, but it is most likely that the adsorption of metal ions to the tubing walls leads to this effect.

As described in Subsection 2.3.1 most of the tubing is polytetrafluoroethylene (PTFE, Teflon). The connections are made of PEEK and the peristaltic tubing is PVC. All of these materials are considered to be inert. Therefore, the memory effects probably come not from reactions with the tubing and connector materials but from adsorption. Even on the inert Teflon surface, molecules will stick to the wall. Especially at higher pH's, this effect has been observed for metals.[150] Coating the surfaces would explain the effect that the signal increases over time and becomes saturated after a certain time. When flushed with water, the memory effect only drops really slowly (hours to almost days), but when washed with an acidic solution (0.1 M HCl) the memory effect is removed fairly quickly (≤ 1 h). The blank after a sufficient flushing is at the same level as the blank before adding

metals to the system, leading to the conclusion that all metal ions are removed efficiently.
For the ambient measurement, this could not be observed, but the total metal concentration is also several orders of magnitude lower. This means that the effect is probably there, but not a problem because the concentration is small enough. For real-world emissions, as can be seen in Chapter 4 with residential wood combustion experiments, this could be a problem because there the metal concentrations can be higher. But because laboratory experiments are usually not too long, a blank correction can be made for the drift, if a couple of blanks were measured before, in the middle, and after the actual measurements.

2.3 Instrument Development of the OOPAAI

In this section all the developments of the OOPAAI are presented. For most part of this section only the final version is presented, but for key components, some previous versions that were working less well or had some challenges are also presented. This is done to avoid that for future improvements the same ideas, that have not worked out in an ideal way, are tested again.

2.3.1 OOPAAI Working Principle Overview

Figure 17 shows a schematic overview of the OOPAAI. The key components of the instrument are: (1) the PILS (PILS, model 4001, Brechtel) where the aerosol particles are collected in the liquid phase; (2) the heating bath where ROS and the other OP-active particle components react with AA to form DHA under physiological conditions (pH 6.8 and 37 °C) and where the condensation reaction occurs between DHA and OPDA to form the fluorescent product DFQ; (3) the detection cell where the fluorophore DFQ is quantified using a spectrometer.

The aerosol is pumped into the instrument using a vacuum pump (N035.1.2AN.18, KNF) at a flow rate of 16 L/min through a sample inlet (Figure 17, black lines) where a solenoid valve allows switching between a HEPA filter (HEPA-CAP 75, Whatman), which removes 99.9% of particles (to allow blank measurements with particle-free air) and without a HEPA filter. The aerosol then passes through four activated charcoal honeycomb denuders (charcoal honeycomb denuders, Ionicon) with a total length of 14 cm to remove all gaseous oxidizing volatile compounds that can result in an increased OP signal. After the charcoal denuder, particles >2.5 µm are removed with a round jet impactor that is part of the PILS. In the

PILS the aerosol particles grow with the supersaturated water vapor to small dropplets. These activated aerosol particles are then collected on the quartz impaction plate at the end of the condensation chamber of the PILS.[151] This quartz impaction plate is washed with a continuous flow of 60 µL/min of AA (200 µM) buffered at pH 6.8 with 10 µM HEPES buffer.
The buffered AA–aerosol mixture is then pumped from PILS into a polyether ether ketone (PEEK) tube through a peristaltic pump operated with a PVC peristaltic tubing (AHF, inner diameter 1.02 mm, white-white) at a flow rate of 60 µL/min flow through a cellulose filter (grade 1 filter, Whatman) to remove any insoluble particles. The reaction mixture then flows through a heating bath filled with ethylene glycol at 37 °C, with a residence time of 20 min. This reaction time of 20 min in the heating bath at body temperature and physiologically representative AA concentrations (200 µM) and physiologically relevant pH (pH 6.8) mimics the conditions in the human lung and the initial reactivity of the aerosol components with AA when the aerosol particles are deposited on the lung lining layer.

The liquid flow is then mixed in a T-piece and two helical mixers (1/16 inch, Stamixco) with a 90 µL flow of OPDA (20 mM in 0.1 M hydrochloric acid) for approximately 2 min before reaching the detector. The short reaction time was optimized to minimize shifting reaction conditions as a result of the low pH. DHA and OPDA react to the fluorescent product DFQ with a 1:1 stoichiometry, which is then detected by fluorescence spectroscopy. AA and OPDA solutions in the reservoir were continuously degassed with 50 mL/min of N_2 to minimize oxidation with oxygen. All liquid flows in the system are constantly monitored using liquid flow meters (SLF3S-0600F, Sensirion).

For fluorescence measurements, the liquid enters the detection cell before being pumped out of the instrument to waste. The detection cell is a home-built unit using a commercial flow through the cell (137-2-40, HELLMA Analytics) with a height of 2 mm, a length of 40 mm and a width of 10 mm. At the end of the detection cell, the cuvette narrows where the inlet and outlet are placed perpendicular to the flow direction (see Figure 17). To enhance light transmission through the cuvette, the narrow sides of the cuvette are polished to make them transparent.
The LED (Roithner Lasertechnik, type UVLED- 365-330-SMD, peak emission wavelength 365 nm) is soldered on a printed circuit board (PCB), which is screwed

to a thermoelectric element to ensure stable temperature conditions and therefore a more stable LED output. The optical fiber from the LED (UV-Vis fiber, FP1500RET SMA, Thorlabs, NA 0.5). is in close contact with the polished short side of the detection cell and excites the solute. The emitted light is then collected from the side of the large surface area of the detection cell with a collimating lens (74-UV, Ocean Insight) and focused on a 1500 µM fiber with a numerical aperture of 0.39 (UV-Vis fiber, FP1500RET SMA, Thorlabs).
The fluorescence detection cell is enclosed in a light-tight box, which has a mirroring surface (reflecting tape) to maximize the collection efficiency of the fluorescence emission. Right in front of the collimating lens, a bandpass filter (FBH430-10, Thorlabs) from 420-440 nm is installed to remove the scattering of the excitation peak. The peak fluorescence emission light at 430 nm is measured using a spectrometer (QePro-UV-VIS, Ocean insight). The fluorescence signal was integrated at over a 10 nm window across the peak emission at 430 nm (425-435 nm). Analog data are collected using a multichannel voltage data logger (1216 series PicoLog, PICO Technologies). A raw spectrum of DFQ, measured with the QePro from Ocean Insight, is shown in Figure 9).

The liquid reservoirs, all tubing, the peristaltic pump, the spectrometer, and the flow cell are enclosed in a compartment inside the aluminum box that is insulated and the temperature is controlled by a thermoelectric cooler (PK 50, ELMEKO) and the corresponding control unit (TPC300, ELMEKO) with two thermistors to measure and regulate the temperature to minimize temperature-related changes in reaction rates (green box in Figure 17). Control of instrument components, as well as data acquisition, is performed using a LabVIEW (National Instruments) script, which sets the input parameters for the peristaltic pump, and monitors the liquid flow rates of the flow meters. A feedback maintains a constant flow at the specified set point. Furthermore, the LabVIEW sotfware collects auxiliary data (various temperatures, and potential errors).
All these components and devices are integrated into an aluminum box (60x60x40 cm) for better thermal stability and easy transport. A fixed position of the different components ensures improved instrument performance and stability, since movement of key components, such as the optical fibers, has a noticeable effect on the fluorescence signal. The vacuum pump is kept externally to minimize vibrations within the instrument. The waste reservoir is also kept externally to minimize the amount of liquid inside the OOPAAI in the event of a leak.

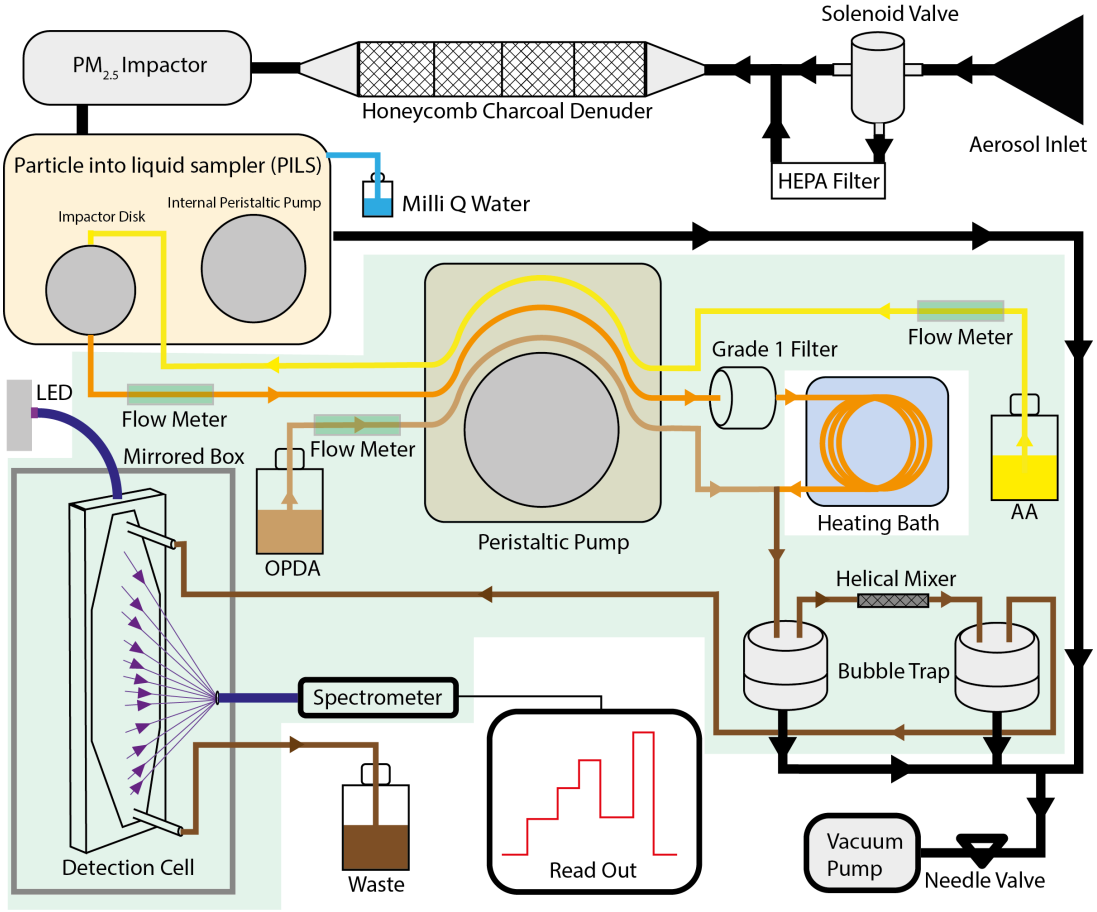

Figure 17: Schematic overview of the OOPAAI. The black lines illustrate air flows where air is pulled into the PILS via a denuder and an impactor. In the PILS the aerosol is collected with a wash flow containing ascorbic acid (yellow line) and pumped into a heating bath via a grade 1 filter (orange line). OPDA (light brown line) is then added, and the condensation reaction of DHA with OPDA to DFQ takes place (dark brown line). After a mixing piece and two bubble traps, the liquid is pumped into the detection cell, where DFQ is excited by an LED and the fluorescent emission is quantified by a spectrometer. All components are mounted in an aluminum, and the components with a light green background are in the thermos-controlled compartment of the OOPAAI.

2.3.2 Particle into Liquid Sampler (PILS)

In an online instrument, efficient transfer of particles from air flow to a continuous liquid flow is a key component in achieving a low LOD, because it is not possible to concentrate the analyte, i.e. the aerosol, over time in a continuous flow system. Therefore, it is crucial to obtain the highest possible ratio of air flow to liquid flow. The first home-built particle collector we used in the first prototype, published by Wragg et al., 2016, [95] operated with a 5 L/min air flow rate and 1 mL/min liquid flow rate.

This particle collector has the advantage of having a filter and therefore has a collection efficiency of almost 100% for water-soluble aerosols and is quite simple and inexpensive. However, the disadvantage is that it can operate only at a maximum air flow rate of 6 L/min and a liquid flow rate of approximately 0.8 mL/min. This limitation is due to the geometry of the particle collector. The spray is disrupted by higher air flow rates or lower liquid flow rates. We did quite some optimizations, but for a higher ratio a completely new design would need to be built. The now used PILS can go up to 16 L/min air flow and down to 0.06 mL/min liquid flow. This is a factor of 26 more aerosols per milliliter that can be extracted, and, in theory, therefore a 26-fold higher sensitivity. Although the disadvantage of pushing the PILS to its limits is that the collection efficiency is not 100% anymore like in the home-built particle collector. The PILS collection efficiency is described in more detail in Chapter 3.

We modified and improved the PILS for our purpose. We changed the wash flow in the PILS by not operating it with the internal peristaltic pump but with an external peristaltic pump (Ismatec™ REGLO Peristaltic Pump, Fischer Scientific) that can adjust flows for each channel independently. Furthermore, the internal bubble trap was removed from the PILS and replaced with two external ones. External bubble traps are placed after mixing with the OPDA contributes to better mixing. To maximize and stabilize the air flow rate to 16 L/min the internal orifice was enlarged and an additional needle valve was added after the pump. With this needle valve, the exact flow could be adjusted and regulated if at the inlet of the PILS a pressure difference occurred.
In the condensation chamber of the PILS the particles grow by supersaturated water vapor before they reach the impaction plate. Although steam is generated around 100 °C, the measured temperature in the condensation chamber, even close (1 cm) to the tip of the heat generator, is only between 35 °Cand 40 °C. Therefore, it is unlikely that the concentrations of OP-active aerosol components will be significantly affected within the PILS.
The extraction efficiency of the PILS was determined by comparing the AA oxidation of aerosols measured directly with the PILS (normal setup as described in Figure 17) and aerosols simultaneously collected on a filter (assuming 100% particle collection efficiency on the filter), which was then extracted and the AA oxidation quantified using the fluorescence detection setup in the OOPAAI. Taking the differences of these two analyzes, the collection efficiency of the PILS

operated under the conditions described here (i.e., very low liquid flow rates and further modifications) was calculated to be 20-25%.

2.3.3 Mixing

To form the fluorescent compound DFQ, AA and OPDA must undergo a condensation reaction where a good mixing of the two solutes is crucial. Mixing is a challenge when it comes to microfluidic systems. With between 60 µL and 150 µL and a diameter below a millimeter for the tubing for most parts of the system the Reynolds number is around 2 which is three orders of magnitude lower than the threshold between laminar and turbulent flows and therefore clearly in the laminar flow regime. In a laminar flow regime, there are no turbulences, and hence no turbulent mixing can take place, only mixing by diffusion. Mixing by only diffusion is much slower and takes a very long time to reach completion. In Figure 18 it is shown in blue and red color what would happen if they were mixed without any mixing device. The red and blue stay on the side which they have entered the T-piece and mix not at all. Even after the bubble trap (in the bottom of Figure 18) with an internal volume of 540 µL the two liquids are still very poorly mixed (large loop from right lower corner to left lower corner in Figure 18A). Also, after 30 cm of the tubing, the blue and red color can still be distinguished. Even in the helical mixer, in the beginning blue and red strains can still be seen, although in the end the liquid is violet, so it can be assumed that the two phases are mixed well. In the final instrument as shown in Figure 17, smaller tubings were used, and therefore also a smaller version of the helical mixing piece. Furthermore, two bubble traps were installed, as well as two helical mixing pieces. With that setup we could ensure that the mixing was complete.

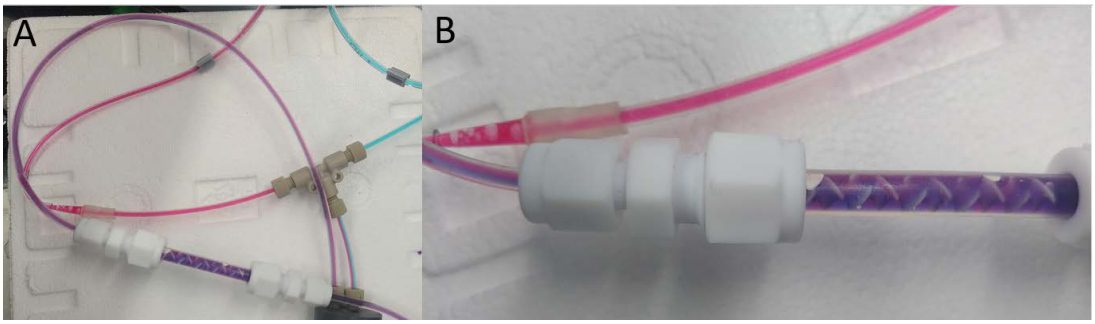

Figure 18: Mixing with a bubble trap and a helical mixing device. In (A), an overview of the blue and red colors that are pumped into a bubble trap and then into a mixing piece is shown. In (B), a zoom-in of the helical mixing piece is shown.

2.3.4 Flow Cell

The key component of an online instrument with a high time resolution and analytes at a very low concentration is an effective detection system. Therefore, we built a flow cell that allowed for a high fluorescence signal collection efficiency while still maintaining a low detection volume. This was necessary because if the volume is too large at low flow rates, the time resolution gets worse because of smear-out effects. To maximize the signal, it would be better to have a large volume because the fluorescence signal is proportional to the width of the probe, but for the time resolution, the smaller the volume of the probe, the better.
To determine the best configuration of this flow cell, many iterations were necessary. The first design used here was the same as described by Wragg et al., 2016 [95] and shows in Figure 19A. This design has multiple drawbacks, first of all, the fluorescence efficiency is not very good. Because of the design, only a small fraction of the light comes into contact with the liquid through the quartz rods. Furthermore, these quartz rods have only a diameter of 2.5 mm so only a small part of the liquid is illuminated.
For the next design, we tried a commercial cuvette (semi-micro cuvette, VWR) that is embedded in a black acetal block to block all the light, as shown in Figure 19B. The cuvette is modified with a whole at the bottom and a lid with another hole to have continuous flow through the cuvette. For this design, the efficiency was very good because there is a lot of liquid and a large volume, resulting in a high fluorescent signal. The advantage of high volume (3 mL) is unfortunately also the major drawback because the flow was not high enough to flush the cuvette at the given flow rates of 2 mL/min. The geometry of a rectangular flow cell leads to dead volumes in the corners, and the flow is present only in a chimney in the middle of the cuvette. This leads to various problems, as that the signal is not stable when randomly the dead volumes are transported into the flow stream due to turbulences or that there is a longer smear out effect.
To overcome these drawbacks, a completely new design was needed, in which the high illuminated area stayed the same, but the volume of the detector cell was reduced. This is also necessary because with the new particle in the liquid sampler, the flow is drastically reduced to 60 mL/min, which would further enhance the effect of dead volume. To achieve this, a commercially available flow-through cell (Hellma Analytics, Switzerland) with a height of 2 mm, a length of 40 mm, and a width of 10 mm was modified.

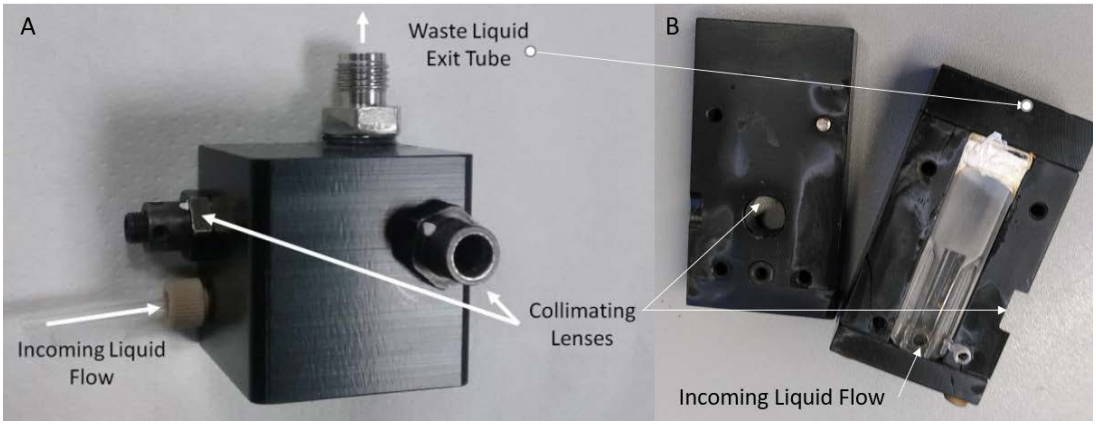

Figure 19: Old designs of the flow cell. In (A) the one used by Wragg et al., 2016 [95] and in (B) the semi-micrometer commercial cuvette in an acetal block similar to that used by Fuller et al., 2014[94]

The detection cell is a home-built unit where a commercial flow-through cell (137-2-40, HELLMA Analytics) is modified to a fluorescent detection cell. For that, all sides of the cells were polished to make them transparent. At the end of the cucette where the inlet and outlet are, the cuvette became narrower (see Figure 17). The fiber from the LED (UV-Vis fiber, FP1500ERT SubMiniature version A (SMA), Thorlabs) with a numerical aperture (NA) of 0.39 is in close contact with the polished short side and excites the solute. The fluorescence is then collected on the long side in a collimating lens (Ocean Insight) and focused on a 1500 µm (UV-Vis fiber, FP1500ERT SMA, NA 0.5 Thorlabs) fiber. The fibers have two different NA, because a higher NA has a higher angle where the light can enter the fiber and is therefore better to collect more light. But for the transmission of the LED it is not suitable to take a high NA fiber, because the transmission of high NA fibers gets worse in the low UV-VIS area.

First we thought that making the case around the cell out of white material would be useful to have a reflective surface to collect more photons. But the problem with a white plastic case is that there is background light. The white plastic does not shield the light 100% from stray light coming from the surrounding, leading to artifacts in the signal. However, this approach did not give a better signal-to-noise ratio. Next, we tried to mirror the inside of the flow cell and to reduce the total volume around the flow cell. Because the mirroring surface is not perfect, a lower volume around the flow cell increases the chance that the photon will enter the fiber and not get absorbed. The major problem with that approach is that the excitation light from the LED also gets reflected, resulting in a huge excitation peak in the spectrometer. To avoid this, a filter was installed

that removed all light of the emission wavelength and only allowed transmission of a 20 nm window for the emitted light from the fluorophor. The Stokes shift for DFQ is quite large, from the excitation at 365 nm and the emission at 430 nm which makes it relatively easy to block the excitation wavelength by applying a filter.

The cuvette is mounted vertically, and the inlet is on the bottom so that any bubbles in the cuvette would quickly travel to the outlet at the top end of the cuvette. The emission light is then analyzed with a spectrometer (QePro, UV-vis, Ocean Insight) where the peak at 430 nm is integrated over a 10 nm window.
In the end, we chose the current design because it had the best performance of all tested versions and is fairly simple. This flow cell design has the advantage that it has a good signal-to-noise ratio, thus making it suitable for low flow rates and weak fluorophors or very low concentrations of analytes. Furthermore, the flow cell is constructed out of quartz and is therefore very durable and chemically inert. The flow cell can also be conveniently placed on the instrument wall and easily removed for maintenance. The entire fluorescence detection cell is housed in a light-tight box, which has a mirroring surface to maximize the emission collection efficiency. Before the collimating lens, a bandwidth filter (FBH430-10, Thorlabs) is installed from 420 nm to 440 nm is installed to remove the scattering of the excitation peak.

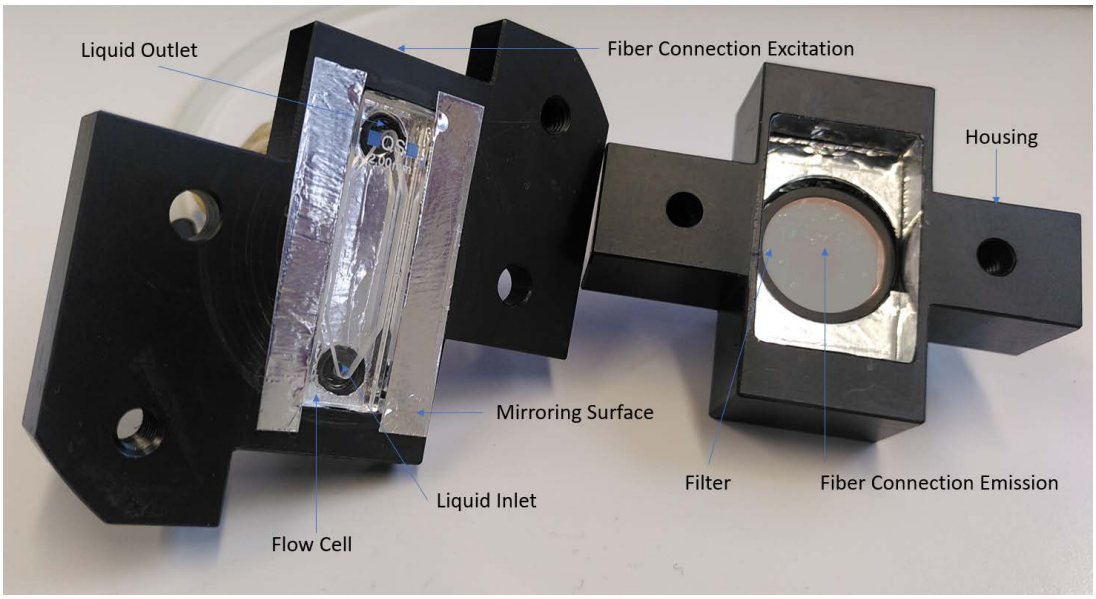

Figure 20: A picture of the final design of the flow cell. The flow cell is taken apart. The actual quartz flow cell can hardly be seen, because it is so transparent. The liquid connections are in the back and not shown here. The fiber connection for the emission is behind the filter and can not be seen in that picture.

In Figure 21 spectra of all different flow cells and mirror and filter combinations that were tested in the newly developed flow cell, as well as some old designs are shown. In (E) the spectra of a flow cell similar to that designed by Fuller et al., 2014 [94] is presented and in (F) the spectra of the block cuvette similar to that used by Wragg et al., 2016 [95] is shown. Both do not show significant differences between the blank and the measurement of 10 µM DHA. In (A), the spectrum of the newly designed flow cell is shown without any mirroring surface and without filter. The difference between the signal and the blank is not very big and the peak from the LED is almost an order of magnitude higher than the fluorescence peak. Therefore, we tried adding mirroring surfaces to the inside to enhance the fluorescence signal. However, as can be seen in (C), this makes it even worse because the LED peak is even larger because of more reflection. However, by removing the LED peak using a bandpass filter, this problem can be solved, as shown in (B). In (D), the spectrum without mirror but with a band-pass filter is shown. This configuration would also be good, but would have half of the signal as in (B).

We also performed some modeling of what the fluorescent intensity might look like and how much fluorescence we can expect to collect. The modeling was done with a round design because we first tried to build a round flow cell where we could also implement lenses to collect more efficiently the light onto the inlet of the fiber. This approach was not successful because we lost more light by the larger geometry and the not perfect reflectance than we gained with the lenses. Therefore, in the end, we decided to keep the flow cell as shown in Figure 20. However, simulations were performed for a flow cell that was a round iteration as shown in Figure 22, but we assume that is should not make a big difference. 1 million rays were simulated from the light source that was placed in the simulation inside the channel where the fiber was connected to the flow cell. In Figure 23 the area is defined where the simulated rays are analyzed and at what angle they impact on that plane.

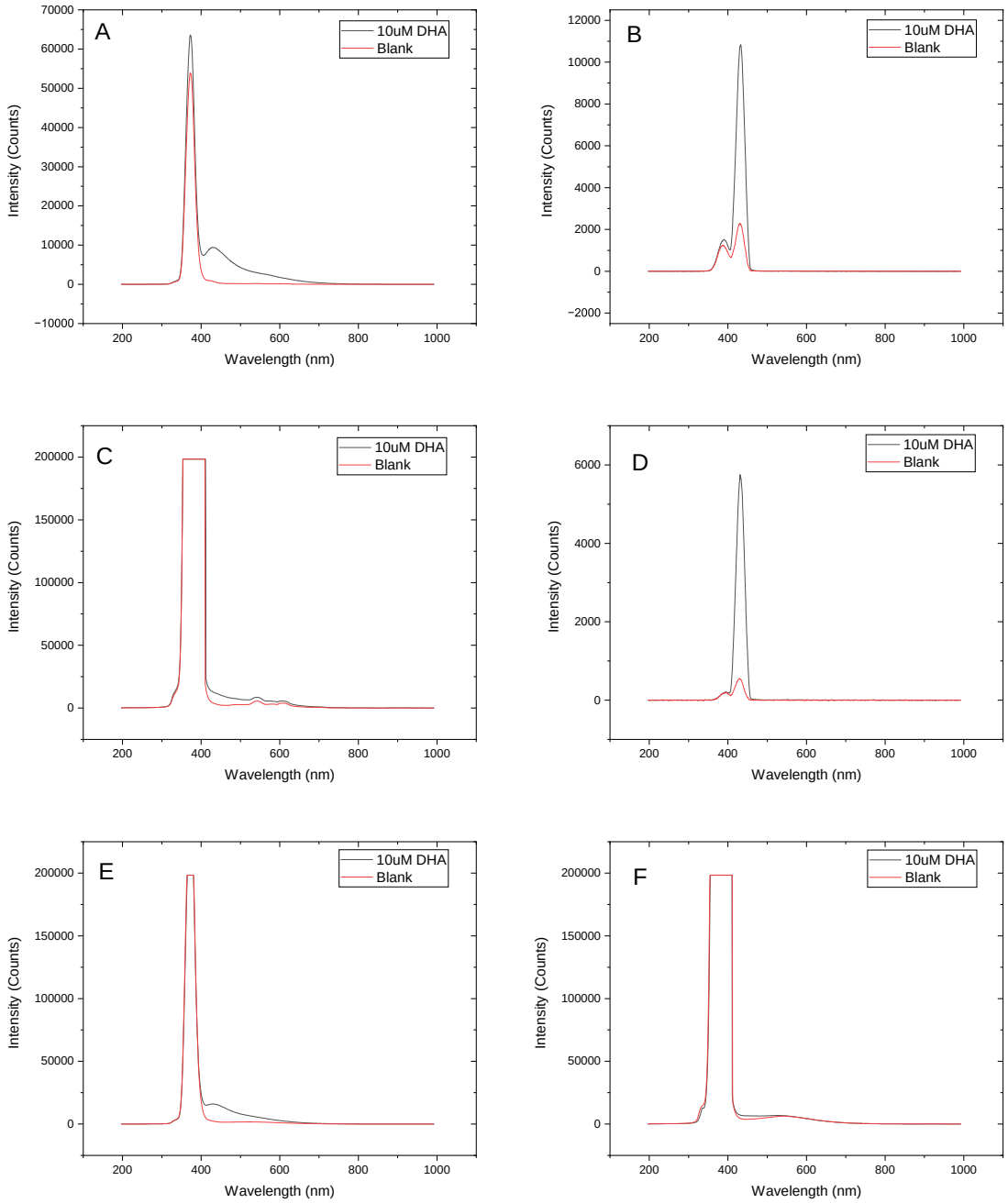

Figure 21: (A) Without a mirrored inside and without a filter. (B) The currently used design of a home-built flow cell, where there is a band pass filter in the flow cell and the inside of the flow cell is mirrored. (C) With a mirrored interior but without a filter. (D) Without a mirror and with a filter. (E) Semi-micrometer commercial cuvette in an acetal block similar to that used by Fuller et al., 2014[94], (F) Block cuvette similar to that used by Wragg et al., 2016[95]

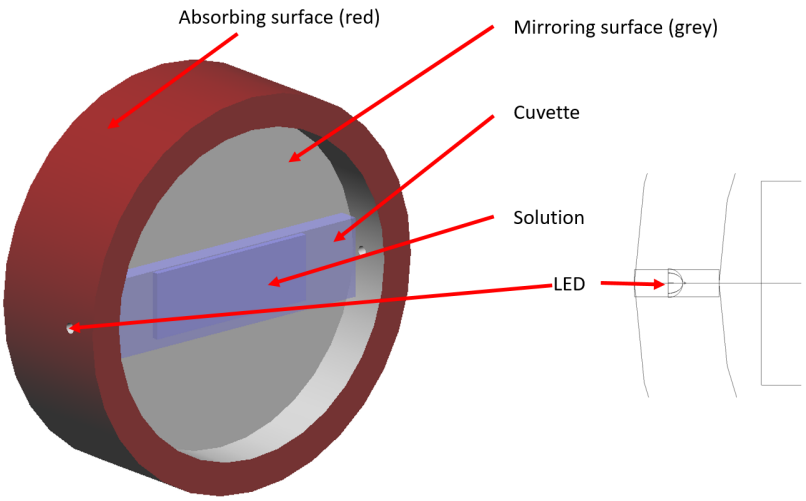

Figure 22: The 3D model used for the modeling. On the right side is a sketch of how the light source was placed for the model.

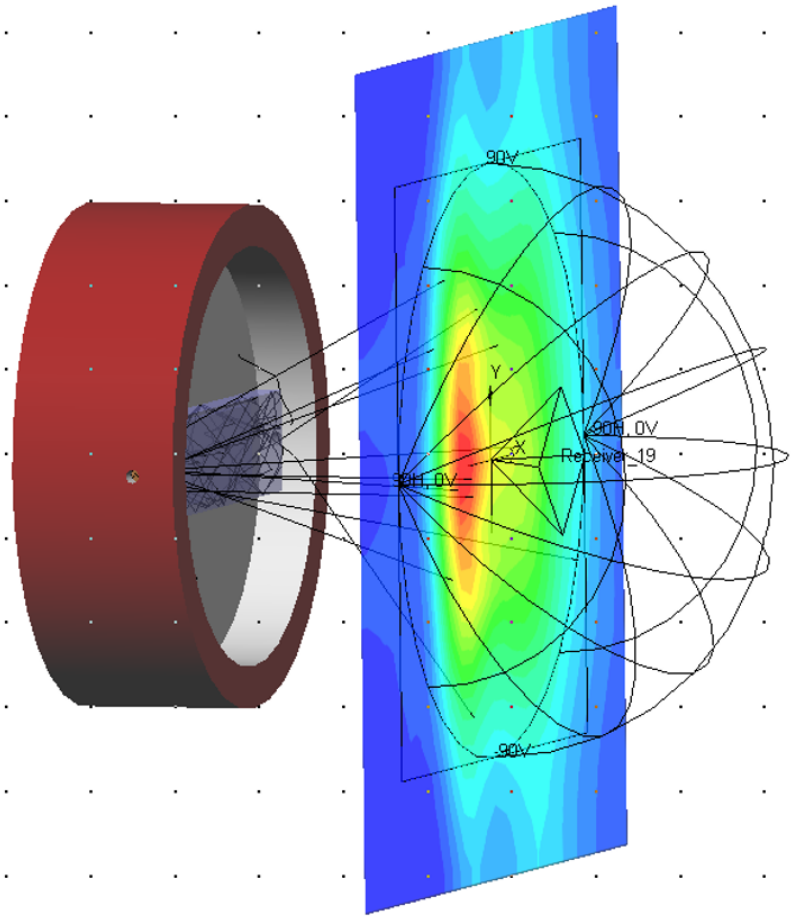

Figure 23: The theoretical mesh that simulated the receiver area and the angle distribution for all of the modeled rays. The more red an area is, the higher is the intensity.

In Figure 24A the intensity of the simulated rays is shown. It is symmetrical in the y-axis, but shifted towards the side where the fiber from the LED is connected to the flow cell. Also in Figure 24B most of the light comes from an angle toward the light source. In the middle where the collection efficiency is the highest, there is a high intensity but not too many rays that come straight to the fiber. With an NA of 0.5 the acceptance angle is 60° and therefore everything outside this angle will not enter the fiber to the detector.
It would be best to add the fiber angled and a little more to where the LED is. Unfortunately, this was difficult to achieve from a mechanical point of view. The bandpass filter had to be mounted in the flow cell cover, so in the end (also for the final design in Figure 20) the SMA connector was added without an angle and in the middle of the flow cell.

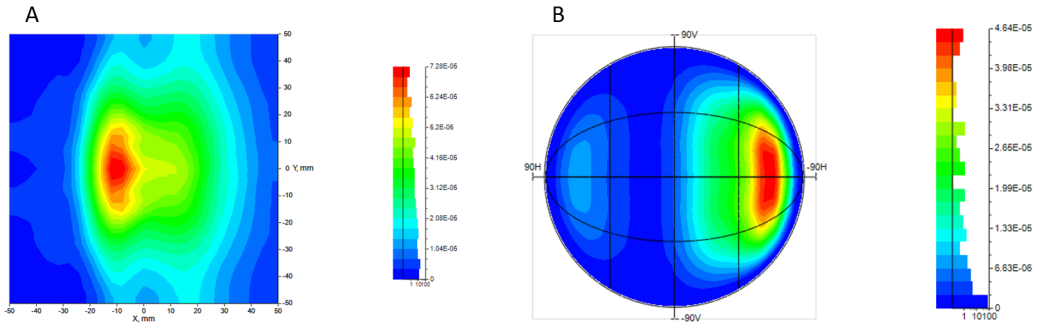

Figure 24: The result of the simulation. In (A) the irradiance by area is expressed in watts per square millimeter, and in (B) the radiance is expressed in watts per steradian.

2.3.5 Time Resolution

The smear out of the signal is a problem because it reduces the time resolution of the instrument. It occurs through diffusion of the solution, but mostly through friction on the wall. In Figure 25 a flow velocity schematic is shown, where the propagation of the front can be seen over time in a tubing. This effect describes why the signal is not a step function, but needs some time to stabilize.

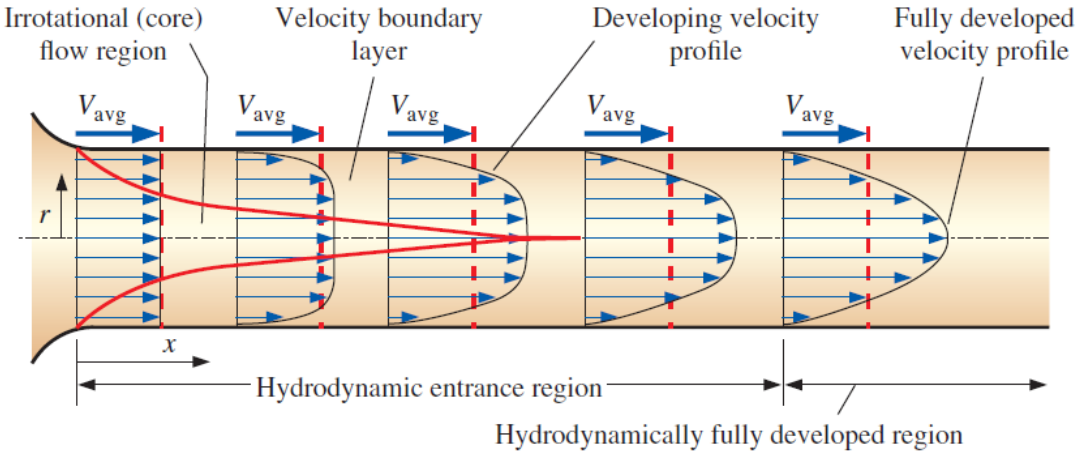

Figure 25: The propagation of a fluid front in a tube. Adapted from [152]

Unfortunately, it is not only the smear out in the tubing but also all other pieces like connectors, bubble trap, and flow cell. In Figure 26 a time laps of red dye entering the flow cell is shown. Only a small amount of red dye was added to a tube connected to the flow cell and pumped through the flow cell with 60 µL. It can be clearly seen that the dye enters in the middle the fastest and takes longer until the whole flow cell is red. The same is true for when the red dye is washed out again. Figure 26 shows very well why a change in the concentration of the analyte does not immediately change the signal. To increase the time resolution these smear out processes would need to be minimized. The system is in a laminar regime with a Reynolds number of around 2, so therefore turbulences can not be the problem. Another approach to reduce smear out would be to increase the flow rates, but they cannot be increased without reducing the concentration of aerosol in the liquid. The smear out is not only a problem, but it helps also to mix the two solutions. As described in Subsection 2.3.3 it is very important, but also difficult, to have good mixing. Unfortunately, high time resolution and good mixing are mutually exclusive. Therefore, it is important to find a good compromise between these two phenomena.

Figure 26: Red dye was pumped through the flow cell. A picture was taken every minute for 20 min. They are shown from top left to bottom right.

2.3.6 Spectrometer

To detect light intensities in fluorescence measurements, there are two classes of devices, both of which have their advantages and disadvantages. Photodiodes are typically smaller, less expensive, and relatively simple to use, making them a good choice for many applications. They can detect light fast in less than 1 µsec, and can detect a wide range of light, from ultraviolet to infrared and have a better signal-to-noise ratio, but have no spectral information. Spectrometers are more complex instruments than photodiodes and are therefore more expensive. They can measure light intensity but also give spectral information. Spectrometers have a longer response time than photodiodes, which can be an issue when measuring fast-changing light sources.

In the first iteration of the OOPAAI, we tried to use a photodiode because it is cheaper and has a better signal-to-noise ratio. During further development, we faced many challenges with the assay and its behavior, especially with metal salts (see Subsection 2.2.9) when we tried to change the pH from acidic to neutral. Furthermore, with the first iteration of the flow cell, we had problems with laminar flow and dead volumes. Without spectral information, it is very difficult to identify such problems. Therefore, we switched to a spectrometer to have additional spectral information. Having spectral information also helped a lot with all kinds of other problems, so in the end we decided to keep the spectrometer also because in the process of improving the sensitivity, we bought an expensive, better model that is better than the cheap photodiode we were using before. If the instrument is not further developed and there is not too much troubleshooting to be done, then it would be possible to switch back to a photodiode (see Section 2.8).

2.3.7 Automation

The first prototype of the instrument was only the assay with a very minimalist benchtop setup where everything had to be done manually. After several development steps it is now an instrument that can be operated autonomously without too much prior knowledge or technical skills. The software is written in LabVIEW and controls all data acquisition. It integrates the fluorescent peak and logs various other parameters like temperature and flows. In Figure 27 the interface of the software is shown. When starting the OOPAAI the parameter in the initialization tab (Figure 27A) need to be set. In a second step, the measurement can be started by the tab shown in Figure 27B. In the main tab the OP signal can be seen, and in other tabs the raw spectrum, temperature, or the flows can be observed. All of these data is logged into a file that is constantly saved.

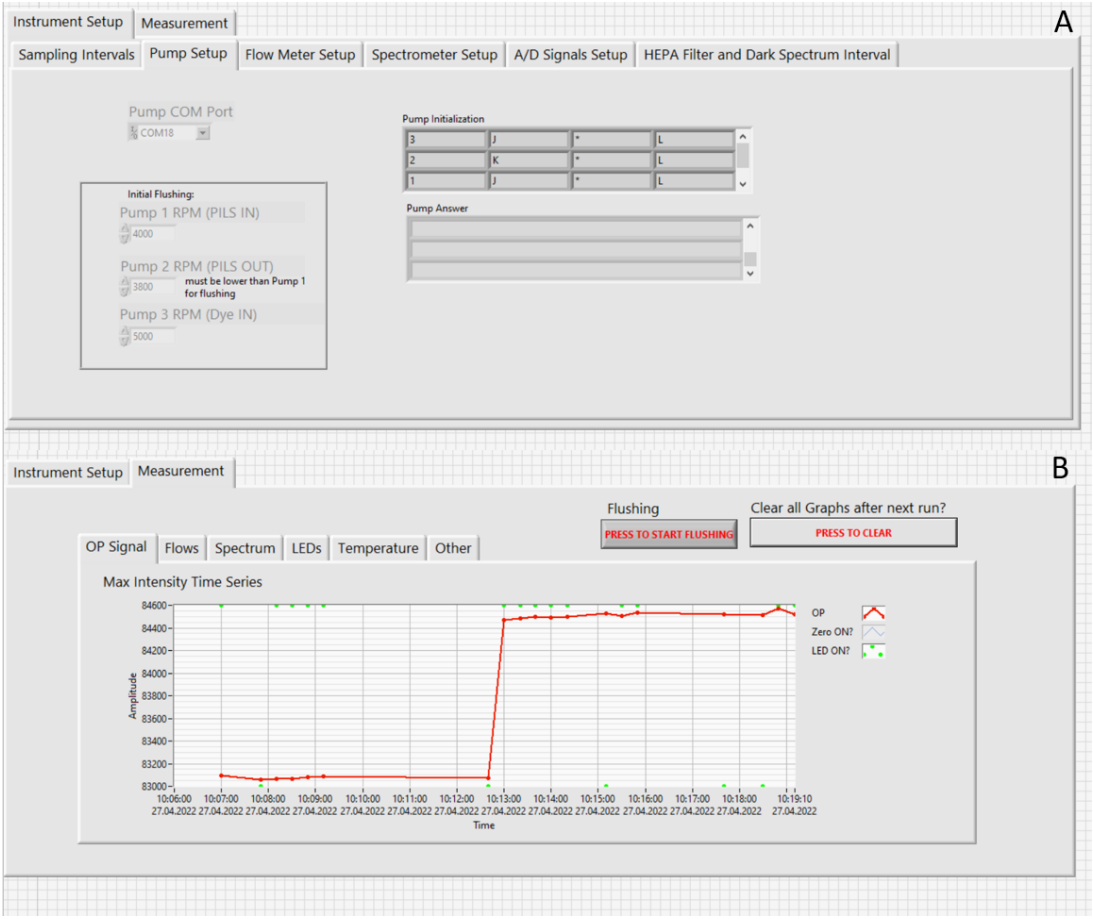

Figure 27: The LabVIEW interface, which consists of two main tabs: (A) The instrument setup where all the initializations can be done and (B) The measurement acquisition where all parameters can be looked at that are also saved, most importantly, the OP signal.

2.3.8 Absorption

Many offline assays that work with ascorbic acid use absorption as a detection method and measure the decay over time of ascorbic acid.[52, 79, 132, 153, 154] The assay measures AA consumption over time, and therefore self-absorption is not a problem because only relative changes are measured. For an online instrument with a very high time resolution, measuring different time points would be possible but just very expensive because basically all the hardware would need to be available multiple times. Another option would be to measure the self-absorption in alternation with the AA and the aerosol and correct it afterwards. But for that a high time resolution is not possible anymore and if there are fast changes in the composition that would lead to higher uncertainties. For ambient measurement that might not be a big problem, because changes are quite slow, but for lab experiments this approach would not work.

Although we were aware of these problems, we tried to build an online ascorbic acid absorption instrument to see if we could overcome these problems. However, in the end, we did not manage to build a working instrument based on absorption spectroscopy and therefore chose fluorescence as the detection method. In the next section, some results from the absorption approach are shown to show why a fully online absorption instrument is hard to achieve and to illustrate the challenges we faced when building it.

We slightly modified the fluorescence OOPAAI and added a liquid wave guide capillary cell (LWCC-3100, WPI) as a detection cell to measure absorption. The LWCC has the advantage of having a longer path than a conventional cuvette, which increases the sensitivity. AA was continuously pumped through the LWCC, with an inner diameter of 55 µm and a length of 1 m.

This internal LWCC tubing consists of a fused silica tube that is covered in a low-refractive index polymer to allow for total reflection. A pressure of approximately 0.1 bar is needed to maintain the optimal operation speed of 1 mL sample of the flow. Instead of a light-emitting diode (LED), a deuterium lamp (DH-mini, Ocean Optics) was used and coupled to the LWCC, by a 600 µm fiber. The same fiber was used to pair the LWCC to the spectrometer.

In Figure 28 a schematic of the setup used for the absorption measurements is shown. The rest of the instrument was the same as described in Figure 17. For the filter extract, the PILS was bypassed and the filter extract was pumped directly from a reservoir vial into the system as described in Subsection 2.3.1. AA solution was prepared in the same way as for the fluorescent approach, only

the concentration was adjusted to 1 µM. A detailed protocol can be found in the Master's Thesis of Benjamin Gfeller.[155]

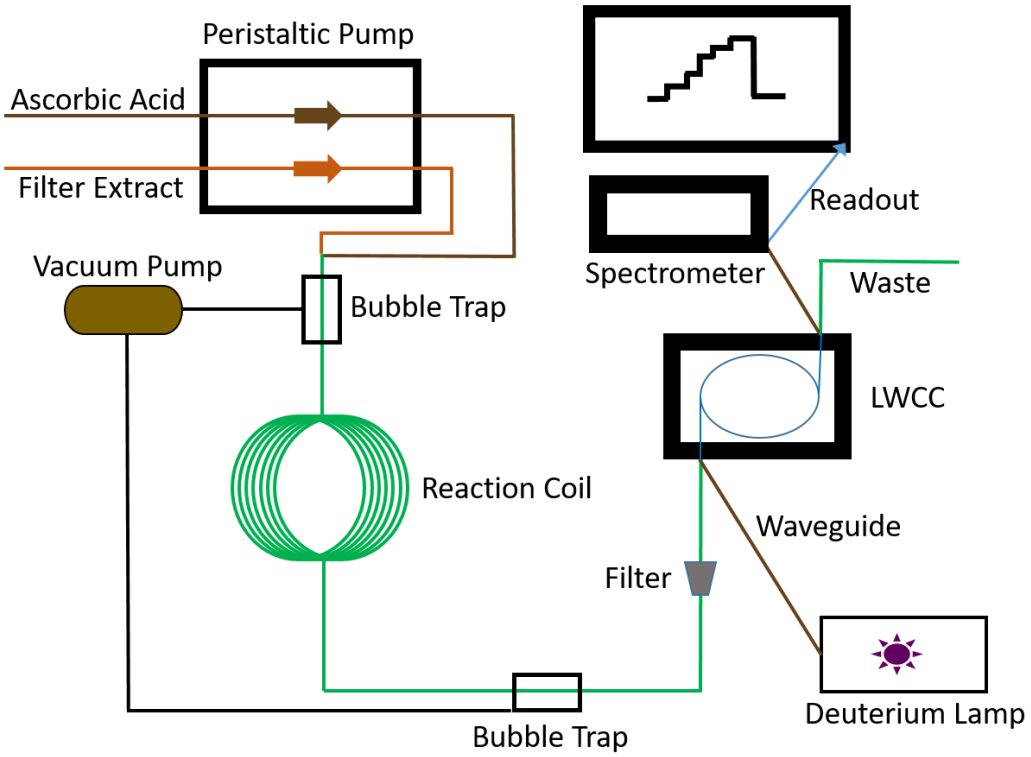

Figure 28: Schematic overview of the absorption measurement. AA and filter extract are pumped into a reaction coil, where bubbles are removed, and then the mixture is pumped into the LWCC, where an absorption measurement is performed.

Absorption of Filter Extracts

The peak wavelength of light where ascorbic acid absorbs light is around 265 nm. Unfortunately, many organic substances also exhibit significant UV absorption, which could interfere with the detection of ascorbic acid at 265 nm.[135, 156] To test the self-absorption of ambient aerosol, a filter extract from the APHH campaign (see [33] for details of the filter collection method) was diluted to four concentrations that correspond to realistic outdoor air pollution up to 30 µg/m^3. The absorption of the AA and filter extracts is measured at 265 nm in 1 m liquid LWCC where the extracts were continuously pumped through. As can be seen in Figure 29 the absorption shoulder of the aerosol contributes substantially to the overall absorption of ascorbic acid. Therefore, measuring both at the same time is impossible without measuring the self-absorption of the aerosol itself first and then subtracting it, and thus it is not practical to design an instrument that

can continuously measure online UV absorption spectra of AA because of the significant self-absorption characteristics of numerous organic chemicals.

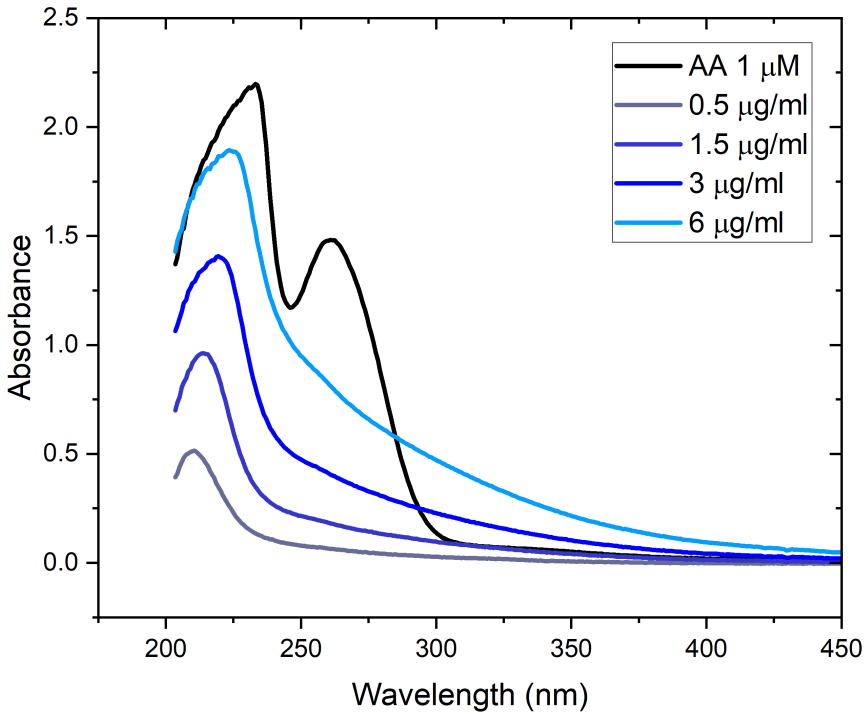

Figure 29: Absorption of AA and filter extract with different concentrations in the ambient range. The black line represents the absorption of pure AA, and all the blue lines are the absorption of pure filter extract without AA.

In Figure 30 the same four concentrations of aerosol are shown again: filter extract (yellow), filter exxtract with AA (blue), AA only (red), calculated difference between AA with filter extract and only filter extract (green). With only a small amount of aerosol such as 0.5 µg/mL (see Figure 30A) there is no big difference. This is good because the self-absorption is very low, but there is no difference between pure AA and AA with filter extract, so it is not possible to resolve that. With increasing concentrations of filter extracts (Figure 30B,C,D), the self absorption is higher and it is not possible to see a decrease in the concentration of AA due to the reaction of AA with components in the filter extract, because self-absorption increases the signal.

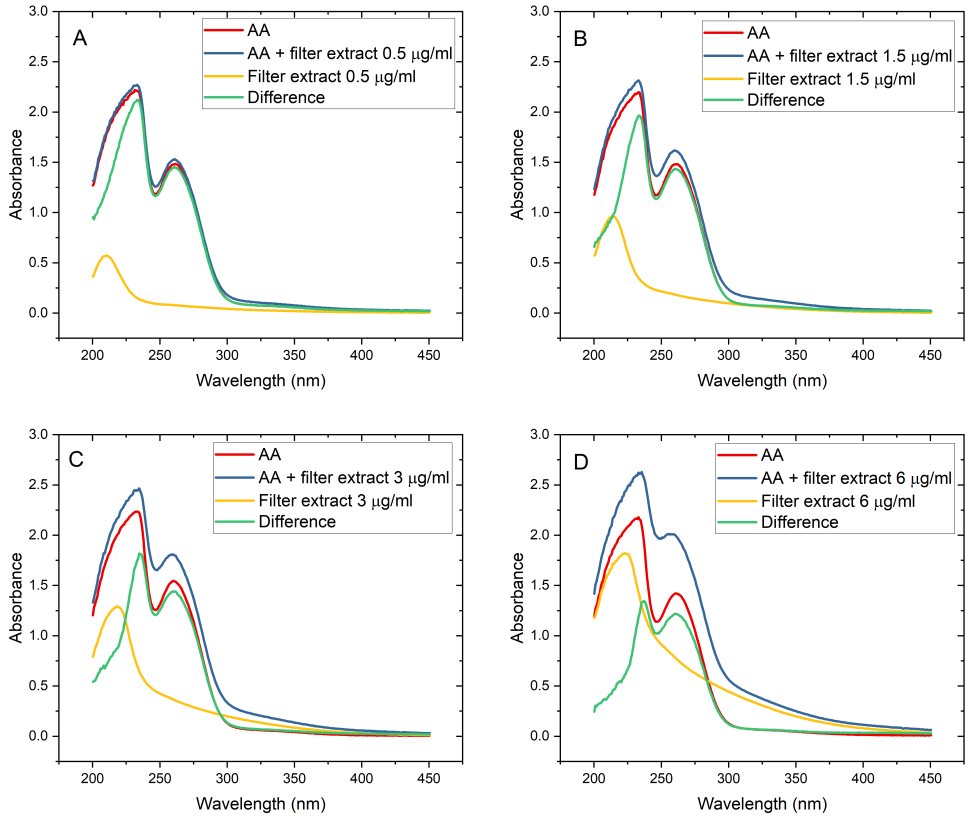

Figure 30: Absorption spectra of four different concentrations of aerosol extract. In red, AA only, in blue, AA mixed with filter extract, in yellow, only filter extract, and in green, the calculated difference between AA plus filter extract and filter extract only is shown. In (A) a filter extract of 0.5 µg/mL is shown, in (B) for 1 µg/mL, in (C) for 3 µg/mL and in (D) for 6 µg/mL.

Note that the absorption in all measurements shown here is high. An absorption of two or more is no longer considered to be in the linear range for most spectrometers, although this value varies with different setups. Because we used a LWCC the sensitivity is very good, but the dynamic range unfortunately is very low. The absorption setup was calibrated with ascorbic acid alone, and with the addition of aerosol, the absorption was even higher. With the LWCC, it is already difficult not to block too much light, because the 1 m long pathway makes the dynamic range very small. However, we used this because it improves the sensitivity compared to standard absorption setups. But it was practically difficult to measure in the dynamic range with unknown compounds, and therefore, we sometimes were above the linear range. We are aware that this is not optimal, but it allows anyways to illustrate the differences, although it might not be in the linear range

anymore. For proper measurements, this would need to be redone with lower absorption values, so that all measurements would be linear over the whole range. Despite the measurement are on the upper limit of what is recommended for absorption, the measurements are still linear. In Figure 31 the absorption at 265 nm of the different filter concentrations are plotted after they have been subtracted from their self-absorption (green line in Figure 30). With this subtraction method, the linear fit gives an adjusted R^2 of 0.99. As shown in Figure 31 With these data, it is nicely shown that the method itself is working, but only for offline measurements, where discreet values are measured by filter collection, and self-absorption is measured separately and subtracted. For an online instrument, this would theoretically be possible but would be more complex and more expensive to achieve. With a fluorescent approach, there are no problems of self-absorption, because the fluorescence is very specific and the aerosol interacts only with the detection by scattering of the LED peak, which can be easily removed by an optical bandpass filter.

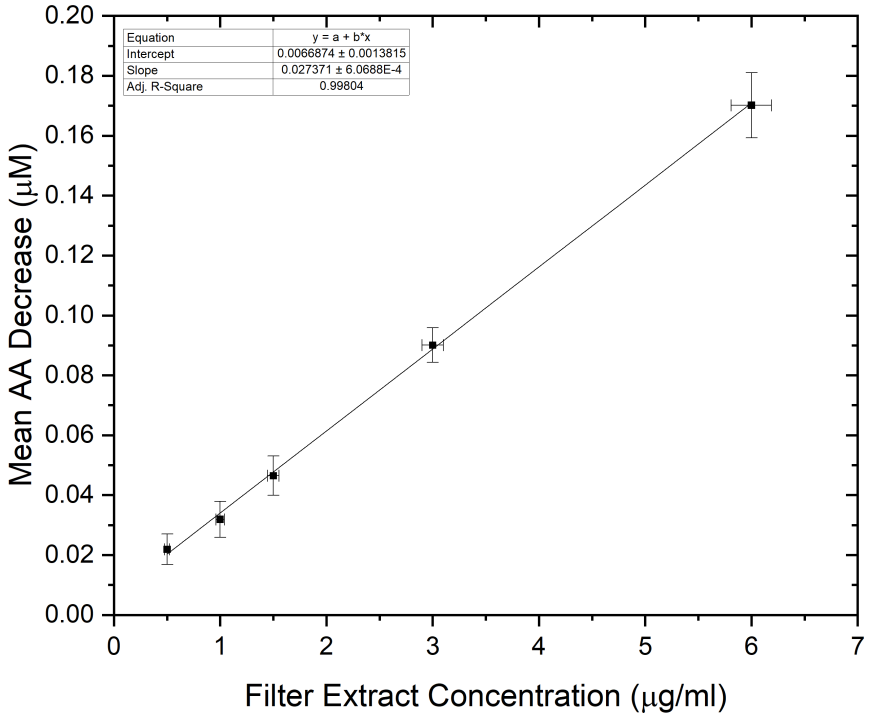

Figure 31: Linear fit of the data shown in Figure 30 with an additional measurement.

Ambient Absorption Measurements

The experiments shown in Figure 29, Figure 30 and Figure 31 are carried out with filters that were collected and then extracted. In Figure 32 a time trace of ambient data measured with the PILS is shown.

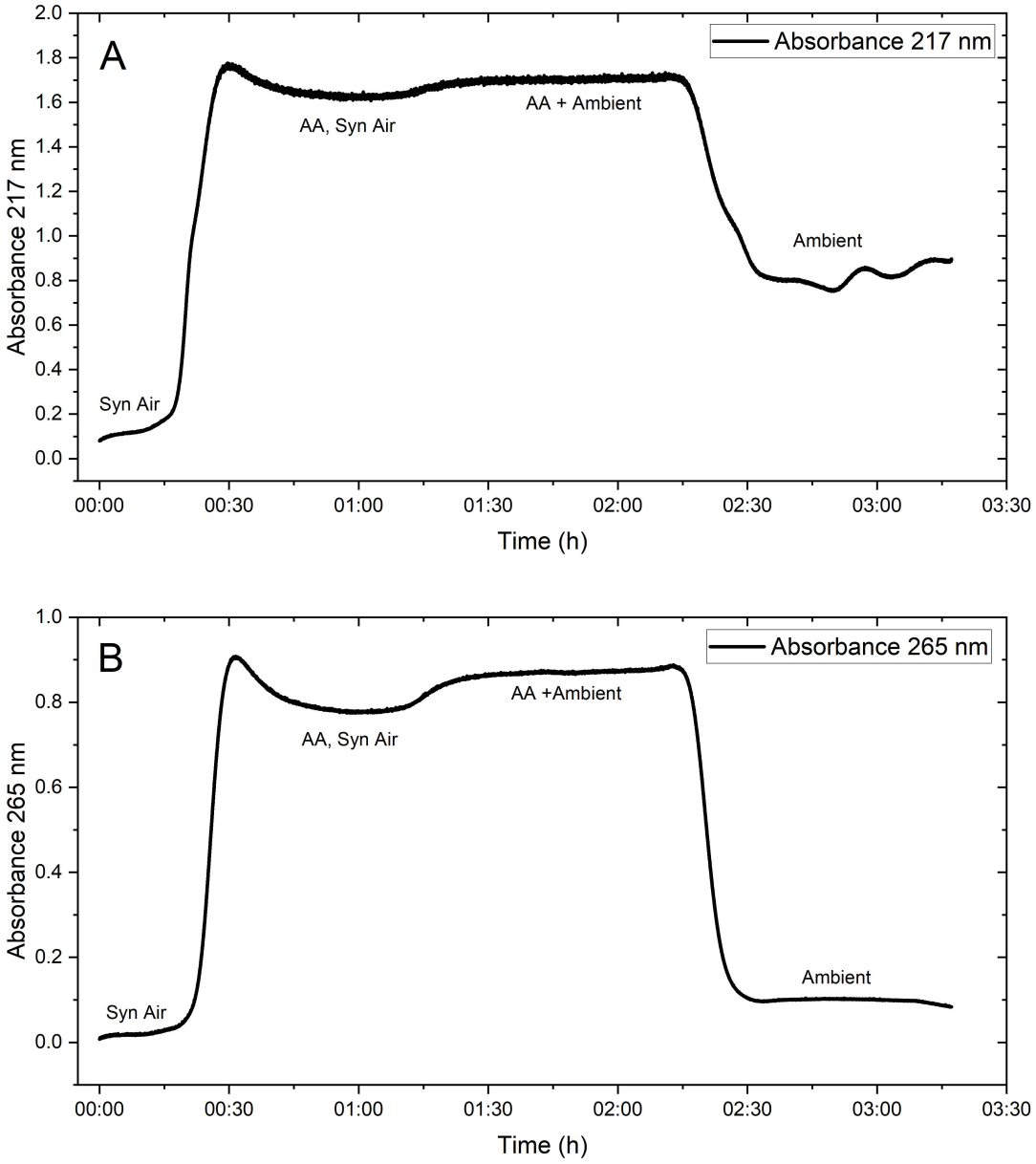

Figure 32: Absorption measured at 217 nm (A) to show the self-absorption of the ambient aerosol and at 265 nm (B) to measure the absorption of AA. In the time trace first, the back ground is measured with only synthetic air, then only AA, after that the actual measurement with AA and ambient aerosol is measured, and in the end only ambient aerosol.

For that, the outflow of the PILS was connected to the LWCC to continuously measure the ambient aerosol. In Figure 32A the time trace of 217 nm is shown for the self-absorption peak, while in Figure 32B the absorption of AA at 265 nm is shown. With ambient aerosol there is almost no difference that can be quantified between AA and AA plus ambient aerosol as a result of the high self-absorption. The difference from AA only to AA plus ambient at 265 nm minus the difference from AA only to AA plus ambient at 217 nm is not above the standard deviation from the time trace. Therefore it is not possible to measure with that absorption setup even if we would

2.4 Instrument Calibration

In this section, all calibration experimenters obtained with OOPAAI are shown. Excluded are results that are obtained during campaigns and, therefore, are presented in other chapters. Because until the end, the instrument was under development to improve certain parts, most of the results shown in this section were not measured with the final instrument. For results that are not measured with the final instrument, a brief note is given to explain what was different from the final version of the instrument presented in Figure 17 and described in Section 2.3. More experiments were conducted, but most of them were to troubleshoot the OOPAAI, so they are described in Appendix C where different problems that can occur and solutions are discussed. Calibrating a novel instrument is crucial to show that the instrument actually works and that the response is linear over the range of interest. Several different calibrations were performed during the development of the OOPAAI with various different compounds to measure the various responses of the OOPAAI. In this section, calibrations are shown in increasing chemical complexity to show the capability of the OOPAAI to measure different compounds.

2.4.1 Calibration of the OOPAAI with DHA

DHA is the first stable oxidation product (see Figure 8) of AA and the proxy for quantifying the oxidative potential of aerosols with the OOPAAI. Therefore, as a first step, it needed to determine how many counts in the spectrometer correspond to how much DHA. A calibration curve with DHA standards must be performed. A solution containing a known amount of DHA was added to the PILS instead of ascorbic acid, and synthetic air without particles was run through the PILS at the same time to avoid changing the setup. The fluorescence signal of the solution

is detected without altering the rest of the setup. The benefits of this calibration technique are that it requires little modification to the instrument setup while preserving a simple, reliable, and quick response system, making it possible to perform this calibration even when the OOPAAI is deployed in the field. To calibrate the device, we pumped liquids with increasingly higher concentrations of DHA through the PILS. In the calibration experiment depicted in Figure 33, nine solutions with DHA concentrations ranging from 0-100 µM were tested for approximately 20 minutes each. In Figure 33 the raw data is shown together with a linear fit (adjusted R-square of 0.999).

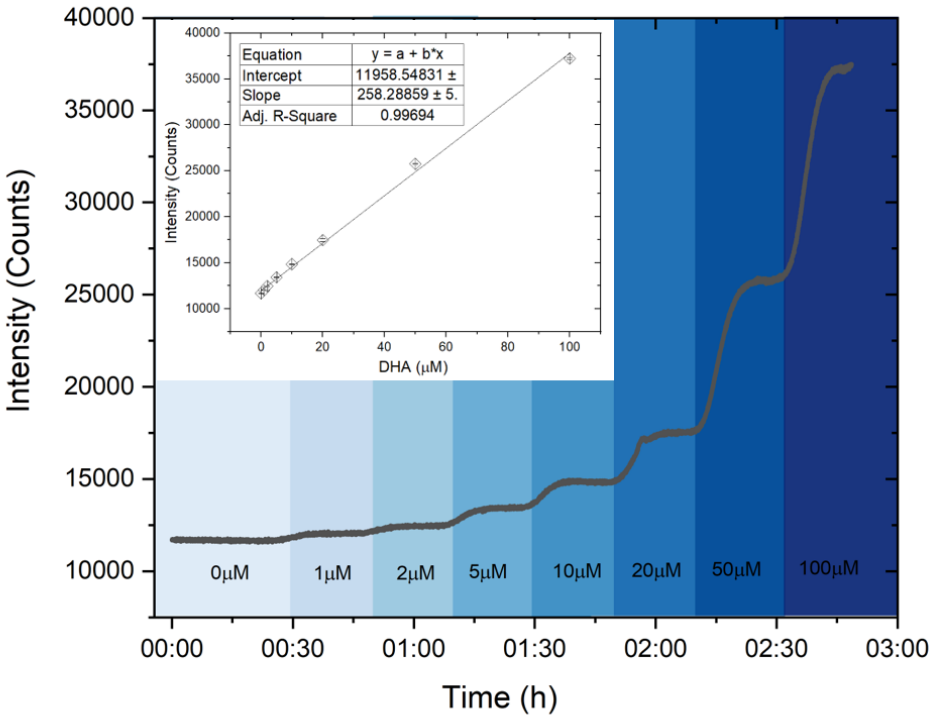

Figure 33: A calibration curve at pH 2 from 0-100 µM DHA. Each concentration of DHA was measured with the setup shown in Figure 17 . The calibration curve is linear (R^2 of 0.999) in the dynamic range of 0-100 µM as shown in the linear fit of the raw data in the upper left corner. Error bars are calculated from the standard deviation of each plateau, but in most cases so small that they are contained in the data point.

The DHA calibration experiments are performed at pH 2 although it would be better to do them under physiologically relevant conditions. Having the same conditions would be better, but because DHA is not stable at higher pH and room temperature (see Table 1)[157] it is better to perform the calibration at pH 2 because then the conditions are more reproducible. In Figure 34 there is

a calibration shown at pH 6.8 where the problem is clearly visible that arises when the calibration is performed at a higher pH. Each plateau has a slope over time because DHA sits in the vial while being pumped into the OOPAAI and degenerates over time. In actual measurements, this is less of a problem because DHA is continuously formed in the instrument and does not already sit as a solution in the vial from the beginning and during the duration of the measurement.

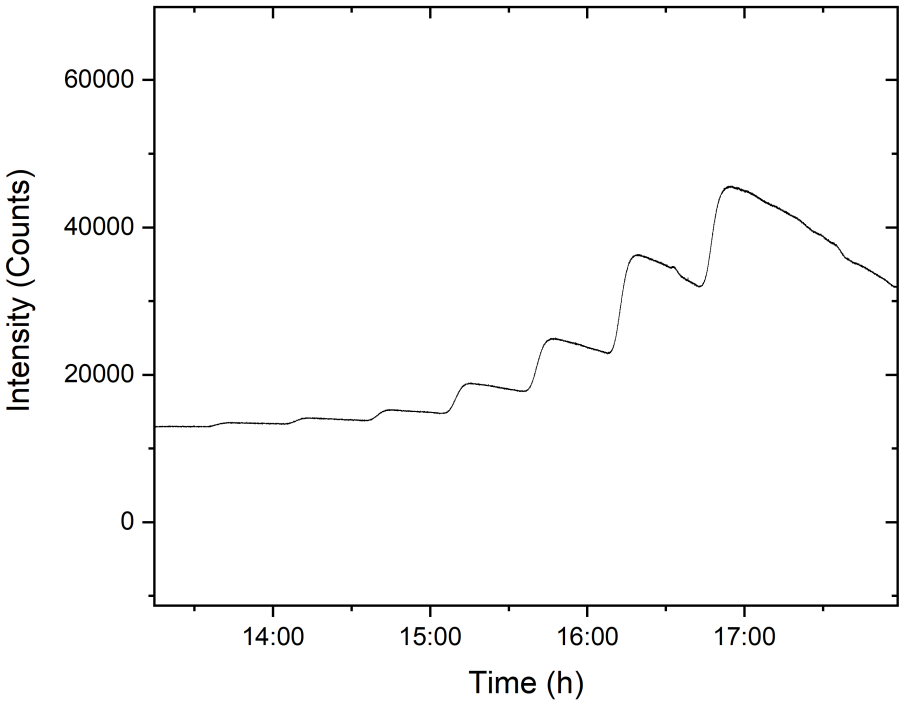

Figure 34: The same calibration (raw counts) as shown in Figure 33, but at pH 6.8 and continuously debubbled with nitrogen, indicating that a calibration at neutral pH is not favorable due to DHA decay in the calibration solutions.

Figure 34 illustrates the effect of increasing the temperature on the decay rate of DHA. The higher the concentration, the more negative the slope resulting from DHA degeneration. Before deciding to measure the calibration curve of DHA at pH 2, the calibration solutions were kept in the refrigerator because DHA degenerates faster at higher temperatures (see Table 1). So, at pH 7 and close to 0 °C the half-life time is 25 h which is also fine for calibration, but it is difficult to keep the solution constant at 0 °C. In the reservoir it is not a problem because the reservoir can be put on ice, but in the tubing the DHA warms up and at 25 °C the half-life time is only 45 min. When the solution is debubbled like in

Figure 34 the solution is heated faster and therefore the decay is even stronger. This is not only a problem because the error of each point becomes larger; it is also a problem for day-to-day variability. The variability between days was so high that the calibrations were highly dependent on the operator rather than the actual instrument. Therefore, we decided to do the calibration at pH 2 for better stability and repeatability. For most applications, relative differences of the OOPAAI results are more important, but absolute values could be calculated by taking into account these temperature-dependent losses.

Table 1: DHA stability with regard to temperature and pH. Data from Huelin et al., 1949 [157]

	0°C.	25°C.	40°C.	70°C.	100°C.
pH					
0	24 hr.	2 hr.	30 min.	6. min	1.5 min.
1	532 days	12 hr.	3 hr.	30 min.	7 min.
2.2	15 days	35 hr.	9 hr.	80 min.	17 min.
3	14 days	34 hr.	8 hr.	50 min.	8 min.
4	12 days	24 hr.	6 hr.	30 min.	3 min.
5	9 days	15 hr.	3 hr.	8 min.	1 min.
6	5 days	43i hr.	35 min.	2 min.	<1 min.
7	24 hr.	45 min.	6 min.	<1 min.	<1 min.

2.4.2 Calibrations with Aqueous Substances

After proving that the condensation reaction works in the instrument, the next step is to show that the oxidation steps of ascorbic acid or the ascorbate anion AH^- (see Figure 8) to DHA also work and are linear. To prove this, calibrations have been conducted with different substances. To test only the aqueous chemistry of OOPAAI, it had to be slightly modified. The PILS is bypassed, and the two liquid pumps that normally pump into and out of the PILS are connected with a T-piece. One pump adds ascorbic acid, while the other pump introduces the oxidative substance (i.e. metal salts or organic filter extract) to the system. After the T-piece, the combined flow passed through the cellulose filter and into the heating bath as described in Figure 17. With this setup, it is possible to introduce an aqueous solution into the system without making significant changes to the OOPAAI. This setup was also described by Campbell et al., 2019 [38] and all calibrations shown in this section were made with that instrument configuration. For the metal salts, the SOA extracted from the filters or the ambient filters was mixed with the AA before entering the heating bath.

Calibration with Metal Salts

AA is highly reactive to redox-active transition metals such as Fe and Cu [81] but also reacts with organic components present in secondary organic aerosols, but less efficiently than with metals.[158] However, in ambient aerosol particles, the mass concentration of organic compounds is often 1-2 orders of magnitude higher than that of redox-active metals [159, 160, 161], so despite the lower sensitivity of the AA assay towards organic constituents, they still have a large impact on the overall OP of the particles measured with AA, and therefore potentially on the oxidative stress that aerosols might generate in the lung.

To determine the sensitivity of the OOPAAI to metals, a calibration curve of different metals was performed. In Figure 36 the raw data from a three-point calibration for Cu(II) and Fe(III) are shown. In Figure 35 an analyzed calibration of Fe(II) is shown where the error bars represent the variability of each measured condition. The linearity with an adjusted R-square of 0.96 of this calibration at pH 6.8 is not as good as with other substances. Most likely, this is also due to the memory effects that metals have in the OOPAAI (see Subsection 2.2.9).

A proof of principle of a preliminary first iteration of the instrument, as published by Campbell et al., 2019, was using the ascorbic acid assay under acidic conditions at pH 2. Ascorbic acid reacts very differently with different metals, depending on the pH. In Figure 36 as an example, the difference of 2.5, 5 and 10 mM Cu(II) sulfate and Fe(III) sulfate under acidic conditions (pH 2) (A) and neutral conditions (pH 7) (B) is shown. Under acidic conditions, Cu(II) and Fe(III) have a very similar oxidative capacity to AA. The formed DHA concentration is very similar for all three concentrations tested and so is the slope (data not shown). Compared to neutral conditions, for Cu(II) the DHA formation is almost an order of magnitude higher than for Fe(III). Although for copper, the measured value might not be accurate because for some concentrations the signal is not plateauing. This effect is described in more detail in Subsection 2.2.9. For Fe(III), the response is lower at neutral pH than under acidic conditions. These two compounds show, as an example, that ascorbic acid reacts differently with different compounds depending on the pH. In Figure 10A the different speciations of Fe(III) at different pH's are shown, indicating that Fe(III) reacts differently when the pH changes. Therefore it is crucial to measure physiological relevant conditions, otherwise the toxicity of some compounds are under or overestimated.

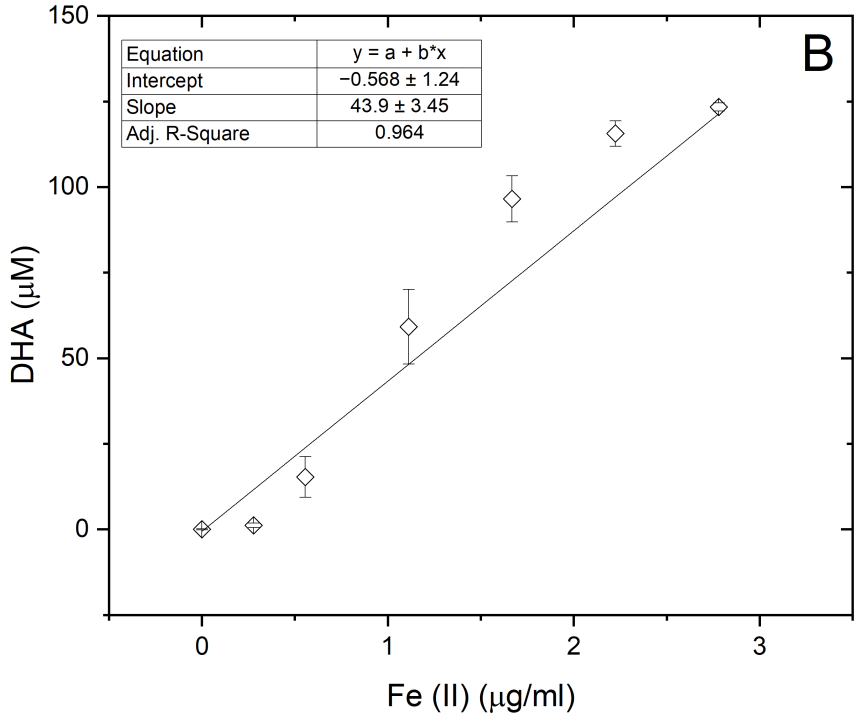

Figure 35: Fe(II) calibration at pH 6.8. Different concentrations of nebulized Fe(II)sulfate were measured and plotted against the resulting DHA concentration. The error bars represent the variability of each concentration measured over time.

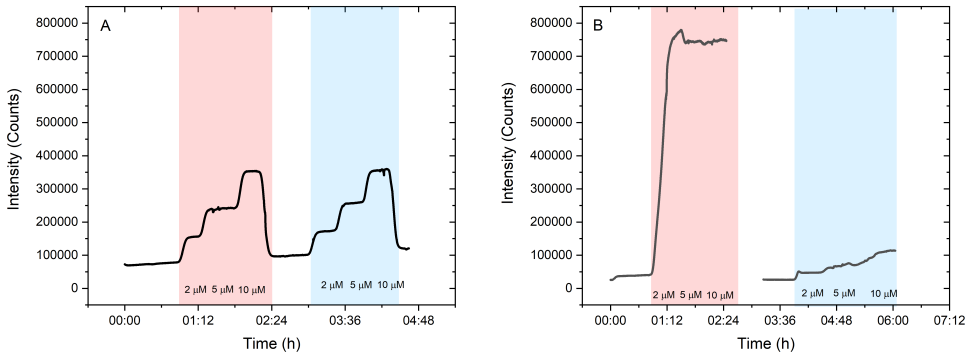

Figure 36: Different responses of Cu(II) and Fe(III) with different pH. In red is 1 µM Cu(II)sulfate in a pH 2 solution of 0.01 M HCl and in blue 1 µM Cu(II)sulfate in pH 7 in 20 mM HEPES

Calibration with SOA

A further characterization of the OOPAAI was performed by calibrating the instrument with an extracted secondary organic aerosol from a filter. As an

example, in Figure 37 a calibration of biogenic α-pinene is shown. With an adjusted R-square of 0.99 the linear response of the OOPAAI is very good.

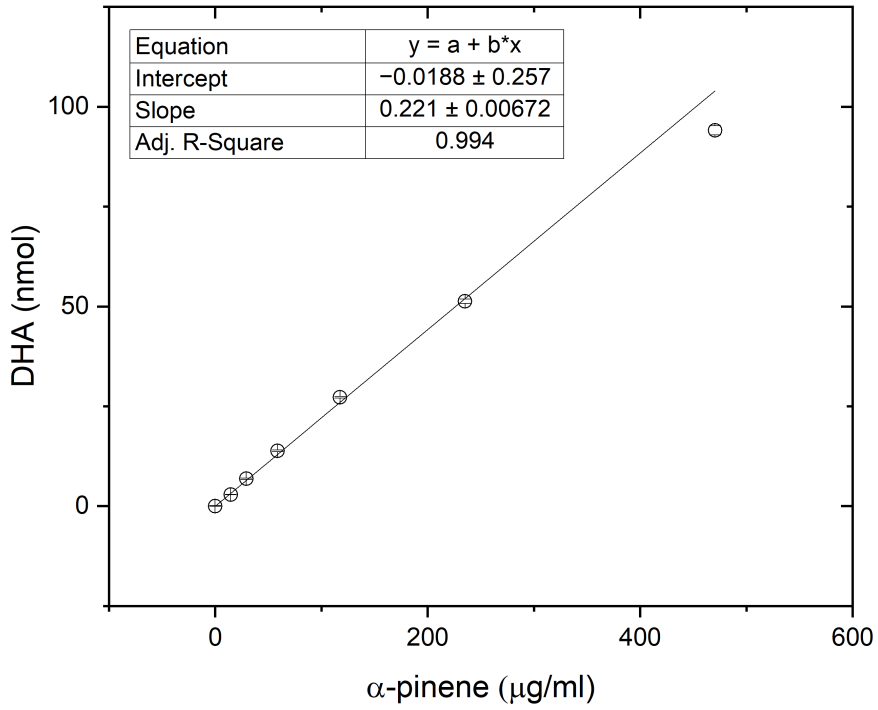

Figure 37: A series of dilutions of α-pinene SOA produced by the OCU and collected on a filter and extracted in water. Error bars represent the measurement variability of each concentration. Most error bars are so small that they are inside the data point.

Calibration with Filter Extract from Ambient Aerosol

The OOPAAI was also characterized with aqueous extracts of ambient aerosol samples collected on filters. This allowed us to evaluate the instrument performance with solutions of complex chemical composition that include a wide range of organic and inorganic components.

Figure 38 shows a series of dilutions of a filter collected in Beijing in 2016 during the Atmospheric Pollution and Human Health campaign (APHH campaign).[162, 163] For these measurements, 10 punches (diameter 1 cm) were extracted in 30 mL of ultra pure chelexed water by vortexing a 50 mL falcon tube for 3 min and then the filter suspension was filtrated with a filter (0.45 µm pore size) and collected in another falcon tube (detailed description of the filter extraction method in Chapter 3 or Campbell et al. 2019 [38]). A good linearity with an adjusted (R^2

of 0.99) is obtained, illustrating that the OOPAAI is also capable of measuring ambient samples and giving a linear relationship in the tested range.

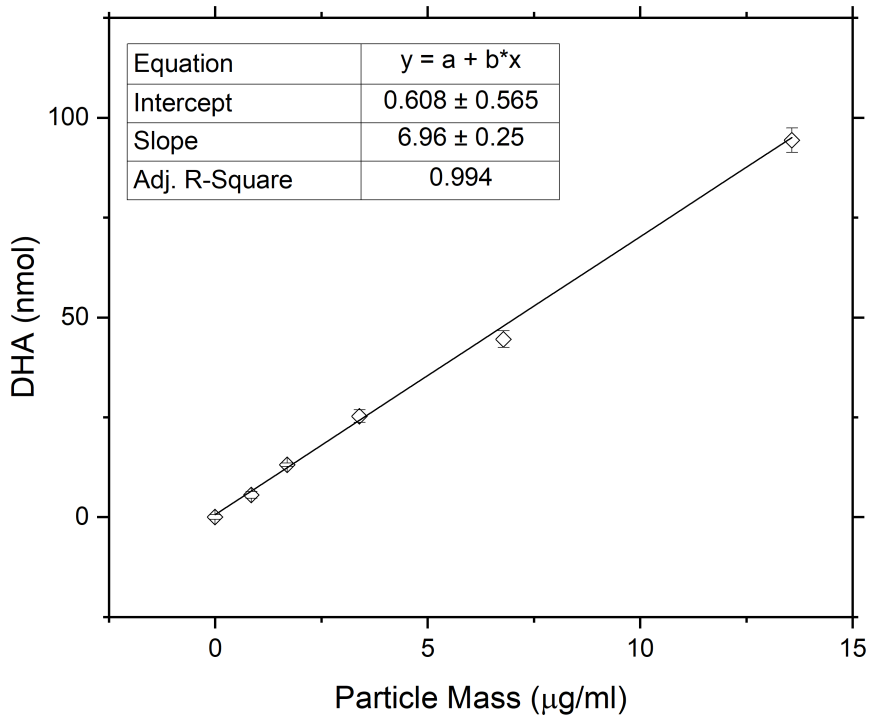

Figure 38: Calibration of the OOPAAI response using particle extracts from a filter collected in an urban location in Beijing, China. A clear linear relationship is obtained between the particle mass and the instrument signal.

2.4.3 Calibrations with Aerosol

In Subsection 2.4.2 the instrument's sensitivity to different substances in solution was shown. As a next step, the capability of the instrument to measure the actual aerosol should be discussed. In Figure 39 a calibration curve of β-pinene-SOA as an example for a biogenic aerosol and naphthalene-SOA as an example for an anthropogenic aerosol is shown. The aerosol generated by the OCU was diluted to generate particle concentrations in the range of around 50 to 1000 µg/m^3 and passed to a home-built charcoal denuder to remove ozone, unreacted VOC residues, and volatile oxidation products that could interfere with the analysis of the OOPAAI and then continuously measured with the OOPAAI. In parallel, a scanning mobility particle sizer (SMPS (3080), DMA (3081), CPC (3776), TSI) was operated. The SMPS was operated with a scan time of 105 and a SOA particle density of 1.4 g/m^3 was assumed.[164] In Figure 38 the OOPAAI

response is shown as a function of the SOA mass per cubic meter for the two types of SOA and illustrates the linear relationship over more than an order of magnitude of particle mass with a real aerosol, in contrast to the filter extract, which was used for the measurements shown in Figure 35 and Figure 37. The abscissa error in Figure 39 is the standard deviation of the variability in the production of the particle mass. The ordinate error represents the standard deviation of the variability of the OOPAAI signal. Naphthalene-SOA particles cause a significantly higher OOPAAI response (i.e. slope) than β-pinene-SOA, which has also been observed by others.[85, 165, 166] This could be because AA reacts very efficiently and catalytically with quinones, which are known oxidation products in naphthalene-SOA, compared with β-pinene-SOA where no quinones are present.[167, 168, 169]

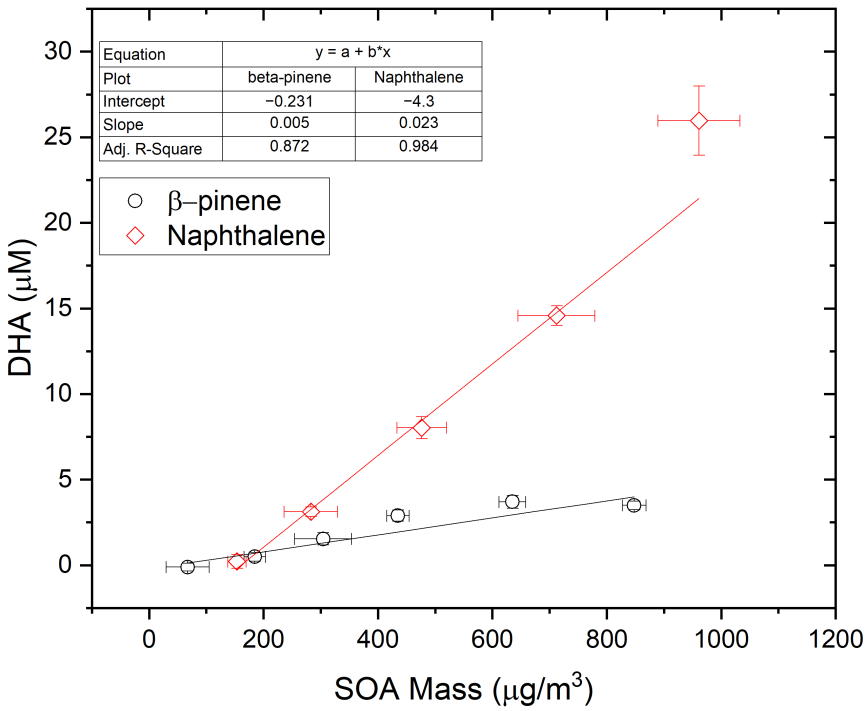

Figure 39: SOA was produced from an anthropogenic and biogenic precursor, respectively, at different mass concentrations using an organic coating unit (OCU, (Keller et al., 2022)).[170] The OOPAAI signal shows a linear response for both types of SOA as a function of particle mass with the anthropogenic SOA being much more reactive toward naphthalene.

2.5 Ambient Measurements

To quantify the response of the OOPAAI for ambient aerosol, some measurements were made with ambient aerosol measured in Basel, Switzerland. In Figure 40A on the left y-axis the signal of the OOPAAI over a couple of days normalized to the volume is shown and with the right y-axis the corresponding $PM_{2.5}$ is plotted. In Figure 40B the mass normalized OOPAAI values are shown in nanomol of DHA per microgram of aerosol. In Equation 6 the calculation of how to normalize the data is given. The first term normalizes the counts of the spectrometer given by the OOPAAI to DHA through the DHA calibration curve. The second term normalizes the OP signal for volume via the liquid and gas flow rate of the OOPAAI. The third term normalizes for the mass of the aerosol. In epidemiology, the OP normalized by volume is more common; then the division by aerosol mass (third term) can be left out. The hourly mean of the mass data of the $PM_{2.5}$ aerosol was measured with a Fidas 200 (PALAS) at Basel St. Johannsplatz by Luftqualität Nordwestschweiz.[171] This station is close to the measurement site where the OOPAAI was operated. In this work, normalized values of volume (per m^3 of air) and particle mass (per microgram of $PM_{2.5}$) values are considered. OP per volume is useful when dealing with exposure or epidemiological research, but OP per mass is likely to be a more informative indicator when investigating how chemical composition affects $PM_{2.5}$.[31]

$$OP\left(\frac{\mu\text{mol}\,DHA}{\mu\text{g Aerosol}}\right) = \frac{Counts - Intercept}{Slope} DHA\big(\mu\text{M}\big) \times \frac{Liquid\,Flow\,Rate\left(\frac{ml}{min}\right)}{Gas\,Flow\,Rate\left(\frac{m^3}{min}\right)} \times \frac{1}{Aerosol\,Mass\left(\frac{\mu g}{m^3}\right)} \tag{6}$$

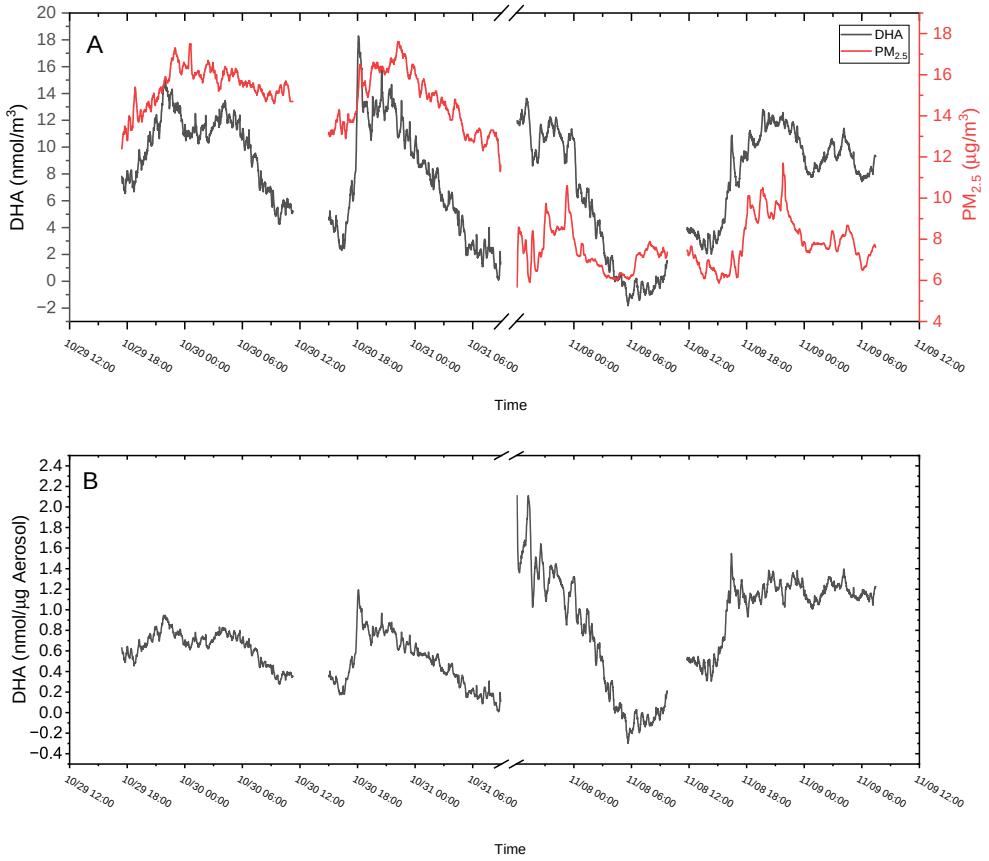

Figure 40: Ambient measurement in Basel. (A) On the left x-axis, DHA in micromol normalized to volume versus time and on the right x-axis $PM_{2.5}$. (B) Mass-normalized DHA values divided by $PM_{2.5}$ mass over time. All gaps in the data are either from changing the solutions or blank measurements.

The volume-normalized signal of the OOPAAI (see Figure 40A) has a very similar trend to the aerosol mass. With that we can show that the OOPAAI measures at a high time resolution the changes in the ambient. But when the signal is mass normalized (see Figure 40B) the data is not a straight horizontal line, which would be the case when the OP-active fraction in the particles would be constant over time. However, this is not the case in Figure 40B, and the trend can still be seen in the mass-normalized values. At very low concentrations, when the signal is close to zero, with variability and a not perfect blank correction, it can happen that the signal is below zero. This effect is amplified in the mass-normalized signal. Values below zero are below the detection limit should be excluded and are only shown here to discuss how this can happen during data analysis.
The hypothesis is that there is a fraction of aerosol that does not change the OP measurement or only slightly but does change the mass of the aerosol (e.g.

nitrates, sulfates) and another fraction that contributes more to the OP and less to the mass (e.g. transition metals or certain organic compounds). In laboratory experiments where we mixed SOA with relatively low reactivity and metals with high reactivity in a ratio of 10:1 together, the OP signal also did not correlate with the mass of the SOA because the metals were more driving the variability of the overall OP more (see Chapter 5) To better understand these compositional changes, more measurements would be required to obtain information on the composition of the aerosol.

2.6 Limit of Detection

The limits of the detection were calculated using the method of taking three times the standard deviation of the blank and are summarized in Table 2. The LODs are presented in µg/ml as well as in µg/m^3 to make them comparable to other measurements. For the experiments that were carried out without PILS the µg/m3 units were estimated with the assumed flow of the OOPAAI and vice versa for the ambient measurements. The detection limit for OOPAAI regarding DHA is 0.1 µg/mL, 0.03 µg/mL for Fe(II), 13 µg/mL for naphthalene SOA and 1.33 µg/mL for ambient SOA in Basel as shown in Table 2. Note that these values have to be treated with caution, because the measurements for the different experiments, and therefore the LOD calculations, were conducted at different stages in the development of the OOPAAI. Unfortunately, there was no time to re-do all the experiments in the end to get properly comparable numbers. But general trends are visible. Metal aerosols have an LOD almost two orders of magnitude lower than that of SOA. This finding was also seen by Campbell et al., 2019 where SOA reacts also less with the AA assay than with metal.[38]

Table 2: Summary of the Limits of Detection (LOD) calculation for DHA, Fe(II), and SOA filter extraction and lab-generated SOA aerosol and ambient particles measured in Basel.

sample	LOD (uM)	Error	LOD(ug/ml)	Error	LOD (ug/m^3)	Error
DHA	0.68	0.12	0.12	0.02	-	-
Fe(II) filter extract	0.10	0.06	0.03	0.02	0.11	0.06
alpha-pinen filter extract	-	-	3.15	0.61	11.83	2.31
Ambient aerosol filter Beijing	-	-	0.18	0.10	0.69	0.39
SOA betaP	-	-	48.49	18.57	181.82	69.62
SOA naph	-	-	12.85	6.34	48.18	23.79
Amient aerosol Basel	-	-	1.33	0.67	5.00	2.50

2.7 Conclusion

A novel automated online OP instrument has been designed, built, and thoroughly characterized. The OOPAAI can continuously quantify OP concentrations in different types of aerosols with a physiologically relevant AA assay (i.e., pH 6.8 and 37 °C) with a very high time resolution of about 5 min. The OP active components in the particles react within seconds after the particles enter the instrument, and thus very short-lived OP components (the majority of the total OP in SOA particles) are quantified, overcoming limitations of current offline-based measurement methods.
The instrument is portable, capable of running autonomously for about three days, thus is well suited for field campaigns and laboratory experiments. The OOPAAI is sensitive to a wide range of different compounds and aerosol types and can measure their OP over a wide range of environments, from ambient to laboratory-generated particles. Its detection limit for urban aerosol is around 5 µg/m^3 and a proof-of-principle deployment at an urban background site in Basel, Switzerland, demonstrated the highly dynamic nature of OP-active components in $PM_{2.5}$, which can only be captured with the fast response, high time resolution, and robust OP measurement facilitated by the OOPAAI.
This novel online instrument characterizes and accurately quantifies OP for the first time in a field study at high time resolution, which will be essential for an improved understanding of sources and formation processes of particle OP and to identify the link between particle OP and particle health effects.

2.8 Outlook and Future Application

The OOPAAI has been developed to a state in which it is possible to measure ambient aerosols autonomously for several days in fairly clean areas (>5 µg/m^3) with a high time resolution with a physiologically relevant assay. Despite these results, there are still many more things that could be improved and optimized for the OOPAAI.

First of all, the box housing is still a prototype and should be optimized. Most of the improvement ideas would refer to more optical things that would just enhance the appearance and make it a little less messy and more handy to operate. In Figure 41 an actual photo of the OOPAAI is shown which in reality looks a little less nice than the schematic described in Figure 17. Having a proper temperature-controlled compartment would be very useful, not only from

an appearance point of view, but also for a more stable operation. So far the insulation of this temperature controlled compartment is not very good, and the walls are prototypes. Because we still needed to change a lot of things and perform some troubleshooting to better understand the instrument, it was useful to have movable parts. But a better insulated compartment, if necessary also with a stronger temperature control unit, would help a lot in obtaining a more stable signal.

When the OOPAAI is operated in the lab, where the temperature change is usually very small, the small oscillation of the temperature control unit, as shown in Figure 11 is not a big problem. But when the ambient temperature changes a lot, as simulated in the data shown in Figure 71, then that could be a problem, especially when the aerosol concentration is very low and therefore the signal difference is very small. Further improvements in the temperature stability of the OOPAAI would definitely be the most important thing to achieve. With that improvement, it would not be limited to a temperature-stabilized laboratory environment to achieve very low LODs.

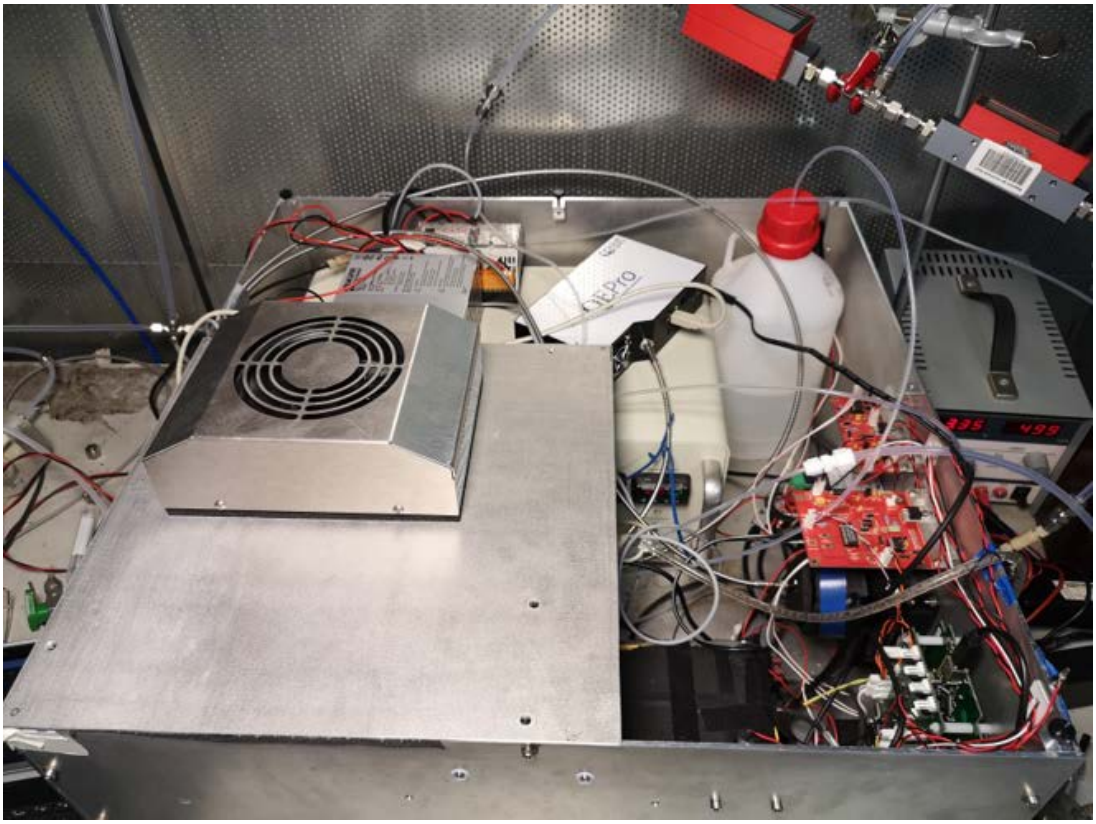

Figure 41: A picture of the OOPAAI in operation. In the left lower corner is the temperature-controlled compartment with the solutions and the flow cell.

Although we have spent quite some time optimizing the flow cell, it could still be further optimized. Together with the group of Prof. Ernest Weingartner of the Fachhochschule Nordwestschweiz, we also tried to build a flow cell in the form of a spiral (see Figure 42) to improve the sensitivity by an optimal use of the geometry and therefore the fluorescence counts. In the modeling phase, this project looked very promising. Although when actual building it there were a lot of practical and technical problems, such as building a perfect spiral with total internal reflection out of quartz and coupling the light into it. But if the detection limit should be lowered even further, then trying to build such a flow cell or just in general optimizing the flow cell would be something that should be done.

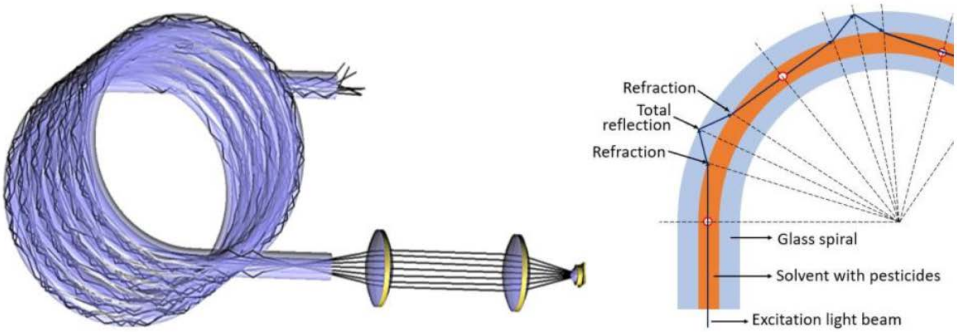

Figure 42: The spiral flow cell. On the left side an overview and on the right side a schematic of the total internal reflection. The light from the excitation should stay in the spiral and only the emitted fluorescence leaves the spiral and is then collected

Another important improvement is the software. Most of the data shown in that thesis were collected with the commercial software from the spectrometer and the commercial software for the flow and temperature sensors and not with the home-built all-operating LabView code. The instrument is running with the LabView code, but there are still some small problems, whereas for longer campaigns, it was just too risky, and therefore, the commercial software was preferred for all the single components. Although the OOPAAI is also working perfectly fine with the commercial software, it has the disadvantage that it is more work for data analysis because the data have different formats, are not synchronized, and have different time intervals. The LabView script would definitely be important if the instrument should also be operated by people outside the lab.

On the electronic side, the LED driver board needs to be improved. In the current version of the instrument, the LED is powered with an external power

supply, which works perfectly fine, but is unnecessary and requires more space. At the moment, the voltage and current of the LED driver board are too low, and therefore the fluorescent signal is lower and the detection limit is higher. Moreover, could the read-out of the PILS be integrated in the PICO logger, where all the rest of the data are logged. Then that could also be integrated in the LabView software.

In the liquid flow regime, there could also be some improvements. Most of the experiments were carried out at the flow rates described in Section 2.3 so with 60 µL of AA and 90 µL of OPDA. We tested some other ratios, but not in a very systematic way, and all of them were not better. In theory, the detection limit should be better if the OPDA flow is lower, because that is only a dilution of the DHA. But with a lower flow of the OPDA the mixing is worse and, therefore, the signal stability is also not as good. But if we could overcome this problem, then maybe with other flow rates a better result could be obtained. Furthermore, the change in flows also slightly alters the pH and residence time (when the tubing length is not adjusted), and therefore, the condensation reaction between DHA and OPDA is different and changes the readout.
We also tried to change the ratio between the flow that entered the PILS (60 µL) and the flow that was pumped out of the PILS (60 µL). The PILS adds via the aerosol that have been grown from the super saturated water vapor a couple of microliters to the flow at the impaction plate. Any difference in liquid flow that exceed the out flow is pumped into the waste. This dilution of the initial flow could be reduced by adding this difference to the flow that is pumping out of the PILS. So as an example the inlet of AA in the PILS could be 60 µL but the outlet flow could be 80 µL, because the water vapor adds 20 µL inside of the PILS. The problem with this approach is that the amount that the PILS adds to the impaction plate varies, depending on the humidity of the air and the number of particles in the aerosol (more particles, more nucleation possibilities for water vapor). We tried to enhanced the output flow to 80 µL and also increased the concentration of the initial AA by that factor to have the same concentration of AA, but unfortunately, the stability was worse. We have not really figured out why this is the case, so it would be good to investigate this a little bit more and investigate different flows in a systematic experiment.
In theory, this matrix between the concentration of OPDA, the flow speeds, the mixing, the PILS dilution, the pH, and the residence time, which are all dependent on each other, could be optimized. However, because this parameter space is quite large and the variables depend on each other, finding the optimum

with experiments would be very time-consuming. In the modeling developed by Shen et al., 2021 [81] most of these parameters are already integrated, so it would be very useful to improve it and run it to minimize the parameter space and find conditions where the detection limit is even better.

Further experiments to understand the mechanism between the OP-active substances and AA would also be very useful. With that knowledge one could better validate the data and compare it to other assays and measurements. Also the condensation reaction between DHA and OPDA and its side reaction would be good to understand better to optimize that part of the assay more. Further research should be conducted to understand the mechanistic effects of the memory effects of transition metals at neutral pH ans also the mixing and reaction rate constant. When these effects are better understood, it would be very useful to try to find materials that are less prone to adsorption of transition metals and maybe do some microfluidic modeling to improve the mixing.
The assay could also be optimized itself. DFQ is not very stable, and the quantum yield is low. With another condensation fluorophor precursor, maybe the fluorophor could be improved.

All the above technical suggestions have the goal of improving the instrument and making it better in terms of scientific output. However, there is also the monetary aspect for future applications. Especially if another instrument or even more than one should be built to do ambient campaigns with a spatial resolution and not only temporal, this is an important aspect. When the chemical reactions and the instrument are understood very well, it might not be necessary to have the spectral resolution of the spectrometer and a cheaper photodiode should also be sufficient. If there would be built more than one, it is also worth considering not building everything in-house. We just did that because we had the expertise for all the electronics, the flow cell or also the hardware parts. This was very useful to make changes in the development process, but once it is no longer a prototype it might be cheaper to buy more parts already assembled. On the other hand, for expensive parts like the PILS that are not too complicated, it might be worth building something similar in-house with just the key components that we need.

If a really low budget version of the instrument should be built, then maybe several components could be omitted or simplified. Parts that are not key

components are flow sensors, the individual operation of the peristaltic pump channels, the second bubble trap, an additional heating bath, the whole electronic that logs all the temperature, etc. But in the current state where it is crucial that all parts are working perfectly to get the sensitivity for ambient measurements, these components should not be removed, otherwise it will become very difficult, once something goes wrong and some troubleshooting is needed.

Not only should the instrument be optimized on a technical level, but also more calibrations and measurements should be performed. As a first step all the calibration experiments should be conducted again with the final instrument to get more comparable results and LODs. Furthermore, it would be interesting to measure more fundamental experiments and correlate this online OP signal from the OOPAAI with other measurements to get a deeper understanding of the working mechanism of the assay. Also would it be interesting to measure more campaigns to compare and correlate the OOPAAI signal to other instruments and measure different aerosols. Finally it would be nice to measure more ambient aerosol also at different places and combined with other measurement methods that provide more chemical composition of the aerosol. With this knowledge of chemical composition the OP signal could be compared and correlated to gain more insight in the toxic components of ambient air pollution. Not only would it be very interesting to measure in parallel with other general aerosol measurement techniques, but also with other online OP and ROS instruments to compare different online ROS and OP measurement techniques to each other.
Because the OOPAAI measure the sum of various OP-active compounds with a physiological assay it might also be very suitable as a parameter for epidemiological studies. So far mostly experiments were done to measure laboratory generated aerosol and ambient aerosol to better understand the chemical pathways and mechanistic effects that could lead to toxicity. But another field of research where the OOPAAI could be used due to his integrative online OP measurement would be epidemiology. The only challenge for that would be to improve the spatial resolution. Epidemiological studies normally need spatial resolution and for that more than one instrument is needed.

3 Measuring the Decay of SOA and Comparing Offline and Online Measurements with Acellular and Cellular Assays

This chapter is based on work published in different papers.
The offline AA data for filter decay will be published in Utinger et al., 2023 (AMTD). The online and offline comparison and also the offline data for DCFH and DTT, as well as the online and offline comparison of human epithelial lung cells, will be published in Campbell et al., 2023 in preparation. The biological method part of this paper is verbatim as published in Campbell et al., 2023 in prep. Some of the cellular data might be published in a further paper that focuses more on biology together with other data from the same campaign, which is not shown here in the near future. The ambient filter data from Beijing is published in Campbell et al., 2021 [33]

Author Contribution
Battist Utinger conducted all the AA offline experiments and the operation of the OOPAAI shown in this chapter. The DCFH and DTT decay experiments were done by Battist Utinger, Alexandre Barth, and Benjamin Gfeller. Alexandre Barth also conducted the online and offline DCFH experiments for the comparison of different compounds. Zaira Leni conducted the biological experiments and wrote the methods for the biology part. Battist Utinger, Steven Campbell, Alexandre Barth and Julian Resch were responisibile for the aerosol generation in the cell campaign. Julian Resch plotted the PCA plots.

Abstract

Numerous adverse health effects have been associated with exposure to ambient particulate matter (PM), according to extensive epidemiological studies. However, there is still great uncertainty about the precise physical and chemical characteristics of the particles that are responsible for these adverse health effects. Moreover, the biological pathways that are induced by aerosols and lead to negative health effects are poorly understood. A key metric for determining particle toxicity are reactive oxygen species (ROS) or the oxidative potential (OP).
To better understand these mechanisms, we measured ambient filter samples with the ascorbic acid (AA) assay and other OP and ROS assays, to quantify the toxicity of aerosols with offline methods, which are standard measurement techniques for OP and ROS measurements. We also measured with the OOPAAI and saw higher OP and ROS signals with the online measurement compared to the offline filter measurements. Therefore, we conducted experiments to investigate the decay of OP-active compounds and ROS in secondary organic aerosols (SOA).

To determine the extent to which reactive OP components in SOA are lost through filter collection, we conducted experiments to quantify the decay of OP-active substances and ROS from biogenic β-pinene SOA. This was done using an offline ascorbic acid (AA) assay, an offline DCFH assay, and an offline DTT assay to investigate the decay of the OP active compounds in SOA. We compared these offline measurements to online measurements, where we could show that for SOA the offline filter measurements hugely underestimate the OP. We investigated this difference also with primary and secondary residential wood combustion and car exhaust, where we could show that the OP is also underestimated by offline measurements for real-world emissions, although by a smaller difference.
Furthermore, to investigate if these online/offline differences in ROS and OP also translate to differences in biological and toxicological effects, we exposed human epithelial lung cells to SOA particles using online and offline methods, and showed that there are different biological responses, demonstrating that particles deposited online onto lungs cells trigger a different set of biological responses than offline deposited particles.

3.1 Introduction

Offline filter-based collection methods are the current standard for ROS and OP measurements. As described in Subsection 1.4.4, most measurements are performed using offline filter analysis.[31] Offline experiments have the advantage that they utilize well-established protocols, are easy to measure, are relatively inexpensive, and therefore easily achieve a good spatial resolution. They also allow the study of particles from locations where online analysis is difficult. The big drawback is that ROS and some OP-active compounds are reactive substances, therefore, short-lived and not stable, and may therefore decay prior to offline filter analysis.

Several different assays are used to measure ROS and OP. The dithiothreitol (DTT) assay is the most widely used assay to measure OP in aerosols.[31, 39, 52, 73, 74, 75] DTT is a surrogate for cellular NADPH. In this process, oxygen is reduced to superoxide (O_2^-). The total generation rate of (O_2^- by aerosols is determined by the consumption rate of DTT. The consumption rate is proportional to the concentration of redox-active species in the aerosol sample. Another widely used assay is the ascorbic acid (AA) assay, which is measured similarly to DTT, where the consumption rate of AA is measured over time.[78, 79, 80] AA is determined by UV-vis absorption and emission spectroscopy in which oxidized AA is condensed with *o*-phenylenediamine to produce a fluorophore.[33, 81]

Furthermore, OP can also be measured with a glutathione (GSH) assay, which is sometimes combined with surrogate lung fluid (SLF), which contains not only glutathione, but also ascorbic acid and uric acid in most methods that use the GSH assay.[31] Offline ROS measurements can be made with the DCFH assay, where filter samples are extracted similar to the other assays and then dichlorofluorescin (DCFH) is added to the aliquot. DCFH is a nonfluorescent reagent that when oxidized in the presence of ROS turns fluorescent (DCF). Before analysis, DCFH and horseradish peroxidase (HRP) were combined in sodium phosphate buffer to catalyze the reactions. The fluorogenic intensity of DCF is then assessed using a spectrometer. To determine the final particle-bound ROS measurement, the fluorescent intensity is translated to H_2O_2 equivalent concentrations using a linear fit and an H_2O_2 calibration curve.[33, 84] The short-lived radicals are best characterized by electron paramagnetic resonance (EPR). EPR is applied primarily to quantify particle-bound radical species [86, 87, 88, 89] or for radicals that are formed when an aerosol is suspended in an aqueous solution.[90, 91]

With these assays, we measured ambient samples to observe trends of OP in the environment to investigate whether seasonal differences in composition could also have an effect on the decay of different compounds present in aerosols. To quantify the lifetime of ROS and OP-active compounds, i.e. how fast they are actually lost over time, we conducted offline experiments to illustrate how stable the OP of biogenic α-pinene SOA is. The decay rate of the OP active compounds was measured with an offline ascorbic acid assay, an offline DCFH assay, and an offline DTT assay. With these experiments, it is possible to estimate the half-life of ROS and OP in the biogenic SOA used. Moreover, a comparison can be made between the offline method and the online instrument to see if the online instrument measures more short-lived ROS/OP. Furthermore, we conducted some biological online and offline experiments with human epithelial lung cells to see if there is also a different response for cellular assays. These experiments were performed in addition to the OP measurement to investigate whether the same trend could also be seen in a more complex system, such as human cells.

3.2 Methods

In this section, all the offline assays that were used are described. The assays were developed and optimized over the years, and therefore they are not exactly the same for all data presented. The versions presented here are the latest and most used. If a slightly different protocol was used, it is mentioned in the results section for that specific experiment.

3.2.1 Reagents

All chemicals were obtained from Sigma-Aldrich and all gases from Carbagas unless otherwise indicated and were used without further purification unless otherwise indicated: ascorbic acid (99%), Dehydroascorbic acid (99%), 0.1 M HCl solution, 0.1 M NaOH solution, Chelex 100 sodium form, $CuSO_4$ (99%), $FeSO_4$ (99%), $Fe_2(SO_4)_3$ (98%), *o*-phenylenediamine ($\geq$99.5%), HEPES (4-(2-hydroxyethyl)-1-piperazineethanesulfonic acid, $\geq$99%), α-pinene ($\geq$98%) β-pinene ($\geq$98%), naphthalene ($\geq$99%), zero grade air, N_2 gas (purity 99.999%). The H_2O used to prepare the solutions was purified with an ultra-high purification water unit (resistivity 18.2 MΩ/cm.

3.2.2 AA Offline Assay Protocol

The offline ascorbic acid assay was performed under conditions that replicate the assay conditions in the OOPAAI (see Chapter 2) to ensure comparability between the offline assay and the online method. Therefore, a fluorescent approach with the same chemical detection was used in which AA is oxidized to DHA, and the amount of DHA is measured by the fluorescent condensation product between DHA and OPDA, DFQ. The chemical reagents were used as described in Subsection 2.2.3 and the preparations of the chemicals were carried out as described in Subsection 2.2.4 with the difference that ascorbic acid is 1800 µM and the OPDA 200 µM. For the AA stock solution of 1800 µM, 15.84 mg of AA are dissolved in 50 mL of a 180 mM HEPES buffer at pH 6.8. The OPDA stock solution is prepared by dissolving 1.08 g of OPDA in 50 mL 0.1 M HCl solution by stirring it for approximately 10 min till all the OPDA crystals are dissolved. At the beginning, the OOPAAI was running under acid conditions and therefore also the AA solution of the offline assay was at pH 2. Most of the experiments shown here were done at neutral pH, but if they were done at acidic pH, that is mentioned.

For the calibration of the offline setup, a DHA calibration curve has to be done similar to as described in Subsection 2.2.3 . For the DHA stock solution 1.74 mg are dissolved in 50 mL of 0.01 M HCl solution and thoroughly mixed. Then a dilution series was: 100 µM, 50 µM, 20 µM, 10 µM, 5 µM, 2 µM, 1 µM. 900 µL of the corresponding calibration solutions for DHA were mixed with 100 µL of the OPDA stock solution (in triplicate) and reacted for 3 min at room temperature and then 900 µL were measured.

For the physical setup, a LED (UVLED-365-330-SMD, Roithner Lasertechnik) with an excitation wavelength of 365 nm is mounted on a TECooler and powered with 0.5 A(current controlled) and is connected with a fiber (600 µm, Ocean Insight) to a cuvette holder (CUV-ALL-UV cuvette holder, Ocean Insight). Perpendicularly, the same fiber is connected to a spectrometer (QePro, Ocean insight) to measure the emission of the fluorophore. The fibers are connected with a collimating lens (SMA, Ocean Insight) to the cuvette holder, and the other two ports of the cuvette holder are equipped with mirrors (Ocean Insight) to amplify the signal.

For filter extraction, the filter has to be cut into small pieces and pushed with a piece of Teflon tubing into a scintillation vial. To avoid contamination with metals, it is important to use only pieces that are not out of metal for cutting and handling the filter. Then 3 mL of ultrapure chelexed water was added and vortexed for

3 min at 3200 rpm and turned around a couple of times while vortexing. While the sample is vortexing, a syringe (5 mL, Luer lock) is filled with water and a filter (0.45 um) is flushed a couple of times to clean it. The filter slurry (quartz filters)/extracted water (teflon filters) in the vial is sucked into the prewashed syringe with a piece of Teflon tube fitted to a Luer lock. The filter slurry is pushed through the syringe filter into another scintillation vial and 800 µL of the filtrate are added to a new vial. This was done three times to obtain the measurements in triplicates. To each of these samples 100 µL of the ascorbic acid stock solution is added and the samples are incubated for 20 min at 37 °C in a heating bath. Then 100 µL of a OPDA stock solution was added and incubated for 3 min at room temperature. 900 µL of the sample was then transferred to a 1 mliter cuvette and the fluorescence emission was measured for approximately 30 sec.

3.2.3 DTT Assay Offline Protocol

The offline DTT assay measures the decay rate of DTT over time through absorbance. The absorbance setup consists of a deuterium lamp (DH-mini, Ocean Insight) that is coupled with an optical fiber with a (600 µm diameter, Ocean Insight) to a cuvette holder (4 Way CUV Cuvette Holder, Ocean Insight) and from there directly to a spectrometer (QePro, Ocean insight). The fibers are connected with a collimating lens (SMA, Ocean Insight) to the cuvette holder, and the other two ports are sealed to avoid disturbing the measurement with stray light. All chemicals for DTT were obtained from Sigma-Aldrich, if not other mentioned reagents, and were prepared with chelexed ultrapure water. The DTT protocol follows, if not mentioned otherwise, the protocol of Cho et al., 2005.[73] Trichloroacetic acid (TCA) is prepared as a 10% solution (20 g TCA in200 mL water) and can be stored up to 1 h. Ethylenediaminetetraacetic acid (EDTA) and Tris(hydroxymethyl)aminomethan (tris-base, Trizma) are stable for up to 2 weeks and are mixed in the following ratio: 20.2 g tris-base, 2.45 g EDTA in aqueous 23.72 mL HCl (1 M and 226.28 mL chelexed ultra pure water. The phosphate buffer is at pH 7.4 and is mixed with 77.8 mL NaH_2PO_4 and can be stored for up to 2 weeks. 5,5-dithio-bis-(2-nitrobenzoic acid) (DTNB, Ellman's reagent) must be made fresh daily with 59.46 mg DTNB in 7.5 mL 0.2 PBS and 7.5 mL of ultra-pure chelexed water. Dithiothreitol (DTT) must also be made fresh every day with 30.8 mg DTT in 20 mL 0.2 M PBS for a 10 mM stock solution. For the working solution 1.125 mL of the stock solution, they are diluted with 48.875 mL PBS.

Filter extraction is performed in the same way as described for AA in Subsection 3.2.2. Then 2.5 mL of the extract is mixed with 2 mL of the working solution of DTT. The vial reacts for 30 sec in the dry heater (38 °C) and 0.6 mL is transferred to 0.6 mL TCA. This vial must already be prepared before proceeding to minimize transfer time. This step is repeated after 2,5,12,22,32 min to get the slope of the decay. The initial concentration of the aerosol should not be such that no more than 20-30% of the initial DTT is consumed. After taking all aliques 60 µL DTNB must react for 5 min and then 0.8 mL of the tris base and EDTA mixture and react for 15 min
For measurement, a quartz cuvette is filled with 800 µL of the final DTT solution and absorption is measured at 412 nm at an integration time of 70 m sec. The variability for triplicates should be less than 5%.

3.2.4 DCFH Assay Offline Protocol

For the DCFH assay, the same setup and filter extraction method as described in Subsection 3.2.2 was used. The here described DCFH assay follows the protocol of Fuller et al., 2014 [94] and Campbell et al., 2021.[33] DCFH was freshly prepared daily using the following procedure: 10 mg of DCFH-DA was dissolved in 10 mL methanol, with vortexing to aid dissolution. For up to a week, this stock solution was kept in the freezer at −18 °C. 2.77 mL of 0.01 M NaOH were added to 338 µL of DCFH-DA in methanol and left to react at room temperature for 30 min in the dark. Then 6.92 mL of 1 M potassium phosphate buffer solution was used to quench the reaction and filled up to 50 mL chelexed ultra pure water. For the HRP solution 1.54 mg HRP was dissolved in 50 mL for a 10 1/µL stock solution (stable for 1 week in the fridge). From this every day a new working solution was prepared by diluting it to a 1.38 units/µL solution with 6.82 mL stock solution 6.82 mL buffer and filling up to 50 mL with chelexed ultrapure water.

3.2.5 SOA Decay Experiment

Secondary organic aerosol (α-pinene) filter samples were collected on filters for offline AA analysis to determine the decay, i.e., the lifetime, of particle OP when collected on a filter. SOA was collected on quartz filters for 100 seconds with a high α-pinene mass (80 mg/m^3) produced by the organic coating unit (OCU, FHNW) and an additional flow tube with ozonolysis. Keller et al., 2022 show that the OCU produces aerosols, which even at high mass concentrations, have a chemical composition that is a realistic representation of ambient SOA.[170] In

the OCU, an organic precursor is oxidized in a small flow chamber by OH and ozone under controlled relative humidity (65%) and temperature conditions (fully described by Keller et al. 2022[170]). After the OCU, an additional flow tube with an ozone flow was added to oxidize any remaining VOC that was not oxidized in the OCU to increase the particle mass. SOA produced from OH-initiated photooxidation of α-pinene is commonly used as an atmospheric representative of SOA.[170, 172] These very high aerosol concentrations were necessary to minimize the collection time and therefore reduce the decay of short-lived OP-active aerosol components.

After the flow tube, the aerosol passed through a charcoal denuder to remove unreacted ozone and VOCs with an efficiency of 99.9%.[38] The filters were then collected and extracted after different time intervals and analyzed with an offline AA assay, using the same chemical conditions as the OOPAAI AA-based assay. A 47 mm quartz filter was extracted directly in 3 mL of 200 µM ascorbic acid, buffered with 20 mM HEPES, and then vortex for 3 min. The slurry is then filtered with a syringe filter (PTFE, pore size 0.45 µm, Agilent) and 900 µL of the extract is reacted 10 min in a 37 °C heating bath. Subsequently, 100 µL OPDA dissolved in 0.1 M HCl was added and reacted for an additional 3 min at room temperature, and then the fluorescent signal was measured with a spectrometer (QePro, Ocean Insight). The fluorescent product DFQ is then excited at $\lambda_e x$=365 nm, with peak fluorescence emission monitored at $\lambda_e x$=430 nm. The filter collection efficiency is assumed to be 100%. The PILS does not have a collection efficiency of 100%,[173] therefore, this difference had to be investigated to compare the online and offline signals. The PILS extraction efficiency is determined by measuring the same amount of aerosol either directly with the PILS or collected on a filter and then extracted and added to the OOPAAI. For this extraction efficiency test of the PILS the measurement is performed with the normal online instrument setup (see Figure 17), but bypassing the PILS when adding the aerosol extracted on the filter. Like that, we could calculate the difference in the signal. The PILS operated under the conditions described here had an extraction efficiency between 20-25%.

3.2.6 Setup for Cell Exposure

Secondary organic aerosol was generated using an OCU [170] and metal aerosol was generated by nebulizing metal salts. The nebulized aerosol was dried with a silica denuder, and for the SOA, the remaining unreacted VOCs and ozone was removed by charcoal denuders. After dilution, the aerosol was transferred to the

nano aerosol chamber *in vivo* toxicity (NACIVT) for cell exposure. The NACIVT is an instrument to expose epithelial cells at an air-liquid interface to aerosols.[70] In parallel, we measured the same aerosol with the OPROSI and the OOPAAI to quantify and correlate ROS and OP. In some cases, due to technical difficulties, we also had to do it separately, but under the exact same conditions.

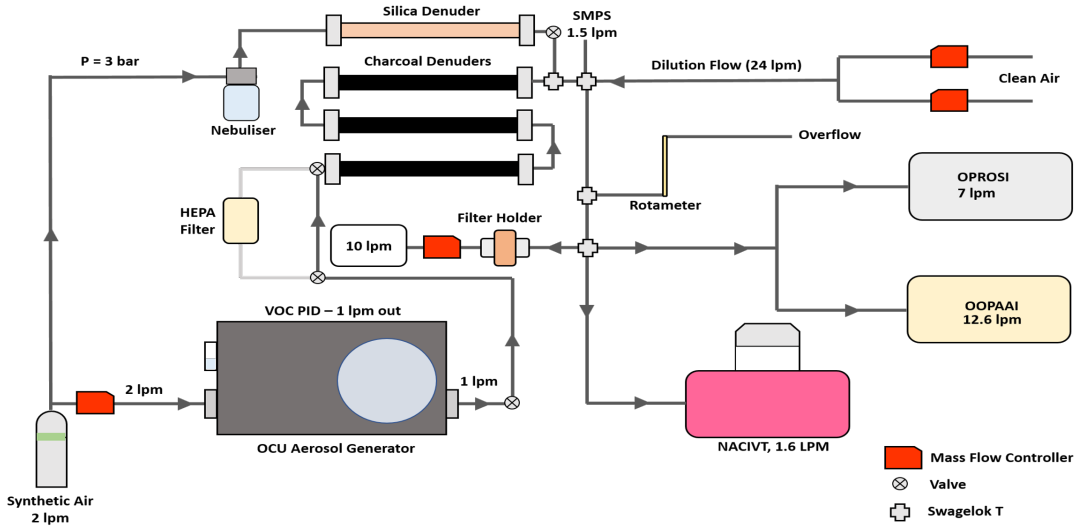

Figure 43: A schematic of the setup used to measure aerosol deposition of human epithelial lung cells and in parallel ROS and OP.

3.2.7 Cell Culture Exposure

Primary bronchial epithelial cells (HBE) were isolated from donor lungs. The normal lung that was deemed not suitable for transplantation was obtained from the Life Alliance Organ Recovery Agency (LAORA) of the University of Miami, Miami, FL, USA. Institutional review board (IRB)-approved consent for research with these tissues was obtained from LAORA and was consistent with the Declaration of Helsinki. The HBEs were kept in two-dimensional submerged culture in bronchial epithelial cell growth medium (BEGM - LHC base medium with supplements, Gibco, Fisher Scientific, Reinach, Switzerland). Subsequently, cells were seeded in 0.33 cm^2 porous Transwell® inserts (Corning International, Fisher Scientific, Reinach, Switzerland) in a chemically defined medium that induces terminal differentiation. Once confluent, the apical medium was removed, establishing an air-liquid interface (ALI), and the epithelium was allowed to differentiate over a 4 week period. ALI cultures of redifferentiated HBE were generated as previously described (Künzi et al. 2015, [174]). Fully differentiated HBE were exposed to the different types of aerosol in the NACIVT at physiological conditions, i.e., 37 °C, 5% CO2, and >85% relative humidity for 60 min. Control

cell cultures were either exposed to particle-free air (p-free air) or left untreated in the incubator. For P-free air exposure, we mounted a HEPA filter between the aerosol exhaust line and the thermodenuder. Particle deposition was observed in real time with Lab View 9.0.1. After exposure, cell cultures were incubated under the same conditions for 4 h before collecting apical wash samples and subsequently incubated for an additional 23 h followed by final sampling. At least three independent HBE cultures were performed for each exposure. For the offline deposition the aerosol was collected on filters and then extracted with PBS buffer and pipetted onto the cell cultures.

3.2.8 Cytotoxicity Analysis

Induction of cell death was measured by the release of cytosolic lactate dehydrogenase (LDH) from damaged cells into the apical compartment. Apical washes were collected 4 h and 24 h post exposure and stored at 4 °C until analysis using the colorimetric cytotoxicity detection kitPLUS (Roche Diagnostics AG, Rotkreuz, Switzerland) according to the manufacturer's instructions. The maximum releasable LDH was estimated in the supernatants of cells lysed with 100 µL 1% Triton-X solution for 10 min at 37 °C. Cytotoxicity is presented as a percentage of maximal releasable LDH activity (absorbance).

3.2.9 Real-time Polymerase Chain Reaction (RT-PCR)

We screened 20 genes to evaluate alterations in signaling pathways related to oxidative stress using Gene globe arrays. Gene expression in HBE was examined by isolation of total ribonuclein acid (RNA) followed by RT-qPCR. Briefly, cells were lysed with RLT buffer (Qiagen, RNeasy® Mini Kit), according to the manufacturer's protocol. RLT buffer was added with β-mercaptoethanol (β-ME) and samples stored at −80 °C until they were further processed. Isolated RNA (500 ng) was reverse transcribed to complementary DNA (cDNA) using the QuantiTect® reverse transcription kit (Qiagen, Hombrechtikon, Switzerland) following the manufacturer's recommendations. Real-time PCR was performed in a reaction volume of 25 µL using the QuantiTect SYBR Green PCR kit (Qiagen) and QuantiTect Primer Assays (Qiagen), amplifying a total of 25 ng cDNA of each sample. Real-time PCR was performed using the Applied Biosystems 7900HT Fast Real Time PCR System with a 15-min initial activation step at 95 °C and 40 cycles with 15 s denaturation at 94 °C, 30 s annealing at 55 °C and 30 s extension at 72 °C. Subsequently, a melting curve was performed to exclude

primer-dimer artifacts and to ensure reaction specificity. Data were normalized to Hypoxanthine-Guanine Phosphoribosyl Transferase (HPRT) using the $\delta\delta$Ct method (Livak and Schmittgen, 2001). Biological replicates (n = 3–9 cultures) were analyzed three times using Applied Biosystems SDS v2.4.

3.2.10 Proteome Profile

The release of 102 cytokines and chemokines from cells was evaluated by high-throughput screening using the Proteom Profiler Human XL Cytokine Array (ARY022, R&D Systems, Minneapolis, MN, USA), which was coated with 102 capturing antibodies in duplicate on a nitrocellulose membrane. The kit contained all the reagents for the assay and was performed according to the manufacturer's instructions. This array of cytokines and chemokines antibodies was used to determine the effects of aerosol exposure on cytokine and chemokine release by HBE-exposed cells. The assay required 500 µL of cell culture supernatants (unstimulated containing 0 µg/mL CDs, LPS stimulated containing 0 µg/mL CDs, and unstimulated containing 500 µg/mL CDs). Membranes were subjected to an ultra-sensitive chromogenic 3,3‘,5,5‘-Tetramethylbenzidine (TMB) membrane substrate (Thermo Scientific, Waltham, MA, USA) to reveal sample–antibody complexes labeled with streptavidin-HRP. Photographs were taken of the blots after the exposure to the substrate. The inflammatory response was evaluated by measuring the release of 102 cytokines and chemokines from cells by high-throughput screening using the Proteome profiler Human XL Cytokine Array (ARY022, R&D Systems, Minneapolis, MN, USA).

3.2.11 Statistical Analysis

All data are expressed as mean values ± standard deviation. Statistical analyzes were performed with GraphPad Prism 7.04 (GraphPad Software Inc. San Diego, USA). For cytotoxicity and release of inflammatory mediators, the arithmetic mean values of each experiment were compared to the mean value of the untreated control by one-way analysis of variance (ANOVA) followed by Dunnett's t test to compare the treated group to the control or the Bonferroni test for multiple comparisons. The principal component analysis (PCA) was performed using SIMCA (Sartorius, Germany).

3.3 Results and Discussion

3.3.1 Ambient Offline AA Analysis

With the offline AA assay, various studies were also conducted for different aerosol samples generated in the laboratory and ambient filter samples. In Zhang et al., in prep and Campbell et al., 2021 AA was performed together with DTT, DCFH, or EPR to obtain a more complete picture on different OP endpoints.[33] The data shown in Figure 44 is obtained with the AA assay as described in Subsection 3.2.2 but at pH 2 under acidic conditions. The exact protocol is also described in the supplementary information of Campbell et al., 2021 [33] where the entire campaign details and the other assays are described. The volume-normalized AA signal (red bars) follows the mass (blue line), especially during summer. But it is not a perfect correlation, where sometimes the signal from the offline AA assay is over-proportional higher. This effect can be seen in the same way, but with a much higher time resolution when measuring online with the OOPAAI (see Figure 40). In winter, the mass of PM is also higher, with an average mass of $PM_{2.5}$ of $98.7 \pm 75.0\,\mu g/m^3$ compared to summer when $PM_{2.5}$ is only $36.7 \pm 16.0\,\mu g/m^3$. Spearman rank correlation of the volume normalized OP of AA with $PM_{2.5}$ (and the other assays) shows a stronger correlation in winter than in summer (data not shown here, more details in Campbell et al. 2021.[33] Calas et al., 2018 [175] saw the same trend for all assays that the correlation is stronger in winter.

The compositional change in ambient aerosol is very large compared to that of laboratory-generated aerosol. In the same campaign as the data collected for Figure 44, Steimer et al., 2020 [96] performed back trajectory modeling showing that if the air came from the very industrialized south of Beijing, the composition was different from that for the lower polluted days, where the aerosol came from more variable directions. In Subsection 3.3.2 we show the decay for only one SOA component (α-pinene) whereas in the ambient environment there are thousands of different compounds that most likely all have different decay rates or are stable or even not OP-active at all. A hypothesis why the signal in summer is lower than in winter could also be due to the fact that there is more photochemistry happening in summer and therefore more short-lived ROS is present in the particles, which may evade detection using offline filter based methods.

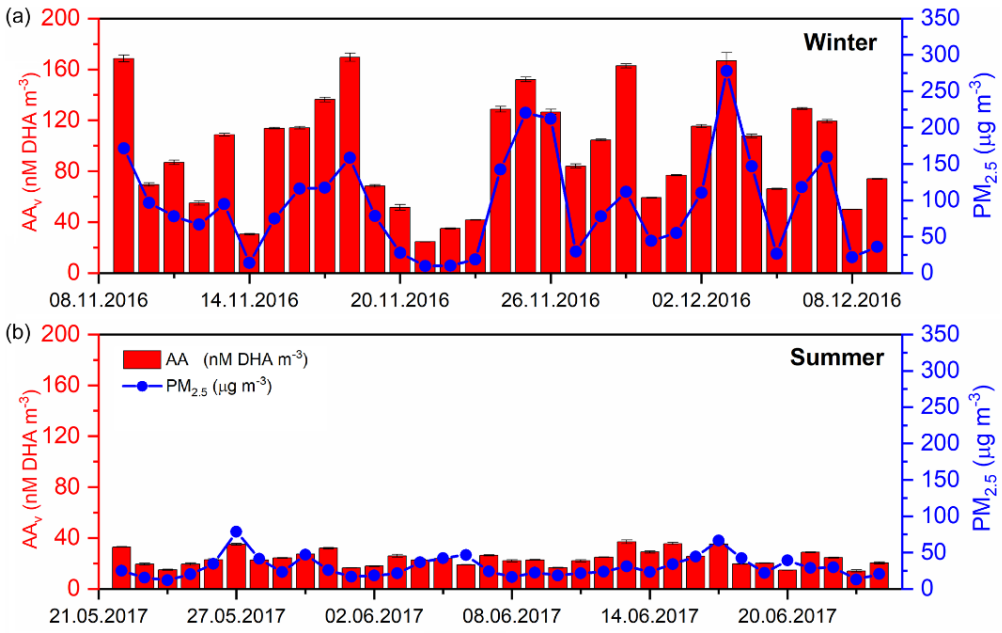

Figure 44: AA offline ambient filter analysis of two seasons from Beijing. Time-averaged (24 h) volume normalized oxidized AA (red bars) and PM2. 5 mass(blue dots), analyzed from 24-h high-volume filters, for both winter 2016 (8 November - 8 December 2016) and summer 2017 (21 May - 24 June 2017)[162, 176] In (A) the filter from winter is shown in nanomolar DHA per cubic meter and in (B) from summer. This figure is published in Campbell et al., 2021 [33]

A recent review by Wang et al., 2023 [177] reported peroxide lifetimes of minutes to days, depending on the peroxide functionality and multiphase loss processes at play. In winter, aerosol emissions are different (more residential wood combustion and heating in general) and therefore could have more stable compounds such as metals or other more stable compounds.[178, 179, 180, 181] Various studies showed seasonal variability of OP due to different transport (i.e., different meteorological) conditions, as shown in Figure 45, or due to different sources.[77, 96, 182, 183, 184] Seasonal differences in OP and ROS measurements might not only come from different compositions, but also from underestimating certain very short-lived compounds that are more present in one season compared to another.

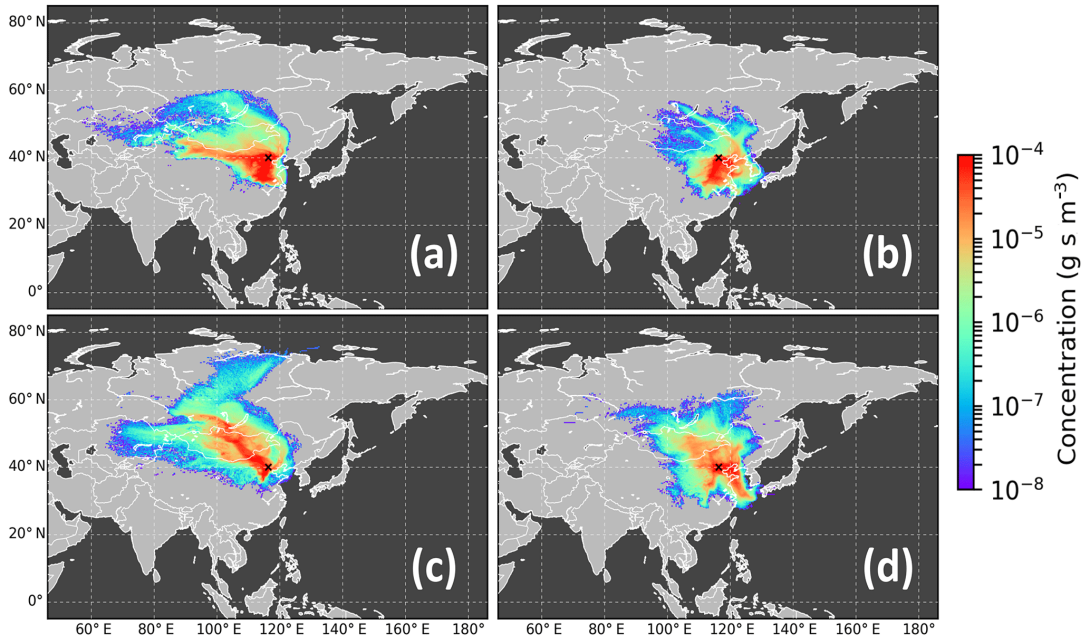

Figure 45: Back trajectories for 72 h. (a) Winter, high-pollution days; (b) summer, high-pollution days; (c) winter, low-pollution days; and (d) summer, low-pollution days. The colors are the relative residence time of the air masses during the last 72 h and the black cross is the measuring station. Figure from Steimer et al., 2018 [127]

In Figure 44 the AA signal is given per volume of air, so the seasonal difference could also be due to higher PM masses in winter. In Figure 46C the mass normalized signal for AA is shown and still the same trend is seen. Furthermore, three different ROS assays are presented (DCFH in (A), EPR in (B), and DTT in (D)). All of these assays show the same trend of a higher OP/ROS signal for the winter. However, for the DCFH assay, the differences are very small. DCFH is known to be mostly sensitive to hydrogen peroxides and other organic peroxides. Under the hypothesis that there is seasonal variability in composition and hence different decay rates for the different aerosol types, it makes sense that there is no large difference for the DCFH assay due to its specific sensitivity to peroxides. Furthermore, as shown in Figure 47 the DCFH assay has the greatest decay of the tested assays when the samples are stored for more than a few days.

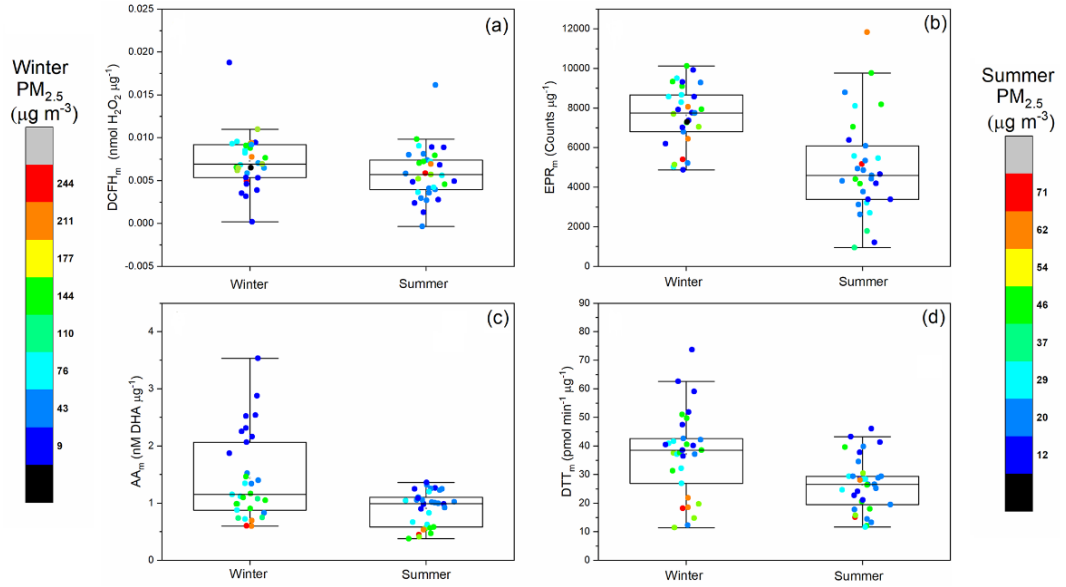

Figure 46: Seasonal differences (winter and summer) of four mass normalized OP/ROS assays: (a) DCFH. (b) EPR, (c) AA and (d) DTT. The individula data points are color-coded for eight different mass bins they are assigned to. Figure from Campbell et al. 2021.[33]

3.3.2 Offline Decay of SOA Measured with the AA, DTT and DCFH Assay

To estimate the kinetics of the OP decay and to compare the offline analysis with the online signal, seven filters were collected and stored between 2 min and 7 d days at room temperature before extraction and analysis in triplicate. Storing the filters in the freezer would slow the decay, but for the filters that were directly analyzed, it is not possible to put them in the freezer. In addition, filters collected in the ambient are often exposed to ambient temperatures for ∼24 hrs prior to freezing or OP analysis. Therefore, to compare the decay over the chosen time interval, we decided to measure the decay at ambient temperature. Figure 47 shows the relative decay of the three assays: AA, DTT and DCFH. They all show the same trend, but not the same decay rate. The second-order decay that is fitted to the data gives for all three assays good correlations. The AA has with an adjusted R-square of almost 1 a very good correlation, but also the DCFH with 0.93 and the DTT with 0.99 have a good adjusted R-square.

The DCFH has the highest decay rate and ROS decreases over the measured time period of one week to 10%. DCFH is most sensitive to hydrogen peroxide, hydroxyl radicals, superoxide, and organic peroxides. All these compounds are highly reactive and therefore short-lived.[33, 94, 95] AA and DTT are also reactive

to these substances that the DCFH assay is, but also to other compounds such as quinones that are less reactive and therefore not so short-lived.[39, 167, 168] So from a mechanistic point of view it makes sense that the DCFH assay measures the fastest decay rates compared to AA and DTT. The oxidation pathway for α-pinene is very complex and can result in many different compounds.[185] The reactions between organic components in SOA and AA is not well understood, as is the case for DTT, where the reactivity of DTT to many organic components in SOA is not well characterized. .[31, 39] Other studies also observed a decay for organic aerosol systems with offline measurements for DCFH.[94, 95, 140] Moreover, this decay was also observed with other measurement techniques such as radical quantification by Campbell et al.,2019 [38] or mass spectrometry of peroxy pinic acid by Steimer et al., 2018.[127]

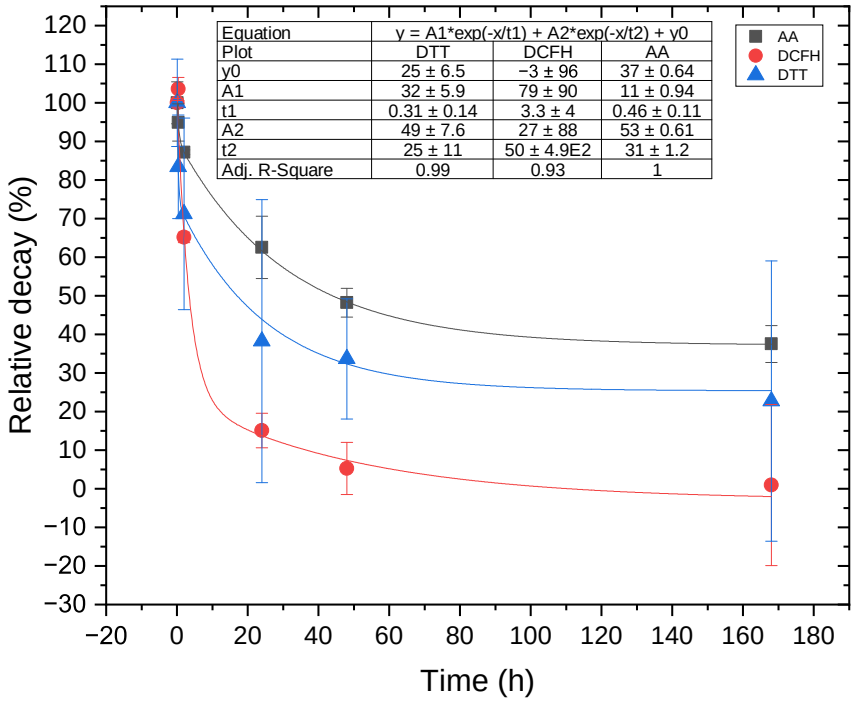

Figure 47: Relative offline decay of DTT, AA, and DCFH. All numbers of each assay are normalized to the first value of each assay and are presented as a percentage of the first initial concentration. A second-order exponential decay fit is performed for each assay. The error bars are in triplicate and are also relative errors to the value.

3.3.3 Online/Offline Comparison

The online instrument described in Chapter 2 measured the same aerosol that was generated for the offline decay (Subsection 3.3.2). The setup was designed so that the length of the tubing and the flows were exactly the same in the offline setup as well as in the online instrument.
The PILS does not have a collection efficiency of 100% and it is different for different aerosol types.[173] Sorooshian et al., 2006 [173] show in their method paper that the PILS collection efficiency is around 90%. Because we operate the PILS under extreme conditions (i.e. much lower liquid flow rates), we determined our particle collection efficiency. The PILS looses particles that are too small and do not grow in the supersaturated water vapor, and they are transported out with the air flow and are therefore not impacted on the impaction plate. Moreover, the liquid inlet flow and the addition of water from the droplets of the PILS need to be slightly higher than the liquid outflow. Otherwise, bubbles in the tubing to the heating bath are produced, which interfere with mixing and measurement. But because the humidity and the concentration of particles can change and therefore the addition of water to the wash flow can vary, and because the peristaltic pumps are not perfectly stable over time, there are additional losses of particles, even if they are impacted.
We used a compound that is chemically very stable to improve the intercomparison between online and offline and that can be used with the existing setting. Therefore, we took quinine, which has a structure similar to that of DFQ and because of that a similar excitation and emission wavelength. Quinine is a fluorescent compound that can be measured directly and does not need to be made fluorescent by another compound. Quinine is very stable and has a very good quantum yield. The quantum yield was so efficient that particular care was taken not to saturate the detector during these experiments. Particles (generated with a nebulizer and an aqueous solution containing quinine) with the same fluorescent intensity have a smaller number and mass distribution compared to SOA particles. Therefore, we added nonfluorescent ammonium sulfate to the mixture to make the particle number and mass distribution more similar to those of SOA because the collection efficiency in the PILS is size dependent.
The quinine and ammonium sulfate solution was nebulized and then either measured with the OOPAAI or collected on a filter and then extracted and inserted into the OOPAAI but with the PILS bypassed. This method assumes that the aerosol is collected with a filter collection efficiency of 100%. The aerosol was also measured with an SMPS to normalize the OOPAAI signal for

the particle mass. With the difference between the measurement directly with the PILS and the measurement in which the aerosol is first collected on a filter and then extracted and added to the same setup, the losses from the PILS could be calculated. With this calculation, we could show that on average 77% of the mass of the aerosol is not collected, and therefore the collection efficienty of the PILS in our setup is 23%. The online data point (red square) shown in Figure 48 is normalized with that factor.
Figure 48 shows the relative decay of DHA over time normalized to the online OOPAAI measurement (red square). The offline measurements (black diamonds) and the online measurements are fitted with a two-phase exponential decay function in the same way as shown in Figure 47. The active components of OP in α-pinene SOA investigated in this study can be broadly divided into three fractions:

- A very reactive first fraction with a half-life of less than a minute. This fraction seems to decay rapidly because the decay from the online measurement to the first online measurement point is already two-thirds of the signal. This fraction will most likely be particle-bound radicals and other very highly-reactive compounds such as organic peroxides.[89]

- A second fraction that decays slower and has a half-life of approximately 20 hours. In this fraction we assume that there are compounds like quinones and peroxides that are not stable, but also do not react immediately.

- A third fraction that is stable over at least a week. This fraction does not decay at all, and we assume that this might be very stable organic compounds or even contaminations from trace metals.

After a week, almost 90% of the active components of the OP are lost. The online signal is more than 2/3 higher than the immediately measured time point (age of particle approximately 2 min). In addition, the point measured immediately offline is almost 2/3 higher than the measurement after a week. This will lead to a huge underestimation of the OP signal when using traditional offline analysis, especially if they are not analyzed immediately.

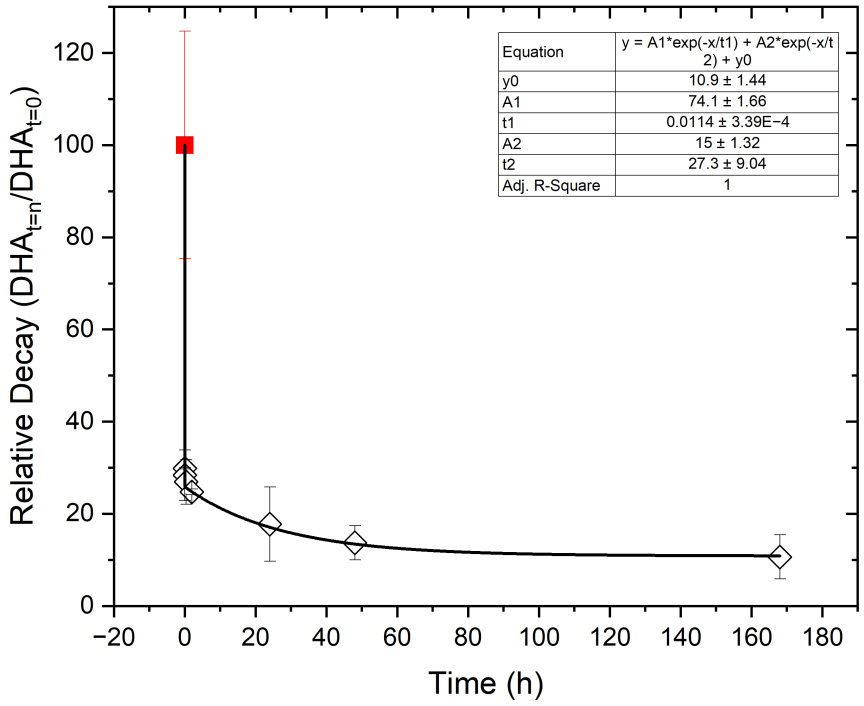

Figure 48: Offline decay of AA oxidation by α-pinene aerosol (black diamonds) and comparison with online quantification using OOPAAI (red square). For the offline decay of OP-active compounds in SOA, DHA concentrations were quantified between 2 min and 7 days. A two-phase exponential decay function is used for the fit and gives an adjusted R^2 of 0.998

Note that the particles for which this decay was quantified are SOA particles produced from OH and O_3-induced photooxidation of α-pinene, without any seed particles, that is, without inorganic components. Biogenic VOC α-pinene was chosen because it is a very well studied SOA precursor in the literature, has a complex organic composition, is an abundant VOC in the atmosphere, and is practically easy to handle.[14] Thus, for particles with different compositions or ambient particles, the ratio of reactive and short-lived to stable OP could be different. The OP decay could be slower or enhanced for SOA produced from different precursors, as well as ambient PM, because of the presence of other reactive components such as redox-active transition metals. However, these experiments demonstrate that the reactive components present in SOA decay on a time scale typical for offline analysis (minutes to weeks). Therefore, to capture this reactive fraction, an online method with fast collection and analysis time is needed for an accurate quantification of the OP of organic aerosol.

3.3.4 Difference in OP and Cytotoxicity of Online and Offline Measurements of Model Particles and Real Combustion Particles.

The online measurements with the OOPAAI were compared with the offline AA filter measurements for a wide range of particle types (Figure 49 and Figure 50). The offline filters were collected in such a manner that exactly the same particle mass was in the extract as with the online instrument. and analyzed approximately an hour after the collection. With this setup, it was possible to measure the difference between more aerosol types than in Figure 48. In Figure 49 the online/offline comparison for three different types of aerosols are presented. In the online measurements, the biogenic β-pinene-SOA has a lower signal than the anthropogenic naphthalene-SOA by approximately a factor of three. Compared to iron(II) sulfate particles, which were chosen here as an example of a redox-active transition metals, both types of SOA exhibit lower OP by over an order of magnitude.

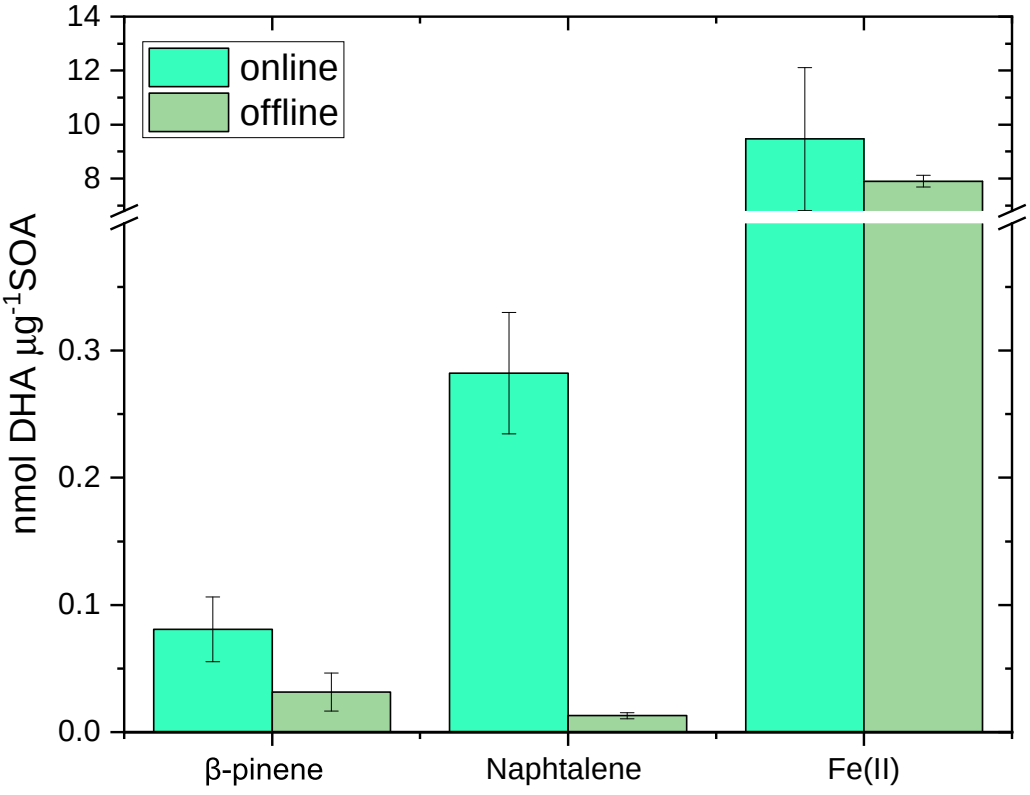

Figure 49: Online and offline measurements of three different aerosols. The OP value in nmol DHA is normalized for all aerosols with the particle mass. The error for the online measurement is the variability of a 1 h measurement and for the offline measurement the error are the standard deviation of triplicates of a filter.

This different reactivity is also shown in Subsection 2.4.2 and discussed there in more detail. The interesting difference when comparing the online and offline measurements is that, for naphthalene, the offline signal is an order of magnitude smaller than that for the corresponding online signal. The β-pinene shows the same trend, although less pronounced (offline signal is factor of 2 to 3 lower than the online signal) than naphthalene. Compared to organic aerosols, the metal shows no significant decay. This finding is in agreement with the decay curve measured in Figure 47 and Figure 48 that organic aerosols decay over time. Unlike labile organic compounds, iron is very stable and will not show a decay over time.

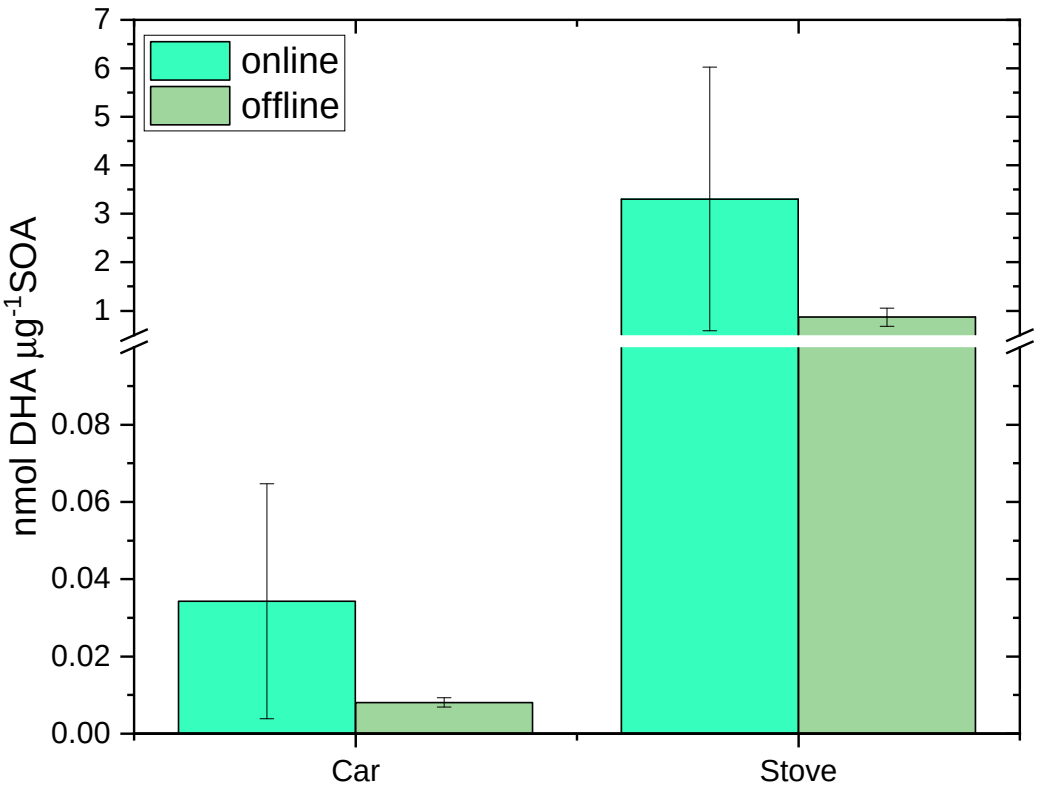

Figure 50: Online and offline measurements of real-world emissions from car exhaust and residential wood combustion. The error is the standard deviation over the measurement time for the online measurements and the standard deviation of triplicate measurements for the offline filter. The error in the online measurement is very high because it is due to the variability of the driving cycles and the batches of wood burning.

We conducted the same experiment not only with laboratory generated SOA particles and nebulized transition metals, but also with two real-world aerosol types generated by aged car exhaust and aged residential wood combustion. The

details of aerosol production and measurements are presented in Chapter 4 and discussed there in more detail. Here, only the difference between the online measurement with the OOPAAI and the offline measurement is shown and discussed, analyzed for the same aerosol collected on a filter and measured 24 h later. Although the decay is less pronounced compared to pure SOA systems in Figure 49 the same trend of a lower mass-normalized signal for offline measurement is consistent. The error for the online measurement is very high due to the signal change initiated by the variability of the car driving cycle and the different batches for the wood combustion (see Chapter 4 for details). So for the offline measurements the error bar is an indication of variability. For the offline filter, this variability is not visible because the filter integrates the changes in the online signal over time, and therefore the error is also smaller.

To investigate whether we can see these differences between online and offline measurements for different aerosols not only in acellular OP experiments but also in cellular experiments, we conducted some experiments with human epithelial lung cells. We tested three different biological endpoints: the LDH assay (Figure 51), gene expression (Figure 52,Figure 53), and protein expression (Figure 54, Figure 55). To determine if the processes of particle deposition mechanically impacts the cells (i.e no chemistry), we nebulized HEPES buffer to form an aerosol that is not toxic. HEPES is a widely used buffer in biology that is considered to be not toxic.[143] To test whether only the handling of cells led to a higher LDH release, a particle free air control was performed and there was no significant difference from the incubator control. For the particle free air control, the system was operating in the same mode as for the particle deposition, but a HEPA filter was mounted inline to remove all particles. The online HEPES measurement had a significant ($p<0.05$) increase of cytotoxicity (LDH) compared to the offline measurement. In the gene and protein expression, this effect is also observed, although there is only a small or no significant effect at all (Figure 52 and Figure 54). For gene analysis, only a fold change of greater than two is normally considered to be significant. Protein analysis is less quantitative than gene expression and only relative changes can be examined. For the same raw data, we show heat maps (Figure 52 and Figure 54) and principal components (PCA) plots (Figure 53 and Figure 55).
If the injury to the cell is mild, local, or other defense mechanisms are involved in addition to an inflammatory response, it is possible that LDH release from cells is higher, although the gene and protein expression of anti-inflammatory

genes and, therefore, proteins are not up-regulated in the same manner.[186] Regarding experiments where cells are exposed to nebulized HEPES particles, the aforementioned explanations could be plausible, although further work is required in order to fully determine why online HEPES particle exposure initiates LDH release. Also, we only measured six replicate cell cultures which is a rather low number for such biological experiments, and in a potential follow-up study the statistics should be improved by using a higher number of inserts for the NACIVT.

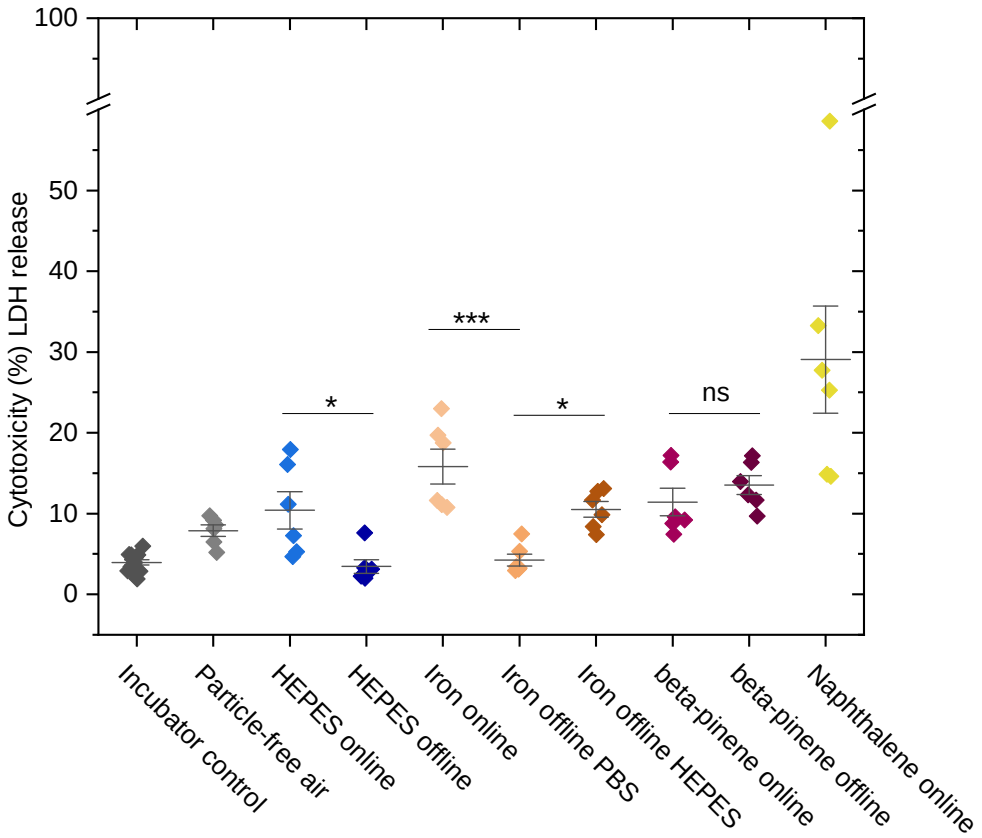

Figure 51: Cytotoxicity measured with the LDH assay of human epithelial lung cells for different types of aerosols. HEPES online and offline are significantly different ($p<0.05$, *). Iron online compared to iron offline with PBS ($p< 0.001$,***) and also iron online with iron offline HEPES (* not shown) and the two different buffers for the iron offline extraction ($p<0.05$) are significantly different. For β-pinene there is no significant difference (ns).

Furthermore, we tested iron particles offline and online and also with different buffers to test the influence of buffer soluton on Fe (II) chemistry, as for example PBS can chelate with Fe (II), potentially influencing it's redox-chemistry and hence OP. This is actually the case, leading to the assumption that for the

analysis of biological effects of metals, not only for the OP and ROS assays (see Subsection 2.2.5), but also for cell assays, it is better to use a buffer that does not chelate metals. Otherwise, the effect of the metals could be underestimated. Note that the lung naturally contains phosphate, but on average more than an order of magnitude less (1 mM than the typical buffer concentration used in cell biology and many acellular OP assays (20 mM). Also, for iron, the cytotoxicity is measured with the LDH assay and is higher for the offline than the online, but especially for the PBS this might also be due to the effect discussed before, i.e., that the PBS chelates the iron, and for the online there is no buffer, because the particles are deposited directly on the cells.

For the gene expression of iron there is for most genes no significant difference between the overall modulation of gene expression between online and offline for single genes, as shown in Figure 52. For the PCA plot the difference is as well very small supporting that finding. For protein expression (Figure 54) the cells that were exposed online with iron have, for most proteins, a higher fold change than the corresponding offline measurements. This can be seen in Figure 55 where the iron online measurement has, for the principle component 2, a very different signal. These diverging results from protein expression to gene expression could be due to post-transcriptional modifications of the RNA in the process of translation where, as an example, slicing can occur leading to different proteins from the same gene, which can lead to an overall increase in protein expression levels. Furthermore, gene transcription can also be regulated at multiple levels such as transciptional and also post-transcriptional modulations, which can then ultimately lead to different translations from the same protein.[187]

These are only speculative hypotheses, which theoretically could be possible, but to really understand the processes in this specific case, the single pathways would need to be studied more closely and more experiments would need to be performed. The PCA plot for the proteins shown in Figure 55 is done with all 104 analyzed proteins compared to the heat map where only selected proteins from the inflammation and oxidative stress pathways were selected. The overall picture is the same because most of the non-selected proteins show very little variation.

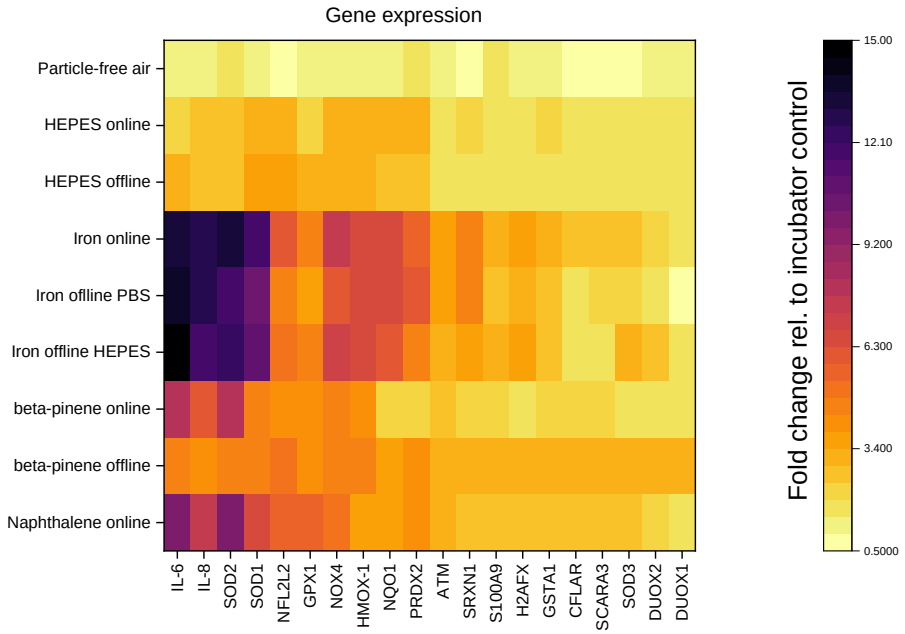

Figure 52: A heat map of gene expression for selected genes that play a role in inflammation and oxidative stress pathways. The colors correspond to the fold changes of the incubator control. The darker the color, the higher the fold change relative to the incubator control.

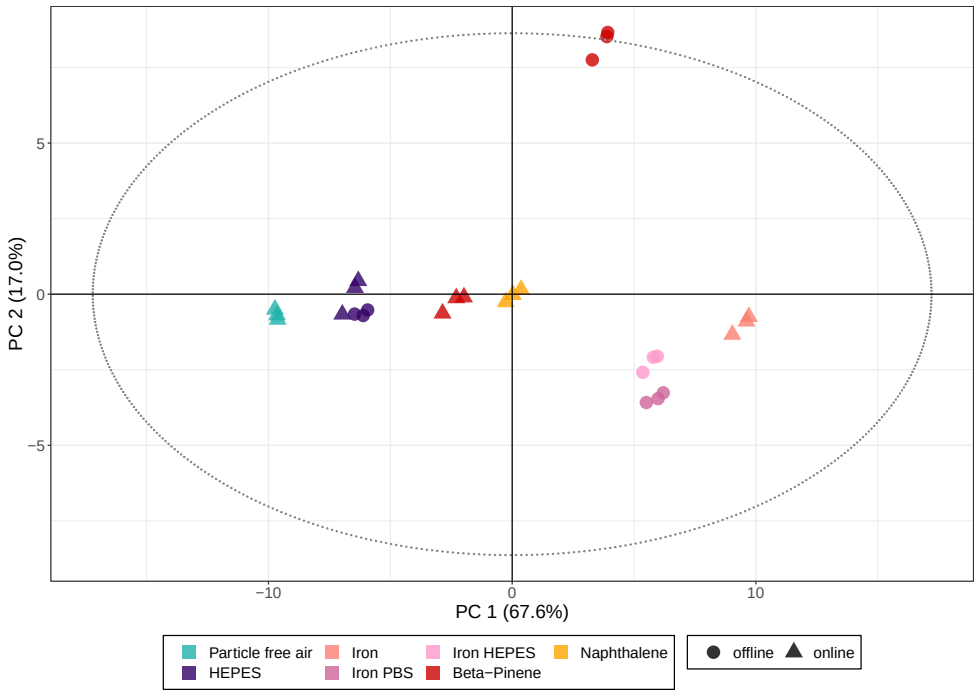

Figure 53: The same raw gene data as in Figure 52 but plotted as a PCA plot. The ellipse represents 95% of the Hotelling's T2 test confidence interval.

For β-pinene-SOA there is no significant difference between online and offline exposure for LDH. For gene expression looking at single genes there is a tendency that online is higher, for example, for IL-8, IL-8 and SOD2, but for protein expression there is no difference at all. Regarding the PCA plot in Figure 53 , offline β-pinene-SOA exposure for the gene expression, especially for the principle component 2, is different from the online β-pinene-SOA and the other aerosols. The different toxicity metrics measured here are quite low for β-pinene-SOA, so maybe due to intrinsically lower toxicity/OP, the difference between online and offline effects are also very small. Therefore we do not observe a significant effect for β-pinene-SOA .

We also performed a dose response curve with β-pinene-SOA (data not shown here) and only after exposure to large mass concentrations (several milligrams per cubic meter resulting in several 10 of nanograms per insert) there was an increase in cellular responses. For naphthalene, there is unfortunately no offline data set, but in a previous campaign we did these experiments and we could see a tendency that the online LDH response is higher. This data is not shown here, because we did not perform gene and protein analyzes to compare and we had some experimental problems. Although we included the online naphthalene measurements in the analysis here to show that there is a significant difference between β -pinene and naphthalene in all measured cellular assays (LDH, gene expression and protein expression). This is also in agreement with our OP data (See section XXX), where we consistently observe higher OP, which we hypothesize is a toxicity metric, for naphthalene SOA compared to β-pinene SOA.

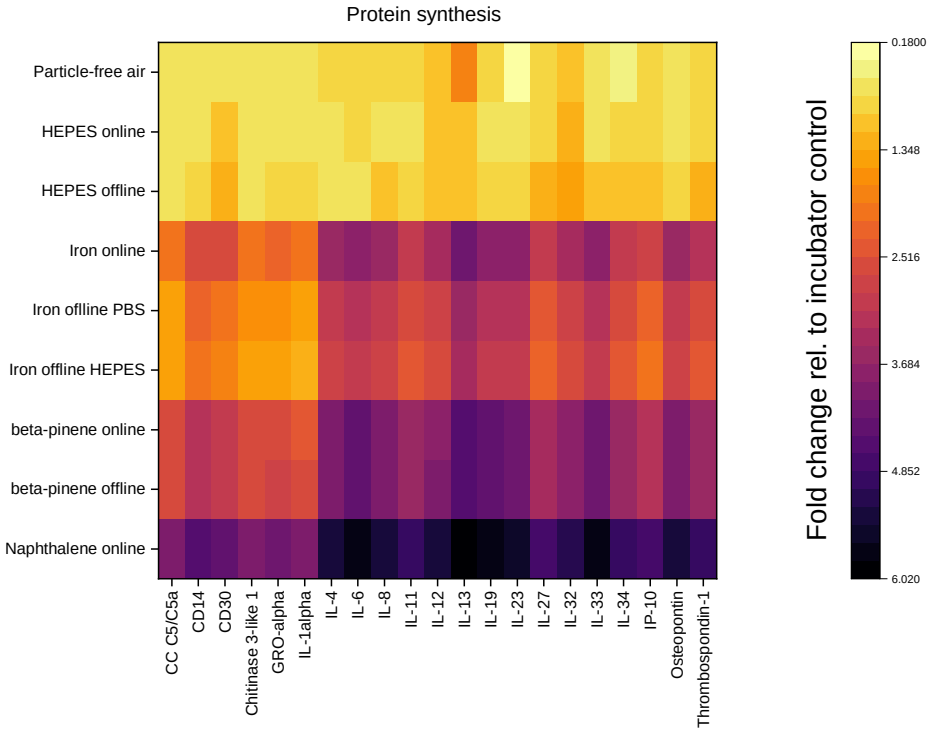

Figure 54: Heat map of protein synthesis for selected proteins that are up-regulated during inflammation and oxidative stress.

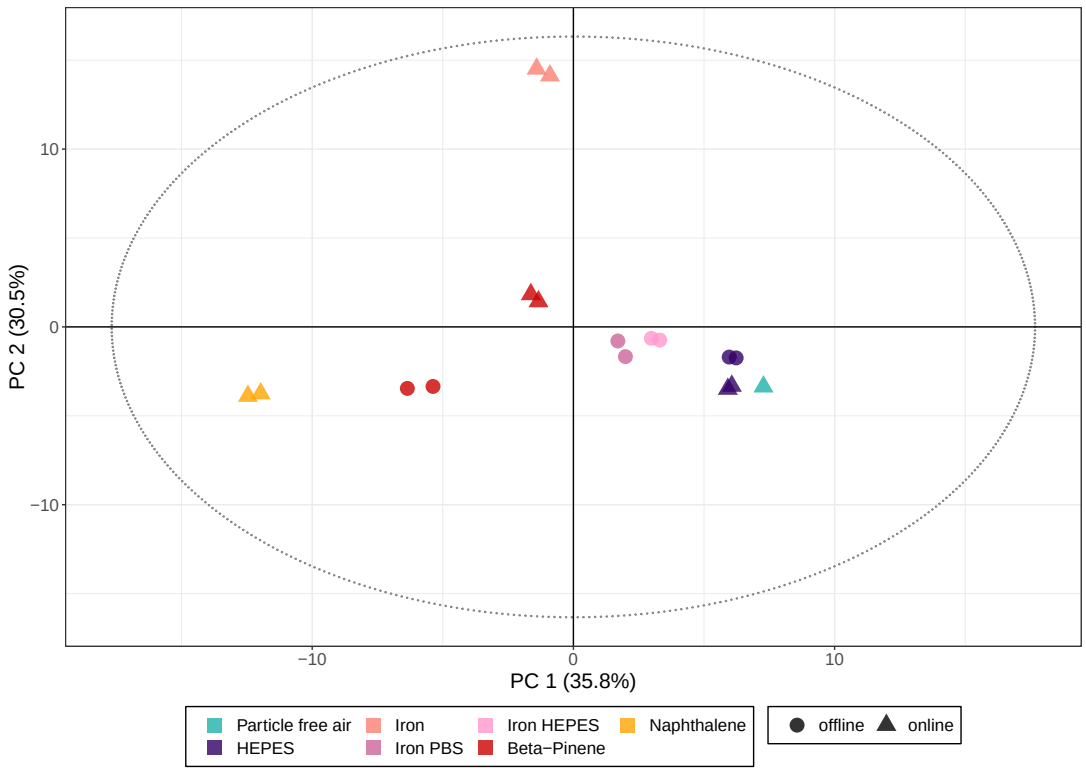

Figure 55: The same protein data as in Figure 54 but plotted as a PCA plot. The ellipse representing 95% of the Hotelling's T2 test.

Different types of aerosol have very different gene and protein expressions. In the LDH release, iron online is slightly higher than the β-pinene-SOA but lower than naphthalene-SOA, although naphthalene SOA has a very high variability. In gene expression analysis, iron has higher fold changes compared to SOA. Naphthalene-SOA has, as for LDH and also for gene expression, more up-regulated genes than β-pinene-SOA. For protein expression, naphthalene SOA again has more up-regulated proteins than β-pinene-SOA, but compared to gene expression, all iron experiments have lower fold changes for almost all selected proteins. So to summarize the biological experiments have more variables and it is difficult to investigate and understand these differences.
The general differences between the online and offline exposure of human epithelial lung cells were not as large as for the OP measurement. Although there are small differences indicating that there might also a variability between the two exposure methods.In particular, the PCA plots show differences for online and offline cell exposures leading to the assumption that the deposition method makes a difference in representing the true biological effects and potential toxicity of the aerosol particles.
All the statements made above were only looking at all genes and proteins that are taking part in an inflammation or an oxidative stress response in bulk, neglecting the individual pathways of the different genes and proteins. Because the focus of this thesis is on the chemical acellular assays and not the biological response, this interpretation would go beyond the scope of this work. In a publication in preparation (Campbell et al., 2023), a more detailed investigation of these biological data will be done.

3.4 Conclusion

In this chapter, the use of offline methods was discussed to measure ambient filters with offline acellular assays. Assay responses correlated with $PM_{2.5}$ mass concentrations, and demonstrated that there are seasonal variations that could be due not only to the different composition, but also to the different decay rates for different classes of compounds. Furthermore, we measured the oxidative potential (OP) of biogenic secondary organic aerosol (SOA) and quantified the decay of OP-active compounds using offline AA, DCFH, and DTT acellular assays. These experiments were used to estimate the half-life of OP active components biogenic SOA and it was shown that, depending on the assay, and therefore which

compounds were measured, 50-90% of the OP-active components in SOA decayed with a half-life of less than 20 h.
Furthermore, the offline method for the AA assay was compared with the online instruments. The OOPAAI has a signal up to a third higher than the immediately measured offline AA signal and even up to 80% higher after a week. These results clearly show that there is a need for an online instrument that continuously measures OP. In particular, they demonstrate the need to have a particle collection system that almost immediately captures particles into the acellular OP assay, capturing the rapidly decaying OP components. The addition of high time resolution allows us to capture dynamically evolving processes on short timescales, as well as detecting also very short-lived OP components, as described in Chapter 2.
To investigate whether there is also a large difference not only for acellular assays, but also for cellular assays between online and offline experiments, we exposed human epithelial lung cells to different aerosols. Compared to the OP and ROS measurements, there was not this clear decay between online and offline exposure, but we could show that the two exposure methods exhibit different responses in LDH, gene expression, and protein expression. It is important to consider these differences when designing experiments, as offline cellular exposure may not truly represent the toxicity of particles, due to the decay of reactive species in aquoeous particle extractions prior to cell exposure. Despite these findings, further investigations need to be done as many open questions remain regarding the mechanisms that lead to observed difference between online and offline cell exposure.

3.5 Outlook and Future Applications

To fully determine whether seasonal variability of OP and ROS is also due to the faster decay of some compounds compared to others, a time-resolved analysis of ambient filter samples would need to be done. But again, there is the same problem, that the vast majority of the decay is happening at the beginning of the storage time and that it is experimentally very challenging to collect ambient filters for only a very short time, with mass loadings sufficient to be detected by offline assays. On the one hand, this hypothesis might only modulate the seasonal difference in a minor way, because most of the OP signal already decays. However, if there are more stable OP-active compounds in one particular season (i.e. metals), then they would not have any effect on the OP measurements at all

compared to more labile SOA, and that could make a large difference. It is very difficult to disentangle the decay from the different reactivity of different aerosols compared to the decay because the decay is also dependent on the composition of the aerosol. In addition, the reactivity of different components within particles (See Chapter 5) also may influence OP and adds additional challenges to fully determine the role of chemical composition on OP. To gain more insight in future experiments, not only should different time points of ambient filters be measured, but also more compositional parameters and with more assays. More assays in give more information and should lead in theory to a better understanding, although increasing the parameter space, makes it also more complex to analyze. Therefore, for future experiments also source apportionments should be considered.

For the OP decay experiments, it would be interesting to try them not only with more assays (i.e. GSH, EPR), but also with different types of aerosols. The data shown in Figure 49 indicate that different SOA systems, but also other compounds, would have different decay rates. Moreover, it would be interesting to conduct these decay curves for more complex aerosol systems. In Figure 50 the difference between online and offline measurements is lower than for pure SOA systems, but still greater than for only transition metals. This indicates that for real-world aerosols, which contain a a lot of chemical compounds, the decay is possibly somewhere in between a strong decay of pure SOA systems with a very high decay, and transition metals with no decay.

Because the ultimate goal is not only to understand the toxicity of laboratory-generated aerosols, or even aerosol from a single emission source, but also from ambient aerosols. Hence, a decay curve for ambient filters would be very interesting to measure. Because we wanted to measure immediately after the aerosol generation and to use as little time as possible between particle generation and analysis, we generated SOA particles with high concentrations. To achieve this for ambient concentrations is particularly challenging as the mass concentrations are very low compared to laboratory-generated aerosol, and therefore we would need to collect for a very long time, defeating the purpose of measuring a decay rate because all the aerosol would already be aged on the filter. But it would definitely be very important to measure a decay curve for ambient aerosol. A possibility would be to measure in a very polluted area with a very high flow rate, so that the collection time could be minimized. Another approach would be to measure the long-term storage over time (e.g.

every month a measurement over a year from the same filter), but at least for the SOA we tested, it seems that the fastest decay occurs rapdily (minutes) after filter collection, so it is likely that this experiment would not give much insight in the decay of an ambient aerosol. In addition, aerosol OP decay in the ambient atmosphere might be different for different locations and seasons or with changing sources of longer time periods (i.e. more electric cars). All such factors might change the temporal stability of the particle OP. To avoid the frequent time-consuming determination of the decay characteristics of aerosol particles at specific locations and times, it would be much simpler and less prone to artifacts to measure with fast, online instruments as presented in Chapter 2 of this thesis.

For cellular assays, more data analysis would need to be performed on the different pathways to better understand the different effects of the different aerosols. Moreover, this could provide more insight as to why the online vs. offline deposition of particles has smaller biological effects than the concentration of OP-components in online vs. offline experiments. Furthermore, it would be beneficial to investigate more SOA systems, different transition metals, and real-world samples to gain a deeper insight and a better understanding of the toxicity of different aerosols.

4 Online Measurement of Reactive Oxygen Species and Oxidative Potential of Fresh and Aged Wood Burning and Gasoline Car Aerosols

This chapter is based on a manuscript in preparation that should be published in the near future.

Author Contribution

This work was carried out as part of the AeroHEALTH campaign in Kuopio, Finland.[188] The AeroHEALTH consortium was involved in this campaign and helped carry out the experiments, especially for the aerosol generation. All the experiments for AA were done by Battist Utinger. The experiments for DCFH were done by Alexandre Barth. The manuscript was written by Battist Utinger and Alexandre Barth. Markus Kalberer supervised the experiments and assisted with the manuscript.

Abstract

Air pollution is the single highest environmental health risk and has adverse effects on human health. In recent years, the importance of the oxidative potential as a metric of particle toxicity in air pollution has become increasingly recognized, as it is believed to play an important role in triggering negative health effects caused by air pollution particles. In this work, the impact of air pollution on human health is investigated, focusing on reactive oxygen species (ROS) and oxidative potential (OP) of aged and fresh wood burning and car exhaust particles. This was done by measuring the OP and ROS with two online instruments that characterized the particle toxicity of the different aerosols together with many other techniques at the aeroHEALTH campaign.

We could show that these novel instruments were capable of measuring the OP- and ROS-content of car exhaust and residential wood combustion emissions online and with a high time resolution of around 5 min. Both instruments did not measure any aerosol toxicity for primary car exhaust emissions, but a substantially signal for aged emissions, leading to the assumption that although there are no primary particles from the car exhaust emission, the secondary organic aerosols forming from the emitted volatile organic compounds have potentially significant toxicity. Different aging conditions lead to divergent OP and ROS measurements, showing that, depending on the assay and aging time, there may be a difference in the aerosol toxicity. Both instruments found that, per particle mass, aged wood burning has an order of magnitude higher toxicity than aged car exhaust particles. This suggests that aged wood burning is a major contributor to air pollution and may be more harmful than car exhaust to human health.

4.1 Introduction

There is a close connection between anthropogenic air pollution and various health effects, according to many different epidemiological studies.[20, 24, 47] Elevated levels of ambient aerosols have been associated with increased hospital admissions and deaths from a variety of diseases, including cancer, respiratory illness, and cardiovascular disease.[68, 118, 119, 120, 121] Air pollution is a complex mixture of gaseous and particulate substances that can have adverse effects on human health. This mixture is composed of both natural and anthropogenic components, with common sources including the burning of fossil fuels, traffic, industrial processes, and agricultural burning. The specific composition and concentrations of pollutants in air pollution can vary depending on a range of factors, including

local sources and meteorological conditions. Understanding the composition of air pollution and its potential health impacts is crucial for developing effective strategies to reduce exposure and protect public health.[12, 174] The WHO (World Health Organization) states in a recent report that air pollution is now recognized as the single largest environmental threat to human health and being a contributing factor of 7 million premature deaths per year.[25]
Despite the strong evidence linking air pollution to negative health outcomes, the specific mechanisms by which aerosol particles cause these effects are only poorly understood. Further research is needed to better understand the chemical and physical properties of aerosols that contribute to their negative health impacts.[31] One potential metric that might explain or contribute to particle toxicity, the oxidative potential (OP), refers to the ability of aerosol particle components to catalytically produce reactive oxygen species (ROS). ROS are highly reactive oxygen-containing molecules such as hydrogen peroxide, hydroxyl radicals, superoxide, and organic peroxides. These can be delivered exogenously via particle exposure or produced endogenously.[38] If present in excess and overwhelming the body's antioxidant capacity, they can damage cellular structures such as membranes, proteins, and DNA, leading to a variety of negative health effects. This phenomenon is generally described as oxidative stress.[189] In recent years, the importance of OP in air pollution has become more and more recognized, as it is believed to play an important role in the adverse health effects of air pollution. Measurements of oxidative potential can be used to assess potential health risks associated with different pollutants and help guide efforts to reduce air pollution and protect public health.
The mass concentrations of $PM_{2.5}$ were shown to be highly influenced by industry, traffic, and domestic fuel burning emissions. In certain regions (e.g., Canada, USA, western Europe), the contribution of secondary particles formed from anthropogenic sources can be as high as 62%.[190] $PM_{2.5}$ originating from anthropogenic sources has a higher oxidative potential than biogenic emissions. Especially during winter, most of the anthropogenic secondary organic aerosol (SOA) comes from biomass burning. At the same time, the OP by mass of anthropogenic SOA is three times higher, as a result of the contribution of the aged biomass burning aerosol, than that of biogenic SOA.[72]
Even at very low ambient concentrations of PM attributed to residential wood combustion (RWC), there is an observable health impact. Annual concentrations of RWC aerosol as low as $0.46\,\mu g/m^3$ can lead to a decrease in life expectancy of 0.1 years.[191] In large urban areas, vehicle exhaust emissions can produce

up to three times as much SOA compared to primary organic aerosol emissions. Extrapolating on a global scale, vehicle exhaust SOA could reach up to 16% of anthropogenic SOA emissions.[192] Studies have shown that the toxicity of exhaust particles thet a cellular level is caused by high mutagenicity or impairment of defense mechanisms.[174, 193, 194]

Traditionally, ROS and OP measurements have been based on the collection of PM filters and subsequent laboratory analysis. However, the time between sample collection and analysis can be significant, potentially leading to an underestimation of PM OP due to the instability of many ROS. Recent studies by Zhang et al., 2021[85] and Utinger et al., 2023 [97] showed that only a small fraction (<10%) of particle-bound ROS in organic aerosol collected on filters is stable on a time scale of up to a week compared to online *in situ* measurements, highlighting the need for rapid collection and analysis of particles. This requires capturing the chemistry of highly reactive aerosol components. Other studies have also shown short half-lives of unstable compounds such as radicals[89], peroxypinic acid[127], and hydroperoxides [128] ranging from minutes to hours. These findings indicate that new direct online measurement methods are needed that can provide immediate ROS and OP measurements.

In this study, the OP and ROS characteristics of two types of exhaust emissions were investigated. The emissions came from a EURO6 gasoline car, as well as a residential wood stove that uses beech wood as fuel. Furthermore, emissions were either sampled directly (primary) or passed through the Photochemical Emission Aging flow tube Reactor (PEAR) to simulate atmospheric aging (secondary) of several days.[195]

We used two recently developed online instruments to quantify OP and particle-bound ROS concentrations. The Online Oxidative Potential Ascorbic Acid Instrument (OOPAAI) measures the aerosol's OP using an online ascorbic acid assay as described by Utinger et al., 2023.[97] For the particle-bound ROS the Online Particle-Bound ROS Instrument (OPROSI) was operated.[95] These measurements allowed us to assess the potential health risks associated with exposure to pollutants emitted from these two sources and provide information on a potential link between atmospheric aging of particles and oxidative stress that leads to adverse health effects. Our measurements were part of the second AeroHEALTH campaign conducted at the University of Eastern Finland in Kuopio at the end of 2021. Our results show fast changes in ROS and OP in aerosol caused by changes in driving conditions or changes in the combustion conditions of the wood stove.

4.2 Material and Methods

Here only a brief overview of the whole campaign is given and only the important parts of this paper are discussed in more detail. More details on the entire AeroHEALTH campaign can be found in Czech et al., 2023 in preparation, and Paul et al.,2023 in preparation.

4.2.1 Reagents

All chemicals were obtained from Sigma-Aldrich unless otherwise indicated and were used without further purification unless otherwise indicated: ascorbic acid (99.0%), Dehydroascorbic acid (99.0%), 0.1 M HCL, 0.1 M NaOH solution, Chelex 100 sodium form, o-phenylenediamine ($\geq$99.5%), HEPES (4-(2-hydroxyethyl)-1-piperazineethanesulfonic acid, $\geq$99%), methanol (99.9%), peroxidase from horseradish (Type VI), DCFH-DA (2,7-Dichlorofluorescin diacetate, 97%), 3% hydrogen peroxide solution, 1 M PBS solution, zero grade air (Model 737–250, Aadco Instruments Inc., USA), N_2 gas (purity 99.999%). The H_2O used to prepare the solutions was purified with a high purification water unit (resistivity 18.2 MΩ/cm.

4.2.2 Chemical Preparation

All chemicals used in this study were made immediately before a measurement, except where otherwise specified. Pure water was additionally prepared using a fritted column and filled with 100 g Chelex 100 resin. The valve was adjusted to a flow of one drop per minute through the resin. The treatment was used to remove trace metals (i.e. copper and iron) from the water and ensure a stable and low transition metal-free background. Otherwise, there could have been an unwanted interference with the AA oxidation from the sample. AA solutions were prepared the night before the experiment in an effort to stabilize the background drift caused by the autooxidation of AA. A 200 mM HEPES stock solution was prepared monthly using chelexed water and stored in a glass bottle (Duran, Schott) in a refrigerator (4 °C). 8.8 mg of AA were dissolved in 25 mL HEPES stock solution and 225 mL chelexed water to form a 200 mM AA working solution. OPDA was prepared by dissolving 0.54 g in250 mL of 0.1 M hydrochloric acid to form a 20 mM working solution. Working solutions were stored in brown HDPE bottles (250 mL Nalgene, Merck) that were rinsed with hydrochloric acid to remove trace amounts of metals.

HRP stock solution was prepared weekly by dissolving 5000 units in 500 mL water and stored in a refrigerator (4 °C). DCFH-DA stock solution was prepared weekly by dissolving 50 mg DCFH-DA in 50 mL methanol and sonicating it for 15 s and stored in a freezer (−20 °C). HRP working solution was prepared using 100 mL of HRP stock solution, 100 mL of 1 M PBS, and 800 mL. DCFH working solution was prepared by letting 4 mL 0.1 M NaOH react with 4.872 mL of the DCFH-DA stock solution for 30 min in the dark. Subsequently, 100 mL of 1 M PBS and water were added to a total volume of 1 L. The HRP and DCFH working solutions were prepared the night before and stored in a refrigerator (4 °C).

4.2.3 Measurement Setup

In Figure 56 a schematic overview of the experimental setup is shown. This figure shows the complexity of the entire setup as well as which instruments and assays were used to quantify and characterize the aerosol toxicity.

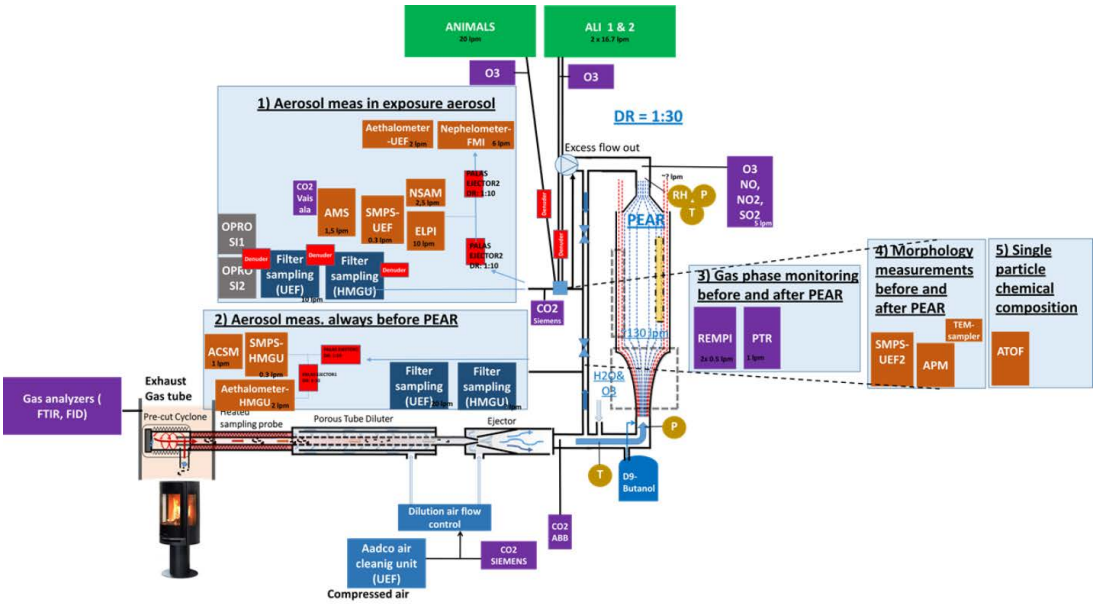

Figure 56: A schematic of the instruments used during the AeroHEALTH campaign. On the bottom left the aerosol emission source is shown (stove in this figure). The aerosol is sampled from the raw exhaust and size selected by a cyclone. It is then transferred to a two-stage dilution system first using a porous tube diluter following an ejection diluter. The aerosol continues to the photochemical emission aging flow tube reactor (PEAR). After the PEAR the aerosol was distributed to the different instruments and further diluted if necessary. For measurements of primary emissions, the PEAR was bypassed. Pictures adapted from campaign planning protocol and Ihalainen et al., 2019 [195]

In Figure 57 a simplified schematic of the instruments that were of interest for our measurements, as well as the important components of the sampling system, are

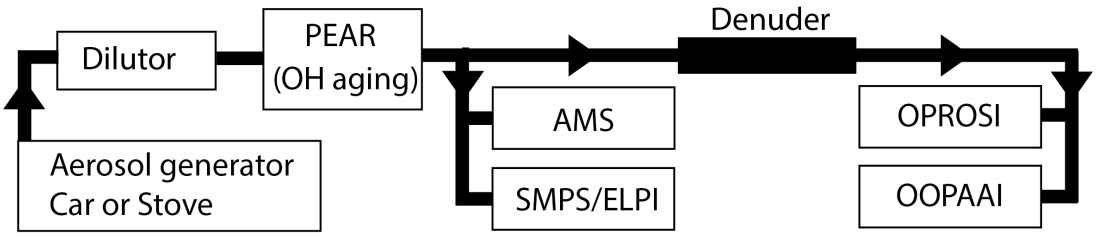

Figure 57: A simplified schematic of Figure 56 where only the components and analysis instruments that are important for this paper are shown. The aerosol is transported and diluted from the emission source to the PEAR and after further dilution and removal of reactive gas-phase components with a denuder, the aerosol was distributed to the different instruments.

shown. The OOPAAI and the OPROSI were sampling the aerosol from a 12 mm line after the PEAR. Due to very high particle concentrations during the wood stove experiments, an additional porous tube diluter was connected and set to a dilution ratio of 1:1.5 to 1:3, depending on experimental conditions. By passing the sample through a high efficiency particle arresting (HEPA) filter (HEPA-CAP150, Whatman), blank measurements during experiments were possible to check for background drifts or gas phase artifacts. Afterwards, two 1 m long home-built activated charcoal (untreated, granular, Sigma-Aldrich) denuders and one additional filled with 8 honey-comb shaped (Ionicon) were connected in line. This was necessary to remove any reactive gas-phase components (i.e. O_3 and organic gases). Having both instruments connected to the same denuders allows for a higher sample flow through them, reducing particle losses.
These losses were characterized at a later time using SOA produced via dark ozonolysis in a flow tube reactor. 0.3 L/min of synthetic air were passed over a heart-shaped flask filled with α-pinene. This flow was mixed with 4.7 L/min coming from an ozone-generating UV lamp (UVP LLC) into a 2.5 L glass flow tube. After the flow tube a dilution flow of 12-20 L/min was added. Similar mass and number concentrations as well as flow rates through the denuders were recreated compared to the aeroHEALTH campaign experiments. By comparing the particle number size distributiuons (SMPS measurements) before and after the denuders, the particle losses were determined to be approximately 10%. The charcoal was regenerated at 230 °C for 24 h every second day.
The key components of the AeroHEALTH campaign were as follows:

- **Aerosol generation (car or stove)**
  The aerosol emitted from the EURO6 gasoline car (Škoda Scala 2021) or

the residential wood stove (Aduro 9-3) was first passed through a cyclone inside the exhaust stream to remove large particles that are not of interest.

- **Dilution system**
  Flowing through a heated sampling line, a two-step dilution system reduced the concentration of the sampled aerosol particles. First in line was a porous tube diluter that could handle the high temperatures of the exhausts. The second was an ejection diluter. The dilution ratio was set at 1:17 during the car and 1:60 during the wood stove experiments. Primary emissions were directly sampled after this point.

- **Aging reactor**
  To simulate atmospheric aging, primary emissions were directed to the PEAR. The high-volume (139 L) cylindrical reactor produces OH by photolyzing ozone at UV light of 254 nm. The ozone concentration as well as the needed humidity are externally controlled and mixed with the aerosol prior to PEAR. With a residence time of approximately 1 min it was possible to achieve photochemical ages of up to 5 d.[195] To calculate the photochemical age, D9 butanol was introduced before the start of an experiment and its decay was measured.

- **Chemical and physical characterization**
  After the PEAR, numerous instruments measured particle and gas phase components. Separate dilutions were necessary in some cases to keep the concentration within the dynamic range of the respective instruments. To monitor the stability of the source as well, certain instruments measured primary emissions in parallel.

  - **Mass and number concentration measurements**
    Electrical Low Pressure Impactor (ELPI, Dekati) to measure the number and size distribution and the mass; Scanning Mobility Particle Sizer (SMPS, TSI) to quantify number and size distribution and the mass; Aerosol Particle Mass Analyzer (APM, Kanomax) for measuring the mass concentration; Nephelometer to measure the concentration of an aerosol.
  - **Morphology**
    Transmission electron microscopy (TEM) grid collection, Nanoparticle Surface Area Monitor (NSAM, TSI) to measure the surface area of nanoparticles.

- **Composition**
  Aethalometer (Magee Scientific) to quantify total organic and soot (black carbon) fractions; Areosol Mass Spectrometer (AMS, Aerodyne) for compositional characterization; Aerosol Time of Flight Mass Spectrometer (ATOF-MS, Photonion) for online characterization of the size and chemical composition of aerosols; Resonance-enhanced multi-photon ionization time-of-flight mass spectrometry (REMPI-TOF-MS, Photonion), to analyze trace species in the gas-phase; Aerosol Chemical Speciation Monitor (ACSM, Aerodyne), to measure the size, composition, and mass of individual aerosol particles; OPROSI (home-built) for online quantification of ROS; OOPAAI (home-built) to measure online OP.
- **Gas-phase**
  PTR-TOF-MS (PTR, Ionicon) to measure VOCs; O_3 analyzer (Model 49i Thermo Scientific); NO_x analyzer(Thermo Scientific); SO_2 analyzer (Thermo Scientific); Fourier Transform Infrared (FTIR, Gasmet) for the chemical composition of the VOCs.
- **Quartz and PTFE filter sampling for offline chemical analysis**.

- **Biological exposure**
  In addition, biological experiments were carried out using model cells. These were exposed using an Air Liquid Interface (ALI, Invitro Cell). Furthermore, the effects on mice were investigated.

  - **Cell cultures** BEAS-2B, bronchial epithelial cells from a human adenocarcinoma a model system for studying the lung biology; A459, a cell line derived from human lung carcinoma; triple culture, apical side: A549and dTHP1 (differentiated macrophages) basal side: MRC5 (fibroblasts).
  - **Animal models**
    Healthy mice; COPD-induced mice.

In Figure 57 a simplified schematic of the instruments that were of interest for our measurements, as well as the important components of the sampling system, are shown. The OOPAAI and the OPROSI were sampling the aerosol from a 12 mm line after the PEAR. Due to very high particle concentrations during the wood stove experiments, an additional porous tube diluter was connected and set to a

dilution ratio of 1:1.5 to 1:3, depending on experimental conditions. By passing the sample through a high efficiency particle arresting (HEPA) filter (HEPA-CAP150, Whatman), blank measurements during experiments were possible to check for background drifts or gas phase artifacts. Afterwards, two 1 m long home-built activated charcoal (untreated, granular, Sigma-Aldrich) denuders and one additional filled with 8 honey-comb shaped (Ionicon) were connected in line. This was necessary to remove any reactive gas-phase components (i.e. O_3 and organic gases). Having both instruments connected to the same denuders allows for a higher sample flow through them, reducing particle losses.
These losses were characterized at a later time using SOA produced via dark ozonolysis in a flow tube reactor. 0.3 L/min of synthetic air were passed over a heart-shaped flask filled with α-pinene. This flow was mixed with 4.7 L/min coming from an ozone-generating UV lamp (UVP LLC) into a 2.5 L glass flow tube. After the flow tube a dilution flow of 12-20 L/min was added. Similar mass and number concentrations as well as flow rates through the denuders were recreated compared to the aeroHEALTH campaign experiments. By comparing the particle number size distributiuons (SMPS measurements) before and after the denuders, the particle losses were determined to be approximately 10%. The charcoal was regenerated at 230 °C for 24 h every second day.

4.2.4 Car Cycles

The car was operated in four cycles of one hour for each experiment and twice per day with a 2 h pause in between. Every cycle consisted of five different driving conditions starting with 5 min and ending with 10 min of idling.

1. Idle for 5 min
2. 50 km/h for 15 min, 4^{th} gear
3. 100 km/h for 15 min, 5^{th} gear
4. 80 km/h for 15 min, 5^{th} gear
5. Idle for 10 min

Chemical blanks were measured in the morning before the experiments, between the two experiments (usually over lnuch time) and after the second experiment in the evening. Furthermore, HEPA blanks were measured during the experiment to characterize gas-phase contributions and denuder efficiency.

4.2.5 Wood Stove Burning

For the wood burning a first batch of beech wood (1.85 kg) was ignited. After 35 min 2 kg of wood was added. In total, six batches of beech wood were added in time intervals of 35 min. After the last addition, the wood was left to burn out under a condition called the ember phase for a total of 65 min. In total, one wood burning experiment lasted for 4 h.

4.2.6 Operation of the OOPAAI and OPROSI

The OPROSI was operated as described in Wragg et al., 2016 [95] and the OOPAAI as described in Chapter 2. Before each experiment, a blank was obtained for both instruments. For the OOPAAI, the instrument was started the evening before and the blank was run overnight. For the OPROSI the blank was started in the morning at least one hour before the experiment started. The filter in the particle collector for the OPROSI and the filter before the heating bath of the OOPAAI were changed daily to avoid excessive contamination from insoluble particles. During the wood burning experiments, this was done in the OPROSI between each 4 hour run.

4.2.7 Data Analysis

The data was first corrected for the blank drift. This was done by applying a fit across all blank measurements. This blank was then subtracted from the raw signal. If the drift was less pronounced in the OOPAAI for the car exhaust measurements, a linear fit was sufficient. However, for stronger drifts as for the RWC, the correction was done by a baseline correction using a B-spline function in OriginPRO (OriginLab 2023). For the OPROSI data, a 3rd order polynomial fit was used. The 1 s raw values from both instruments were averaged to 10 s to match the ELPI data, which was used to normalize the instrument signals for particle mass. A calibration was performed once per week to convert the raw signal to DHA and H_2O_2 equivalents. The data was then further normalized for mass or volume. The conversion is shown in Equation 7.[97, 99]

$$OP\left(\frac{\mu\text{mol}\,DHA}{\mu\text{g Aerosol}}\right) = \frac{Counts - Intercept}{Slope} DHA\big(\mu\text{M}\big)\, x \\ \frac{Liquid\,Flow\,Rate\left(\frac{ml}{min}\right)}{Gas\,Flow\,Rate\left(\frac{m^3}{min}\right)}\, x\, \frac{1}{Aerosol\,Mass\left(\frac{\mu g}{m^3}\right)} \tag{7}$$

The first term normalizes the counts of the spectrometer given by the OOPAAI into DHA via the DHA calibration curve. The second term normalizes the OP signal for volume via the liquid and gas flow rate of the OOPAAI. The third term normalizes for the mass of the aerosol. For the OPROSI the calculation is done analogously to Equation 7. Instead of DHA H_2O_2 equivalents are calculated.

4.3 Results and Discussion

The OOPAAI and the OPROSI were always measuring the same aerosol in parallel and for all experiments both results are shown and differences and similarities are discussed.

4.3.1 Car Exhaust

Time Resolution and Primary Aerosol

In Figure 58, blank corrected data of one measurement day is shown (signal intensity vs. time). For the primary aerosol, both the OOPAAI and the OPROSI could not detect any signal as can be seen during the first experiment in the morning (left side of Figure 58 from 08:00 to 12:00). As part of the EURO6 regulations, the car's exhaust system is fitted with a gasoline particulate filter (GPF). This reduced primary exhaust emissions to $<5\,\mu g/m^3$, thus possible particle OP and ROS are below the detection limit. However, other papers have shown a significantly higher aerosol mass without a GPF.[196] In contrast to the primary emissions, ROS and OP from secondary particle emissions in the afternoon were strongly enhanced compared to the blank. The fourth cycle during the secondary emissions was used as a blank measurement and signals decay back to blank values within 5-10 min. This shows that there were no gas-phase artifacts since both instruments were at the same level as during the chemical blank before the experiment.

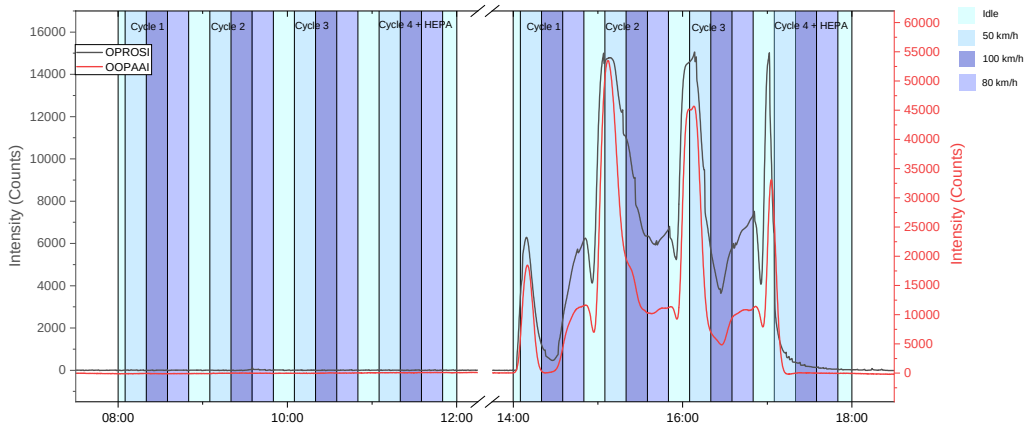

Figure 58: Blank-corrected signal intensities as time traces of the OOPAAI and OPROSI measuring OP and ROS in primary and secondary car emissions. The different colored markings correspond to the different conditions of the driving cycles. The primary car exhaust aerosol was measured from 08:00. to 12:00 where the last hour was a HEPA blank and the secondary aerosol was measured from 14:00 to 18:00 where the last hour was again a HEPA blank.

Volume Normalized OP and ROS Measurement in Secondary Emissions

OP and ROS measurements during aging experiments are given as volume normalized values, as can be seen in Figure 59. Although the instruments have different hardware components and run with different chemical assays, they show a very similar pattern for the driving cycle. Both also generally follow the particle mass very well (as measured by the ELPI and also shown in Figure 59), although they do not correlate all the time. The secondary emissions are known to consist only of SOA from gas-phase origins since there are no or only very few primary particles due to the GPF. Both instruments are sensitive to SOA, as shown in previous studies (see also Figure D.5 for the OOPAAI).[95, 97] The absolute values differ and a direct comparison is not possible because the exact composition of the aerosol is unknown due to its complexity. The OOPAAI is also sensitive to transition metals and other organic compounds in contrast to the OPROSI. Since there are only minor differences between the two instrument responses, it can be concluded that these compounds (i.e., metals) are only present in small concentrations in the tail pipe emissions. During the last hour of the experiment, a particle-free blank was measured. Even though the secondary emissions are still sampled, both instruments return to blank level, proving the efficiency of the denuders to remove any reactive gas-phase components.

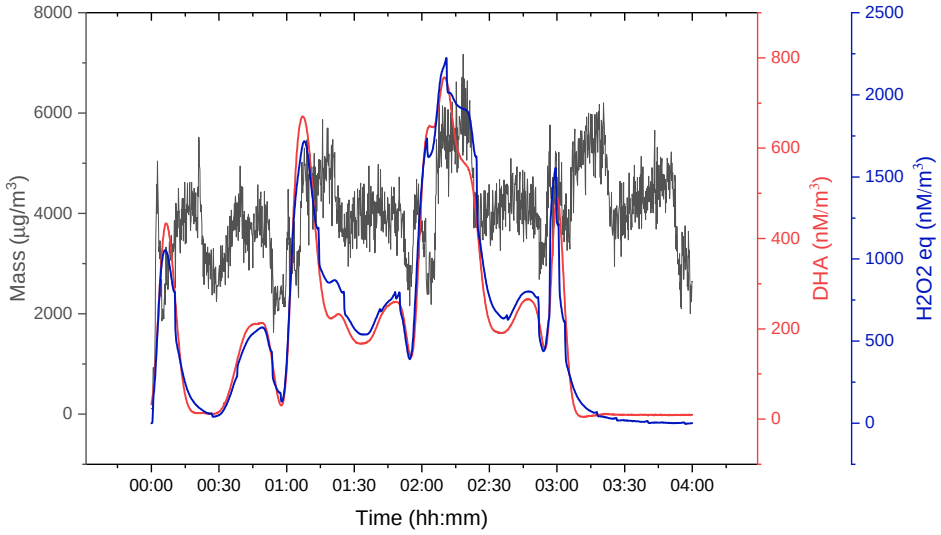

Figure 59: Volume normalized measurement of secondary car emissions. In black is the particle mass measured with the ELPI in µg/m^3. In red and blue the volume normalized signal of the OOPAAI and OPROSI in nM [DHA] m^{-3} and nM [H_2O_2] eq. m^{-3}, respectively. One experiment consisted of four repetitions of the driving cycle, but the last one was used for a particle-free blank to ensure proper operation of the charcoal denuders.

Different Photochemical Ages during Secondary Car Emissions

Two different aging conditions were investigated. A photochemical age of approximately 2 d was estimated for the "short aging". The "long aging" was equivalent to approximately 5 d. In Figure 60 the mass normalized values of all 15 cycles measured by the OOPAAI are averaged. The highest values are measured during the transition from idle to 50 km/h. All the other conditions are on a similar level with few differences. The transition from idle to 50 km/h also shows the highest variability. The intensities of the OP signal during cold starts at the beginning of an experiment, which usually have very high emissions of NO_x, CO, and total hydrocarbon (THC), are not distinguishable. Thus, they cannot be the reason for the variability. The highest agreement between all measurements is visible during the 80 km/h. This is especially the case for short aging (A). The differences between the two agings are otherwise only visible during the transition period during idle. Long aging (B) shows a trend of up to 40% higher for the OP measured with the OOPAAI but within the standard deviation of the different cycles. The other driving conditions show no change. There is also no significant

difference from the cold start to the other cycles when the motor is already warm. This could be due to the large amount of NO_x in the beginning that reduces the OH and O_3 concentrations and therefore the oxidation of the VOCs and eventually the formation of SOA and the aging of the aerosol.[197]
The ROS content as measured by the OPROSI is shown in Figure 61 with the same graphical presentation as in Figure 60. In general, both instruments observe the same pattern. The differences in ROS between driving conditions are similar to those in OP measured with the OOPAAI. The highest values are also observed during the transition from idle to 50 km/h. During 80 km/h the variability is the smallest. However, the increase at the beginning of 100 km/h is stronger. In contrast to the OP measured with the AA, the ROS signal was increased during short aging (A). The signals were 30-70% higher depending on the driving condition. The greatest increase is in the idle to 50 km/h period as well as at the beginning of 100 km/h. Zhang et al., 2021 [85] also measured an increase in OP_{DCFH} with longer aging times for two simple SOA systems (β-pinene and naphthalene as precursors). Another study by Platt et al., 2014 [198] showed for the ROS concentration a slight increase in the beginning for a two-stroke combustion system with higher photochemical ages.

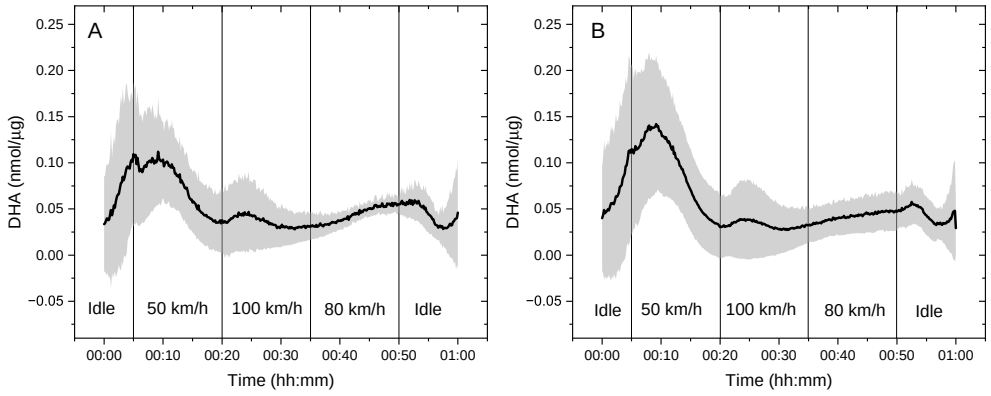

Figure 60: Mass-normalized OP from the OOPAAI 2 d (A) and 5 d (B) aging of car emissions. The average of 15 driving cycles is represented in one cycle. The error band shown is the standard deviation.

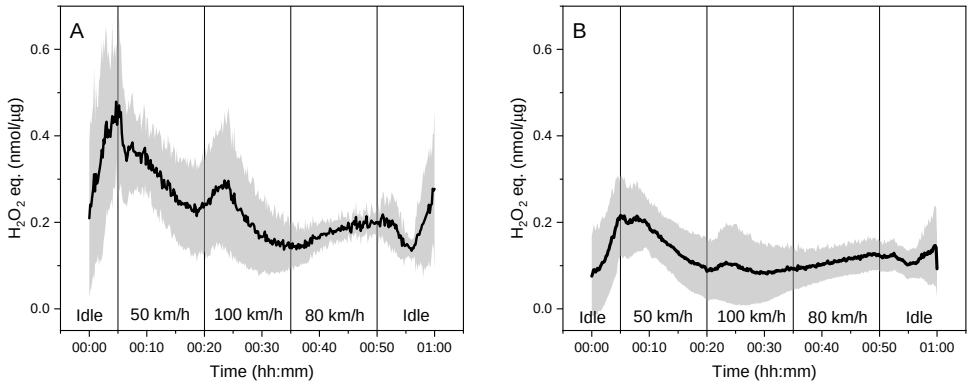

Figure 61: Mass-normalized ROS signal of the OPROSI 2 d (A) and 5 d (B) aging of car emissions. The average of 10 driving cycles for short aging and 11 cycles for long aging is represented in one cycle. The error band represents the standard deviation.

4.3.2 Residential Wood Combustion (RWC)

For the RWC experiment, the same measurements were performed. Primary emissions and two aging conditions for secondary emissions were investigated. Compared to the car experiments, the RWC results show a higher variability. This is observed by both instruments as well as in the particle mass concentration. This has already been shown in a variety of other experiments.[199, 200]

Primary and Secondary Residential Wood Combustion

The OOPAAI has a much stronger blank drift over the course of an RWC experiment compared to the car exhaust measurements. This drift is removed by the blank correction so not visible in the final data shown here, although it might be a source of larger errors. This continuous increase of the blank over time can be explained by the very high load of insoluble particles. Specifically, soot contamination accumulates inside the PILS and the liquid filter. This effect was reversible to some extent, meaning that the OOPAAI could return to normal operation. However, the time required for this was outside the practical range during the campaign. This strong drift caused difficulties for the blank calculation during data analysis. Due to the fit used for the correction, it can happen that the actual blank is underestimated or overestimated and therefore negative values are possible. Compared to the range of positive signals, these were negligible in absolute terms (see Figure 62). The OPROSI was similarly affected, but to a smaller extent. Unlike primary car emissions, both instruments show a response for primary RWC particles. The OOPAAI observes an increase of OP_{AA} over the

blank value. In Figure 62 blank corrected raw signal from the OOPAAI is shown for primary emissions in the morning (8:00-12:00) and for secondary emissions in the afternoon (14:00-18:00) as a comparison. The individual additions of pieces of wood to the fire are clearly resolved. Each increase and subsequent decrease is a new batch of wood. On the contrary, the OPROSI remains at blank level or shows negative signals for the primary emissions. This could be due to an artifact of the large soot content of the aerosol. Similar to the OOPAAI, the soot accumulates and potentially interacts with the assay. The high surface area of the soot could inactivate the reagents of the assay (e.g., HRP), disrupting the blank. Furthermore, the high content of antioxidant compounds frequently found in wood smoke could also cause a signal decrease.[201] To the authors' knowledge, no such effect is described in the literature, and further investigations would need to be carried out on a mechanistic level of the assays.

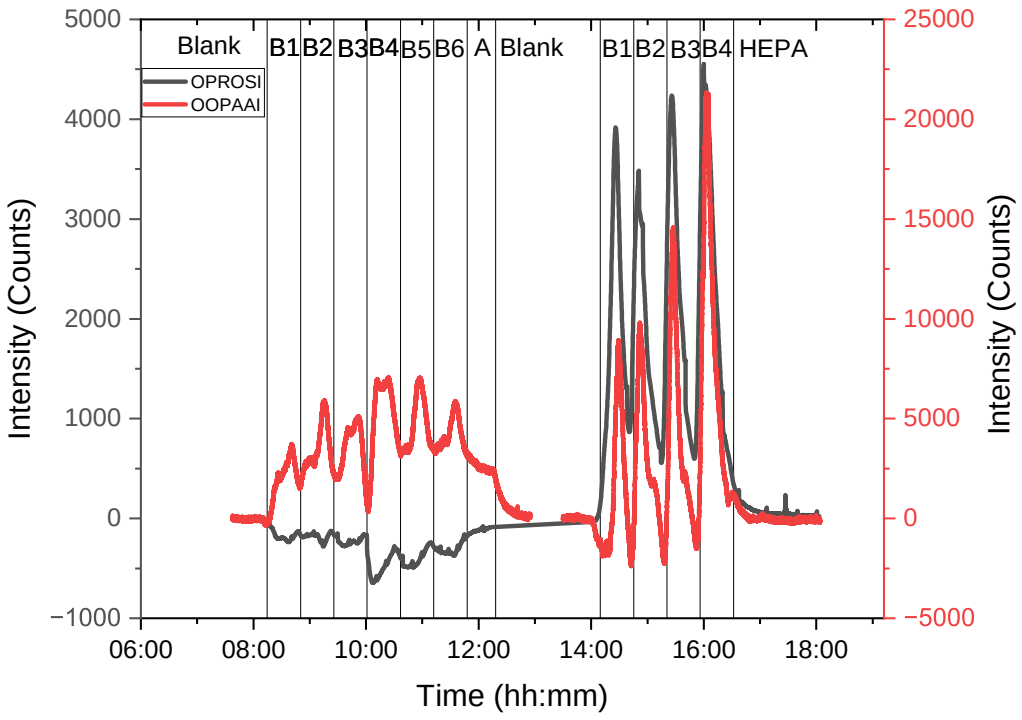

Figure 62: Blank-corrected raw counts as time traces of the OOPAAI measuring primary and secondary RWC. The data shown is not continuous. The two experiments (morning and afternoon) were performed on different days.

Volume Normalized OP Measurement of Fresh and Aged Residential Wood Combustion

In Figure 63 a typical set of volume normalized measurements of the OOPAAI and the OPROSI and the particle mass of the ELPI is shown. In contrast to the car exhaust measurements, the OOPAAI and the OPROSI measurements are not as congruent, leading to the assumption that the aerosol composition is more complex than for the car, where we can assume that we only measure SOA from not fully burned gasoline VOCs. Also, the OPROSI and the OOPAAI do not correlate as well with the particle mass as is the case for the car exhaust (see Figure 59). The mass of the aerosol in general is more variable in the stove as well as between individual batches. After six batches of RWC the amber phase started, where almost no aerosol was generated. The OOPAAI and the OPROSI show a similar pattern for the secondary aerosol, although the OOPAAI signal reaches blank level, due to its slightly higher time resolution.

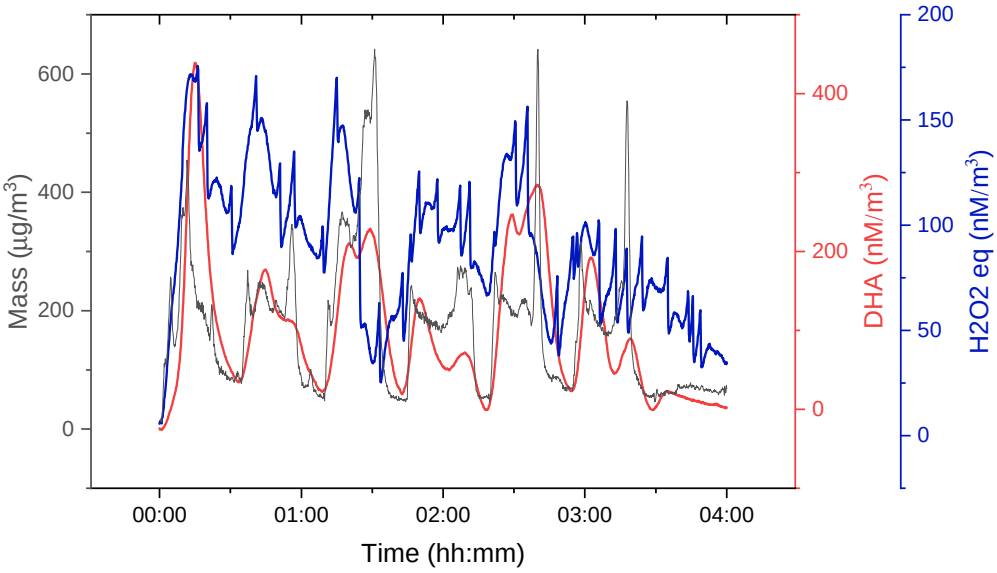

Figure 63: Volume normalized measurement of aged wood stove aerosol. In black is the particle mass measured with the ELPI in micrograms per cubic meter. In red, the volume normalized signal of the OOPAAI in nanomoles of DHA per cubic meter and in blue the OPROSI measurement in H_2O_2 equivalents per cubic meter.

RWC: Different Aging Conditions

For residential wood combustion, two different aging conditions were tested with a rather short aging of 1.4 ± 0.2 d and a longer aging of 3.3 ± 0.4 d. In Figure 64 the mass normalized average of the OOPAAI measurements of primary aerosol

and two different aging conditions are shown with the standard deviation as an error band. The amber phase is not considered in these figures. The primary aerosol shows aging similar to that of the short aging, but with less variability in the first phase of the batch. In contrast, the longer aging has a significantly lower OP signal and has less variability during the batch, meaning that the OP measurement per mass does not differ a lot from the total mass of the aerosol. For shorter aging, there is almost two times more OP signal for the second half than for the start of the batch. Variability between batches is also quite high for the second half of the batch (between 20-35 min), when the mass was generally lower. With these high variabilities, we cannot show a significant difference between aging conditions, although there is a trend that longer aging has a lower OP signal per mass. This might be due to decomposition or evaporation of some OP-active compounds during longer aging. For car exhaust, longer aging leads to higher OP signal per mass, which is a major difference compared to the residential wood burning particles. Therefore, depending on the VOC precursors, the concentration of oxidizing species (i.e. NO_x, OH, O_3), humidity and temperature of different aging times can have different outputs with respect to OP and ROS measurements. To get a better understanding of these very complex processes, more mechanistic experiments would need to be done.

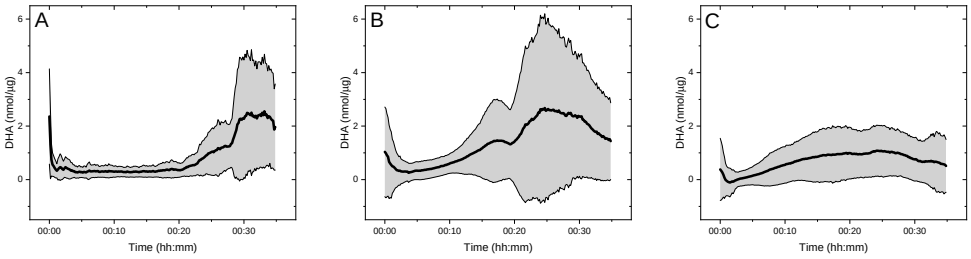

Figure 64: OOPAAI mass-normalized OP of primary, short, and long aging from wood burning. In (A) the average of 21 batches of primary aerosol from wood combustion. In (B) the average of 16 batches from wood burning from the mass normalized short aging experiments. In (C) 17 batches of wood burning, but with a longer aging. The error is plotted as an error band from the standard deviation of the different measurements.

In Figure 65 the same analysis is shown for the OPROSI as in Figure 64 but without the primary aerosol. The DCFH assay did not measure a signal above the blank level for the primary aerosol or sometimes even negative values. Values close to zero are not possible to mass normalize because the normalized value is then very large, which is a mathematical artifact. Compared to the OOPAAI, the short aging results in a lower signal for the OPROSI compared to the long

aging. The variability for the short aging is substantially lower than for the long aging, where the variability is very similar to the short aging of the OOPAAI. Hodshire et al., 2019 [202] show in a recent review that, for ambient but also for laboratory experiments, longer aging leads to increased oxidation. Also the aged soot particles can lead to a higher toxicity.[203] More oxidized aerosol is generally associated with higher oxidative potential. This is because the more oxidized an aerosol is, the more reactive it becomes.[85, 204, 205, 206] However, for certain SOA systems it is also observed that more aging (more oxidation) does not induce a higher oxidative potential / toxicity [68], as was also illustrated for the SOA particles of car exhaust shown in Figure 61.

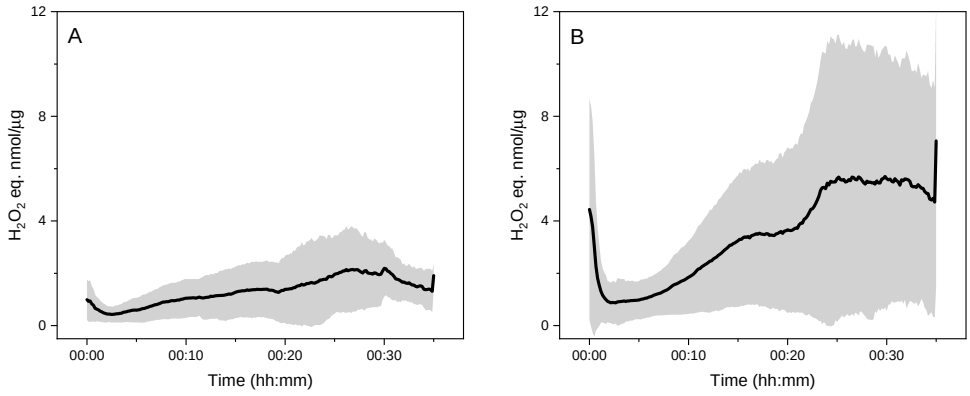

Figure 65: OPROSI mass-normalized ROS concentrations for short and long aging from wood burning. (A) Average of 16 batches of wood burning from the mass normalized short aging experiments. (B) 20 batches of wood burning but with longer aging. The variability between batches is plotted as an error band from the standard deviation of the different measurements.

4.3.3 Difference between Car Exhaust and RWC

Aged RWC aerosol leads for both assays to an order of magnitude higher mass normalized OP and ROS signal, respectively, compared to car exhaust, as can be seen in Figure 60 and Figure 61 compared to Figure 64 and Figure 65. There are some differences for the different aging times, but they are small compared to the compositional changes of the two different aerosol types. One possible explanation might be the higher content of polyaromatic hydrocarbons (PAHs) in wood smoke compared to car exhaust.[207] PAHs are known to be toxic [208] and also in Figure 77 and Figure 76 we could show that oxidized PAHs such as quinones lead to a high OP respectively ROS signal of the AA and DCFH assay. One of the dominant sources for PAHs are in many regions wood burning emissions.[209, 210] Gianelle et al., 2013 found that benzo(a)pyrene, a well known

toxic PAH, [211] is higher in RWC than car exhaust.[212] Brown et al.,2005 show a higher cancer potency and mutagenicity during the wood burning season, indicating that the higher PAH content also leads to a higher toxicity not only for acellular measurements, but also for cellular measurements and potentially disease development.[213]

4.4 Conclusion

It was possible to measure with both instruments a highly time-resolved OP and ROS signal for aged car emissions and primary and aged wood stove emissions. Furthermore, we could show that different aging conditions have adverse effects on different types of aerosol and their toxicity. For the OOPAAI longer aging leads to a slightly increased OP signal for car exhaust particle and a decreased OP signal for the RWC. For the OPROSI shorter aging leads to a higher ROS content for the car exhaust, but a smaller ROS signal for RWC. For both instruments, aged RWC gives an order of magnitude higher signal than the aged car exhaust, leading to the conclusion that RWC is more toxic than car exhaust. Compared to car exhaust, RWC has a higher content of PAHs which are especially in the oxidized forms as quinones well know to be very toxic.

4.5 Outlook and Future Applications

At the aeroHEALTH campaign many other measurements were performed, as shown in Figure 56. Unfortunately, not all of this data is yet analyzed and available. Once more data is available it would be nice to correlate the OP and the ROS signal also with other physical, chemical, and biological data to further investigate the results that we obtained with our measurements.
To better understand the chemical details that lead to these differences in a further analysis, the specific reactions of individual compounds with the assays should be investigated. The OOPAAI and the OPROSI measure only one integrated toxicity value for the very complex aerosol system. This is very helpful especially when correlating it with biological endpoints, but to understand mechanistic aspects, i.e., why one aerosol is more toxic than the other, more compounds-specific experiments and measurements need to be done. For SOA systems and transition metals, we tried to explore such mechanistic pathways better in Chapter 5. When all physical and especially chemical data is available form this campaign the differences in the OP/ROS data for emission sources with the different aging conditions should be further investigated with a more

chemical mechanistic approach to pinpoint the single components that lead to higher toxicity in the integrated OOPAAI or OPROSI signal.

For the cellular assays and the animal models it would be interesting to see if the biological measurements also see an order of magnitude higher toxicity for the RWC than for the car exhaust when normalized for particle mass. Furthermore, for the shorter and longer aging conditions it would be interesting if the biological measurements correlate better with the measurement performed with the OPROSI or the OOPAAI.
By combining all these measurements, a more complete analysis could be performed and more insight in the different mechanistic pathways of the toxicity of these emissions could be gained. It would be interesting not only to analyze further the data from this campaign, but also to compare it to other emission sources. We are also measuring emissions from an aircraft turbine and from a ship engine. Unfortunately, for this thesis, these experiments are still ongoing before submission, but for a further comparison of the RWC emissions and the car exhaust, we could gain a more complete insight by investigating these other emissions.

5 Iron and Copper Alter the Oxidative Potential of Secondary Organic Aerosol: Insights from Online Measurements, and Model Development

This chapter is a verbatim of a manuscript that is currently in the process of being submitted to Environmental Science & Technology

Author Contribution

Steven Campbell wrote most of the manuscript. Battist Utinger conducted all of the ascorbic acid measurements, operated the OOPAAI and analyzed the data and wrote minor parts of the manuscript. Alexandre Barth was operating the OPROSI and performing the data analysis for the DCFH. Steven Campbell was measuring the OH assay. Steven Campbell, Battist Utinger, and Alexandre Barth operated the aerosol generation. Suzanne Paulson and Steven Campbell developed and applied the kinetic model and Markus Kalberer supervised the experiments and assisted with the manuscript.

Abstract

The oxidative potential (OP) of particulate matter has been widely suggested as key metric describing atmospheric particle toxicity. OP measurements of ambient particles have demonstrated that secondary organic aerosol (SOA) and redox-active transition metals such as iron and copper are key drivers of particle OP. However, their relative contributions to OP, as well as the influence of metal-organic interactions and particulate chemistry on OP, remains uncertain. In this work, we simultaneously deploy two online instruments for the first time, providing robust quantification of particle OP. We utilize online AA (OP_{AA}) and 2,7-dichlorofluoroscein (OP_{DCFH}) instruments to investigate the influence of Fe(II) and Cu(II) on the OP of secondary organic aerosol (SOA).
In addition, we quantify OH production (OP_{OH}) from these particle mixtures in the presence of synthetic lung fluid (SLF). We observe a range of synergistic and antagonistic interactions when Fe(II) and Cu(II) are mixed with representative biogenic (β-pinene, BSOA) and anthropogenic (naphthalene, NSOA) SOA. A general decrease in OP_{DCFH} is observed when BSOA and NSOA are mixed with both Fe(II) and Cu(II). However, synergistic enhancements of OP_{AA} and OP_{OH} are observed when BSOA is mixed with Cu(II), and NSOA is mixed with Fe(II) and Cu(II). A newly developed kinetic model revealed some of the key reactions between BSOA and NSOA components, transition metals, and ascorbate (AH^-), driving OP_{AA}. Model predictions agree well with OP_{AA} measurements, highlighting that metal-ascorbate and naqthoquinone-ascrobate reactions are important drivers of OP_{AA}. The simultaneous application of multiple online OP methods, as well as a kinetic model, provides new insights into the interaction of SOA and metals and their influence on particle oxidative properties.

5.1 Introduction

Decades of large-scale epidemiological studies have consistently linked exposure to airborne particulate matter with an aerodynamic diameter $< 2.5\,\mu m$ (PM2.5) with adverse health outcomes.[20, 47] The World Health Organization recently updated guideline annual exposure limits for PM2.5 from $10\,\mu g/m^3$ to $5\,\mu g/m^3$. With this recent update, 99% of the world's population now live in places that exceed these guideline limits. However, the specific properties of particles which are most damaging to human health, such as their size, shape and chemical composition, and their mechanisms of toxicity upon exposure, remain largely uncertain.[31]

The promotion of oxidative stress, defined as an imbalance of the oxidant to antioxidant ratio in favor of the former, overwhelming the lung's natural antioxidant defenses upon particle deposition, has been widely suggested as a key mechanism describing particle toxicity. Reactive oxygen species (ROS), a term typically referring to the hydroxyl radical (OH), hydroperoxyl radical (HO_2), superoxide (O_2^{-}), hydrogen peroxide (H_2O_2), and in some cases including organic peroxides (ROOH) and organic radicals, are key drivers of oxidative stress.[214] The catalytic production of ROS by redox-active particle components with subsequent depletion of antioxidants is defined as oxidative potential (OP).[31]

There are a range of acellular chemical assays which are utilised to measure particle OP, including but not limited to; 2,7-dichlorofluoroscein (DCFH), the ascorbic acid (AA) assay, the terephthalate assay (TA) and the dithiothreitol (DTT) assay. These assays are sensitive to a broad range of chemical components which likely contribute to particle OP, including H_2O_2 and organic peroxides (DCFH), [94, 95] redox-active transition metals (DTT/AA), [33, 39, 215] water-soluble organic carbon (WSOC), quinones (DTT/AA) and hydroxyl radicals (TA).[83, 169, 216, 217] Several studies in the literature have demonstrated that total organic carbon (OC), [74, 175] as well as specific organic fractions including WSOC and secondary organic aerosol (SOA), [91, 92] quinones, [169, 216] and humic-like substances (HULIS), [218] as well as redox-active transition metals including Cu, Fe and Mn, [33, 39, 215] are key drivers of particle OP. However, only a few studies have probed the chemical interaction of these species.[215, 219, 220] Processes such as metal-organic ligand formation, influencing metal solubility and redox chemistry, [221, 222] and chemical reactions between organic aerosol components with metals, such as Fenton-like peroxide decomposition by Fe(II), [223] likely change the oxidative properties of these key species. Thus, metal-organic chemistry in particles likely influence the physical and chemical properties of PM, including OP, and subsequently the health implications of these particle components.

Traditional methods for measuring PM OP have largely relied on the collection of particle samples on filters, with analysis occurring typically several hours, days, weeks or even months after particle collection. Offline sampling may then underestimate OP, as highly reactive components such as organic peroxides can decompose prior to analysis.[94] In a recent study by Zhang et al.,2012 [85] we showed that up to 90% of particle-bound ROS are lost prior to offline analysis due to the $\sim$ 24 hour time delay between particle collection on a filter prior to analysis. This emphasizes the importance of online methods for robust quantification of

particle OP, in particular for SOA, which can be rich in organic peroxides that have a range of lifetimes from minutes to several days, depending on the peroxide molecular structure and multiphase loss processes at play.[177]
Recently, we developed an online methodology which can directly measure particle OP in situ, with immediate liquid extraction in the presence of the OP assay, and a time resolution of approximately 10 min. We have developed two iterations of this instrument; the Online Particle-bound ROS Instrument (OPROSI), [95] which utilises the DCFH assay, and the Online Oxidative Potential Ascorbic Acid Instrument (OOPAAI), [38, 97] another instrument version which adopts an ascorbic acid-based assay. These instruments allow highly time-resolved, accurate quantification of OP_{DCFH} (OPROSI) and OP_{AA} (OOPAAI), also capturing short-lived ROS and OP-active components which filter-based methods may miss and therefore underestimate. Thus, the simultaneous application of two unique online methods provides robust quantification of particle oxidative properties which contribute to particle OP.
In this work, we deploy the OPROSI and OOPAAI simultaneously for the first time, probing both online OP_{DCFH} and OP_{AA}. We investigate the effects of mixing redox-active transition metals (Fe(II), Cu(II), some of the most abundant metals in ambient aerosol particles) with biogenic (BSOA, using β-pinene as the precursor) and anthropogenic (NSOA, using naphthalene as the precursor) SOA particles. BSOA and NSOA have significantly different chemical composition, as well as originating from different sources in the atmosphere. In addition, OH measurements (OP_{OH}) were performed on filters collected simultaneously with online measurements. The metals produce a range of synergistic and antagonistic effects on OP_{DCFH}, OP_{AA}, and OP_{OH}. We also develop a detailed kinetic model, building on our previous work by Shen et al., [81] incorporating chemistry describing the reaction of naphthoquinones with ascorbic acid, ROS, Fe(II) and Cu(II), as well as organic peroxide chemistry.

5.2 Material and Methods

5.2.1 Reagents

Reagents were all purchased from Merck unless otherwise stated. L-ascorbic acid ($\geq$ 99%), L-dehydroascorbic acid, H2O2 solution (3%) Chelex 100 sodium form, 1 M HCl solution, 0.1 M NaOH solution, CuSO4 ($\geq$ 99%), FeSO4 ($\geq$ 99%), $Fe_2(SO4)_3$ ($\geq$ 98%), o-phenylenediamine ($\geq$ 99.5%), β-pinene (98%), naphthalene (98%), 1 M PBS solution, HEPES ($\geq$99.5%), horseradish peroxidase

(Type VI) and 2,7-dichlorofluoroscein diacetate (98%). Disodium terepthalate and 2-hydroxyterepthalic acid for OP_{OH} measurements were purchased from TCI (USA). All aqueous solutions were prepared using water obtained from a high-purity water unit (resistivity $\geq 18.2\,M\Omega/cm$). Ultra pure water was further purified by flowing through a 10 cm column packed with Chelex-resin at a flow rate of 1 drop per minute, to minimize background contributions from transition metals.[38]

5.2.2 Particle production and Online Measurement of Aerosol Particle OP DCFH and AA

Aerosol particles in this study were produced using a nebulizer (for Fe(II) an Cu(II) seed particle, and an organic coating unit (OCU) [170] for the production of BSOA and NSOA, which is described in detail in Section D.1 in the Supplementary Information. Particle masses were in the range of 320-408 $\mu g/m^3$ for SOA and 5 – 34 µg m-3 Fe(II) and Cu(II) nebulized aerosol particles (Table 3). Experiments where SOA and metals were mixed in the same mass range, with a ∼10:1 ratio for SOA:Fe(II), and a ∼50:1 SOA : Cu(II), aiming to broadly represent metal-SOA ratios observed in previous studies in polluted urban environments.[33, 224] For experiments involving mixtures of both SOA and metal particles, the particles are well mixed as opposed to two particle populations in parallel, as evidenced by the one mode observed in the particle size distribution in Figure 74.

Online measurements of aerosol particle OP were performed using two instruments developed within our group. The online particle bound ROS instrument (OPROSI), based on the chemistry of DCFH, and the Online Oxidative Potential Ascorbic Acid Instrument (OOPAAI), which is a modified version that utilises a fluorescence-based AA assay. Detailed descriptions of the instruments can be found in Wragg et al., 2016 [95] Campbell et al.[38] and Utinger et al., 2023 [97] Additional information is also given in Section D.2 and Section D.3 in the supplementary information, respectively, and a brief operational overview will be provided here.

The functionality, design and operating procedure for the OPROSI is extensively described in Wragg et al., 2016 [95] and Fuller et al., 2014 [94] Briefly, the aerosol samples are continuously drawn into the instrument through an activated charcoal denuder to remove gas phase artefacts such as VOCs, O3 and H_2O_2, [89] before entering a homebuilt particle sampler. Particles are collected onto a wetted filter continuously sprayed with a solution of horseradish peroxidase (HRP) in 10% PBS buffer, which immediately reacts with ROS present in the particles and is

collected in a 10 mL liquid reservoir. The HRP solution is then immediately mixed with 2,7-diclhorofluoroscein (DCFH), which is subsequently oxidized to form a fluorescent product DCF by the ROS-HRP solution in a reaction bath maintained at 37 °C for 15 min. DCF is then quantified via fluorescence spectroscopy. The fluorescence response of the instrument is calibrated with known concentrations of hydrogen peroxide (H_2O_2), and thus OP_{DCFH} concentrations are expressed in H_2O_2 equivalent concentrations per unit volume (per cubic meter) or per unit particle mass (per microgram). The assay has demonstrated sensitivity, in particular to hydrogen peroxides and organic peroxides.[94, 95]
The direct-to-liquid sampling and high time resolution of this instrument therefore is particularly sensitive to short-lived ROS components, which react within seconds after sampling with HRP.[94, 95] The OOPAAI is described in detail in Utinger et al., 2023 [97] and Section D.3 in the supplementary material. Particles are continuously measured using a commercial PILS (Brechtel, USA) and immediately sampled into a wash flow containing 200 µM Ascorbic acid (AA), where the particle AA mixture is reacted for 10 min at 37 °C in a heated bath. The OOPAAI measures OP_{AA} by quantifying the formation of dehydroascorbic acid (DHA), the dominant oxidation product of ascorbic acid (AA), by reacting DHA with o-phenylenediamine (OPDA) forming a fluorescent product 3-(1,2-dihydroxyethyl)-fluoro-[3,4-b]quinoxaline-1-one (DFQ), where we then quantify the concentration of DFQ using fluorescence spectroscopy ($\lambda_{ex} = 365$ nm), $\lambda_{em} = 430$ nm). The OOPAAI is calibrated using known concentrations of DHA, and hence the OP_{AA} here is then expressed in terms of nmol DHA per unit volume (m^{-3}) or unit mass (µg/m^3).

5.2.3 Offline Filter Collection

For the offline analysis, the aerosol particles were collected on PTFE membrane filters (Whatman, TE 35, 0.2 µm pore size) at a flow rate of 5 L/min. To reduce any background contamination, they were soaked and washed with methanol before use. The OCU was optimised to maximise the SOA output. All 5 lamps as well as the highest amount of VOC were in use. A total mass of 920 ± 166 µg was collected per filter. This resulted in a collection time of 20 min for the BSOA and 60 min for the NSOA samples. The loaded filters were stored at −20 °C after collection.

5.2.4 Quantification of OP from OH

Hydroxyl radical production (OP_{OH}) was quantified using the terephthalate probe (TA).[83] TA reacts selectively with OH to produce the highly fluorescent product 2-hydroxyterepthalate (hTA), which is then detected at $\lambda_{ex}/\lambda_{em}$ 320/420 nm. A 325 nm peak emission LED (M325F4, Thorlabs) is coupled to a cuvette cell (CVH100), using quartz cuvettes to ensure efficient UV transmission, and a QEpro (Ocean insight) high precision spectrometer to facilitate fluorescence detection. SOA samples were extracted into 10 nm TA at pH 6.8, in HEPES buffer containing 200 µM AA at particle concentrations equivalent to those sampled using the OPROSI and OOPAAI. Equivalent concentrations of $Fe(II)SO_4$ and $Cu(II)SO_4$ that were sampled by the OPROSI and OOPAAI experiments were added to SOA filter samples to probe the influence of SOA-metal mixtures on OP_{OH}.

5.2.5 Chemical Kinetics Model Development

The model describing iron, copper, ROS chemistry, hydroperoxide and quinone chemistry in the presence of AA is presented in Figure D.5 in the Supplementary Information. It includes 137 individual reactions, and builds on the previous model presented by Shen et al., 2021 [81] which describes the redox chemistry of ascorbic acid (AA) with ROS, Fe(II)/Fe(III) and Cu(I)/Cu(II). It also includes reactions describing the AA assay measuring DHA formation (OP_{AA}) as described in Campbell et al., 2019 which is used in this work.[38] In this study, we further developed the model by adding the following reactions; chemistry describing the reaction of naphthoquinones with ascorbic acid, ROS, Fe(III) and Cu(II), as well as organic peroxide chemistry, terephthalate probe reactions with OH, iron-HULIS complexation and subsequent reactions, based on the data presented in Gonzalez et al., 2018 [83] as well as HEPES and phosphate buffer chemistry (Figure D.5). Reactions and rate constants were synthesized from the literature and referenced appropriately in Figure D.5. The kinetic model is solved using the Kinetics Pre-Processor (KPP) version 2.2.3, [225] utilizing the Rosenbrock solver and gfortran compiler.

The model was run using the experimental conditions in the OOPAAI for each individual experiment. The pH was initially set at pH 7 and then equilibrated at pH 6.8 by using 10 mM HEPES buffer in the model input (R130-131, Figure D.5). The model was run at pH 6.8 for 10 minutes, and then at pH 2 for 2 minutes to simulate the experimental conditions in the OOPAAI as described in Shen et al., 2021 [81] and Campbell et al., 2019 [38] The majority of the rate

constants presented in Figure D.5 are determined at room temperature, whereas measurements using the OOPAAI are conducted at 37 °C, which may introduce uncertainty regarding model calculations.

5.3 Results and Discussion

5.3.1 Online OP from DCFH and AA of BSOA, NSOA Fe(II) and Cu(II)

OP_{DCFH}

OP_{DCFH} and OP_{AA} for individual BSOA, NSOA and transition metals are summarized in Figure 66. Representative online data is presented in Figure 75. NSOA shows almost a factor of two greater OP_{DCFH} compared to BSOA, with an OP_{DCFH} of 0.25 ± 0.01 nmol H_2O_2 equivalent µg-1 and 0.11 ± 0.02 nmol H_2O_2 equivalent µg-1, respectively (Figure 66A). This observation is in good agreement with our previous study investigating NSOA and BSOA using the OPROSI.[85] OP_{DCFH} observed previously for limonene and oleic acid SOA were 0.4 nmol and 0.58 nmol H_2O_2 equivalent µg-1, respectively.[94, 226] Therefore, SOA derived from different precursors of both biogenic and anthropogenic origin have substantially different OP_{DCFH}, with up to approximately a factor 3 difference depending on the SOA precursor. No online OP_{DCFH} signal was observed when nebulized Cu(II) or Fe(II) particles were sampled with the OPROSI, as the DCFH assay is predominantly sensitive to hydrogen peroxide and organic peroxides.[94, 95]

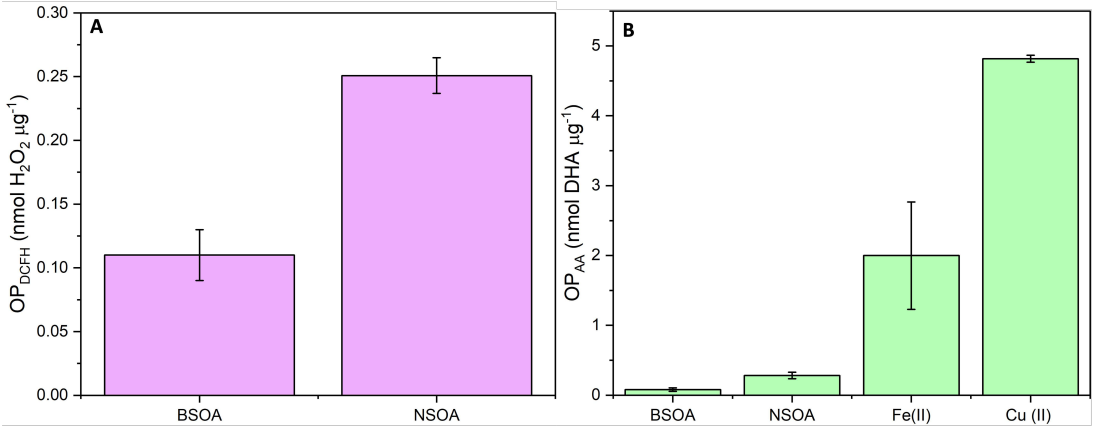

Figure 66: (A) OP_{DCFH} and (B) OP_{AA} values measured for BSOA, NSOA Fe(II) and Cu(II). Error bars represent standard deviation observed over three experimental repeats. For Cu(II) and Fe(II), no OP_{DCFH} signal was observed.

OP_{AA}

OP_{AA} values, expressed in nmol DHA μg^{-1}, are presented in Figure 66B. As is the case with OP_{DCFH}, higher intrinsic OP_{AA} is observed for NSOA (0.28 ± 0.05 nmolDHA/µg) compared to BSOA (0.08 ± 0.02 nmol DHA/µg). Increased NSOA activity for OP_{AA} may be due to the present of naphthoquinones in NSOA; Experiments where OP_{AA} was measured for metals and species which may be present in NSOA is shown in Figure 77, where 1,2-napthoquionone (1,2NQN), shows greater OP_{AA} compared to equivalent concentrations of peroxides, highlighting that quinones in NSOA may be key drivers of OP_{AA}. Redox active transition metals, particularly Fe(II) (1.99 ± 0.76 nmol DHA/µg) and Cu(II) (4.81 ± 0.22 nmol DHA/µg), exhibit an order of magnitude higher OP_{AA} compared to BSOA and NSOA. The sensitivity of the AA assay towards redox-active transition metals, in particular Fe(II) and Cu(II) has been well documented in previous studies.[33, 81] A recent study by Shen et al., 2021 [81] has suggested that redox-active transition metals catalytically react with AA (and ascorbate, AH^-, the dominant form of AA at pH 6.8), providing a pathway for direct oxidation of AH^- by transition metals such as Fe(III) (produced in these experiments from Fe(II) oxidation) and Cu(II), resulting in the formation of DHA, through the following reactions: [81]

$$Fe(III) + AH^- + O_2 \rightarrow Fe(III) + H_2O_2 + DHA - H^+ \quad k = 2.8 \times 10^6 M^{-1} s^{-1} \quad (8)$$

$$Cu(II) + AH^- + O_2 \rightarrow Cu(II) + H_2O_2 + DHA - H^+ \quad k = 4.7 \times 10^6 M^{-1} s^{-1} \quad (9)$$

Therefore, given the higher rate constant in Equation 9, enhanced direct DHA production is expected in the case of Cu(II) compared to Fe(II). According to model runs using visual MINTEQ (v.3.1) (Figure 78 and Figure 79), Fe(III) will exist almost entirely as the insoluble form $Fe(OH)_2^+$ at pH 6.8, which may further limit its ability to participate in Equation 8 compared to Cu(II).

5.3.2 Influence of Fe(II) and Cu(II) on OP from DCFH of NSOA and BSOA

We investigated the influence of mixing Fe(II) and Cu(II) seed particles with BSOA and NSOA on OP_{DCFH} and OP_{AA} using the OPROSI and OOPAAI,

respectively. For all measurements, the two instruments were run in parallel using the experimental apparatus described in Figure 73. Comparison of OP_{DCFH} for BSOA and NSOA mixed transition metal seeds is presented in Figure 67.

For both BSOA and NSOA, OP_{DCFH} activity generally decreases when both Fe(II) and Cu(II) seed particles are present. Compared to BSOA only (0.11 ± 0.02 nmol H_2O_2 equivalent/µg), the intrinsic mass-normalised OP_{DCFH} of BSOA + Cu(II) and BSOA + Fe(II) decreases (0.03 ± 0.006 , 0.06 ± 0.015 H_2O_2 equivalent /µg, respectively). The DCFH assay predominantly measures H_2O_2, organic hydroperoxides and organic peroxides.[94, 95] BSOA has been shown to be particularly rich in ROOH/ROOR.[227] Tong et al., 2018 [92] measured the yield of organic peroxides for BSOA and NSOA as 42 ± 24% and 19 ± 7%, respectively.

In addition, they reported mass normalised H_2O_2 production from BSOA and NSOA in H2O (5.47 ± 1.24, 0.67 ± 0.66 ng/µg, respectively) and in SLF (4.52 ± 0.08, 16.3 ± 4.4 ng/µg, respectively). Therefore, the observed decrease in OP_{DCFH} for BSOA and NSOA in the presence of Fe(II) and Cu(II) may well be due to the enhanced decomposition of H_2O_2, organic hydroperoxides (ROOH) and organic peroxides (ROOR) by Fenton-like reactions with Fe(II) and Cu(II).

We tested the OP_{DCFH} of a range of peroxide standards including cumene hydroperoxide, benzoyl peroxide and t-butyl hydroperoxide, commercially available peroxides that may act as surrogates for peroxides expected in BSOA and NSOA, and mixtures of these peroxides with Fe(II) and Cu(II) (Figure 76). A decrease in OP_{DCFH} is observed when organic peroxides are mixed with Fe(II) and Cu(II). Interestingly, a greater decrease in OP_{DCFH} is observed when peroxides are mixed with Cu(II) compared to Fe(II), in agreement with our observations for BSOA + Cu(II) (Figure 67). Cu(II) reactions with H_2O_2 (k = 480 M^{-1} s^{-1} [228] have been demonstrated to be faster than the Fenton reaction between Fe(II) (k = 78 M^{-1} s^{-1}) and H_2O_2, proceeding as follows:

$$Cu(II) + H_2O_2 \rightarrow Cu(I) + O_2^{\cdot -} - 2H^+ \quad k = 480 M^{-1} s^{-1} \tag{10}$$

$$Cu(I) + H_2O_2 \rightarrow OH^{\cdot} + OH^- - 2H^+ \quad k = 4.7 \times 10^3 M^{-1} s^{-1} \tag{11}$$

Therefore, enhanced peroxide decomposition via Cu(II) chemistry (liberating ROS, $O_2^{\cdot -}$ and OH) could explain the enhanced decrease of BSOA and NSOA OP_{DCFH}

of Cu(II) compared to Fe(II). There is limited literature data regarding the reaction of Cu(II) and Fe(II) Fenton-like reactions with larger organic peroxides or hydroperoxides. Fang et al., 2020 [223] demonstrated that ISOPOOH, a peroxide prevalent in isoprene-derived SOA, is rapidly consumed by Fe(II), at a rate substantially greater than for the Fenton reaction with H_2O_2 ($k \sim 4\times10^{10}$ M^{-1} s^{-1} compared to $k \sim 75$ M^{-1} s^{-1}

Thus, some organic peroxides present in BSOA may also exhibit similar enhanced Fenton-like reactivity towards Fe(II). It has also been demonstrated that Fe(II) reaction with organic peracids, which are common labile peroxides in BSOA, [127] is potentially rapid; for example, the rate constant for Fe(II) plus peracetic acid (PAA) is 5×10^{-4} M^{-1} s^{-1} [229] at circumneutral pH compared to that of Fe(II) + H_2O_2 (78 M^{-1} s^{-1}) [230] , likely due to (1) the lower ΔGf associated with Fe(II) + PAA (-299.8) compared to Fe(II) + H_2O_2 (-118.5), [229] (2) reduced bond energy of O-OH for PAA (90.4 kcal/mol) compared to H_2O_2 (88.4 kcal/mol) [229, 231] and (3) higher reduction potential of PAA (1.96 V) compared to H_2O_2 (1.76 V), thus making the Fe(II) + PAA Fenton-like reaction more favorable compared to Fe(II) + H_2O_2, a process which could also be at play here.[232, 233, 234] Given the higher rate constant between Cu(II) and H_2O_2, it is plausible that enhanced degradation of ROOR/ROOH in the presence of Cu(I) and Cu(II) would also be observed, thus resulting in enhanced decrease of particle-bound peroxides compared to Fe(II) (Figure 76).

Furthermore, NSOA formed via photooxidation is known to produce quinones and semiquinone radicals, which when extracted in water can react with O_2 to form superoxide ($O_2^{\cdot-}$) and therefore potentially produce more ROS compared to BSOA.[68] Similar to BSOA, the largest decrease in OP_{DCFH} is also observed when NSOA and Cu(II) are mixed, likely due to the enhanced destruction of both organic peroxides and H_2O_2 produced by NSOA by Cu(II) and Cu(I). Wang et al., 2018 [220] demonstrated using 1^H NMR that Cu(II) complexes with components present in photo oxidised NSOA, with dominant chemical components such as 1,2 naphthoquinone or 2,3 dihydroxy naphthalene, resulting in a decrease in DTT activity due to limited redox chemistry as a result of Cu(II) complexation.[220] This phenomena may explain the decrease in OP_{DCFH} observed here, where the ability of quinones and semiquinones to produce H_2O_2 is reduced as a result of Cu(II) complexation. Interestingly, a modest increase in OP_{DCFH} is observed when Fe(II) is mixed with NSOA. There are limited studies looking at the interaction of NSOA components with Fe(II) and Fe(III) directly. However, a few studies have investigated the chemistry of quinones and hydroquinones with Fe(II)/Fe(III);

Li et. al., 2012 [235] showed enhanced OH production from anthraquinone and Fe(II), likely due to enhanced redox cycling of semiquinone chemistry. Jiang et al., 2015 [236] demonstrated that Fe(III) interacts with 1,4 hydroquinone, producing semiquinone radicals, which can in turn produce ROS and H_2O_2, although under more acidic conditions (pH 5) than this study. In addition, Zanca et al., 2017 [237] measured the yield of humic-like substances (HULIS) in NSOA formed in a potential aerosol mass flow reactor (PAM) to be around 30%. HULIS has been shown to enhance the redox chemistry of Fe(II), [219] another process which may explain the enhanced ROS production from Fe(II) and NSOA.

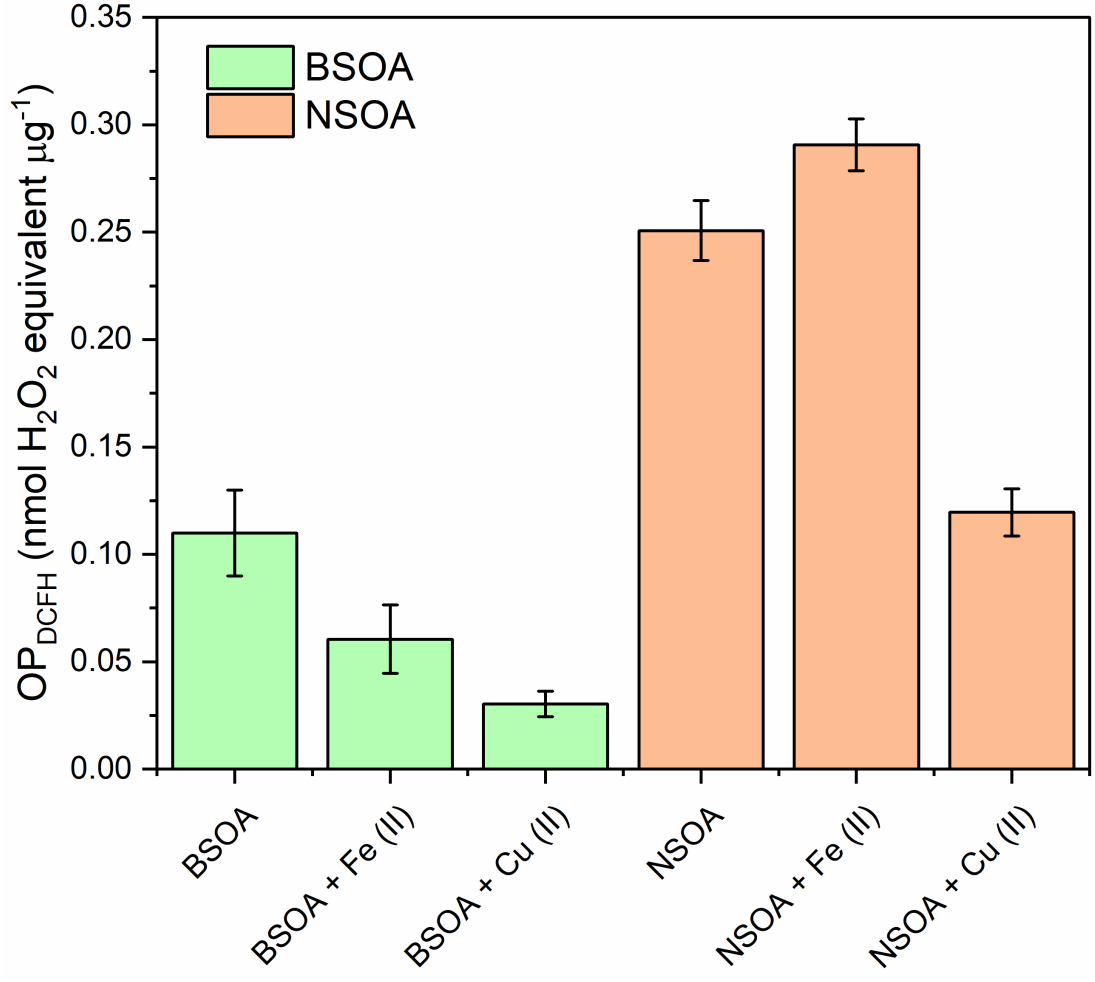

Figure 67: OP_{DCFH} for pure BSOA (green) and NSOA (orange), and mixtures of BSOA and NSOA with Fe(II) and Cu(II) seed particles. Error bars represent the standard deviation over four experimental repeats (BSOA and NSOA), and average signal observed over a 1-hour continuous online sampling period for SOA-metal mixtures.

5.3.3 Synergistic and Antagonistic Effects of Transition Metals on OP from AA and OH

In addition to online OP_{DCFH} measurements, the online OP_{AA} of Fe(II) and Cu(II) mixed with BSOA and NSOA was investigated. Results are presented in Figure 68, which shows the relative increase or decrease in OP_{AA} when a transition metal and SOA are mixed, relative to the sum of their individual OP_{AA}. Note that these values are not mass normalised, due to the much higher intrinsic OP_{AA} activity of Cu(II) and Fe(II) per mass compared to BSOA and NSOA (Figure 66). There are clear synergistic and antagonistic effects based on the transition metal, and the type of SOA. Suppression of BSOA OP_{AA} is observed when BSOA is mixed with Fe(II) (Figure 68), decreasing from 39.4 pmol DHA /min (combined sum of OP_{AA} for Fe(II) and BSOA, Figure 69A) to 29.7 pmol DHA /min when mixed. Complexation of Fe(II) with chemical components common in BSOA, such as carboxylic acids and aldehydes, may limit the redox activity of Fe(II) via complexation.[238] In contrast, a substantial increase in OP_{AA} is observed when Cu(II) seed particles are mixed with BSOA (345 pmol DHA /min) relative to the sum of the individual OP_{AA} of BSOA and Cu(II) (117.4 pmol DHA /min). This coincides with the greatest decrease in online OP_{DCFH} (Figure 67), where a decrease in OP_{DCFH} suggests that there is larger decrease in peroxide content in BSOA when Cu(II) is present compared to Fe(II). The reaction of Cu(II) with ROOH/ROOR present in BSOA may then produce hydroxyl radicals or other organic radicals via Fenton-like chemistry, potentially leading to a more pronounced increase in DHA formation (i.e., an increase in OP_{AA}). Enhanced AA loss and OH production has previously been observed for mixtures of Cu(II), H_2O_2 and AA.[239, 240] This may indicate that the reaction of Cu(II)/Cu(I) and ROOH/ROOR, in the presence of AA may enhance OH production and DHA formation. AA, and ascorbate (AH-), the deprotonated form of AA, which will be dominant form under the experimental conditions here (pH 7.4) is known to be relatively unreactive towards peroxides, [241] and may be even less sensitive to larger organic peroxides and hydroperoxides with increased steric hindrance. Therefore, the rapid conversion of peroxides to hydroxyl or alkoxyl radicals by Cu(II) in SOA liberates more reactive species which oxidize AH^- much more rapidly than peroxides, given the rate constant for $AH^- + H_2O_2$ ($k = 1.6\times10^{-2}$ $M^{-1}sec^{-1}$) [241] compared to that of $AH^- + OH$ ($k = 7.9 \times10^{-9}$ $M^{-1}sec^{-1}$), hence potentially increasing the OP_{AA} of the particles via enhanced anti-oxidant depletion. Cu(II) complexation may play an additional role here in enhancing AA loss, DHA production and OH production; Yan et al., 2022 [242] demonstrated

that Cu(II) mixed with water soluble organic carbon (WSOC) lead to enhanced OH production and AA loss, and Lin et al., 2020 [238] showed that mixtures of Cu(II) and complexing ligands such as citrate, malonate and oxalate also enhance OH production and AA loss. Therefore, the interaction of BSOA components and Cu(II) can potentially enhance the OP_{AA} of the particles. For NSOA, synergistic enhancements of OP_{AA} are observed for NSOA + Cu(II) and Fe(II). The greatest% enhancement is observed for NSOA + Fe(II), from 43.8 pmol/min to 77.3 pmol/min; this could be driven by interactions with quinones, or complexation with HULIS-like molecules formed during naphthalene photooxidation, which contain a range of functionalised aromatic moieties.[68, 219]Enhanced OP_{AA} is also observed when NSOA is mixed with Cu(II), increasing from 121.2 pmol DHA min^{-1} to 163.9 pmol DHA min^{-1}. In the case of Cu(II), enhanced decomposition of H_2O_2, which has been shown to be produced from NSOA upon extraction, by Cu(II) could increase OH production and hence OP_{AA}. In addition, the presence of organic ligands in NSOA such as naphthoquinones, hydroquinones or HULIS-like molecules in NSOA could enhance the redox potential of the metals themselves. For instance, this could enhance their direct oxidation pathways leading to DHA formation and AA degradation and hence an increased OP_{AA}.[81]

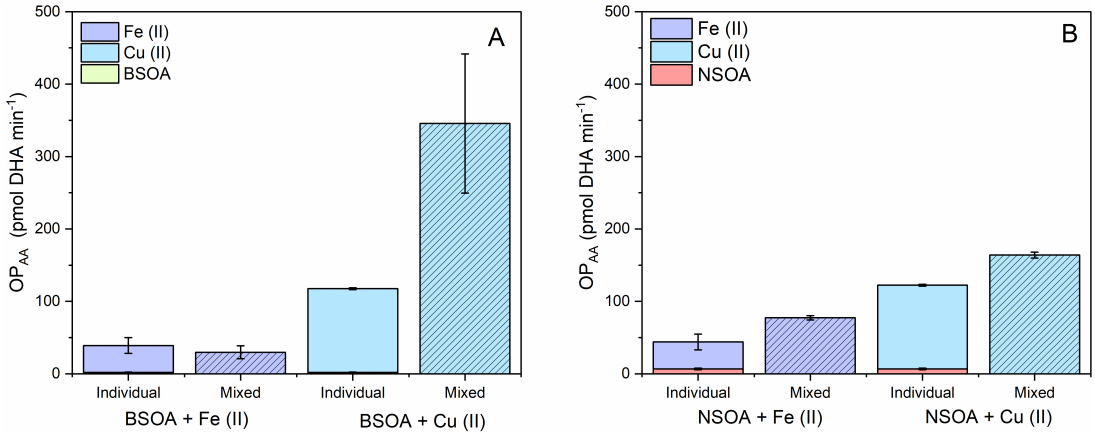

Figure 68: OP_{AA} for (A) BSOA and (B) NSOA, plus Fe(II) and Cu(II) seed particles, comparing the sum of the individual OP_{AA} responses of BSOA, NSOA, Fe(II) and Cu(II) (Figure 66B) with mixtures of SOA and metal seeds. Error bars represent the standard deviation of the online signal observed over 1-hour sampling.

For both BSOA and NSOA, we hypothesise that transition metals participate in Fenton-like chemistry with particle-phase peroxides, either formed during particle formation via VOC photooxidation, or with hydrogen peroxide which has been shown to be formed during BSOA and NSOA extraction in aqueous media.[92] The reaction of metals with peroxides liberates more reactive ROS species such as OH

and organic radicals, which leads to enhanced DHA formation, enhancing OP_{AA}. To test this, we also measured OP_{OH} from mixtures of BSOA and NSOA with Fe(II) and Cu(II)) all in the presence of AA. These experiments were conducted the same particle concentrations, AA concentrations and metal/SOA mixing ratios as for the OOPAAI measurements for each condition discussed earlier for a direct comparison, the results of which are presented in Figure 69A.

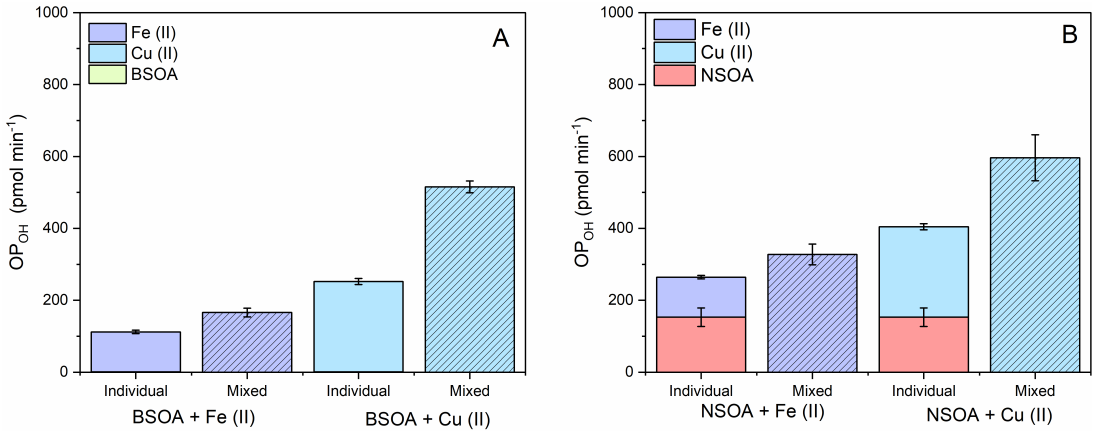

Figure 69: OP_{OH} measured for individual components and mixtures of (A) BSOA with Fe(II) and Cu(II) and (B) NSOA with Fe(II) and Cu(II), all in the presence of AA. Hatched lines indicate experiments where SOA and metal particles are mixed. Note BSOA only OP_{OH} values are substantially lower 0.7 ± 0.06 pmol/min than others plotted in this Figure. OP_{OH} experiments were performed at metal and SOA mass concentrations equivalent to OP_{AA} measurements.

OP_{OH} measurements are in broad agreement with observed OP_{AA} values. As was the case with OP_{AA}, we observe a synergistic enhancement of OP_{OH} for both BSOA and NSOA in the presence of transition metals, notably the redox-active Fe(II) and Cu(II). OP_{OH} for BSOA is substantially lower than NSOA, 0.07 ± 0.06 pmol/min compared to 153 ± 25 pmol/min, respectively. This result agrees with OP_{DCFH} and OP_{AA} of BSOA and NSOA (Figure 66). For BSOA, addition of Fe(II) and Cu(II) enhances OH production compared to the sum of their individual OH production rates in the presence of AA, with BSOA + Fe(II) + AA and BSOA + Cu(II) + AA OH production rates of 186 pmol/min and 515 ± 16 pmol/min respectively. Higher OP_{OH} production is also observed for NSOA + Fe(II) and Cu(II), with 327 ± 28 pmol/min and 596 ± 64 pmol/min respectively. OP_{OH} measurements are in broad agreement with OP_{AA} measurements, as well with decrease in OP_{DCFH}, which we hypothesise is likely due to decomposition of H_2O_2 and ROOH/ROOR from SOA by transition metals upon aqueous extraction, forming more OH and hence increasing OP_{OH}.

5.3.4 Kinetic Modeling of OP from AA

Modelling results and measurement data for DHA formation from AA oxidation (OP_{AA}) from BSOA, NSOA, Fe(II), Cu(II) and SOA-metal mixtures are presented in Figure 70. In addition, pie-charts within Figure 70 for each experimental condition indicate the contribution of key reactive species towards modelled OP_{AA}. Overall, the model is in relatively good agreement regarding measured OP_{AA} (i.e. DHA formation) especially for Fe(II) and Cu(II), as well as BSOA and NSOA (Figure 70).

Metals + AA: The model suggests that Fenton-like chemistry involving Fe(II)/Cu(I) + H_2O_2 → OH + OH- only plays a minor role promoting DHA formation, consistent with the study by Shen et al. 25 Instead, direct reactions of Fe(III), formed from Fe(II) oxidation, and Cu(II) with AH^-, the dominant deprotonated form at pH 7.4 are the dominant pathways for DHA formation (∼92%, ∼99%, respectively, Figure 70), via the catalytic reactions of ascorbate (AH-) under these reaction conditions.[223]

BSOA + AA: Production of DHA from BSOA in the model comes predominantly from OH formation from the homolysis of organic peroxides (ROOH), producing OH and the alkoxyl radical (RO);[92]

$$ROOH \rightarrow Ro^{\cdot} + OH^{\cdot} k = 0.0015 s^{-1} \tag{12}$$

OP_{AA} is very sensitive to the combination of the k assumed for Equation 12 and the assumed concentration of ROOH in the particle phase. It is well predicted by the model when considering the estimated first order rate constant k = 0.0015 s-1 and a ROOH yield of ∼80% (assuming an average molar mass of 205 g/mol for BSOA), which is within the range of reported ROOH yields of 30-90% previously observed in BSOA.[227] RO contributes substantially less to DHA formation in the BSOA model, despite being formed in equal amounts to OH; the rate constant of AA/AH- + RO (k = 1×10^{-4} 1/M sec) is orders of magnitude lower compared to that of AA/AH- + OH (k = 7.9×10^{-9} 1/M sec-71×10^{-10} 1/M sec.[243, 244]

NSOA + AA: The NSOA-specific model was built from an additional 16 reactions from the literature (R90-106, Figure D.5) and reported yields of 1,2NQN and 1,4NQN from naphthalene photooxidation.[169] The resulting model is in very good agreement with the OP_{AA} measurements, coming within about 95%. To the authors' knowledge, this model is the first to include the ascorbic acid and naphthoquinones specific to NSOA, including different rate constants for

quinone isomers and ascorbic acid/ascorbate. Direct reactions of quinones with AA/AH- dominate DHA formation; 1,2 naphthoquinone (1,2NQN) is responsible for ∼90% of DHA formation via the reactions of 1,2NQN with AA/AH-, producing the ascorbyl radical ($A^{\cdot-}$) which promptly undergoes disproportionation to form DHA (R12, R13, R90-100, Figure D.5). The reaction between AA and 1,4 naphthoquinone (1,4-NQN) contributes an additional 10% to DHA formation through an analogous mechanism to (1,2-NQN).

BSOA + AA + Fe(II): The model is less successful in reproducing the OP_{AA} measurements regarding Fe(II) + BSOA. The Fe(II) + BSOA model assumes Fenton-like reactions between ROOH present in BSOA and Fe(II) (R112, Figure D.5). However, OP_{AA} measurements (Figure 68) show that the OP_{AA} signal from Fe(II) + BSOA is less than the sum of OP_{AA} from Fe(II) and BSOA separately when Fe(II) and BSOA are mixed (Figure 68). Although the source of the discrepancy is not clear, the kinetic model does not consider complexation of Fe(II) by chelating organics present in BSOA, such as carboxylic acids and carbonyl groups, which have been shown to enhance and suppress Fe(II) redox activity. In addition, (di-)carboxylic acids such as pinic and pinonic acid are abundant oxidation products in BSOA.[238, 245] The interaction of these species with Fe(II) which is not included in the model, may explain this discrepancy.

NSOA + AA + Fe(II)/Cu(II): The model is in reasonably good agreement with OP_{AA} measurements for Fe(II) + NSOA, slightly underpredicting OP_{AA}. NSOA formed via photooxidation has been shown to contain large quantities of HULIS-like molecules, with yields reported up to 30%.[237] HULIS has been shown to complex Fe(II), enhancing the rate of redox reactions.[83] The model includes an estimate of Fe(II) complexation by HULIS-like molecules derived from experiments using Suwannee River Fulvic Acid (SRFA) as a surrogate for HULIS, as described in Gonzalez et al., 2018 [83] The enhanced Fenton chemistry associated with Fe(II)-HULIS + H_2O_2 (R120 Figure D.5) increases the contribution of OH contributions to DHA formation to 22% compared to 11% for Fe(II) only. This mechanism broadly describes the synergistic enhancement of the measured OP_{AA} of Fe(II) + NSOA, highlighting the potentially important role of metal-organic complexation regarding increased OP_{AA}. In contrast to Fe(II) + NSOA, for Cu(II) + NSOA the model underpredicts DHA formation and does not capture the synergy observed in the measurements, instead predicting a value that is essentially equal to the sum of Cu(II) and NSOA measured separately. The Cu(II) + NSOA model does not contain any HULIS-Cu(II) complexation, which

may influence Cu(II) redox chemistry in a manner analogous to Fe(II)-HULIS, however there is currently no literature data to describe this phenomenon.

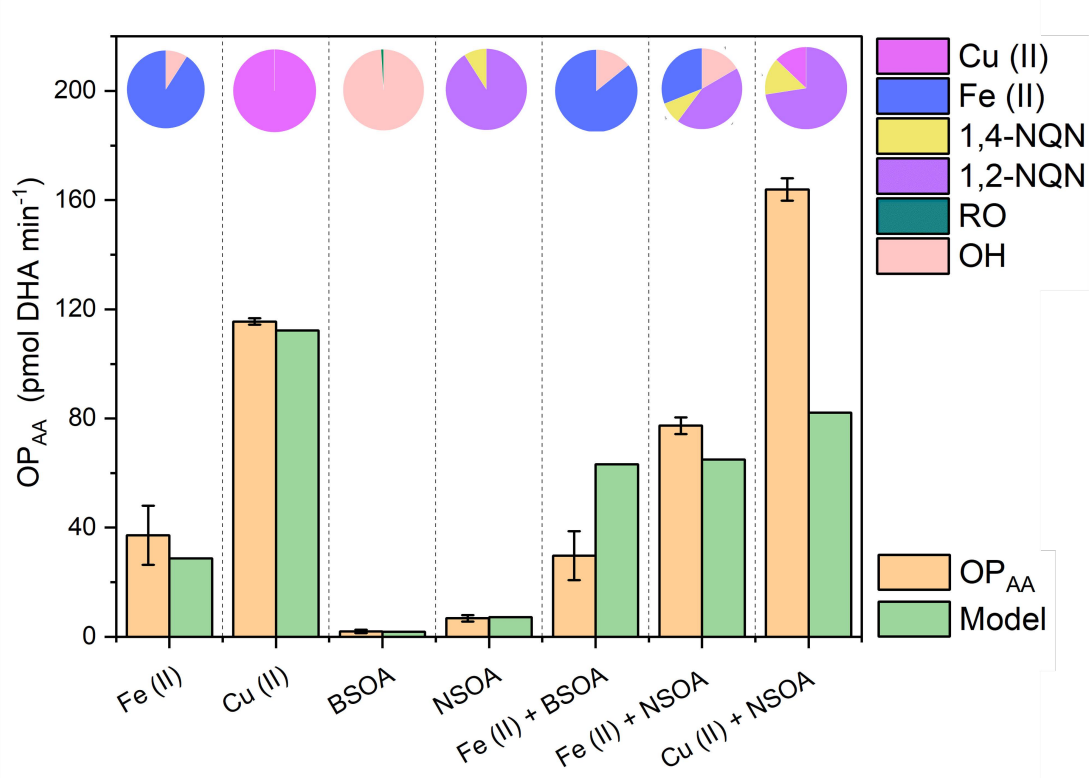

Figure 70: Comparison of OP_{AA} measurements (orange bars) with kinetic model results (green bars). Pie charts indicate relative contributions of key redox-active species in the model towards DHA formation.

5.4 Summary and Atmospheric Implications

The oxidative potential (OP) of particulate matter has been widely suggested as a key metric describing particle toxicity. The emergence of acellular OP assays has led to a rapid increase in research interest and application of OP measurements globally. In some cases, OP measurements outperform the policy standard of PM2.5 mass concentrations regarding prediction of health outcomes.[31] However, large uncertainty remains regarding the relationship between particle chemical composition, including particle-phase interactions of chemical species and aqueous-phase chemistry occurring in e.g. the lung, and OP. Developing our understanding of the relationship between aerosol chemical composition, often with unique emission sources, and OP is crucial in order to develop more source-specific air pollution mitigation strategies. In particular, understanding the chemical interactions of key components such as SOA and redox-active transition metals and their influence on OP is crucial. This is particularly important as contributions of

non-exhaust emissions, dominant sources of Cu and Fe in an urban environment, are predicted to steadily grow in the future due to increase in electric car use and lack of policy focused on non-exhaust emissions.[246]

This study presents the first simultaneous application of two online methods to quantify OP_{AA} and OP_{DCFH} in a laboratory setting, providing robust and accurate quantification of the oxidative properties of biogenic and anthropogenic SOA. The simultaneous application of online instruments capture rapid chemistry that traditional filter-based method may not fully characterize, particularly the reaction of labile and reactive peroxides, which our previous study shows decrease by up to 90% prior to offline analysis.[85] All assays show that NSOA, a surrogate for anthropogenic SOA, has intrinsically higher OP_{DCFH}, OP_{AA} and OP_{OH}, in agreement with our previous studies.[71, 85]

OP_{DCFH} measurements indicate the enhanced destruction of organic peroxides by redox-active Fe(II) and Cu(II) chemistry, leading to a decrease in OP_{DCFH} in both BSOA and NSOA. Complimentary online OP_{AA} and filter based OP_{OH} measurements show synergistic enhancements of OP_{AA} when SOA is mixed with Fe(II) and Cu(II). Interestingly, OP_{AA} and OP_{OH} are particularly enhanced when Cu(II) is mixed with BSOA. A decrease in OP_{DCFH}, which predominantly measures organic peroxides, would suggest that decomposition of peroxides by Cu(II) liberates more reactive species such as $O_2^{\cdot-}$ and OH, which oxidise AH^- faster than peroxides, therefore leading to an increase in OP_{AA} and OP_{OH}.

Our kinetic model provides additional insight into the mechanisms that lead to observed OP_{AA} for SOA, Fe(II), Cu(II) and metal-SOA mixtures, where in general the model is in good agreement with OP_{AA} measurements; model results suggest that the direct reactions of Fe(II)/Fe(III) and Cu(II), as well as 1,2-NQN with AH^- are key contributors to OP_{AA}. Fe(II)-HULIS reactions may be at least partially responsible for observed enhancement of OP_{AA} and OP_{OH} when Fe(II) and NSOA are mixed. The key results of this study demonstrate that the interaction of Fe(II) and Cu(II) with NSOA and BSOA results in a range of synergistic and antagonistic enhancements. Furthering our understanding of key chemical mechanisms that influence OP will provide vital information regarding the influence of chemical composition on OP and hence health relevant properties of particles, helping to build towards more targeted and efficient air pollution mitigation strategies.

5.5 Outlook and Future Applications

With the OPROSI and the OOPAAI and the OH assay we could show synergistic and antagonistic effects when SOA and transition metal are mixed. The OOPAAI can also be used to investigate mechanistic effects, especially if it is combined with other assays. The AA assay is sensitive to a lot of different compounds, so even with simply aerosol systems it is quite hard to identify the single mechanistic pathways. Therefore, for future studies looking at mechanistic effects, it would be important to include other assays that can measure single pathways and single compounds, such as the OH assay. It might also be interesting to combine these results with other bottom-up measurement techniques such as mass-spectrometry to correlate compositional information of the aerosol with these integrated OP results. Another future improvement of this study could also be to measure with another OP assay such as DTT, which is more sensitive to other compounds such as quinones and therefore might give other insights into the mechanistic pathways.

Furthermore, it would also be crucial to investigate more aerosol systems and their combinations of SOA and transition metals to gain a better understanding of these synergistic and antagonistic effects. For future experiments, real-world aerosols such as combustion could also be a possibility to mix with SOA or metals to investigate the enhancing effects that might occur.

For the model, more reactions could be incorporated to improve it, so that it is in even better agreement with the measurements. Also, it could be expanded respectively redeveloped to other OP assays, such as the DCFH assay, which was also used in this study. Moreover, more experiments should be performed to better estimate the rate constants. Especially for this model, it would be useful to have them under physiologically relevant conditions (37 °C and $\sim$ pH 7).

6 Summary, Conclusion and Outlook

Despite of a vast amount research there are still many uncertainties regarding the composition of aerosols and how to measure their toxicity for human health. The research conducted in this thesis was motivated by the hypothesis that many OP-active and thus potentially toxic aerosol components may be short-lived and hence are underestimated by classical analysis methods. Thus an analytical method needs to be developed that is fast (i.e. sec-min) to explore the lifetime of OP and quantify the losses for the entire OP concentrations.
An instrument that can measure OP with a high time resolution and in the ambient atmosphere would be highly advantageous because conditions are often changing quickly in the atmosphere such as changes in wind direction or rush hours. To understand the evolution of OP and its sources, a high time resolution is highly desirable, because many other instrument that measures changes in the atmosphere have a time resolutions of seconds to minutes, which would making it easier to correlate and compare OP and other measurements. Such an instrument should reflect the antioxidant defense of the human lung as closely as possible with respect to chemical reactivity in terms of assay, pH and temperature, but also for the kinetics of the reaction time to mimic the biology in the human lung as closely as possible.
Therefore, we developed a novel instrument with high time resolution and physiological assay and characterized it. Various laboratory-generated aerosols, from model systems to real-world emissions, were measured. Additionally, ambient aerosols were investigated and correlated with aerosol mass measurements. Furthermore, various campaigns were conducted with this novel instrument. The key findings and future applications of that work are presented extensively at the end of each chapter in the corresponding conclusion and outlook sections. Here, only a brief summary of the most important points of each chapter is made.

Chapter 2

In this chapter, we presented the development of a novel, portable, online instrument that can measure laboratory and ambient aerosol with a high time resolution physiological relevant assay. The online oxidative potential ascorbic acid instrument (OOPAAI) is working under a physiological pH of 6.8 and using an physiological relevant anti-oxidant, ascorbic acid, as a proxy to quantify the oxidative potential of aerosol particles. This is done using a modified particle into liquid sampler that can collect aerosols in an efficient way with a high yield. The

detection of the oxidized ascorbic acid is done via a specific fluorescent detection approach with a home-built flow cell that can collect the emitted fluorescence light in an optimized way resulting in a good signal-to-noise ratio. The OOPAAI can measure stable and automated over several days.
The OOPAAI was used to measure many different aerosols generated in the laboratory, such as different transition metals, biogenic and anthropogenic secondary organic aerosols, and also mixtures of them. Furthermore, we measured also real-world emissions from car exhaust and residential wood burning (see Chapter 4). These different emissions were measured as primary aerosol, and as secondary, oxidized aerosol. We measured with the OOPAAI ambient aerosol with a detection limit of $5\,\mu g/m^3$.

The OOPAAI is still a prototype and for future work there are a lot of details that could be improved such as a better temperature controlled compartment or a even further improved optical system. For measurements and campaigns, it would be very interesting to measure more lab aerosols of different sources and composition and investigate more mechanistic details of the oxidation reaction of AA by OP active substances. Furthermore, more emission sources and different atmospheric aging conditions could be investigated and correlated to other OP metrics, physical parameters, or biological end points. For ambient measurements, longer measurement campaigns would be interesting where also the composition of the aerosol is monitored in parallel, to gain a deeper understanding which parts of the aerosol are actually contributing to the OP metric measured by the OOPAAI in the ambient particles.

Chapter 3
In this chapter, the decay of offline measured compounds was characterized showing that a large fraction of reactive compounds is lost when the OP measurements are carried out on the offline filters compared to online analysis with the OOPAAI. These experiments were done with not only the ascorbic acid assay but also with DTT and DCFH which showed a similar decay trend for biogenic SOA. Moreover, we could show that there is also a significant decay for the real world emissions of car exhaust and residential wood combustion. Furthermore, we investigated human epithelial lung cells with various different aerosols in order to determine whether there is also a significant difference between online and offline experiments for cellular assays and not only for acellular assays. Although the measurements for cellular systems were not as clear in the difference for online

and offline and we could not show a decay for SOA the different measurement methods seem to have different pathways that lead to different toxicological effects.

In the future, these decay experiments should also be performed with different aerosols and more complex aerosol systems preferably also with ambient aerosol. Another improvement would be if other acellular assays could be measured to better identifying the chemical nature and the sources of these short-lived OP compounds. Moreover, it would be important to further investigate the biological assays and end points to better understand the mechanistic pathways in biological systems from the different exposure techniques.

Chapter 4

In this chapter, we could show that the OOPAAI and the OPROSI are capable of measuring real-world and fast-changing emissions from car exhaust and residential wood combustion with a high time resolution. Furthermore, we could show that various aging conditions have other effects on different aerosol types and their toxicity. For both assays, the residential wood combustion gives an order of magnitude higher OP, respectively ROS signal.

To investigate these differences more closely between different aging conditions and different emissions sources, further investigations of the various measurements of this campaign could be done in future experiments. The OP and ROS signals should be correlated with not only the chemical composition data, but also with the various biological experiments conducted in this study.

Chapter 5

This chapter highlights the more mechanistic investigations that can be performed with the OOPAAI. Developing our understanding of the relationship between aerosol chemical composition and OP is crucial in order to develop more source-specific air pollution mitigation strategies. In particular, understanding the chemical interactions of key components such as SOA and redox-active transition metals and their influence on OP is crucial. We measured SOA from different precursors and different transition metals and their mixtures and showed that synergistic or antagonistic effects can occur. Naphthalene SOA has a higher OP than β-pinene SOA for all the assays (AA, DCFH, OH) we used.

The AA and OH OP assays showed synergistic enhancement for transition metals and SOA, whereas the DCFH OP assay showed an antagonistic effect. The kinetic model performed in this study is in good agreement with our measurements. The better understanding of these synergistic and antagonistic effects provides vital information regarding the influence of chemical composition on OP and hence health relevant properties of particles, helping to find more targeted and efficient air pollution mitigation strategies.

7 References

[1] J. H. Seinfeld and S. N. Pandis, J. H. Seinfeld, and S. N. Pandis, *Atmospheric Chemistry and Physics: From Air Pollution to Climate Change SECOND EDITION*. 2006, pp. 628–674, ISBN: 9780471720171 (cit. on pp. 1, 5, 200).

[2] *Figure TS.7 — IPCC*. [Online]. Available: https://www.ipcc.ch/report/ar5/wg1/technical-summary/figts-07-2/ (cit. on p. 1).

[3] P. J. Beggs, „Environmental Allergens: from Asthma to Hay Fever and Beyond“, *Current Climate Change Reports*, vol. 1, no. 3, pp. 176–184, Sep. 2015, ISSN: 21986061. DOI: 10.1007/S40641-015-0018-2/FIGURES/3. [Online]. Available: https://link.springer.com/article/10.1007/s40641-015-0018-2 (cit. on p. 1).

[4] S. Tang *et al.*, „Aerosol transmission of SARS-CoV-2? Evidence, prevention and control“, *Environment International*, vol. 144, p. 106 039, Nov. 2020, ISSN: 0160-4120. DOI: 10.1016/J.ENVINT.2020.106039 (cit. on p. 1).

[5] W. W. Nazaroff, „Indoor aerosol science aspects of SARS-CoV-2 transmission“, *Indoor Air*, vol. 32, no. 1, Jan. 2022, ISSN: 16000668. DOI: 10.1111/INA.12970 (cit. on p. 1).

[6] M. C. Jarvis, „Aerosol Transmission of SARS-CoV-2: Physical Principles and Implications“, *Frontiers in Public Health*, vol. 8, p. 813, Nov. 2020, ISSN: 22962565. DOI: 10.3389/FPUBH.2020.590041/BIBTEX (cit. on p. 1).

[7] J. W. Tang, Y. Li, I. Eames, P. K. Chan, and G. L. Ridgway, „Factors involved in the aerosol transmission of infection and control of ventilation in healthcare premises“, *Journal of Hospital Infection*, vol. 64, no. 2, pp. 100–114, Oct. 2006, ISSN: 0195-6701. DOI: 10.1016/J.JHIN.2006.05.022 (cit. on p. 1).

[8] Rachael. M.Jones and Lisa M. Brosseau, „Aerosol Transmission of Infectious Disease on JSTOR“, *Journal of Occupational and Environmental Medicine*, 2015. [Online]. Available: https://www.jstor.org/stable/48501269#metadata_info_tab_contents (cit. on p. 1).

[9] D. W. Dockery *et al.*, „An Association between Air Pollution and Mortality in Six U.S. Cities“, *New England Journal of Medicine*, vol. 329, no. 24, pp. 1753–1759, Dec. 1993, ISSN: 0028-4793. DOI: 10.1056/NEJM199312093292401. [Online]. Available: http://www.nejm.org/doi/10.1056/NEJM199312093292401 (cit. on pp. 1, 5, 11).

[10] N. Englert, „Fine particles and human health—a review of epidemiological studies“, *Toxicology Letters*, vol. 149, no. 1-3, pp. 235–242, Apr. 2004, ISSN: 03784274. DOI: 10.1016/j.toxlet.2003.12.035. [Online]. Available: https://linkinghub.elsevier.com/retrieve/pii/S0378427403005022 (cit. on p. 1).

[11] R. C. Puett *et al.*, „Particulate {Matter} {Air} {Pollution} {Exposure}, {Distance} to {Road}, and {Incident} {Lung} {Cancer} in the {Nurses}' {Health} {Study} {Cohort}“, *Environ Health Perspect*, vol. 122, no. 9, pp. 926–932, 2014, ISSN: 0091-6765. DOI: 10.1289/ehp.1307490. [Online]. Available: http://www.ncbi.nlm.nih.gov/pmc/articles/PMC4154215/ (cit. on pp. 1, 5).

[12] B. Brunekreef and S. T. Holgate, „Air pollution and health.“, *Lancet (London, England)*, vol. 360, no. 9341, pp. 1233–42, Oct. 2002, ISSN: 0140-6736. DOI: 10.1016/S0140-6736(02)11274-8. [Online]. Available: http://www.ncbi.nlm.nih.gov/pubmed/12401268 (cit. on pp. 1, 5, 10, 11, 20, 23, 113).

[13] A. H. Goldstein and I. E. Galbally, „Known and Unexplored Organic Constituents in the Earth's Atmosphere“, *Environmental Science & Technology*, vol. 41, no. 5, pp. 1514–1521, Mar. 2007, ISSN: 0013-936X. DOI: 10.1021/es072476p. [Online]. Available: https://pubs.acs.org/doi/10.1021/es072476p (cit. on p. 3).

[14] J. H. Kroll and J. H. Seinfeld, „Chemistry of secondary organic aerosol: Formation and evolution of low-volatility organics in the atmosphere“, *Atmospheric Environment*, vol. 42, no. 16, pp. 3593–3624, May 2008, ISSN: 13522310. DOI: 10.1016/j.atmosenv.2008.01.003. [Online]. Available: https://linkinghub.elsevier.com/retrieve/pii/S1352231008000253 (cit. on pp. 3, 98).

[15] J. H. Murillo *et al.*, „Temporal and spatial variations in organic and elemental carbon concentrations in PM10/PM2.5 in the metropolitan area of Costa Rica, Central America“, *Atmospheric Pollution Research*, vol. 4, no. 1, pp. 53–63, 2013, ISSN: 13091042. DOI: 10.5094/APR.2013.006. [Online]. Available: http://www.sciencedirect.com/science/article/pii/S1309104215304001 (cit. on p. 4).

[16] W. Dechapanya, M. Russel, and D. Allen, „Characterization of Nonpolar Organic Fine Particulate Matter in Houston, Texas Special Issue of Aerosol Science and Technology on Findings from the Fine Particulate Matter Supersites Program“, *Aerosol Science and Technology*, vol. 38, no. sup1, pp. 60–67, 2004, ISSN: 0278-6826. DOI: 10.1080/02786820390229444. [Online]. Available: http://dx.doi.org/10.1080/02786820390229444 (cit. on p. 4).

[17] J. A. de Gouw *et al.*, „Budget of organic carbon in a polluted atmosphere: Results from the New England Air Quality Study in 2002“, *Journal of Geophysical Research D: Atmospheres*, vol. 110, no. 16, pp. 1–22, 2005, ISSN: 01480227. DOI: 10.1029/2004JD005623 (cit. on p. 4).

[18] M. Hallquist *et al.*, „The formation, properties and impact of secondary organic aerosol: current and emerging issues“, *Atmos. Chem. Phys.*, vol. 9, no. 14, pp. 5155–5236, 2009, ISSN: 1680-7324. DOI: 10.5194/acp-9-5155-2009. [Online]. Available: http://www.atmos-chem-phys.net/9/5155/

2009/%5Cnhttp://www.atmos-chem-phys.net/9/5155/2009/acp-9-5155-2009.pdf (cit. on p. 4).

[19] B. J. Finlayson-Pitts and J. N. Pitts, „Chemistry of the Upper and Lower Atmosphere: Theory, Experiments, and Applications“, p. 969, 2000. [Online]. Available: http://www.sciencedirect.com/science/book/9780122570605 (cit. on p. 4).

[20] J. E. Hart *et al.*, „The association of long-term exposure to PM2.5 on all-cause mortality in the Nurses' Health Study and the impact of measurement-error correction“, *Environmental Health*, vol. 14, no. 1, p. 38, May 2015, ISSN: 1476-069X. DOI: 10.1186/s12940-015-0027-6. [Online]. Available: http://ehjournal.biomedcentral.com/articles/10.1186/s12940-015-0027-6%20https://pubmed.ncbi.nlm.nih.gov/25926123/ (cit. on pp. 5, 10, 20, 23, 112, 134).

[21] F. J. Kelly and I. S. Mudway, „Protein oxidation at the air-lung interface“, *Amino Acids 2003 25:3*, vol. 25, no. 3, pp. 375–396, Jul. 2003, ISSN: 1438-2199. DOI: 10.1007/S00726-003-0024-X. [Online]. Available: https://link.springer.com/article/10.1007/s00726-003-0024-x (cit. on p. 5).

[22] F. J. Kelly and J. C. Fussell, „Size, source and chemical composition as determinants of toxicity attributable to ambient particulate matter“, *Atmospheric Environment*, vol. 60, pp. 504–526, 2012, ISSN: 13522310. DOI: 10.1016/j.atmosenv.2012.06.039. [Online]. Available: http://dx.doi.org/10.1016/j.atmosenv.2012.06.039 (cit. on pp. 5, 9).

[23] L. Künzi *et al.*, „Responses of lung cells to realistic exposure of primary and aged carbonaceous aerosols“, *Atmospheric Environment*, vol. 68, pp. 143–150, Apr. 2013, ISSN: 13522310. DOI: 10.1016/j.atmosenv.2012.11.055 (cit. on pp. 5, 23).

[24] F. Laden, J. Schwartz, F. E. Speizer, and D. W. Dockery, „Reduction in fine particulate air pollution and mortality: Extended follow-up of the Harvard Six Cities Study“, *American Journal of Respiratory and Critical Care Medicine*, vol. 173, no. 6, pp. 667–672, Mar. 2006, ISSN: 1073449X. DOI: 10.1164/rccm.200503-443OC. [Online]. Available: https://pubmed.ncbi.nlm.nih.gov/16424447/ (cit. on pp. 5, 12, 23, 112).

[25] World Helath Organitation, „WHO global air quality guidelines“, 2021 (cit. on pp. 5, 10, 23, 113).

[26] G. Oberdörster *et al.*, *Principles for characterizing the potential human health effects from exposure to nanomaterials: Elements of a screening strategy*, Oct. 2005. DOI: 10.1186/1743-8977-2-8. [Online]. Available: https://particleandfibretoxicology.biomedcentral.com/articles/10.1186/1743-8977-2-8 (cit. on pp. 5, 24).

[27] T. Y. Poh *et al.*, „Inhaled nanomaterials and the respiratory microbiome: clinical, immunological and toxicological perspectives“, *Particle and Fibre Toxicology 2018 15:1*, vol. 15, no. 1, pp. 1–16, Nov. 2018, ISSN: 1743-8977. DOI: 10.1186/S12989-018-0282-0. [Online]. Available: https://particleandfibretoxicology.biomedcentral.com/articles/10.1186/s12989-018-0282-0 (cit. on p. 6).

[28] M. Geiser *et al.*, „Ultrafine particles cross cellular membranes by nonphagocytic mechanisms in lungs and in cultured cells“, *Environmental Health Perspectives*, vol. 113, no. 11, pp. 1555–1560, Nov. 2005, ISSN: 00916765. DOI: 10.1289/ehp.8006. [Online]. Available: https://ehp.niehs.nih.gov/doi/10.1289/ehp.8006 (cit. on pp. 6, 13).

[29] H. M. Braakhuis, V. Park, I. Gosens, W. H. De Jong, and F. R. Cassee, „Physicochemical characteristics of nanomaterials that affect pulmonary inflammation“, Tech. Rep., 2014. DOI: 10.1186/1743-8977-11-18. [Online]. Available: http://www.particleandfibretoxicology.com/content/11/1/18 (cit. on p. 7).

[30] P. J. Gallimore and M. Kalberer, „Characterizing an extractive electrospray ionization (EESI) source for the online mass spectrometry analysis of organic aerosols“, *Environmental Science and Technology*, vol. 47, no. 13, pp. 7324–7331, 2013, ISSN: 0013936X. DOI: 10.1021/es305199h (cit. on p. 7).

[31] J. T. Bates *et al.*, „Review of Acellular Assays of Ambient Particulate Matter Oxidative Potential: Methods and Relationships with Composition, Sources, and Health Effects“, *Environmental Science and Technology*, vol. 53, no. 8, pp. 4003–4019, 2019, ISSN: 15205851. DOI: 10.1021/acs.est.8b03430 (cit. on pp. 8, 12, 14, 15, 23, 24, 38, 71, 82, 95, 113, 134, 135, 150).

[32] Z. Leni, L. Künzi, and M. Geiser, „Air pollution causing oxidative stress“, *Current Opinion in Toxicology*, vol. 20-21, pp. 1–8, Apr. 2020, ISSN: 24682020. DOI: 10.1016/J.COTOX.2020.02.006 (cit. on p. 8).

[33] S. J. Campbell *et al.*, „Atmospheric conditions and composition that influence PM_{2.5} oxidative potential in Beijing, China“, *Atmospheric Chemistry and Physics*, vol. 21, no. 7, pp. 5549–5573, Apr. 2021, ISSN: 1680-7324. DOI: 10.5194/acp-21-5549-2021. [Online]. Available: https://acp.copernicus.org/articles/21/5549/2021/ (cit. on pp. 8, 14, 15, 24, 57, 80, 82, 86, 91, 92, 94, 135, 137, 141, 188).

[34] S. Stevanovic *et al.*, „Influence of oxygenated organic aerosols (OOAs) on the oxidative potential of diesel and biodiesel particulate matter“, *Environmental Science and Technology*, vol. 47, no. 14, pp. 7655–7662, 2013, ISSN: 15205851. DOI: 10.1021/es4007433. [Online]. Available: https://pubs.acs.org/sharingguidelines (cit. on p. 8).

[35] L. A. Morio *et al.*, „Tissue injury following inhalation of fine particulate matter and hydrogen peroxide is associated with altered production of inflammatory mediators and antioxidants by alveolar macrophages“, *Toxicology and applied pharmacology*, vol. 177, no. 3, pp. 188–199, Dec. 2001, ISSN: 0041-008X. DOI: 10.1006/TAAP.2001.9316. [Online]. Available: https://pubmed.ncbi.nlm.nih.gov/11749118/ (cit. on p. 8).

[36] K. Donaldson *et al.*, „Oxidative stress and calcium signaling in the adverse effects of environmental particles (PM10)“, *Free Radical Biology and Medicine*, vol. 34, no. 11, pp. 1369–1382, Jun. 2003, ISSN: 08915849. DOI: 10.1016/S0891-5849(03)00150-3. [Online]. Available: https://pubmed.ncbi.nlm.nih.gov/12757847/ (cit. on p. 8).

[37] S. Rezaei *et al.*, „Physiochemical characteristics and oxidative potential of ambient air particulate matter (PM 10) during dust and non-dust storm events: a case study in Tehran, Iran“, 2018. DOI: 10.1007/s40201-018-0303-9. [Online]. Available: https://doi.org/10.1007/s40201-018-0303-9 (cit. on p. 8).

[38] S. J. Campbell *et al.*, „Development of a physiologically relevant online chemical assay to quantify aerosol oxidative potential“, *Analytical Chemistry*, 2019, ISSN: 15206882. DOI: 10.1021/acs.analchem.9b03282 (cit. on pp. 8, 14, 17, 19, 22, 25, 26, 38, 65, 68, 73, 87, 95, 113, 136, 137, 139, 188, 202).

[39] J. G. Charrier and C. Anastasio, „On dithiothreitol (DTT) as a measure of oxidative potential for ambient particles: Evidence for the importance of soluble \newline transition metals“, *Atmospheric Chemistry and Physics*, vol. 12, no. 19, pp. 9321–9333, 2012, ISSN: 16807316. DOI: 10.5194/acp-12-9321-2012 (cit. on pp. 8, 14, 82, 95, 135).

[40] S. D. Pouwels, J. K. Burgess, E. Verschuuren, and D. J. Slebos, „The cellular composition of the lung lining fluid gradually changes from bronchus to alveolus“, *Respiratory Research*, vol. 22, no. 1, pp. 1–4, Dec. 2021, ISSN: 1465993X. DOI: 10.1186/S12931-021-01882-X/FIGURES/1. [Online]. Available: https://respiratory-research.biomedcentral.com/articles/10.1186/s12931-021-01882-x (cit. on pp. 8, 18).

[41] F. J. Kelly, M. Cotgrove, and I. S. Mudway, „Respiratory tract lining fluid antioxidants: the first line of defence against gaseous pollutants.“, *Central European Journal of Public Health*, vol. 4 Suppl, pp. 11–14, Jan. 1996, ISSN: 1210-7778. [Online]. Available: https://europepmc.org/article/med/9167049 (cit. on p. 8).

[42] A. W. Ng, A. Bidani, and T. A. Heming, „Innate Host Defense of the Lung: Effects of Lung-lining Fluid pH“, *Lung*, vol. 182, pp. 297–317, 2004. DOI: 10.1007/s00408-004-2511-6 (cit. on p. 8).

[43] J. Lepeule, F. Laden, D. Dockery, and J. Schwartz, „Chronic exposure to fine particles and mortality: An extended follow-up of the Harvard six cities study from 1974 to 2009“, *Environmental Health Perspectives*, vol. 120, no. 7, pp. 965–970, Jun. 2012, ISSN: 00916765. DOI: 10.1289/ehp.1104660. [Online]. Available: https://pubmed.ncbi.nlm.nih.gov/22456598/ (cit. on pp. 10, 20).

[44] WHO, *BreatheLife Campaign*. [Online]. Available: https://breathelife2030.org/ (cit. on p. 10).

[45] M. L. Bell and D. L. Davis, „Reassessment of the lethal London fog of 1952: novel indicators of acute and chronic consequences of acute exposure to air pollution.“, *Environmental Health Perspectives*, vol. 109, no. Suppl 3, p. 389, 2001, ISSN: 00916765. DOI: 10.1289/EHP.01109S3389. [Online]. Available: /pmc/articles/PMC1240556/?report=abstract%20https://www.ncbi.nlm.nih.gov/pmc/articles/PMC1240556/ (cit. on p. 11).

[46] F. Laden, J. Schwartz, F. E. Speizer, and D. W. Dockery, „Reduction in fine particulate air pollution and mortality: Extended follow-up of the Harvard Six Cities Study“, *American Journal of Respiratory and Critical Care Medicine*, vol. 173, no. 6, pp. 667–672, Mar. 2006, ISSN: 1073449X. DOI: 10.1164/rccm.200503-443OC. [Online]. Available: https://pubmed.ncbi.nlm.nih.gov/16424447/ (cit. on p. 11).

[47] J. Lepeule, F. Laden, D. Dockery, and J. Schwartz, „Chronic exposure to fine particles and mortality: An extended follow-up of the Harvard six cities study from 1974 to 2009“, *Environmental Health Perspectives*, vol. 120, no. 7, pp. 965–970, Jun. 2012, ISSN: 00916765. DOI: 10.1289/ehp.1104660. [Online]. Available: https://pubmed.ncbi.nlm.nih.gov/22456598/ (cit. on pp. 11, 23, 112, 134).

[48] K. J. Colonna, P. Koutrakis, P. L. Kinney, R. M. Cooke, and J. S. Evans, „Mortality Attributable to Long-Term Exposure to Ambient Fine Particulate Matter: Insights from the Epidemiologic Evidence for Understudied Locations“, *Cite This: Environ. Sci. Technol*, vol. 2022, pp. 6799–6812, 2022. DOI: 10.1021/acs.est.1c08343. [Online]. Available: https://doi.org/10.1021/acs.est.1c08343 (cit. on p. 11).

[49] UK GOV, *Statement on the differential toxicity of particulate matter according to source or constituents: 2022 - GOV.UK*, 2022. [Online]. Available: https://www.gov.uk/government/publications/particulate-air-pollution-health-effects-of-exposure/statement-on-the-differential-toxicity-of-particulate-matter-according-to-source-or-constituents-2022 (cit. on p. 12).

[50] J. T. Bates *et al.*, „Reactive Oxygen Species Generation Linked to Sources of Atmospheric Particulate Matter and Cardiorespiratory Effects“, *Environmental Science and Technology*, vol. 49, no. 22, pp. 13 605–13 612, Oct. 2015, ISSN: 15205851. DOI: 10.1021/acs.est.5b02967. [Online]. Available: https://pubmed.ncbi.nlm.nih.gov/26457347/%20https://pubs.acs.org/sharingguidelines (cit. on pp. 12, 24).

[51] J. Y. Abrams *et al.*, „Associations between ambient fine particulate oxidative potential and cardiorespiratory emergency department visits“, *Environmental Health Perspectives*, vol. 125, no. 10, pp. 1–9, Oct. 2017, ISSN: 15529924. DOI: 10.1289/EHP1545. [Online]. Available: /pmc/articles/PMC5933307/%20/pmc/articles/PMC5933307/?report=abstract%20https://www.ncbi.nlm.nih.gov/pmc/articles/PMC5933307/ (cit. on pp. 12, 24).

[52] T. Fang *et al.*, „Oxidative potential of ambient water-soluble PM2.5 in the southeastern United States: Contrasts in sources and health associations between ascorbic acid (AA) and dithiothreitol (DTT) assays“, *Atmospheric Chemistry and Physics*, vol. 16, no. 6, pp. 3865–3879, 2016, ISSN: 16807324. DOI: 10.5194/acp-16-3865-2016 (cit. on pp. 12, 14, 56, 82).

[53] A. Yang, N. A. H. Janssen, B. Brunekreef, F. R. Cassee, G. Hoek, and U. Gehring, „Children's respiratory health and oxidative potential of PM 2.5 : the PIAMA birth cohort study“, *Occup. Environ. Med*, 2016. DOI: 10.1136/oemed-2015-103175. [Online]. Available: http://www. (cit. on p. 12).

[54] N. A. Janssen *et al.*, „Associations between three specific a-cellular measures of the oxidative potential of particulate matter and markers of acute airway and nasal inflammation in healthy volunteers“, *Occupational and Environmental Medicine*, vol. 72, no. 1, pp. 49–56, 2015, ISSN: 14707926. DOI: 10.1136/oemed-2014-102303 (cit. on p. 12).

[55] R. J. Delfino, N. Staimer, T. Tjoa, D. L. Gillen, J. J. Schauer, and M. M. Shafer, „Airway inflammation and oxidative potential of air pollutant particles in a pediatric asthma panel“, *Journal of Exposure Science and Environmental Epidemiology*, vol. 23, no. 5, pp. 466–473, 2013, ISSN: 15590631. DOI: 10.1038/jes.2013.25 (cit. on p. 12).

[56] C. L. Maikawa *et al.*, „Particulate Oxidative Burden as a Predictor of Exhaled Nitric Oxide in Children with Asthma“, *Environmental health perspectives*, vol. 124, no. 10, pp. 1616–1622, Oct. 2016, ISSN: 1552-9924. DOI: 10.1289/EHP175. [Online]. Available: https://pubmed.ncbi.nlm.nih.gov/27152705/ (cit. on p. 12).

[57] S. Weichenthal *et al.*, „Oxidative burden of fine particulate air pollution and risk of cause-specific mortality in the Canadian Census Health and Environment Cohort (CanCHEC)“, *Environmental Research*, vol. 146, pp. 92–99, 2016, ISSN: 10960953. DOI: 10.1016/j.envres.2015.12.013. [Online]. Available: http://dx.doi.org/10.1016/j.envres.2015.12.013 (cit. on p. 12).

[58] L. S. Joanna Borlaza *et al.*, „Personal exposure to PM 2.5 oxidative potential and its association to birth outcomes“, DOI: 10.1038/s41370-022-00487-w. [Online]. Available: https://doi.org/10.1038/s41370-022-00487-w (cit. on p. 12).

[59] R. W. Atkinson *et al.*, „Short-term associations between particle oxidative potential and daily mortality and hospital admissions in London“, *International Journal of Hygiene and Environmental Health*, vol. 219, no. 6, pp. 566–572, 2016, ISSN: 1618131X. DOI: 10.1016/j.ijheh.2016.06.004. [Online]. Available: http://dx.doi.org/10.1016/j.ijheh.2016.06.004 (cit. on p. 12).

[60] C. Canova *et al.*, „PM10 oxidative properties and asthma and COPD“, *Epidemiology*, vol. 25, no. 3, pp. 467–468, 2014, ISSN: 15315487. DOI: 10.1097/EDE.0000000000000084. [Online]. Available: https://journals.lww.com/epidem/Fulltext/2014/05000/PM10_Oxidative_Properties_and_Asthma_and_COPD.21.aspx (cit. on p. 12).

[61] Q. Q. Wu, L. B. Huang, H. Liang, Y. Zhao, D. Huang, and Z. M. Chen, „Heterogeneous reaction of peroxyacetic acid and hydrogen peroxide on ambient aerosol particles under dry and humid conditions: kinetics, mechanism and implications“, *Atmos. Chem. Phys*, vol. 15, pp. 6851–6866, 2015. DOI: 10.5194/acp-15-6851-2015. [Online]. Available: www.atmos-chem-phys.net/15/6851/2015/ (cit. on p. 13).

[62] N. Pechacek, M. Osorio, J. Caudill, and B. Peterson, „Evaluation of the toxicity data for peracetic acid in deriving occupational exposure limits: A minireview“, *Toxicology Letters*, vol. 233, no. 1, pp. 45–57, Feb. 2015, ISSN: 0378-4274. DOI: 10.1016/J.TOXLET.2014.12.014 (cit. on p. 13).

[63] N. Liang *et al.*, „Chronic exposure to traffic-related air pollution reduces lipid mediators of linoleic acid and soluble epoxide hydrolase in serum of female rats“, *Environmental Toxicology and Pharmacology*, vol. 93, p. 103 875, Jul. 2022, ISSN: 1382-6689. DOI: 10.1016/J.ETAP.2022.103875 (cit. on p. 13).

[64] A. N. Larcombe, M. A. Janka, B. J. Mullins, L. J. Berry, A. Bredin, and P. J. Franklin, „The effects of electronic cigarette aerosol exposure on inflammation and lung function in mice“, *American Journal of Physiology - Lung Cellular and Molecular Physiology*, vol. 313, no. 1, pp. L67–L79, 2017, ISSN: 15221504. DOI: 10.1152/AJPLUNG.00203.2016/ASSET/IMAGES/LARGE/ZH50051772360009.JPEG. [Online]. Available: https://journals.physiology.org/doi/10.1152/ajplung.00203.2016 (cit. on p. 13).

[65] T. Ihantola *et al.*, „Influence of wood species on toxicity of log-wood stove combustion aerosols: A parallel animal and air-liquid interface cell exposure study on spruce and pine smoke“, *Particle and Fibre Toxicology*, vol. 17, no. 1, Jun. 2020, ISSN: 17438977. DOI: 10.1186/S12989-020-00355-1 (cit. on p. 13).

[66] M. Pardo *et al.*, „Mechanisms of lung toxicity induced by biomass burning aerosols“, *Particle and Fibre Toxicology*, vol. 17, no. 1, pp. 1–15, Jan. 2020, ISSN: 17438977. DOI: 10.1186/S12989-020-0337-X/FIGURES/5. [Online]. Available: https://link.springer.com/articles/10.1186/s12989-

020-0337-x%20https://link.springer.com/article/10.1186/s12989-020-0337-x (cit. on p. 13).

[67] M. S. Happo *et al.*, „Pulmonary inflammation and tissue damage in the mouse lung after exposure to PM samples from biomass heating appliances of old and modern technologies“, *Science of The Total Environment*, vol. 443, pp. 256–266, Jan. 2013, ISSN: 0048-9697. DOI: 10.1016/J.SCITOTENV.2012.11.004 (cit. on p. 13).

[68] S. Offer *et al.*, „Effect of Atmospheric Aging on Soot Particle Toxicity in Lung Cell Models at the Air-Liquid Interface: Differential Toxicological Impacts of Biogenic and Anthropogenic Secondary Organic Aerosols (SOAs)“, *Environmental health perspectives*, vol. 130, no. 2, pp. 1–19, Feb. 2022, ISSN: 1552-9924. DOI: 10.1289/EHP9413. [Online]. Available: https://ehp.niehs.nih.gov/doi/10.1289/EHP9413%20https://pubmed.ncbi.nlm.nih.gov/35112925/ (cit. on pp. 13, 24, 30, 112, 130, 143, 146).

[69] M. N. Delaval *et al.*, „Responses of reconstituted human bronchial epithelia from normal and health-compromised donors to non-volatile particulate matter emissions from an aircraft turbofan engine“, *Environmental Pollution*, vol. 307, p. 119 521, Aug. 2022, ISSN: 0269-7491. DOI: 10.1016/J.ENVPOL.2022.119521 (cit. on p. 13).

[70] N. Jeannet *et al.*, „Acute toxicity of silver and carbon nanoaerosols to normal and cystic fibrosis human bronchial epithelial cells“, 2015. DOI: 10.3109/17435390.2015.1049233. [Online]. Available: https://www.tandfonline.com/action/journalInformation?journalCode=inan20 (cit. on pp. 13, 88).

[71] M. Pardo *et al.*, „Exposure to naphthalene and β-pinene-derived secondary organic aerosol induced divergent changes in transcript levels of BEAS-2B cells“, *Environment International*, vol. 166, no. June, p. 107 366, Aug. 2022, ISSN: 01604120. DOI: 10.1016/j.envint.2022.107366. [Online]. Available: https://linkinghub.elsevier.com/retrieve/pii/S0160412022002938 (cit. on pp. 13, 30, 151).

[72] K. R. Daellenbach *et al.*, „Sources of particulate-matter air pollution and its oxidative potential in Europe“, *Nature*, vol. 587, no. 7834, pp. 414–419, Nov. 2020, ISSN: 0028-0836. DOI: 10.1038/s41586-020-2902-8. [Online]. Available: https://doi.org/10.1038/s41586-020-2902-8%20http://www.nature.com/articles/s41586-020-2902-8 (cit. on pp. 14, 30, 38, 113).

[73] A. K. Cho *et al.*, „Redox activity of airborne particulate matter at different sites in the Los Angeles Basin“, *Environmental Research*, vol. 99, no. 1, pp. 40–47, 2005, ISSN: 00139351. DOI: 10.1016/j.envres.2005.01.003 (cit. on pp. 14, 82, 85).

[74] M. Lin and J. Z. Yu, „Dithiothreitol (DTT) concentration effect and its implications on the applicability of DTT assay to evaluate the oxidative potential of atmospheric aerosol samples“, *Neotropical Entomology*, vol. 251, pp. 938–944, Aug. 2019, ISSN: 16788052. DOI: 10.1016/j.envpol.2019.05.074. [Online]. Available: https://doi.org/10.1016/j.envpol.2019.05.074 (cit. on pp. 14, 82, 135).

[75] D. Gao, T. Fang, V. Verma, L. Zeng, and R. J. Weber, „A method for measuring total aerosol oxidative potential (OP) with the dithiothreitol (DTT) assay and comparisons between an urban and roadside site of water-soluble and total OP“, *Atmospheric Measurement Techniques*, vol. 10, no. 8, pp. 2821–2835, Aug. 2017, ISSN: 18678548. DOI: 10.5194/amt-10-2821-2017 (cit. on pp. 14, 17, 25, 30, 82).

[76] J. G. Charrier and C. Anastasio, „Rates of Hydroxyl Radical Production from Transition Metals and Quinones in Surrogate Lung Fluid“, *Environmental Science and Technology*, vol. 49, no. 15, pp. 9317–9325, 2016, ISSN: 15205851. DOI: 10.1021/acs.est.5b01606 (cit. on p. 14).

[77] A. Patel and N. Rastogi, „Oxidative potential of ambient fine aerosol over a semi-urban site in the Indo-Gangetic Plain“, *Atmospheric Environment*, vol. 175, no. August 2017, pp. 127–134, 2018, ISSN: 18732844. DOI: 10.1016/j.atmosenv.2017.12.004. [Online]. Available: https://doi.org/10.1016/j.atmosenv.2017.12.004 (cit. on pp. 14, 92).

[78] I. S. Mudway *et al.*, „An in vitro and in vivo investigation of the effects of diesel exhaust on human airway lining fluid antioxidants“, *Archives of Biochemistry and Biophysics*, vol. 423, no. 1, pp. 200–212, Mar. 2004, ISSN: 00039861. DOI: 10.1016/j.abb.2003.12.018. [Online]. Available: https://pubmed.ncbi.nlm.nih.gov/14871482/ (cit. on pp. 14, 82).

[79] M. R. Perrone, I. Bertoli, S. Romano, M. Russo, G. Rispoli, and M. C. Pietrogrande, „PM2.5 and PM10 oxidative potential at a Central Mediterranean Site: Contrasts between dithiothreitol- and ascorbic acid-measured values in relation with particle size and chemical composition“, *Atmospheric Environment*, vol. 210, pp. 143–155, Aug. 2019, ISSN: 18732844. DOI: 10.1016/J.ATMOSENV.2019.04.047. [Online]. Available: https://doi.org/10.1016/j.atmosenv.2019.04.047 (cit. on pp. 14, 56, 82).

[80] T. Fang, V. Verma, H. Guo, L. E. King, E. S. Edgerton, and R. J. Weber, „A semi-automated system for quantifying the oxidative potential of ambient particles in aqueous extracts using the dithiothreitol (DTT) assay: Results from the Southeastern Center for Air Pollution and Epidemiology (SCAPE)“, *Atmospheric Measurement Techniques*, vol. 8, no. 1, pp. 471–482, Jan. 2015, ISSN: 18678548. DOI: 10.5194/amt-8-471-2015. [Online]. Available: https://amt.copernicus.org/articles/8/471/2015/ (cit. on pp. 14, 17, 25, 82).

[81] J. Shen, P. T. Griffiths, S. J. Campbell, B. Utinger, M. Kalberer, and S. E. Paulson, „Ascorbate oxidation by iron, copper and reactive oxygen species: review, model development, and derivation of key rate constants“, *Scientific Reports 2021 11:1*, vol. 11, no. 1, pp. 1–14, Apr. 2021, ISSN: 2045-2322. DOI: 10.1038/s41598-021-86477-8. [Online]. Available: https://www.nature.com/articles/s41598-021-86477-8 (cit. on pp. 14, 18, 26, 36, 37, 66, 78, 82, 136, 139, 141, 146, 188).

[82] K. J. Godri *et al.*, „Particulate matter oxidative potential from waste transfer station activity“, *Environmental Health Perspectives*, vol. 118, no. 4, pp. 493–498, 2010, ISSN: 00916765. DOI: 10.1289/ehp.0901303 (cit. on pp. 15, 24).

[83] D. H. Gonzalez, X. M. Kuang, J. A. Scott, G. Olimpio Rocha, and S. E. Paulson, „Terephthalate Probe for Hydroxyl Radicals: Yield of 2-Hydroxyterephthalic Acid and Transition Metal Interference“, *Analytical Letters*, vol. 51, pp. 2488–2497, 2018, ISSN: 0003-2719. DOI: 10.1080/00032719.2018.1431246. [Online]. Available: https://www.tandfonline.com/action/journalInformation?journalCode=lanl20 (cit. on pp. 15, 135, 139, 149).

[84] P. Venkatachari, P. K. Hopke, B. D. Grover, and D. J. Eatough, „Measurement of particle-bound reactive oxygen species in rubidoux aerosols“, *Journal of Atmospheric Chemistry*, vol. 50, no. 1, pp. 49–58, Jan. 2005, ISSN: 01677764. DOI: 10.1007/s10874-005-1662-z. [Online]. Available: https://link.springer.com/article/10.1007/s10874-005-1662-z (cit. on pp. 15, 24, 82).

[85] Z.-H. H. Zhang *et al.*, „Are reactive oxygen species (ROS) a suitable metric to predict toxicity of carbonaceous aerosol particles?“, *Atmospheric Chemistry and Physics Discussions*, vol. 22, no. August, pp. 1–29, Feb. 2021, ISSN: 1680-7316. DOI: 10.5194/acp-2021-666. [Online]. Available: https://doi.org/10.5194/acp-22-1793-2022%20https://ui.adsabs.harvard.edu/abs/2022ACP....22.1793Z/abstract (cit. on pp. 15, 24, 38, 70, 114, 125, 130, 135, 140, 151, 188).

[86] W. Gehling and B. Dellinger, „Environmentally Persistent Free Radicals and Their Lifetimes in PM 2.5 Observed decay rates along with initial radical concentrations“, *Environ. Sci. Technol*, vol. 47, p. 40, 2013. DOI: 10.1021/es401767m. [Online]. Available: https://pubs.acs.org/sharingguidelines (cit. on pp. 15, 82).

[87] A. M. Arangio, H. Tong, J. Socorro, U. Pöschl, and M. Shiraiwa, „Quantification of environmentally persistent free radicals and reactive oxygen species in atmospheric aerosol particles“, *Atmospheric Chemistry and Physics*, vol. 16, no. 20, pp. 13 105–13 119, Oct. 2016, ISSN: 16807324. DOI: 10.5194/acp-16-13105-2016 (cit. on pp. 15, 82).

[88] H. Chen, Y. Liu, H. Li, Y. Zhang, and S. Yao, „Non-oxidation reduction strategy for highly selective detection of ascorbic acid with dual-ratio fluorescence and colorimetric signals“, *Sensors and Actuators, B: Chemical*, vol. 281, no. June 2018, pp. 983–988, 2019, ISSN: 09254005. DOI: 10.1016/j.snb.2018.11.020. [Online]. Available: https://doi.org/10.1016/j.snb.2018.11.020 (cit. on pp. 15, 82).

[89] S. J. Campbell, S. Stevanovic, B. Miljevic, S. E. Bottle, Z. Ristovski, and M. Kalberer, „Quantification of Particle-Bound Organic Radicals in Secondary Organic Aerosol“, *Environmental Science & Technology*, vol. 53, no. 12, pp. 6729–6737, Jun. 2019, ISSN: 0013-936X. DOI: 10.1021/acs.est.9b00825. [Online]. Available: https://pubs.acs.org/doi/10.1021/acs.est.9b00825 (cit. on pp. 15, 25, 82, 97, 114, 137, 201).

[90] H. Tong *et al.*, „Hydroxyl radicals from secondary organic aerosol decomposition in water“, *Atmospheric Chemistry and Physics*, vol. 16, no. 3, pp. 1761–1771, Feb. 2016, ISSN: 16807324. DOI: 10.5194/acp-16-1761-2016 (cit. on pp. 15, 82).

[91] H. Tong *et al.*, „Reactive oxygen species formed in aqueous mixtures of secondary organic aerosols and mineral dust influencing cloud chemistry and public health in the Anthropocene“, *Faraday Discussions*, vol. 200, no. 0, pp. 251–270, Aug. 2017, ISSN: 13645498. DOI: 10.1039/c7fd00023e. [Online]. Available: https://pubs.rsc.org/en/content/articlehtml/2017/fd/c7fd00023e%20https://pubs.rsc.org/en/content/articlelanding/2017/fd/c7fd00023e (cit. on pp. 15, 82, 135).

[92] H. Tong *et al.*, „Reactive Oxygen Species Formed by Secondary Organic Aerosols in Water and Surrogate Lung Fluid“, *Environmental Science and Technology*, vol. 52, no. 20, pp. 11 642–11 651, Oct. 2018, ISSN: 15205851. DOI: 10.1021/acs.est.8b03695 (cit. on pp. 15, 135, 142, 146, 148).

[93] K. C. Edwards *et al.*, „Effects of Nitrogen Oxides on the Production of Reactive Oxygen Species and Environmentally Persistent Free Radicals from α-Pinene and Naphthalene Secondary Organic Aerosols“, *The Journal of Physical Chemistry A*, Oct. 2022, ISSN: 1089-5639. DOI: 10.1021/ACS.JPCA.2C05532. [Online]. Available: https://pubs.acs.org/doi/full/10.1021/acs.jpca.2c05532 (cit. on p. 15).

[94] S. Fuller, F. Wragg, J. Nutter, and M. Kalberer, „Comparison of on-line and off-line methods to quantify reactive oxygen species (ROS) in atmospheric aerosols“, *Atmospheric Environment*, vol. 92, pp. 97–103, Aug. 2014, ISSN: 13522310. DOI: 10.1016/j.atmosenv.2014.04.006. [Online]. Available: https://linkinghub.elsevier.com/retrieve/pii/S1352231014002787 (cit. on pp. 15, 17, 24, 25, 47, 49, 50, 86, 94, 95, 135, 137, 138, 140, 142, 201).

[95] F. P. Wragg, S. J. Fuller, R. Freshwater, D. C. Green, F. J. Kelly, and M. Kalberer, „An automated online instrument to quantify aerosol-bound reactive oxygen species (ROS) for ambient measurement and health-relevant aerosol studies“, *Atmospheric Measurement Techniques*, vol. 9, no. 10,

pp. 4891–4900, 2016, ISSN: 18678548. DOI: 10.5194/amt-9-4891-2016 (cit. on pp. 15, 17, 18, 25, 30, 43, 46, 47, 49, 50, 94, 95, 114, 121, 123, 135–138, 140, 142, 201).

[96] S. S. Steimer *et al.*, „Seasonal Differences in the Composition of Organic Aerosols in Beijing: a Study by Direct Infusion Ultrahigh Resolution Mass Spectrometry“, *Atmospheric Chemistry and Physics Discussions*, no. January, pp. 1–26, 2020, ISSN: 1680-7316. DOI: 10.5194/acp-2019-1009 (cit. on pp. 15, 91, 92).

[97] B. Utinger *et al.*, „An automated online field instrument to quantify the oxidative potential of aerosol particles via ascorbic acid oxidation“, *Atmospheric Measurement Techniques*, vol. 16, no. 10, pp. 2641–2654, May 2023, ISSN: 1867-8548. DOI: 10.5194/amt-16-2641-2023. [Online]. Available: https://amt.copernicus.org/articles/16/2641/2023/ (cit. on pp. 15, 22, 114, 121, 123, 136–138, 202).

[98] J. Resch, K. Wolfer, A. Barth, and M. Kalberer, „Technical note: Effects of storage conditions on molecular-level composition of organic aerosol particles“, DOI: 10.5194/egusphere-2023-840. [Online]. Available: https://doi.org/10.5194/egusphere-2023-840 (cit. on p. 16).

[99] F. P. Wragg, „PhD Wragg Francis“, vol. 54, no. 3, pp. 1103–1117, 2016 (cit. on pp. 16, 121).

[100] A. Carlino, M. P. Romano, M. G. Lionetto, D. Contini, and M. R. Guascito, „An Overview of the Automated and On-Line Systems to Assess the Oxidative Potential of Particulate Matter“, *Atmosphere 2023, Vol. 14, Page 256*, vol. 14, no. 2, p. 256, Jan. 2023, ISSN: 2073-4433. DOI: 10.3390/ATMOS14020256. [Online]. Available: https://www.mdpi.com/2073-4433/14/2/256/htm%20https://www.mdpi.com/2073-4433/14/2/256 (cit. on p. 16).

[101] Y. Wang, P. K. Hopke, L. Sun, D. C. Chalupa, and M. J. Utell, „Laboratory and Field Testing of an Automated Atmospheric Particle-Bound Reactive Oxygen Species Sampling-Analysis System“, *Journal of Toxicology*, vol. 2011, 2011. DOI: 10.1155/2011/419476 (cit. on p. 17).

[102] L. E. King and R. J. Weber, „Development and testing of an online method to measure ambient fine particulate reactive oxygen species (ROS) based on the 2',7'-dichlorofluorescin (DCFH) assay“, *Atmospheric Measurement Techniques*, vol. 6, no. 7, pp. 1647–1658, 2013, ISSN: 18671381. DOI: 10.5194/amt-6-1647-2013. [Online]. Available: www.atmos-meas-tech.net/6/1647/2013/ (cit. on p. 17).

[103] J. Zhou *et al.*, „Development, characterization and first deployment of an improved online reactive oxygen species analyzer“, *Atmospheric Measurement Techniques*, vol. 11, no. 1, pp. 65–80, Jan. 2018, ISSN: 18678548. DOI: 10.5194/AMT-11-65-2018 (cit. on p. 17).

[104] W. Huang *et al.*, „Development of an automated sampling-analysis system for simultaneous measurement of reactive oxygen species (ROS) in gas and particle phases: GAC-ROS“, *AtmEn*, vol. 134, pp. 18–26, Jun. 2016, ISSN: 1352-2310. DOI: 10.1016/J.ATMOSENV.2016.03.038. [Online]. Available: https://ui.adsabs.harvard.edu/abs/2016AtmEn.134...18H/abstract (cit. on p. 17).

[105] Y. Sameenoi *et al.*, „Microfluidic electrochemical sensor for on-line monitoring of aerosol oxidative activity“, *Journal of the American Chemical Society*, vol. 134, no. 25, pp. 10 562–10 568, 2012, ISSN: 00027863. DOI: 10.1021/ja3031104 (cit. on p. 17).

[106] A. Eiguren-Fernandez, N. Kreisberg, and S. Hering, „An online monitor of the oxidative capacity of aerosols (o-MOCA)“, *Atmospheric Measurement Techniques*, vol. 10, no. 2, pp. 633–644, 2017, ISSN: 18678548. DOI: 10.5194/amt-10-633-2017 (cit. on p. 17).

[107] J. V. Puthussery, C. Zhang, and V. Verma, „Development and field-testing of an online instrument for measuring the real-time oxidative potential of ambient particulate matter based on dithiothreitol assay“, *Atmospheric Measurement Techniques*, vol. 11, no. May, pp. 1–25, 2018, ISSN: 18678548. DOI: 10.5194/amt-11-5767-2018 (cit. on p. 17).

[108] H. Yu, J. V. Puthussery, and V. Verma, „A semi-automated multi-endpoint reactive oxygen species activity analyzer (SAMERA) for measuring the oxidative potential of ambient PM _{2.5} aqueous extracts“, *Aerosol Science and Technology*, vol. 54, no. 3, pp. 304–320, Mar. 2020, ISSN: 0278-6826. DOI: 10.1080/02786826.2019.1693492. [Online]. Available: https://www.tandfonline.com/doi/full/10.1080/02786826.2019.1693492 (cit. on p. 17).

[109] K. E. Berg, K. M. Clark, X. Li, E. M. Carter, J. Volckens, and C. S. Henry, „High-throughput, semi-automated dithiothreitol (DTT) assays for oxidative potential of fine particulate matter“, *Atmospheric Environment*, no. October, p. 117 132, 2019, ISSN: 18732844. DOI: 10.1016/j.atmosenv.2019.117132. [Online]. Available: https://doi.org/10.1016/j.atmosenv.2019.117132 (cit. on p. 17).

[110] M. Deutsch and C. Weeks, „Microfluorometric Assay for Vitamin C“, *J. Assoc. Off. Anal. Chem*, no. 48, p. 1248, 1965 (cit. on pp. 18, 19, 27, 33, 38).

[111] K. Iqbal, A. Khan, and M. Muzaffar Ali Khan Khattak, „Biological Significance of Ascorbic Acid (Vitamin C) in Human Health-A Review“, *Pakistan Journal of Nutrition*, vol. 3, no. 1, pp. 5–13, 2004 (cit. on p. 18).

[112] P. Zhang and S. T. Omaye, „Antioxidant and prooxidant roles for β-carotene, α-tocopherol and ascorbic acid in human lung cells“, *Toxicology in Vitro*, vol. 15, no. 1, pp. 13–24, Feb. 2001, ISSN: 0887-2333. DOI: 10.1016/S0887-2333(00)00054-0 (cit. on p. 18).

[113] C. E. Cross *et al.*, „Oxidants, antioxidants, and respiratory tract lining fluids“, *Environmental Health Perspectives*, vol. 102, no. suppl 10, p. 185, 1994, ISSN: 00916765. DOI: 10.1289/ehp.94102s10185. [Online]. Available: /pmc/articles/PMC1566988/?report=abstract%20https://www.ncbi.nlm.nih.gov/pmc/articles/PMC1566988/ (cit. on p. 18).

[114] J. C. Deutsch, „Ascorbic acid oxidation by hydrogen peroxide.“, *Analytical Biochemistry*, vol. 255, no. 1, pp. 1–7, Jan. 1998, ISSN: 00032697. DOI: 10.1006/abio.1997.2293. [Online]. Available: http://www.sciencedirect.com/science/article/pii/S0003269797922934%5Cnhttp://www.sciencedirect.com/science/article/pii/S0003269797922934/pdf?md5=605d36b9707f3cec04f55c654efe5b25&pid=1-s2.0-S0003269797922934-main.pdf (cit. on p. 18).

[115] H. Loertzer, S. Bauer, W. Mörke, P. Fornara, and H. J. Brömme, „Formation of Ascorbate Radicals as a Measure of Oxidative Stress: An In Vitro Electron Spin Resonance-Study Using 2,2-Azobis (2-Amidinopropane) Dihydrochloride as a Radical Generator“, *Transplantation Proceedings*, vol. 38, no. 3, pp. 674–678, 2006, ISSN: 00411345. DOI: 10.1016/j.transproceed.2006.01.043 (cit. on p. 18).

[116] G. Burini, „Development of a quantitative method for the analysis of total l-ascorbic acid in foods by high-performance liquid chromatography“, *Journal of Chromatography A*, vol. 1154, no. 1-2, pp. 97–102, 2007, ISSN: 00219673. DOI: 10.1016/j.chroma.2007.03.013 (cit. on pp. 19, 33).

[117] E. Koike and T. Kobayashi, „Chemical and biological oxidative effects of carbon black nanoparticles“, *Chemosphere*, vol. 65, no. 6, pp. 946–951, Nov. 2006, ISSN: 00456535. DOI: 10.1016/j.chemosphere.2006.03.078 (cit. on p. 24).

[118] K. Donaldson, V. Stone, A. Seaton, and W. MacNee, „Ambient particle inhalation and the cardiovascular system: Potential mechanisms“, *Environmental Health Perspectives*, vol. 109, no. SUPPL. 4, pp. 523–527, 2001, ISSN: 00916765. DOI: 10.1289/ehp.01109s4523. [Online]. Available: http://ehpnet1.niehs.nih.gov/docs/2001/suppl-4/523-527donaldson/abstract.html (cit. on pp. 24, 112).

[119] N. Li, M. Hao, R. F. Phalen, W. C. Hinds, and A. E. Nel, „Particulate air pollutants and asthma: A paradigm for the role of oxidative stress in PM-induced adverse health effects“, *Clinical Immunology*, vol. 109, no. 3, pp. 250–265, 2003, ISSN: 15216616. DOI: 10.1016/j.clim.2003.08.006 (cit. on pp. 24, 112).

[120] A. Baulig *et al.*, „Involvement of reactive oxygen species in the metabolic pathways triggered by diesel exhaust particles in human airway epithelial cells“, *American Journal of Physiology - Lung Cellular and Molecular Physiology*, vol. 285, no. 3 29-3, Sep. 2003, ISSN: 10400605. DOI: 10.1152/ajplung.00419.2002. [Online]. Available: https://pubmed.ncbi.nlm.nih.gov/12730081/ (cit. on pp. 24, 112).

[121] A. K. Prahalad, J. Inmon, L. A. Dailey, M. C. Madden, A. J. Ghio, and J. E. Gallagher, „Air pollution particles mediated oxidative DNA base damage in a cell free system and in human airway epithelial cells in relation to particulate metal content and bioreactivity“, *Chemical Research in Toxicology*, vol. 14, no. 7, pp. 879–887, 2001, ISSN: 0893228X. DOI: 10.1021/tx010022e. [Online]. Available: https://pubmed.ncbi.nlm.nih.gov/11453735/ (cit. on pp. 24, 112).

[122] S. E. Lehman, A. S. Morris, P. S. Mueller, A. K. Salem, V. H. Grassian, and S. C. Larsen, „Silica nanoparticle-generated ROS as a predictor of cellular toxicity: Mechanistic insights and safety by design“, *Environmental Science: Nano*, vol. 3, no. 1, pp. 56–66, Feb. 2016, ISSN: 20518161. DOI: 10.1039/c5en00179j. [Online]. Available: https://pubs.rsc.org/en/content/articlehtml/2016/en/c5en00179j%20https://pubs.rsc.org/en/content/articlelanding/2016/en/c5en00179j (cit. on p. 24).

[123] M. Steenhof *et al.*, „In vitro toxicity of particulate matter (PM) collected at different sites in the Netherlands is associated with PM composition, size fraction and oxidative potential - the RAPTES project“, *Particle and Fibre Toxicology*, vol. 8, no. 1, p. 26, Sep. 2011, ISSN: 17438977. DOI: 10.1186/1743-8977-8-26. [Online]. Available: http://www.particleandfibretoxicology.com/content/8/1/26%20http://particleandfibretoxicology.biomedcentral.com/articles/10.1186/1743-8977-8-26%20https://link.springer.com/articles/10.1186/1743-8977-8-26%20https://link.springer.com/article/10.1186/1743-8977-8-26 (cit. on p. 24).

[124] A. Yang, N. A. Janssen, B. Brunekreef, F. R. Cassee, G. Hoek, and U. Gehring, „Children's respiratory health and oxidative potential of PM2.5: The PIAMA birth cohort study“, *Occupational and Environmental Medicine*, vol. 73, no. 3, pp. 154–160, Mar. 2016, ISSN: 14707926. DOI: 10.1136/oemed-2015-103175. [Online]. Available: https://pubmed.ncbi.nlm.nih.gov/26755634/ (cit. on p. 24).

[125] K. J. Godri *et al.*, „Increased oxidative burden associated with traffic component of ambient particulate matter at roadside and Urban background schools sites in London“, *PLoS ONE*, vol. 6, no. 7, 2011, ISSN: 1932203. DOI: 10.1371/journal.pone.0021961 (cit. on p. 24).

[126] V. Verma *et al.*, „Physicochemical and oxidative characteristics of semi-volatile components of quasi-ultrafine particles in an urban atmosphere“, *Atmospheric Environment*, vol. 45, no. 4, pp. 1025–1033, Feb. 2011, ISSN: 13522310. DOI: 10.1016/j.atmosenv.2010.10.044. [Online]. Available: http://dx.doi.org/10.1016/j.atmosenv.2010.10.044%20https://experts.illinois.edu/en/publications/physicochemical-and-oxidative-characteristics-of-semi-volatile-co (cit. on pp. 24, 30).

[127] S. S. Steimer *et al.*, „Synthesis and characterisation of peroxypinic acids as proxies for highly oxygenated molecules (HOMs) in secondary organic aerosol“, *Atmospheric Chemistry and Physics*, vol. 18, no. 15, pp. 10 973–10 983, 2018, ISSN: 16807324. DOI: 10.5194/acp-18-10973-2018 (cit. on pp. 25, 93, 95, 114, 143).

[128] J. Zhao *et al.*, „Assessment of reactive oxygen species generated by electronic cigarettes using acellular and cellular approaches“, *Journal of Hazardous Materials*, vol. 344, pp. 549–557, 2018, ISSN: 18733336. DOI: 10.1016/j.jhazmat.2017.10.057. [Online]. Available: http://dx.doi.org/10.1016/j.jhazmat.2017.10.057 (cit. on pp. 25, 114).

[129] M. F. Akhtar, M. Hanif, and N. M. Ranjha, „Methods of synthesis of hydrogels... A review“, *Saudi Pharmaceutical Journal*, vol. 24, no. 5, pp. 554–559, 2016, ISSN: 13190164. DOI: 10.1016/j.jsps.2015.03.022 (cit. on p. 25).

[130] Y. Wang, P. K. Hopke, L. Sun, D. C. Chalupa, and M. J. Utell, „Laboratory and Field Testing of an Automated Atmospheric Particle-Bound Reactive Oxygen Species Sampling-Analysis System“, *Journal of Toxicology*, vol. 2011, pp. 1–9, 2011, ISSN: 1687-8191. DOI: 10.1155/2011/419476. [Online]. Available: http://www.hindawi.com/journals/jt/2011/419476/ (cit. on p. 25).

[131] A. Calas *et al.*, „The importance of simulated lung fluid (SLF) extractions for a more relevant evaluation of the oxidative potential of particulate matter“, *Scientific Reports*, vol. 7, no. 1, pp. 1–12, Dec. 2017, ISSN: 20452322. DOI: 10.1038/s41598-017-11979-3 (cit. on p. 25).

[132] M. C. Pietrogrande, I. Bertoli, F. Manarini, and M. Russo, „Ascorbate assay as a measure of oxidative potential for ambient particles: Evidence for the importance of cell-free surrogate lung fluid composition“, *Atmospheric Environment*, vol. 211, no. May, pp. 103–112, Aug. 2019, ISSN: 18732844. DOI: 10.1016/j.atmosenv.2019.05.012. [Online]. Available: https://doi.org/10.1016/j.atmosenv.2019.05.012 (cit. on pp. 25, 30, 56).

[133] S. Englard and S. Seifter, „THE BIOCHEMICAL FUNCTIONS OF ASCORBIC ACID“, 1986. [Online]. Available: www.annualreviews.org (cit. on p. 26).

[134] L. Li *et al.*, „Ascorbic Acid Facilitates Neural Regeneration After Sciatic Nerve Crush Injury“, *Frontiers in Cellular Neuroscience*, vol. 13, p. 108, Jan. 2019, ISSN: 16625102. DOI: 10.3389/FNCEL.2019.00108. [Online]. Available: /pmc/articles/PMC6437112/%20/pmc/articles/PMC6437112/?report=abstract%20https://www.ncbi.nlm.nih.gov/pmc/articles/PMC6437112/ (cit. on p. 26).

[135] J. E. Birdwell and A. S. Engel, „Characterization of dissolved organic matter in cave and spring waters using UV-Vis absorbance and fluorescence spectroscopy“, *Organic Geochemistry*, vol. 41, no. 3, pp. 270–280, Mar. 2010, ISSN: 01466380. DOI: 10.1016/J.ORGGEOCHEM.2009.11.002 (cit. on pp. 27, 57).

[136] S. Huang, W. Gan, M. Yan, X. Zhang, Y. Zhong, and X. Yang, „Differential UV–vis absorbance can characterize the reaction of organic matter with ClO2“, *Water Research*, vol. 139, pp. 442–449, Aug. 2018, ISSN: 0043-1354. DOI: 10.1016/J.WATRES.2018.04.006 (cit. on p. 27).

[137] A. Bonifacie, A. Promeyrat, G. Nassy, P. Gatellier, V. Santé-Lhoutellier, and L. Théron, „Chemical reactivity of nitrite and ascorbate in a cured and cooked meat model implication in nitrosation, nitrosylation and oxidation“, *Food Chemistry*, vol. 348, p. 129 073, Jun. 2021, ISSN: 0308-8146. DOI: 10.1016/J.FOODCHEM.2021.129073 (cit. on p. 27).

[138] X. Wu, Y. Diao, C. Sun, J. Yang, Y. Wang, and S. Sun, „Fluorimetric determination of ascorbic acid with o - phenylenediamine“, *Talanta*, vol. 59, no. 1, pp. 95–99, 2003 (cit. on p. 27).

[139] J. A. Rodrigues, I. M. Valente, L. M. Gonçalves, J. G. Pacheco, and A. A. Barros, „Polarographic determination of vitamin C after derivatization with o-phenylenediamine“, *Collection of Czechoslovak Chemical Communications*, vol. 75, no. 7, pp. 731–741, Jul. 2010, ISSN: 1212-6950. DOI: 10.1135/CCCC2010026 (cit. on p. 27).

[140] P. Zhang, X. Zhang, X. Zhao, G. Jing, and Z. Zhou, „Activation of peracetic acid with zero-valent iron for tetracycline abatement: The role of Fe(II) complexation with tetracycline“, *Journal of Hazardous Materials*, vol. 424, no. November 2021, 2022, ISSN: 18733336. DOI: 10.1016/j.jhazmat.2021.127653 (cit. on pp. 30, 95).

[141] Y. Yoshimura, Y. Matsuzaki, T. Watanabe, K. Uchiyama, K. Ohsawa, and K. Imaeda, „Effects of Buffer Solutions and Chelators on the Generation of Hydroxyl Radical and the Lipid Peroxidation in the Fenton Reaction System“, *J. Clin. Biochem. Nutr*, vol. 13, pp. 147–154, 1992 (cit. on p. 30).

[142] Jon Petter Gustafsson, *Visual MINTEQ*, 2014. [Online]. Available: https://vminteq.lwr.kth.se/ (cit. on p. 30).

[143] C. Shipman, „Evaluation of 4-(2-hydroxyethyl)-1-piperazineëthanesulfonic acid (HEPES) as a tissue culture buffer“, *Proceedings of the Society for Experimental Biology and Medicine. Society for Experimental Biology and Medicine (New York, N.Y.)*, vol. 130, no. 1, pp. 305–310, 1969, ISSN: 0037-9727. DOI: 10.3181/00379727-130-33543. [Online]. Available: https://pubmed.ncbi.nlm.nih.gov/5762514/ (cit. on pp. 30, 101).

[144] C. M. H. Ferreira, I. S. S. Pinto, E. V. Soares Bc, and H. M. V. M. Soares, „(Un)suitability of the use of pH buffers in biological, biochemical and environmental studies and their interaction with metal ions – a review“, 2015. DOI: 10.1039/c4ra15453c. [Online]. Available: www.rsc.org/advances (cit. on p. 30).

[145] Y. Ding, T. Lin, J. Shen, Y. Wei, and C. Wang, „In situ reaction-based ratiometric fluorescent assay for alkaline phosphatase activity and bioimaging“, *Spectrochimica Acta Part A: Molecular and Biomolecular Spectroscopy*, vol. 282, p. 121 698, Dec. 2022, ISSN: 1386-1425. DOI: 10.1016/J.SAA.2022.121698 (cit. on pp. 33, 34).

[146] X. Sun and M. Hagner, „Mixing Aqueous Ferric Chloride and O-Phenylenediamine Solutions at Room Temperature: A Fast, Economical Route to Ultralong Microfibrils of Assemblied O-Phenylenediamine Dimers“, 2007. DOI: 10.1021/la701378y. [Online]. Available: https://pubs.acs.org/sharingguidelines (cit. on p. 33).

[147] S. Liu, X. Qin, J. Tian, L. Wang, and X. Sun, „Photochemical preparation of fluorescent 2,3-diaminophenazine nanoparticles for sensitive and selective detection of Hg(II) ions“, *Sensors and Actuators, B: Chemical*, vol. 171-172, pp. 886–890, Aug. 2012, ISSN: 09254005. DOI: 10.1016/J.SNB.2012.05.089 (cit. on p. 33).

[148] C. C. Winterbourn, „Toxicity of iron and hydrogen peroxide: the Fenton reaction“, *Toxicology Letters*, vol. 82-83, no. C, pp. 969–974, 1995, ISSN: 03784274. DOI: 10.1016/0378-4274(95)03532-X (cit. on p. 37).

[149] J. M. Vislisel, F. Q. Schafer, and G. R. Buettner, „A simple and sensitive assay for ascorbate using a plate reader“, *Analytical Biochemistry*, vol. 365, no. 1, pp. 31–39, Jun. 2007, ISSN: 00032697. DOI: 10.1016/j.ab.2007.03.002. [Online]. Available: /pmc/articles/PMC2129083/?report=abstract%20https://www.ncbi.nlm.nih.gov/pmc/articles/PMC2129083/%20https://linkinghub.elsevier.com/retrieve/pii/S000326970700139X (cit. on p. 38).

[150] M. Andersen, K. Raulund-Rasmussen, B. Strobel, and H. Hansen, „Adsorption of Cadmium, Copper, Nickel, and Zinc to a Poly(tetrafluorethene) Porous Soil Solution Sampler“, *Journal of Environmental Quality*, vol. 31, no. 1, pp. 168–175, Jan. 2002, ISSN: 00472425. DOI: 10.2134/jeq2002.1680. [Online]. Available: http://doi.wiley.com/10.2134/jeq2002.1680 (cit. on p. 39).

[151] R. J. Weber, D. Orsini, Y. Daun, Y. N. Lee, P. J. Klotz, and F. Brechtel, „A Particle-into-Liquid Collector for Rapid Measurement of Aerosol Bulk Chemical Composition“, *https://doi.org/10.1080/02786820152546761*, vol. 35, no. 3, pp. 718–727, 2001, ISSN: 02786826. DOI: 10.1080/02786820152546761. [Online]. Available: https://www.tandfonline.com/doi/abs/10.1080/02786820152546761 (cit. on p. 41).

[152] *fluid dynamics - Does the Flow Rate of a Pipe Change with its Length? - Physics Stack Exchange*. [Online]. Available: https://physics.stackexchange.com/questions/533371/does-the-flow-rate-of-a-pipe-change-with-its-length (cit. on p. 53).

[153] D. Zhao, J. Li, C. Peng, S. Zhu, J. Sun, and X. Yang, „Fluorescence Immunoassay Based on the Alkaline Phosphatase Triggered in Situ Fluorogenic Reaction of o-Phenylenediamine and Ascorbic Acid“, *Analytical Chemistry*, 2019, ISSN: 15206882. DOI: 10.1021/acs.analchem.8b05203. [Online]. Available: https://pubs.acs.org/sharingguidelines (cit. on p. 56).

[154] P. Shahpoury, T. Harner, G. Lammel, S. Lelieveld, H. Tong, and J. Wilson, „Development of an antioxidant assay to study oxidative potential of airborne particulate matter“, *Atmospheric Measurement Techniques*, vol. 12, no. 12, pp. 6529–6539, Dec. 2019, ISSN: 18678548. DOI: 10.5194/amt-12-6529-2019 (cit. on p. 56).

[155] B. Gfeller, E. Meyer, and M. Kalberer, „Development of an Ascorbic Acid Absorbance based Particulate Matter Toxicity Metric and Synthesis of Metal Nanoparticles for Health Studies MASTER'S THESIS for the Master in Physics“, Tech. Rep., 2022 (cit. on p. 57).

[156] J. Huang, Y. Liu, H. Hou, and T. You, „Simultaneous electrochemical determination of dopamine, uric acid and ascorbic acid using palladium nanoparticle-loaded carbon nanofibers modified electrode“, *Biosensors and Bioelectronics*, vol. 24, no. 4, pp. 632–637, 2008, ISSN: 09565663. DOI: 10.1016/j.bios.2008.06.011 (cit. on p. 57).

[157] F. E. Huelin, „Investigations on the stability and determination of dehydroascorbic acid“, *Australian Journal of Biological Sciences*, vol. 2, no. 4, pp. 346–354, 1949, ISSN: 00049417. DOI: 10.1071/BI9490346 (cit. on pp. 63, 65).

[158] M. C. Pietrogrande, L. Romanato, and M. Russo, „Synergistic and Antagonistic Effects of Aerosol Components on Its Oxidative Potential as Predictor of Particle Toxicity“, *Toxics 2022, Vol. 10, Page 196*, vol. 10, no. 4, p. 196, Apr. 2022, ISSN: 2305-6304. DOI: 10.3390/TOXICS10040196. [Online]. Available: https://www.mdpi.com/2305-6304/10/4/196/htm%20https://www.mdpi.com/2305-6304/10/4/196 (cit. on p. 66).

[159] S. M. Hama, R. L. Cordell, J. Staelens, D. Mooibroek, and P. S. Monks, „Chemical composition and source identification of PM10 in five North Western European cities“, *Atmospheric Research*, vol. 214, pp. 135–149, Dec. 2018, ISSN: 01698095. DOI: 10.1016/J.ATMOSRES.2018.07.014 (cit. on p. 66).

[160] A. I. Calvo, C. Alves, A. Castro, V. Pont, A. M. Vicente, and R. Fraile, „Research on aerosol sources and chemical composition: Past, current and emerging issues“, *Atmospheric Research*, vol. 120-121, pp. 1–28, Feb. 2013, ISSN: 0169-8095. DOI: 10.1016/J.ATMOSRES.2012.09.021 (cit. on p. 66).

[161] M. Kamphus *et al.*, „Chemical composition of ambient aerosol, ice residues and cloud droplet residues in mixed-phase clouds: single particle analysis during the Cloud and Aerosol Characterization Experiment (CLACE 6)“, *Atmos. Chem. Phys*, vol. 10, pp. 8077–8095, 2010. DOI: 10.5194/acp-10-

8077-2010. [Online]. Available: www.atmos-chem-phys.net/10/8077/2010/ (cit. on p. 66).

[162] Z. Shi *et al.*, „Introduction to the special issue "In-depth study of air pollution sources and processes within Beijing and its surrounding region (APHH-Beijing)"", *Atmospheric Chemistry and Physics*, vol. 19, no. 11, pp. 7519–7546, Jun. 2019, ISSN: 1680-7324. DOI: 10.5194/acp-19-7519-2019. [Online]. Available: https://acp.copernicus.org/articles/19/7519/2019/ (cit. on pp. 68, 92).

[163] S. J. Campbell, „Supplement of Atmospheric conditions and composition that influence PM 2 . 5 oxidative potential in Beijing , China Section S1 : APHH site location", *Atmospheric Chemistry and Physics*, no. 21, pp. 5549–5573, 2021. DOI: 0.5194/acp-21-5549-2021 (cit. on p. 68).

[164] E. Kostenidou, S. N. Pandis, R. K. Pathak, S. N. Pandis, E. Kostenidou, and S. N. Pandis, „An Algorithm for the Calculation of Secondary Organic Aerosol Density Combining AMS and SMPS Data", *http://dx.doi.org/10.1080/02786820701666270*, vol. 41, no. 11, pp. 1002–1010, Oct. 2007, ISSN: 15217388. DOI: 10.1080/02786820701666270. [Online]. Available: https://www.tandfonline.com/doi/abs/10.1080/02786820701666270 (cit. on p. 69).

[165] W. Y. Tuet *et al.*, „Chemical oxidative potential of secondary organic aerosol (SOA) generated from the photooxidation of biogenic and anthropogenic volatile organic compounds", *Atmospheric Chemistry and Physics*, vol. 17, no. 2, pp. 839–853, 2017, ISSN: 16807324. DOI: 10.5194/acp-17-839-2017 (cit. on p. 70).

[166] P. H. Chowdhury, Q. He, T. Lasitza Male, W. H. Brune, Y. Rudich, and M. Pardo, „Exposure of Lung Epithelial Cells to Photochemically Aged Secondary Organic Aerosol Shows Increased Toxic Effects", *Environmental Science and Technology Letters*, vol. 5, no. 7, pp. 424–430, Jul. 2018, ISSN: 23288930. DOI: 10.1021/ACS.ESTLETT.8B00256/ASSET/IMAGES/LARGE/EZ-2018-00256Y{_}0002.JPEG. [Online]. Available: https://pubs.acs.org/doi/full/10.1021/acs.estlett.8b00256 (cit. on p. 70).

[167] V. A. Roginsky, T. K. Barsukova, and H. B. Stegmann, „Kinetics of redox interaction between substituted quinones and ascorbate under aerobic conditions", *Chemico-Biological Interactions*, vol. 121, no. 2, pp. 177–197, 1999, ISSN: 00092797. DOI: 10.1016/S0009-2797(99)00099-X (cit. on pp. 70, 95).

[168] N. S. Isaacs and R. Van Eldik, „A mechanistic study of the reduction of quinones by ascorbic acid", *Journal of the Chemical Society. Perkin Transactions 2*, no. 8, pp. 1465–1467, 1997, ISSN: 03009580. DOI: 10.1039/a701072i (cit. on pp. 70, 95).

[169] R. D. McWhinney, S. Zhou, and J. P. Abbatt, „Naphthalene SOA: Redox activity and naphthoquinone gas-particle partitioning“, *Atmospheric Chemistry and Physics*, vol. 13, no. 19, pp. 9731–9744, 2013, ISSN: 16807316. DOI: 10.5194/ACP-13-9731-2013 (cit. on pp. 70, 135, 148).

[170] A. Keller *et al.*, „The organic coating unit, an all-in-one system for reproducible generation of secondary organic matter aerosol“, *Aerosol Science and Technology*, vol. 56, no. 10, pp. 947–958, Sep. 2022, ISSN: 0278-6826. DOI: 10.1080/02786826.2022.2110448. [Online]. Available: https://www.tandfonline.com/doi/full/10.1080/02786826.2022.2110448 (cit. on pp. 70, 86, 87, 137, 200).

[171] Lufthygine Amt beider Basel, *Luftqualität Nordwestschweiz*. [Online]. Available: https://luftqualitaet.ch/messdaten/datenarchiv/abfrage (cit. on p. 71).

[172] C. Giorio *et al.*, „Online Quantification of Criegee Intermediates of α-Pinene Ozonolysis by Stabilization with Spin Traps and Proton-Transfer Reaction Mass Spectrometry Detection“, 2017. DOI: 10.1021/jacs.6b10981. [Online]. Available: https://pubs.acs.org/sharingguidelines (cit. on p. 87).

[173] A. Sorooshian *et al.*, „Modeling and Characterization of a Particle-into-Liquid Sampler (PILS)“, *http://dx.doi.org/10.1080/02786820600632282*, vol. 40, no. 6, pp. 396–409, Jul. 2006, ISSN: 15217388. DOI: 10.1080/02786820600632282. [Online]. Available: https://www.tandfonline.com/doi/abs/10.1080/02786820600632282 (cit. on pp. 87, 96).

[174] L. Künzi *et al.*, „Toxicity of aged gasoline exhaust particles to normal and diseased airway epithelia“, *Scientific Reports*, vol. 5, pp. 1–10, 2015, ISSN: 20452322. DOI: 10.1038/srep11801 (cit. on pp. 88, 113, 114).

[175] A. Calas *et al.*, „Comparison between five acellular oxidative potential measurement assays performed with detailed chemistry on PM10 samples from the city of Chamonix (France)“, *Atmospheric Chemistry and Physics*, vol. 18, no. 11, pp. 7863–7875, Jun. 2018, ISSN: 16807324. DOI: 10.5194/acp-18-7863-2018. [Online]. Available: https://www.atmos-chem-phys.net/18/7863/2018/ (cit. on pp. 91, 135).

[176] J. Xu *et al.*, „Source Apportionment of Fine Aerosol at an Urban Site of Beijing Using a Chemical Mass Balance Model“, *in preparation*, 2020 (cit. on p. 92).

[177] S. Wang, Y. Zhao, A. W. H. Chan, M. Yao, Z. Chen, and J. P. D. Abbatt, „Organic Peroxides in Aerosol: Key Reactive Intermediates for Multiphase Processes in the Atmosphere“, *Chemical Reviews*, Jan. 2023, ISSN: 0009-2665. DOI: 10.1021/ACS.CHEMREV.2C00430. [Online]. Available: https://pubs.acs.org/doi/full/10.1021/acs.chemrev.2c00430 (cit. on pp. 92, 136, 188).

[178] A. Kocbach Bølling *et al.*, „Health effects of residential wood smoke particles: the importance of combustion conditions and physicochemical particle properties“, *Particle and Fibre Toxicology 2009 6:1*, vol. 6, no. 1, pp. 1–20, Nov. 2009, ISSN: 1743-8977. DOI: 10.1186/1743-8977-6-29. [Online]. Available: https://particleandfibretoxicology.biomedcentral.com/articles/10.1186/1743-8977-6-29 (cit. on p. 92).

[179] L. Qi, M. Chen, X. Ge, Y. Zhang, and B. Guo, „Seasonal Variations and Sources of 17 Aerosol Metal Elements in Suburban Nanjing, China“, *Atmosphere 2016, Vol. 7, Page 153*, vol. 7, no. 12, p. 153, Nov. 2016, ISSN: 2073-4433. DOI: 10.3390/ATMOS7120153. [Online]. Available: https://www.mdpi.com/2073-4433/7/12/153/htm%20https://www.mdpi.com/2073-4433/7/12/153 (cit. on p. 92).

[180] J. Orasche *et al.*, „Comparison of emissions from wood combustion. Part 2: Impact of combustion conditions on emission factors and characteristics of particle-bound organic species and polycyclic aromatic hydrocarbon (PAH)-related toxicological potential“, *Energy and Fuels*, vol. 27, no. 3, pp. 1482–1491, Mar. 2013, ISSN: 08870624. DOI: 10.1021/EF301506H/SUPPL{_}FILE/EF301506H{_}SI{_}001.PDF. [Online]. Available: https://pubs.acs.org/doi/full/10.1021/ef301506h (cit. on p. 92).

[181] M. C. Pietrogrande, C. Colombi, E. Cuccia, U. D. Santo, and L. Romanato, „Seasonal and Spatial Variations of the Oxidative Properties of Ambient PM2.5 in the Po Valley, Italy, before and during COVID-19 Lockdown Restrictions“, *International Journal of Environmental Research and Public Health 2023, Vol. 20, Page 1797*, vol. 20, no. 3, p. 1797, Jan. 2023, ISSN: 1660-4601. DOI: 10.3390/IJERPH20031797. [Online]. Available: https://www.mdpi.com/1660-4601/20/3/1797 (cit. on p. 92).

[182] D. Paraskevopoulou *et al.*, „Yearlong variability of oxidative potential of particulate matter in an urban Mediterranean environment“, *Atmospheric Environment*, vol. 206, no. February, pp. 183–196, 2019, ISSN: 18732844. DOI: 10.1016/j.atmosenv.2019.02.027. [Online]. Available: https://doi.org/10.1016/j.atmosenv.2019.02.027 (cit. on p. 92).

[183] D. A. Lack, X. X. Tie, N. D. Bofinger, A. N. Wiegand, and S. Madronich, „Seasonal variability of secondary organic aerosol: A global modeling study“, *Journal of Geophysical Research: Atmospheres*, vol. 109, no. D3, p. 3203, Feb. 2004, ISSN: 2156-2202. DOI: 10.1029/2003JD003418. [Online]. Available: https://onlinelibrary.wiley.com/doi/full/10.1029/2003JD003418%20https://onlinelibrary.wiley.com/doi/abs/10.1029/2003JD003418%20https://agupubs.onlinelibrary.wiley.com/doi/10.1029/2003JD003418 (cit. on p. 92).

[184] G. Bergametti *et al.*, „Seasonal variability of the elemental composition of atmospheric aerosol particles over the northwestern Mediterranean“, *Stockholm Uni Press*, vol. 41, no. 3, pp. 353–361, Jan. 2017. DOI: 10.3402/TELLUSB.V41I3.15092. [Online]. Available: https://www.tandfonline.com/doi/abs/10.3402/tellusb.v41i3.15092 (cit. on p. 92).

[185] X. Zhang *et al.*, „Formation and evolution of molecular products in α-pinene secondary organic aerosol“, *Proceedings of the National Academy of Sciences of the United States of America*, vol. 112, no. 46, pp. 14 168–14 173, Nov. 2015, ISSN: 10916490. DOI: 10.1073/PNAS.1517742112/SUPPL{_}FILE/PNAS.1517742112.SAPP.PDF. [Online]. Available: https://www.pnas.org/doi/abs/10.1073/pnas.1517742112 (cit. on p. 95).

[186] J. Hammond, B. A. Maher, T. Gonet, F. Bautista, and D. Allsop, „Oxidative Stress, Cytotoxic and Inflammatory Effects of Urban Ultrafine Road-Deposited Dust from the UK and Mexico in Human Epithelial Lung (Calu-3) Cells“, *Antioxidants*, vol. 11, no. 9, p. 1814, Sep. 2022, ISSN: 20763921. DOI: 10.3390/ANTIOX11091814/S1. [Online]. Available: https://www.mdpi.com/2076-3921/11/9/1814/htm%20https://www.mdpi.com/2076-3921/11/9/1814 (cit. on p. 102).

[187] L. A. Urry, M. L. (L. Cain, S. A. Wasserman, P. V. Minorsky, J. B. Reece, and N. A. Campbell, „Campbell Biology“, vol. 11th, 2017 (cit. on p. 103).

[188] AeroHEALTH Consortium, *AeroHEALTH > Helmholtz International Laboratory*, 2021. [Online]. Available: https://www.aerohealth.eu/en/index.html (cit. on p. 111).

[189] G. Pizzino *et al.*, „Oxidative Stress: Harms and Benefits for Human Health“, 2017. DOI: 10.1155/2017/8416763. [Online]. Available: https://doi.org/10.1155/2017/8416763 (cit. on p. 113).

[190] F. Karagulian *et al.*, „Contributions to cities' ambient particulate matter (PM): A systematic review of local source contributions at global level“, *Atmospheric Environment*, vol. 120, pp. 475–483, Nov. 2015, ISSN: 1352-2310. DOI: 10.1016/J.ATMOSENV.2015.08.087 (cit. on p. 113).

[191] H. Orru *et al.*, „Health impacts of PM2.5 originating from residential wood combustion in four nordic cities“, *BMC Public Health*, vol. 22, no. 1, pp. 1–13, Dec. 2022, ISSN: 14712458. DOI: 10.1186/S12889-022-13622-X/FIGURES/3. [Online]. Available: https://bmcpublichealth.biomedcentral.com/articles/10.1186/s12889-022-13622-x (cit. on p. 113).

[192] R. Bahreini *et al.*, „Gasoline emissions dominate over diesel in formation of secondary organic aerosol mass“, *Geophysical Research Letters*, vol. 39, no. 6, p. 6805, Mar. 2012, ISSN: 1944-8007. DOI: 10.1029/2011GL050718. [Online]. Available: https://onlinelibrary.wiley.com/doi/full/10.1029/2011GL050718%20https://onlinelibrary.wiley.com/doi/abs/10.1029/2011GL050718%20https://agupubs.onlinelibrary.wiley.com/doi/10.1029/2011GL050718 (cit. on p. 114).

[193] A. K. Agarwal *et al.*, „Toxicity of exhaust particulates and gaseous emissions from gasohol (ethanol blended gasoline)-fuelled spark ignition engines“, *Environmental Science: Processes & Impacts*, vol. 22, no. 7, pp. 1540–1553, Jul. 2020, ISSN: 20507895. DOI: 10.1039/D0EM00082E. [Online]. Available: https://pubs.rsc.org/en/content/articlehtml/

2020/em/d0em00082e%20https://pubs.rsc.org/en/content/articlelanding/2020/em/d0em00082e (cit. on p. 114).

[194] A. K. Agarwal *et al.*, „Toxicity and mutagenicity of exhaust from compressed natural gas: Could this be a clean solution for megacities with mixed-traffic conditions?“, *Environmental Pollution*, vol. 239, pp. 499–511, Aug. 2018, ISSN: 0269-7491. DOI: 10.1016/J.ENVPOL.2018.04.028 (cit. on p. 114).

[195] M. Ihalainen *et al.*, „A novel high-volume Photochemical Emission Aging flow tube Reactor (PEAR)“, *Aerosol Science and Technology*, vol. 53, no. 3, pp. 276–294, Mar. 2019, ISSN: 15217388. DOI: 10.1080/02786826.2018.1559918/SUPPL{_}FILE/UAST{_}A{_}1559918{_}SM0097.DOCX. [Online]. Available: https://www.tandfonline.com/doi/abs/10.1080/02786826.2018.1559918 (cit. on pp. 114, 116, 118).

[196] S. M. Platt *et al.*, „Secondary organic aerosol formation from gasoline vehicle emissions in a new mobile environmental reaction chamber“, *Atmospheric Chemistry and Physics*, vol. 13, no. 18, pp. 9141–9158, 2013, ISSN: 16807316. DOI: 10.5194/ACP-13-9141-2013 (cit. on p. 122).

[197] A. Zare *et al.*, „Analysis of cold-start NO2 and NOx emissions, and the NO2/NOx ratio in a diesel engine powered with different diesel-biodiesel blends“, *Environmental Pollution*, vol. 290, p. 118 052, Dec. 2021, ISSN: 0269-7491. DOI: 10.1016/J.ENVPOL.2021.118052 (cit. on p. 125).

[198] S. Platt *et al.*, „Two-stroke scooters are a dominant source of air pollution in many cities“, *Nature Communications*, vol. 5, no. 1, p. 3749, Sep. 2014, ISSN: 2041-1723. DOI: 10.1038/ncomms4749. [Online]. Available: http://www.nature.com/articles/ncomms4749 (cit. on p. 125).

[199] M. F. Heringa *et al.*, „Time-Resolved Characterization of Primary Emissions from Residential Wood Combustion Appliances“, *Environmental Science & Technology*, vol. 46, no. 20, pp. 11 418–11 425, Oct. 2012, ISSN: 0013-936X. DOI: 10.1021/es301654w. [Online]. Available: https://pubs.acs.org/doi/10.1021/es301654w (cit. on p. 126).

[200] E. D. Vicente, M. A. Duarte, A. I. Calvo, T. F. Nunes, L. Tarelho, and C. A. Alves, „Emission of carbon monoxide, total hydrocarbons and particulate matter during wood combustion in a stove operating under distinct conditions“, *Fuel Processing Technology*, vol. 131, pp. 182–192, Mar. 2015, ISSN: 0378-3820. DOI: 10.1016/J.FUPROC.2014.11.021 (cit. on p. 126).

[201] J. Kjällstrand and G. Petersson, „Phenolic antioxidants in wood smoke“, *Science of The Total Environment*, vol. 277, no. 1-3, pp. 69–75, Sep. 2001, ISSN: 0048-9697. DOI: 10.1016/S0048-9697(00)00863-9 (cit. on p. 127).

[202] A. L. Hodshire *et al.*, „Aging Effects on Biomass Burning Aerosol Mass and Composition: A Critical Review of Field and Laboratory Studies“, *Environmental Science and Technology*, vol. 53, no. 17, pp. 10 007–10 022, Apr. 2019, ISSN: 15205851. DOI: 10.1021/ACS.EST.9B02588/ASSET/IMAGES/LARGE/ES9B02588{_}0004.JPEG. [Online]. Available: https://pubs.acs.org/doi/full/10.1021/acs.est.9b02588 (cit. on p. 130).

[203] M. Pardo *et al.*, „Atmospheric aging increases the cytotoxicity of bare soot particles in BEAS-2B lung cells“, *https://doi.org/10.1080/02786826.2023.2178878*, pp. 1–17, Feb. 2023, ISSN: 0278-6826. DOI: 10.1080/02786826.2023.2178878. [Online]. Available: https://www.tandfonline.com/doi/abs/10.1080/02786826.2023.2178878 (cit. on p. 130).

[204] E. Z. Nordin *et al.*, „Influence of ozone initiated processing on the toxicity of aerosol particles from small scale wood combustion“, *Atmospheric Environment*, vol. 102, pp. 282–289, Feb. 2015, ISSN: 1352-2310. DOI: 10.1016/J.ATMOSENV.2014.11.068 (cit. on p. 130).

[205] S. Wang *et al.*, „Dynamic Wood Smoke Aerosol Toxicity during Oxidative Atmospheric Aging“, *Environmental Science and Technology*, vol. 57, pp. 1246–1256, 2023, ISSN: 15205851. DOI: 10.1021/ACS.EST.2C05929/ASSET/IMAGES/LARGE/ES2C05929{_}0006.JPEG. [Online]. Available: https://pubs.acs.org/doi/full/10.1021/acs.est.2c05929 (cit. on p. 130).

[206] J. Li *et al.*, „Effects of atmospheric aging processes on in vitro induced oxidative stress and chemical composition of biomass burning aerosols“, *Journal of Hazardous Materials*, vol. 401, p. 123 750, Jan. 2021, ISSN: 0304-3894. DOI: 10.1016/J.JHAZMAT.2020.123750 (cit. on p. 130).

[207] A. Kocbach, Y. Li, K. E. Yttri, F. R. Cassee, P. E. Schwarze, and E. Namork, „Physicochemical characterisation of combustion particles from vehicle exhaust and residential wood smoke“, *Particle and Fibre Toxicology*, vol. 3, no. 1, pp. 1–10, Jan. 2006, ISSN: 17438977. DOI: 10.1186/1743-8977-3-1/FIGURES/4. [Online]. Available: https://link.springer.com/articles/10.1186/1743-8977-3-1%20https://link.springer.com/article/10.1186/1743-8977-3-1 (cit. on p. 130).

[208] L. Cao *et al.*, „Oxidative damage mediates the association between polycyclic aromatic hydrocarbon exposure and lung function“, *Environmental Health: A Global Access Science Source*, vol. 19, no. 1, pp. 1–10, Jul. 2020, ISSN: 1476069X. DOI: 10.1186/S12940-020-00621-X/TABLES/4. [Online]. Available: https://ehjournal.biomedcentral.com/articles/10.1186/s12940-020-00621-x (cit. on p. 130).

[209] L. Poulain *et al.*, „Atmospheric Chemistry and Physics Diurnal variations of ambient particulate wood burning emissions and their contribution to the concentration of Polycyclic Aromatic Hydrocarbons (PAHs) in Seiffen, Germany“, *Atmos. Chem. Phys*, vol. 11, pp. 12 697–12 713, 2011. DOI:

10.5194/acp-11-12697-2011. [Online]. Available: www.atmos-chem-phys.net/11/12697/2011/ (cit. on p. 130).

[210] T. Ancelet, P. K. Davy, W. J. Trompetter, A. Markwitz, and D. C. Weatherburn, „Carbonaceous aerosols in a wood burning community in rural New Zealand“, *Atmospheric Pollution Research*, vol. 4, no. 3, pp. 245–249, Jul. 2013, ISSN: 1309-1042. DOI: 10.5094/APR.2013.026 (cit. on p. 130).

[211] N. Verma, M. Pink, A. W. Rettenmeier, and S. Schmitz-Spanke, „Review on proteomic analyses of benzo[a]pyrene toxicity“, *PROTEOMICS*, vol. 12, no. 11, pp. 1731–1755, Jun. 2012, ISSN: 1615-9861. DOI: 10.1002/PMIC.201100466. [Online]. Available: https://onlinelibrary.wiley.com/doi/full/10.1002/pmic.201100466%20https://onlinelibrary.wiley.com/doi/abs/10.1002/pmic.201100466%20https://analyticalsciencejournals.onlinelibrary.wiley.com/doi/10.1002/pmic.201100466 (cit. on p. 131).

[212] V. Gianelle *et al.*, „Benzo(a)pyrene air concentrations and emission inventory in Lombardy region, Italy“, *Atmospheric Pollution Research*, vol. 4, no. 3, pp. 257–266, Jul. 2013, ISSN: 1309-1042. DOI: 10.5094/APR.2013.028 (cit. on p. 131).

[213] L. E. Brown, K. R. Trought, C. I. Bailey, and J. H. Clemons, „2,3,7,8-TCDD equivalence and mutagenic activity associated with PM10 from three urban locations in New Zealand“, *The Science of the total environment*, vol. 349, no. 1-3, pp. 161–174, Oct. 2005, ISSN: 0048-9697. DOI: 10.1016/J.SCITOTENV.2005.01.008. [Online]. Available: https://pubmed.ncbi.nlm.nih.gov/16198678/ (cit. on p. 131).

[214] A. M. Knaapen, P. J. Borm, C. Albrecht, and R. P. Schins, „Inhaled particles and lung cancer. Part A: Mechanisms“, *International Journal of Cancer*, vol. 109, no. 6, pp. 799–809, 2004, ISSN: 00207136. DOI: 10.1002/ijc.11708 (cit. on p. 135).

[215] J. G. Charrier, N. K. Richards-Henderson, K. J. Bein, A. S. McFall, A. S. Wexler, and C. Anastasio, „Oxidant production from source-oriented particulate matter - Part 1: Oxidative potential using the dithiothreitol (DTT) assay“, *Atmospheric Chemistry and Physics*, vol. 15, no. 5, pp. 2327–2340, 2015, ISSN: 16807324. DOI: 10.5194/acp-15-2327-2015 (cit. on p. 135).

[216] X. M. Kuang *et al.*, „Aerosol-Borne Quinones and Reactive Oxygen Species Generation by Particulate Matter Extracts“, *Aerosol Science and Technology*, vol. 40, no. 16, pp. 4880–4886, 2006, ISSN: 0013936X. DOI: 10.1021/es0515957. [Online]. Available: http://dx.doi.org/10.1080/02786826.2016.1271938 (cit. on p. 135).

[217] Q. Xiong, H. Yu, R. Wang, J. Wei, and V. Verma, „Rethinking Dithiothreitol-Based Particulate Matter Oxidative Potential: Measuring Dithiothreitol Consumption versus Reactive Oxygen Species Generation“, *Environmental Science and Technology*, vol. 51, no. 11, pp. 6507–6514, 2017, ISSN: 15205851. DOI: 10.1021/acs.est.7b01272 (cit. on p. 135).

[218] V. Verma *et al.*, „Organic Aerosols Associated with the Generation of Reactive Oxygen Species (ROS) by Water-Soluble PM _{2.5}“, *Environmental Science & Technology*, vol. 49, no. 7, pp. 4646–4656, Apr. 2015, ISSN: 0013-936X. DOI: 10.1021/es505577w. [Online]. Available: https://pubs.acs.org/doi/10.1021/es505577w (cit. on p. 135).

[219] D. H. Gonzalez, C. K. Cala, Q. Peng, and S. E. Paulson, „HULIS Enhancement of Hydroxyl Radical Formation from Fe(II): Kinetics of Fulvic Acid-Fe(II) Complexes in the Presence of Lung Antioxidants“, *Environmental Science and Technology*, vol. 51, no. 13, pp. 7676–7685, 2017, ISSN: 15205851. DOI: 10.1021/acs.est.7b01299 (cit. on pp. 135, 144, 146).

[220] Y. Wang *et al.*, „The Secondary Formation of Organosulfates under the Interactions between Biogenic Emissions and Anthropogenic Pollutants in Summer of Beijing“, *Atmospheric Chemistry and Physics Discussions*, pp. 1–37, 2018, ISSN: 1680-7375. DOI: 10.5194/acp-2018-262 (cit. on pp. 135, 143).

[221] J. Wei, H. Yu, Y. Wang, and V. Verma, „Complexation of Iron and Copper in Ambient Particulate Matter and Its E ff ect on the Oxidative Potential Measured in a Surrogate Lung Fluid“, *Environmental Science and Technology*, vol. 53, no. 3, pp. 1661–1671, 2019, ISSN: 0013-936X. DOI: 10.1021/acs.est.8b05731 (cit. on p. 135).

[222] A. S. Wozniak, R. U. Shelley, S. D. McElhenie, W. M. Landing, and P. G. Hatcher, „Aerosol water soluble organic matter characteristics over the North Atlantic Ocean: Implications for iron-binding ligands and iron solubility“, *Marine Chemistry*, vol. C, no. 173, pp. 162–172, Jul. 2015, ISSN: 0304-4203. DOI: 10.1016/J.MARCHEM.2014.11.002. [Online]. Available: https://www.infona.pl//resource/bwmeta1.element.elsevier-d614ae04-1db6-335a-9499-21e4a47d96af (cit. on p. 135).

[223] T. Fang, P. S. Lakey, J. C. Rivera-Rios, F. N. Keutsch, and M. Shiraiwa, „Aqueous-Phase Decomposition of Isoprene Hydroxy Hydroperoxide and Hydroxyl Radical Formation by Fenton-like Reactions with Iron Ions“, *Journal of Physical Chemistry A*, vol. 124, no. 25, pp. 5230–5236, Jun. 2020, ISSN: 15205215. DOI: 10.1021/ACS.JPCA.0C02094/ASSET/IMAGES/LARGE/JP0C02094{_}0004.JPEG. [Online]. Available: https://pubs.acs.org/doi/full/10.1021/acs.jpca.0c02094 (cit. on pp. 135, 143, 148).

[224] Y. X. Sun, S. F. Wang, X. H. Zhang, and Y. F. Huang, „Simultaneous determination of epinephrine and ascorbic acid at the electrochemical sensor of triazole SAM modified gold electrode“, *Sensors and Actuators,*

B: Chemical, vol. 113, no. 1, pp. 156–161, 2006, ISSN: 09254005. DOI: 10.1016/j.snb.2005.02.042 (cit. on p. 137).

[225] V. Damian, A. Sandu, M. Damian, F. Potra, and G. R. Carmichael, „The kinetic preprocessor KPP - A software environment for solving chemical kinetics“, *Computers and Chemical Engineering*, vol. 26, no. 11, pp. 1567–1579, Nov. 2002, ISSN: 00981354. DOI: 10.1016/S0098-1354(02)00128-X (cit. on p. 139).

[226] P. J. Gallimore *et al.*, „Multiphase composition changes and reactive oxygen species formation during limonene oxidation in the new Cambridge Atmospheric Simulation Chamber (CASC)“, *Atmos. Chem. Phys.*, vol. 17, pp. 9853–9868, 2017, ISSN: 1680-7375. DOI: 10.5194/acp-2017-186. [Online]. Available: https://www.atmos-chem-phys-discuss.net/acp-2017-186/ (cit. on p. 140).

[227] K. S. Docherty, W. Wu, Y. B. Lim, and P. J. Ziemann, „Contributions of organic peroxides to secondary aerosol formed from reactions of monoterpenes with O 3“, *Environmental Science and Technology*, vol. 39, no. 11, pp. 4049–4059, 2005, ISSN: 0013936X. DOI: 10.1021/es050228s (cit. on pp. 142, 148).

[228] P. Zhou *et al.*, „Generation of hydrogen peroxide and hydroxyl radical resulting from oxygen-dependent oxidation of l-ascorbic acid via copper redox-catalyzed reactions“, *RSC Advances*, vol. 6, no. 45, pp. 38 541–38 547, 2016, ISSN: 20462069. DOI: 10.1039/c6ra02843h (cit. on p. 142).

[229] J. Kim, T. Zhang, W. Liu, P. Du, J. T. Dobson, and C. H. Huang, „Advanced Oxidation Process with Peracetic Acid and Fe(II) for Contaminant Degradation“, *Environmental Science and Technology*, vol. 53, no. 22, pp. 13 312–13 322, 2019, ISSN: 15205851. DOI: 10.1021/acs.est.9b02991 (cit. on p. 143).

[230] J. De Laat and T. G. Le, „Kinetics and modeling of the Fe(III)/H2O2 system in the presence of sulfate in acidic aqueous solutions“, *Environmental Science and Technology*, vol. 39, no. 6, pp. 1811–1818, 2005, ISSN: 0013936X. DOI: 10.1021/es0493648 (cit. on p. 143).

[231] R. Bianchini, L. Calucci, C. Lubello, and C. Pinzino, „Intermediate free radicals in the oxidation of wastewaters“, *Research on Chemical Intermediates*, vol. 28, no. 2-3, pp. 247–256, 2002, ISSN: 09226168. DOI: 10.1163/156856702320267154 (cit. on p. 143).

[232] C. Zhang, P. J. Brown, and Z. Hu, „Thermodynamic properties of an emerging chemical disinfectant, peracetic acid“, *Science of the Total Environment*, vol. 621, pp. 948–959, 2018, ISSN: 18791026. DOI: 10.1016/j.scitotenv.2017.10.195. [Online]. Available: https://doi.org/10.1016/j.scitotenv.2017.10.195 (cit. on p. 143).

[233] T. Luukkonen and S. O. Pehkonen, „Peracids in water treatment: A critical review“, *Critical Reviews in Environmental Science and Technology*, vol. 47, no. 1, pp. 1–39, 2017, ISSN: 15476537. DOI: 10.1080/10643389.2016.1272343. [Online]. Available: http://dx.doi.org/10.1080/10643389.2016.1272343 (cit. on p. 143).

[234] M. Panizza and G. Cerisola, „Electrochemical generation of H2O2 in low ionic strength media on gas diffusion cathode fed with air“, *Electrochimica Acta*, vol. 54, no. 2, pp. 876–878, 2008, ISSN: 00134686. DOI: 10.1016/j.electacta.2008.07.063 (cit. on p. 143).

[235] Y. Li, T. Zhu, J. Zhao, and B. Xu, „Interactive enhancements of ascorbic acid and iron in hydroxyl radical generation in quinone redox cycling“, *Environmental Science and Technology*, vol. 46, no. 18, pp. 10 302–10 309, 2012, ISSN: 0013936X. DOI: 10.1021/es301834r (cit. on p. 144).

[236] C. Jiang, S. Garg, and T. D. Waite, „Hydroquinone-Mediated Redox Cycling of Iron and Concomitant Oxidation of Hydroquinone in Oxic Waters under Acidic Conditions: Comparison with Iron-Natural Organic Matter Interactions“, *Environmental Science and Technology*, vol. 49, no. 24, pp. 14 076–14 084, 2015, ISSN: 15205851. DOI: 10.1021/acs.est.5b03189 (cit. on p. 144).

[237] N. Zanca *et al.*, „Characterizing source fingerprints and ageing processes in laboratory-generated secondary organic aerosols using proton-nuclear magnetic resonance (1H-NMR) analysis and HPLC HULIS determination“, *Atmospheric Chemistry and Physics*, vol. 17, no. 17, pp. 10 405–10 421, 2017, ISSN: 16807324. DOI: 10.5194/acp-17-10405-2017 (cit. on pp. 144, 149).

[238] M. Lin, J. Z. Yu, J. Zhen Yu, and J. Z. Yu, „Assessment of interactions between transition metals and atmospheric organics: ascorbic acid depletion and hydroxyl radical formation in organic-metal mixtures“, *Environmental Science and Technology*, vol. 54, no. 3, pp. 1431–1442, 2020, ISSN: 15205851. DOI: 10.1021/acs.est.9b07478. [Online]. Available: https://dx.doi.org/10.1021/acs.est.9b07478 (cit. on pp. 145, 146, 149).

[239] E. Vidrio, H. Jung, and C. Anastasio, „Generation of hydroxyl radicals from dissolved transition metals in surrogate lung fluid solutions“, *Atmospheric Environment*, vol. 42, no. 18, pp. 4369–4379, 2008, ISSN: 13522310. DOI: 10.1016/j.atmosenv.2008.01.004 (cit. on p. 145).

[240] J. G. Charrier, A. S. McFall, N. K. Richards-Henderson, and C. Anastasio, „Hydrogen peroxide formation in a surrogate lung fluid by transition metals and quinones present in particulate matter“, *Environmental Science and Technology*, vol. 48, no. 12, pp. 7010–7017, 2014, ISSN: 15205851. DOI: 10.1021/es501011w (cit. on p. 145).

[241] R. R. Grinstead, „The Oxidation of Ascorbic Acid by Hydrogen Peroxide. Catalysis by Ethylenediaminetetraacetato-Iron(III)“, *Journal of the American Chemical Society*, vol. 82, no. 13, pp. 3464–3471, 1960, ISSN: 15205126. DOI: 10.1021/ja01498a057 (cit. on p. 145).

[242] Y. Yan *et al.*, „The complexation between transition metals and water-soluble organic compounds (WSOC) and its effect on reactive oxygen species (ROS) formation“, *Atmospheric Environment*, vol. 287, no. November 2021, p. 119 247, 2022, ISSN: 13522310. DOI: 10.1016/j.atmosenv.2022.119247. [Online]. Available: https://linkinghub.elsevier.com/retrieve/pii/S1352231022003120 (cit. on p. 145).

[243] G. R. Buettner and F. Q. Schafer, „Ascorbate (Vitamin C), its Antioxidant Chemistry“, *Free Radical Biology and Medicine*, no. Vitamin C, pp. 319–335, 2006 (cit. on p. 148).

[244] J. L. Redpath and R. L. Willson, „Reducing compounds in radioprotection and radiosensitization: model experiments using ascorbic acid“, *International journal of radiation biology and related studies in physics, chemistry, and medicine*, vol. 23, no. 1, pp. 51–65, 1973, ISSN: 0020-7616. DOI: 10.1080/09553007314550051. [Online]. Available: https://pubmed.ncbi.nlm.nih.gov/4567291/ (cit. on p. 148).

[245] C. K. Remucal and D. L. Sedlak, „The role of iron coordination in the production of reactive oxidants from ferrous iron oxidation by oxygen and hydrogen peroxide“, *ACS Symposium Series*, vol. 1071, pp. 177–197, 2011, ISSN: 19475918. DOI: 10.1021/BK-2011-1071.CH009. [Online]. Available: https://pubs.acs.org/doi/abs/10.1021/bk-2011-1071.ch009 (cit. on p. 149).

[246] J. C. Fussell *et al.*, „A Review of Road Traffic-Derived Non-Exhaust Particles: Emissions, Physicochemical Characteristics, Health Risks, and Mitigation Measures“, *Environmental Science and Technology*, vol. 56, no. 11, pp. 6813–6835, Jun. 2022, ISSN: 15205851. DOI: 10.1021/ACS.EST.2C01072/ASSET/IMAGES/LARGE/ES2C01072{_}0004.JPEG. [Online]. Available: https://pubs.acs.org/doi/full/10.1021/acs.est.2c01072 (cit. on p. 151).

[247] Bio-Rad LAboratories, „Chelex ® 100 and Chelex 20 Chelating Ion Exchange Resin Instruction Manual“, *Manual*, (cit. on p. 195).

Appendices

A Further Contributions

In addition to the work presented in the main text I contributed to other projects and publications. In this appendix further publications that are not presented as a full chapter in the main text (as Chapter 2 (respectively Figure D.5), Chapter 4 and Chapter 5) are presented shortly.

- For the publication of Campbell et al., 2019 [38] I conducted most of the measurements to characterize the prototype of the OOPAAI and was involved with data analysis. In this publications we showed the development of an physiological relevant online chemical assay to quantify aerosol oxidative potential.
- I also analyzed offline filter samples with the AA and DCFH assay for the publication of Wang et al., 2023 [177]. In this publication we investigated the aerosol toxicity of wood smoke during oxidative atmospheric aging.
- In the publication of Zhang et el., 2021 [85] I was involved in the offline filter measurements of DCFH and DTT. In this paper we investigated if ROS is a suitable metric to predict toxicity of carbonaceous aerosol particles.
- In the publication of Shen et al., 2021 [81] I contributed the online measurements of AA under two different pHs (acidic and neutral) for the model. In this paper we investigated ascorbate oxidation by iron, copper and reactive oxygen species.
- In Campbell et al., 2021 [33] I measured for all the ambient filters of both seasons with the AA the OP. In this paper we showed the influence on atmospheric conditions and compositions of $PM_{2.5}$ in Beijing, China.
- In a manuscript in preparation we want to show the difference between offline and online measurement methods for acellular and acellular assays. I contributed for the offline and online AA measurements, and I was involved in the biological analysis of the offline and online experiments. Furthermore, I conducted AA, DCFH and DTT measurements to quantify the decay of biogenic aerosol over time.

- In a manuscript in preparation we want to show different toxicity measurements (acellular and cellular) for different locations. For this study I also contributed offline AA, DCFH and DTT measurements.
- There are further campaigns and measurement I participated, but there it is not yet clear if something will be published and if so if my contributions will be part of the publication.

B OOPAAI Operating Manual

In this section, the preparation of all chemicals needed for the OOPAAI is discussed and how to operate it and perform basic data analysis.

B.1 Preparation of Chemicals

First, ultrapure water must be chelexed overnight. Chelex raisin 100 (100 g) is filled in a column (750 mL) with frit and water is added and slowly, one drop per minute or a little faster, drips through. If possible, chelex the water twice. Use Nalgene bottles and no glass to minimize metal contamination. All bottles were washed first with HCl and then with chelexed ultra pure water before using them. Ascorbic acid must be buffered to maintain pH 6.8. For the preparation of the buffer, a stock solution of HEPES 200 mM (MW: 238 g/mol is needed. Add HEPES to a bottle and dissolve in chelexed water (a stir bar helps to speed up the process), adjust the pH with sodium hydroxide (1 M is best, but it is also possible to use 0.1 M) to pH 6.8 and then fill the bottle to the final volume. For the working solution, dilute the buffer stock solution 1:10 with chelexed water to obtain a solution of 20 mM.
For the ascorbic acid solution, dissolve 8.8 mg ascorbic acid (MW: 176 g/mol) in 250 mL buffer to get a 200 µM ascorbic acid solution. For OPDA (MW: 108 g/mol), weigh 1.08 g and dissolve it by stirring in 500 mL 0.1 M hydrochloric acid (From a 1 M stock solution diluted with ultra pure water) to get a 20 mM solution.

B.2 Operating the OOPAAI

The OOPAAI must be turned on and looked at to ensure that everything is properly connected and all cables are connected. Before turning the LED on, start the software because correction spectra have to be recorded. The PILS bottle should be filled at least once a day. One should be very careful that the PILS never runs dry and that there is always water in the bottle; otherwise, the signal will be disturbed. So far the LED is operated with an external power supply that needs to be set to current control 500 mA. The corresponding voltage is then around 3.3 V. If operated with the external OceanView Software (Version 2.0.12, Ocean Insight), open the software make a blank measurement and set the integration to a 1000 m sec. Leave the other things to the default. Open a time series tab and integrate from 425 nm to 435 nm and set the time after it should stop to 1'000'000 and circular. Chose a name and a folder and timeseries as data

format and press save. Also, open the Sensirion flow control software by first choosing "USB cable" and then select "flow sensor 6". Set the integration time at 100 ms and set the moving averaging to a 100. Then monitor the flow and adjust the three flows at the pump if necessary. If operated with the LabView Software, just start the LabView script and follow the steps to calibrate the flows. and then start the measurement.

B.3 DHA Calibration Curve

For the calibration curve dissolve 1.74 mg DHA (MW: 174 g/mol) in 50 mL HCl 0.01 M (pH 2) (200 µM). Shake or stir well and wait some minutes until all DHA is dissolved. Then make a series of dilutions (with HCl) from the stock solution (200, 100, 50, 20, 10, 5, 2, 1 µM). Pump it with normal flow rates through the OOPAAI (with PILS (air flow on) and heating bath). The solution should be made immediately before the start of the calibration curve and stored in the refrigerator.

B.4 Data Analysis

The raw data first need to be detrended and blank subtracted for any blank drift that can occur during measurement. At the current development stage of the OOPAAI, it is unfortunately not possible to automatically detrend the data, because there are too many uncertainties and variables that change over measurements from different days. Therefore, a manual routine with Excel and Origin was developed to analyze the data.

- Open the .txt file from the spectrometer in Excel via browse and save as excel file.
- Correct for time delay in the OOPAAI and time zone difference to UTC, make the date time out of epoch time.
- normalize with blank drift and blank offset, and then import it in origin (close excel).
- To normalize it, plot the epoch time normalized to zero with origin take blank value (mark the area with the selection tool, click on the arrow, and then copy to the new workbook).
- Plot new workbook, make linear fit (1. order or 3. order if data have a very strong/weird drift), add the intercept and slope in Excel (without error).

- Re-import to origin, move headers up, and delete all text, plot date time vs. detrended counts.
- If necessary (blank still not good), do a baseline correction in origin: Analysis tab, Peaks and Baselines, Peak analyzer Select subtract baseline mode, user defined, 2^{nd} derivation leave rest as suggested and adjust points for blank
- Add "subtracted from intensity" from origin to Excel.
- To normalize the data to DHA instead of counts, average the data to the interval of the mass measurement, and then take the averaged counts, subtract the intercept and divide by the slope of the DHA calibration curve.
- Mass normalize it by multiplying the concentration of DHA by the liquid flow rate of the OOPAAI divided by the air flow rate of the OOPAAI and the mass concentration of the aerosol measured.
- For volume normalization the DHA value does not need to be divided by mass.

C OOPAAI Troubleshooting

In this appendix all important problems and their possible solutions are described that have occurred during the development and the operation of the OOPAAI. The development of a novel instrument leads to many unexpected errors, but most of them could be solved during the process of improving OOPAAI, although there is still the possibility that new errors can occur. When troubleshooting the instrument, always remember that a problem could also arise from multiple sources.

C.1 Stability Issues of the Blank and High Blanks

Unfortunately blank stability issues or a too high blank, in general, are one of the recurring problems, which can have multiple reasons. If the blank is not stable at the beginning, which is normal, the system needs up to 2 h to stabilize. Therefore, it is highly recommended to start the blank a day before a measurement series starts and let a blank measurement run over night.

The reason that leads most often to blank problems is contamination of a part. First, always check the filter (cellulose Grade 1) in the filter holder. This needs to be replaced daily if high PM loads are measured, especially during lab experiments. But it should be replaced at least weekly, even when measuring ambient air. Normally the filter gets quite fast black even when the mass loadings are not too high.

If experiments were conducted with transition metals, they will adsorb to the walls of the tubing and connectors and the PILS. Therefore, it is necessary to flush the system (the flow must be $\geq 2\,\mathrm{mL}$) for at least 15 min with hydrochlocric acid (HCl, 0.1 M). The low pH of hydrochloric acid will make the transition metal particles more soluble and wash them out. After flushing with HCl, it is necessary to flush with ultra pure water because the inner part (cone to the impaction plate) of the PILS is made of anodized aluminum. If HCl is too long in contact with that piece, the anodized layer is removed, and the aluminum starts oxidizing. So, from time to time also check that piece and if it is not black anymore replace it.

A minor problem was adsorption of organic aerosols. But if flushing with HCl did not help it is worth flushing the system with methanol. There it is very important to remove the bubble traps because the membranes of the babble trap start to leak if they get in contact with methanol. Furthermore, it is not possible

to use the peristaltic pump because the tubing of the peristaltic pump is also not compatible with methanol. The easiest way is to fill a syringe with methanol and flush all the tubings manually.
Another component that could be contaminated is the PILS. There, the most likely part of contamination is the impaction plate. This can be easily removed and washed. Next to the impaction plate is the wick (metal mesh), which also needs to be replaced from time to time (depending on what is measured, but at least every half a year). The condensation chamber of the PILS can also become dirty over time, so if the blank is not stable or higher than usual, it might become necessary to take the whole PILS apart and clean all PILS components as well. The round jet impactor in front of the PILS that removes particles larger than 2.5 µm needs to be cleaned also from time to time, but was never the problem for blank drifts.
The tubings of the peristaltic pump wear out over time, so they should be changed as well if they are not good anymore or if it is not possible to clean them anymore (i.e. soot). Before replacing them, it is possible to turn them around because they have three stoppers, so they can also be used from the other side as well. When changing the tubing, it is very important to precondition them before using them. When they are new, the back pressure of the PILS is bigger than the capacity of the peristaltic pump. It is best to let them run with water for at least 24 h before using them so that they could stabilize. This can be done externally with a spare peristaltic pump. If the new tubing is still not working the cassette of the peristaltic pump needs to be pushed down (gently, otherwise the motor of the peristaltic pump is under too high load) a little bit at high flow rates and hold that for a couple of minutes. The tubing should get softer and should then transport the liquid through the pump without additional force. When the flow of the tubing is less (or more) than it should be, this can change the blank drastically. So, it is very important to always check the flow rates of all three channels with the flow sensors. If the reading of the pump and the flow sensors differ a lot, it might be worth to calibrate the pump again.
If the PILS runs out of water then that will also affect the blank, so always make sure that there is enough water in the reservoir for the PILS. The flow for the steam in the PILS must be checked from time to time as well, because changes in the amount of liquid can alter the operation of the pILS and therefore also lead to a slightly different blank.

Lab temperature can also lead to blank drifts in various ways. In Figure 71 the difference of around 6 °C is shown. The dip in the data is when the air conditioning is fully on and the top bit is without air conditioning.

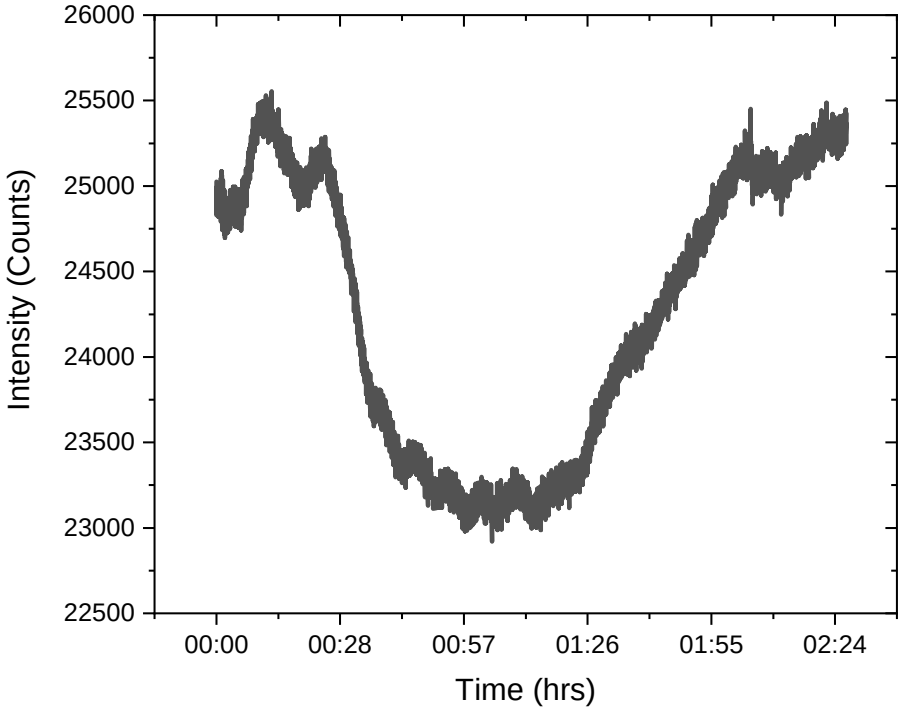

Figure 71: Temperature differences in the lab. In the dip in the middle of the graph, the temperature is around 6 °C colder than in the beginning. The temperature was reduces after 30 min
and increased after 90 min.

If the temperature in the lab is drifting slowly, the solutions, particularly the AA will decompose to DHA by auto-oxidation from dissolved O_2 and other contamination's like trace metals, faster and lead to a slightly increasing blank over time. If the blank is too high, then the solutions might also be contaminated. In this case, it is the easiest to just make new solutions. If that still does not solve the high blank levels, it is worth checking the chelex100 resin. The chelex100 needs to be regenerated from time to time (done as described in the Bio-Rad manual [247]).

A further problem can occur when the humidity is too high and when it starts to condensate at the ELMEKO cooling unit. When that happens, the water drips down and can lead to condensate entering the flow through the cell. If there

is water or water vapor on the filter or SMA lens, that leads to scattering and therefore to more light and a higher signal.
The gas phase can also contribute to an increased signal, and if the capacity of the charcoal denuder is reduced, this can lead to a higher blank and also to a higher signal. This is not as easy to detect because the absolute level of the blank always varies a little because of slightly different liquid flow rates and therefore different residence times or because of inaccuracies from the weighing of the chemicals. The absolute blank level can also be changed slightly when the OOPAAI is connected to an external air flow system. The air flow is not regulated actively (only a critical orifice) and therefore change in pressure change the amount of air that is going through the PILS and the internal pressure of the PILS. This can changes the amount of particles collected per milliliter, but also the blank. Even connecting a longer air sampling tubing gives back pressure and changes the blank slightly. So it is very important to measure the blank always by using the final setup by which also the aerosol is measured (incl. the sampling tubing length), but just with an HEPA filter on. The HEPA does not give any back pressure and therefore does not change the level of the blank.

C.2 Software

If there is a software problem, a restart usually solves the problem. If not, check if all hardware components are plugged in and are working properly. If that also doesn't solve the problem, check the Labview code.

C.3 Electronic Parts

If the blank is too low or there is no signal at all, the most likely issue is a broken or misaligned LED. To check if the LED is misaligned, remove the black cover around the LED and center the LED in the middle of the TECooler. The LED light can still be visible, but it is possible that the UV part is not working anymore. To verify that a 200 µM quinine sulfate solution in 0.1 M HCl is added to a cuvette in the offline setup where the LED is mounted. Quinine is a useful proxy to test the LED power, because it has a similar excitation wavelength and is very stable compared to DFQ. The offline setup should be configured in the following way; power supply 500 mA current controlled, two mirrors mounted on the cuvette holder, the cuvette orientated so that the narrow side points in the direction of the spectrometer and the long side (1 cm) to the LED where the lid shutter is, 600 µm fibers, the ocean insight software should be on the "quick view"

tab and the integration time should be set to 100 m sec. The slit should be the "no slit" that is normally used in the OOPAAI. When all these parameters are the same and the LED is still good, the spectra should look like the spectrum shown in Figure 72. If the LED gets focused on a white surface, the individual pads of the LED can be seen, and this should show if one of the elements is broken. If only one is broken, that does not change much the total intensity, but if there are more, then it might be worth changing the LED.

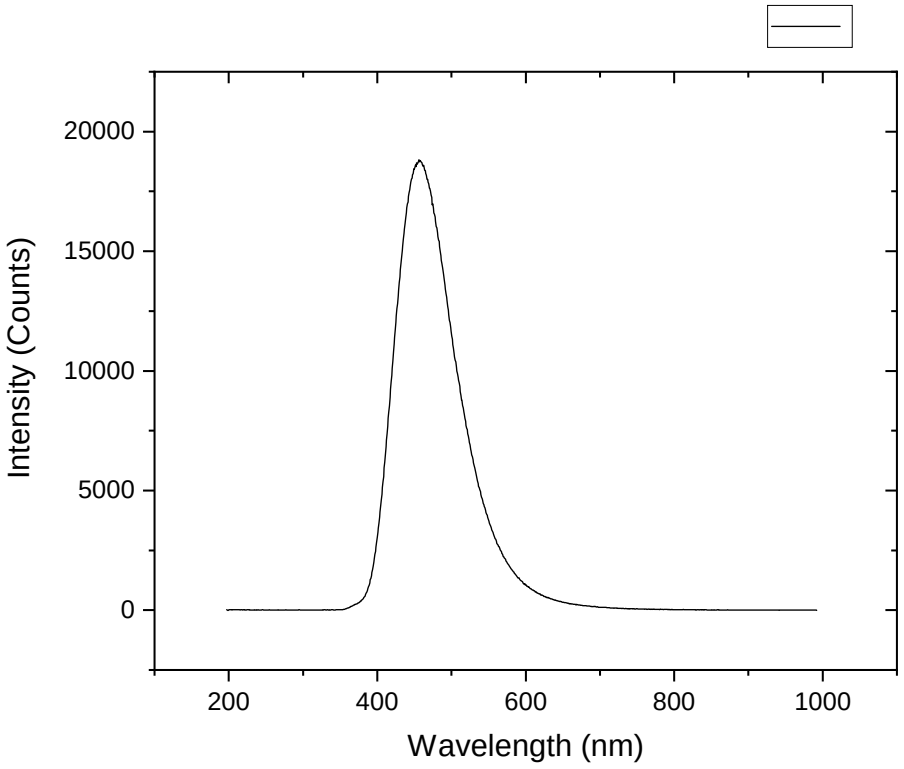

Figure 72: Standard spectra of quinine to test if the LED is still working.

If the blanks drift downward, that is usually an indication that the system is still dirty. Just flush with HCl (at least 10 min) and afterwards with water to neutralize the pH. Then start a new blank and wait till the blank stabilizes itself. This should normally take not more than 1 h. The blank now should be lower than before. If that is not the case then impurities in the liquid system might have not been the problem or they are so strong that the flushing time was not enough. In that case let the HCl stay in the system overnight and flush it again the next day for at least 30 min. These types of problem occur most often if high concentrations of transition metals entered the system, especially copper. Copper adheres to the walls and is very difficult to remove.

C.4 Spikes in Signal

If there are spikes in the signal for a short time, i.e. only one or a couple of data points, that are higher in the signal, then this is likely due to bubbles passing through the flow through the cell and indicates that the bubble trap membrane is not working properly anymore and need to be replaced. First flush the system with water, then remove the bubble traps and screw them loose. Replace the membrane, clean the housing and put them back together and install them in the OOPAAI.

C.5 Sensitivity Decrease of the Signal

At around 10 µg ambient mass concentration the OOPAAI should give a signal of around 200 counts with the Ocean Insight software set at 1000 m sec integration time and an integration window from 425-435 nm. If that is not achieved anymore check the temperature of the PILS. If the tip temperature of the PILS is not between 97 °C and 100 °C the steam flow is not perfect and the collection efficiency is not optimal. Run the PILS for 2 h dry to remove all the water that is at the temperature sensor in the PILS that could alter the correct readout. Check the flow speed of the liquid flow into the PILS, which should be 1.5 mL/min. If these measure do not help a new steam injector assembly from Brechtel needs to be bought for the PILS.
Furthermore, measure the air flow of the OOPAAI which should be above 15 L/min. If that is not the case, either the vacuum pump is not working properly anymore or the tubing/critical orifice/impactor is clogged. If that is the case, clean everything and figure out where the reduced flow originates.

C.6 Calibration Procedure

If in the DHA calibration the linearity is not at least 0.99 for the adjusted R^2 then either the dilution series is not exact enough or there is a general problem with the stability of the liquid flows. If only the value of 200 mM is too high, then not all DHA was dissolved before starting the dilution series. DHA takes some minutes to dissolve fully so it is necessary to wait till all is dissolved. If the higher concentration points in the calibration are too low, then the DHA decomposed, which is an indication that the solutions are not fresh anymore.

C.7 Lower HCl Background

The HCl background (only HCl in the cuvette) should be around 12'000 counts with 1000 m sec integration time and a integration window of 10 nm from 425 nm to 435 nm. The first thing is to check if the LED is misaligned. Disconnect the fiber, remove the cover and visually check if the LED is in the center of the TECooler. It is also possible to see, when the cover is on the TECooler, if the light is aligned. For that, just hold a piece of paper approximately 10 cm from the SMA lens away and see if the LED is a square. The LED consists of 4x4 small squares, and if the focus is right even these 16 squares can be seen. This is also good for checking if one or more of these elements are not working because that could also be a reason for a lower intensity. If that is the case, replace the LED and see if the intensity gets higher again. Another problem that can appear is that condensate drips onto or finally into the flow cell when the humidity is very high. This can give more scattering, and depending where the droplet is, it leads to less signal but sometimes also to more signal. Another issue can also be that the fiber is not properly connected to the flow cell. This can be seen when the fiber is touched, even slight movements of the fiber change the signal quite a bit.

C.8 Wobbly Signal

This can either be from temperature instabilities (See Figure 71) where the signal is disturbed by changing ambient temperature (turn air conditioning on if possible). Against that not too much can be done. The only way is to try to stabilize the outside temperature. The other problem can be unstable liquid flows of the OOPAAI. The easiest thing is to exchange the or at least switch the tubing of the peristaltic pump around.

D Supplementary Information: Iron and Copper Alter the Oxidative Potential of Secondary Organic Aerosol: Key Insights from Online Measurements, and Model Development

D.1 Metal Particle and Secondary Organic Aerosol Generation using the Organic Coating Unit (OCU)

A flow through system consisting of various components to facilitate the production of secondary organic aerosol, metal seed particles and mixed metal-organic particles prior to analysis with the OPROSI and OPOAAI is displayed in Figure 73. Fe(II) and Cu (II) particles were produced using a homebuilt nebulizer containing a 0.4 mM solution of FeSO4 or CuSO4. The resulting particles were dried with a silica denuder, and then passed through an organic coating unit (OCU) (see Keller et al.).[170] In short, the OCU maintains a steady concentration of the gas phase volatile organic compound (VOC) precursor, which is maintained via a PID voltage feedback.

For BSOA production, 1 mL of β-pinene was placed in a VOC reservoir at room temperature with a steady gas flow passed over the surface. For NSOA production, 1 g of naphthalene was placed in the VOC reservoir and heated to 80 °C using a water bath to volatilize the naphthalene into the gas phase. The VOCs were then passed through a cylindrical quartz photooxidation chamber (76 mL volume) surrounded by 5 low pressure mercury lamps (4 W UVC with 254 nm and 185 nm emission lines, type GPH212T5VH/2, Heraeus, Germany), which produce both O_3 and OH radicals via the photolysis of O_2 under humid conditions. Only one UV lamp was turned on for all photooxidation experiments presented in this study, resulting in a maximum O_3 concentration of 2 x 1013 molecules cm^{-}3 and an estimated OH concentration in the chamber of 1 x 109 molecules cm-3 in the absence of VOCs, with a constant gas flow of 1 L minthrough the oxidation chamber.

We expect predominantly OH-initiated β-pinene SOA due to the greater rate constant associated with OH reaction (7.9 x 10-11 molecules cm-3 s-1) at the exocyclic double bond compared to O_3 (1.5 x 10-17 molecules cm 3 s-1), whereas naphthalene oxidation proceeds only through OH initiated oxidation.[1] All

experiments were performed at 70% RH in the chamber, which was maintained using a humidifier in the OCU. The resulting SOA mixture is then passed through a series of charcoal denuders to remove gas phase VOCs (Figure 73) and remove 99.9% O_3.[89]

Gas phase VOC concentrations were monitored online using a proton transfer time-of-flight mass spectrometer (PTR-ToF-MS, 3000, Ionicon, Innsbruck, Austria). Particle number size distributions, were constantly monitored using a scanning mobility particle sizer (SMPS, TSI). A particle density of $1.3\,\mathrm{g\,cm^3}$ was assumed to calculate particle mass distributions. O_3 concentrations were continuously monitored using an O_3 analyzer (Model 49i, Thermo Scientific). The particle-bound ROS concentrations and particle oxidative potential were then measured online using the OPROSI and OOPAAI, respectively, the operational procedures of which are described below. This results in a more dominant formation of hydroperoxides and can be considered as representative of conditions encountered in the unpolluted atmosphere.

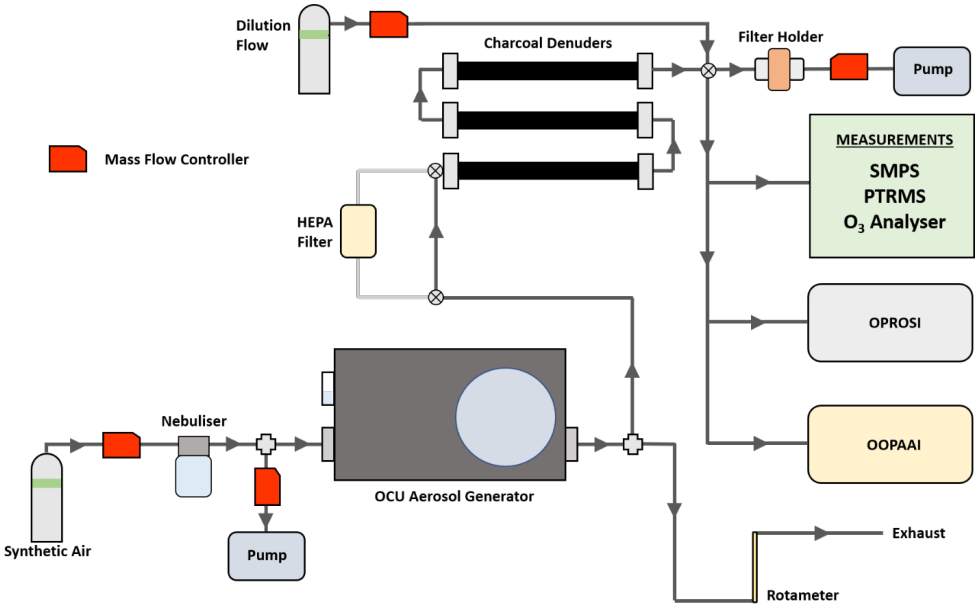

Figure 73: Schematic representation of the experimental setup used in this study.

D.2 OPROSI (Online Instrument to Quantify OP from DCFH

The functionality, design and operating procedure for the OPROSI is extensively described in Wragg et al.[95] and Fuller et al.[94] Briefly, the aerosol is continuously drawn into the instrument via an aerosol conditioning unit, which consists firstly of

a stainless steel cyclone (2.5 µm cut-off at 5 L/min URG-2000-30E-5-2.5-S, URG) and charcoal denuder, before entering a homebuilt particle sampler. Particles are collected onto a filter sprayed with a solution of horseradish peroxidase (HRP) in 10% PBS buffer, which immediately reacts with ROS present in the particles and is collected in a 1 mL liquid reservoir. The HRP solution is then immediately mixed with 2,7-diclhorofluoroscein (DCFH), which is subsequently oxidized to form a fluorescent product DCF by the ROS-HRP solution in a reaction bath maintained at 37 °C for 15 min. The DCF is then quantified via fluorescence spectroscopy. The fluorescence response of the instrument is calibrated with known concentrations of hydrogen peroxide (H_2O_2), and thus ROS concentrations are expressed in H_2O_2 equivalent concentrations per unit volume (m-3) or per unit particle mass (ug-1). The assay has demonstrated sensitivity in particular to hydrogen peroxides and organic peroxides.5,4 The direct-to-liquid sampling and high time resolution of this instrument therefore is particularly sensitive to short-lived ROS components, which react within seconds after sampling.5,4

D.3 OOPAAI (Online Instrument to Quantify OP from AA)

The initial iteration of the OOPAAI is described in detail in Campbell et al., [38] was used, with substantial modifications, including technical and chemical improvements presented in the following description, most notably running the assay with a HEPES buffer at pH 6.8 (Utinger et al).[97] The OOPAAI measures OPAA by measuring the formation of dehydroascorbic acid (DHA), an oxidation product of ascorbic acid (AA), by reacting DHA with o-phenylenediamine (OPDA) forming a fluorescent product 3-(1,2-dihydroxyethyl)-fluoro-[3,4-b]quinoxaline-1-one (DFQ), where we then monitor the concentration of DFQ using fluorescence spectroscopy. Aerosol particles are continuously collected for online OP analysis using a commercially available particle-into-liquid sampler (PILS, Brechtel, USA), where the wash flow was modified to contain the AA reagent, ensuring rapid reaction of AA of aerosol particle components with direct-to-liquid particle sampling. The sample is then washed off the impactor with a flow rate of 60 µl/min and the resulting AA-particle aqueous sample is reacted for 10 minutes at 37 °C. The reaction solution is then mixed with OPDA at a flow of 90 µl/min and pumped into another reaction coil at room temperature for 2 min, where the DHA + OPDA reaction occurs, forming the fluorescent product DFQ. The concentration of DFQ is then monitored using a homebuilt flow through fluorescence cell which

consisted of a modified flow-through quartz cuvette (Hellma Analytics). DFQ is excited by a high-power UV LED (Roithner Lasertechnik, type UVLED- 365-330-SMD) at 365 nm via an optical fiber (Thorlabs, 1500 µm, NA 0.39). The fluorescence emission light is then collected through a collimating lens (Ocean Insight) via an optical fiber (Thorlabs, 1500 µm, NA 0.50) and then detected using a spectrometer (Ocean Insight, QePro). The OOPAAI is calibrated using known concentrations of DHA, and hence the OP here is then expressed in terms of nmol DHA per unit volume (m^{-3}) or unit mass (µg $/m^3$).

D.4 Reaction Conditions

Particle mass concentrations used in this study are presented in Table S1. A particle mass concentration range between 245-408 µg/m^3 for SOA produced from the OCU and 5-34 µg m-3 for metal particles. OH concentrations in the photolysis chamber were estimated to be ∼1 x 109 cm^{-3} , based on the rate of decay of gas phase naphthalene present in the system.

Table 3: Reaction conditions (particle mass, metal mass, O_3, OH, RH,) – emphasize metal ratio

Experiment	Average Organic SOA (µg m-3)	Metal (µg m-3)
NAP + Fe(II)	351	34
NAP + Fe(III)	352	33
NAP + Cu (II)	356	5.74
BP + Fe(II)	245	34
BP + Fe(III)	321	37
BP + Cu (II)	408	5.4

D.5 Representative Online Data

The representative size distributions of SOA, metal and a SOA-metal mixture are presented in Figure 74. We assume that the SOA and metals during the mixed aerosol experiments are internally mixed due to the one mode observed in the size distribution. Using the experimental setup described in Figure 66, online particle-bound ROS and particle OP were quantified for ß-pinene-derived SOA (BSOA), naphthalene derived SOA (NSOA) and redox active transition metals including Fe(II) and Cu (II). Figure 74 shows a representative plot illustrating the online raw signal response of the OPROSI over 3.5 hours quantifying OPDCFH of pure Cu (II), pure BSOA or Cu (II) + BSOA particles. Total particle mass

(smps measurements) is also displayed. Particles are well mixed as evidenced by the growth of particle size distribution, and one mode observed for SOA + metal mixtures in the OCU (Figure 74).

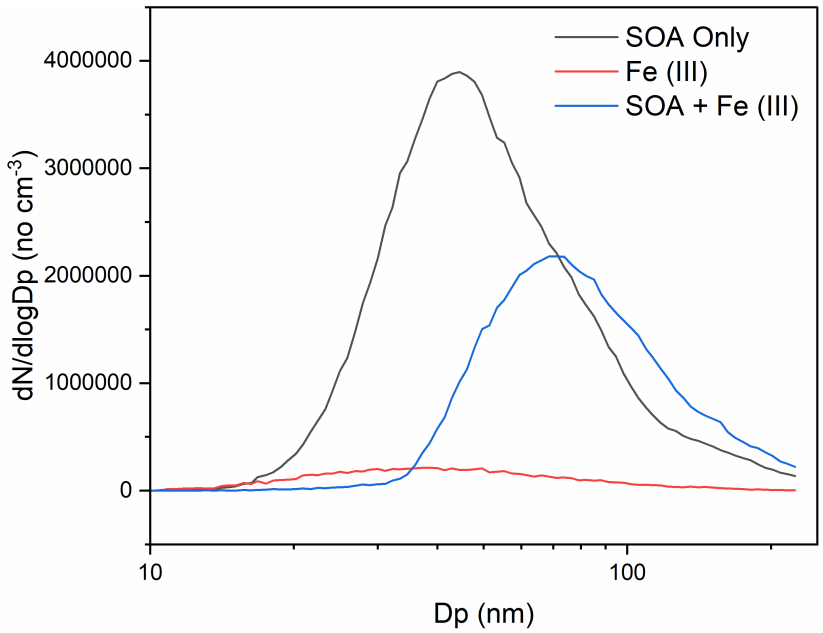

Figure 74: Size distributions of secondary organic aerosol, nebulised Fe2SO4 and a mixture of both, showing well mixed aerosol SOA/metal aerosol particles.

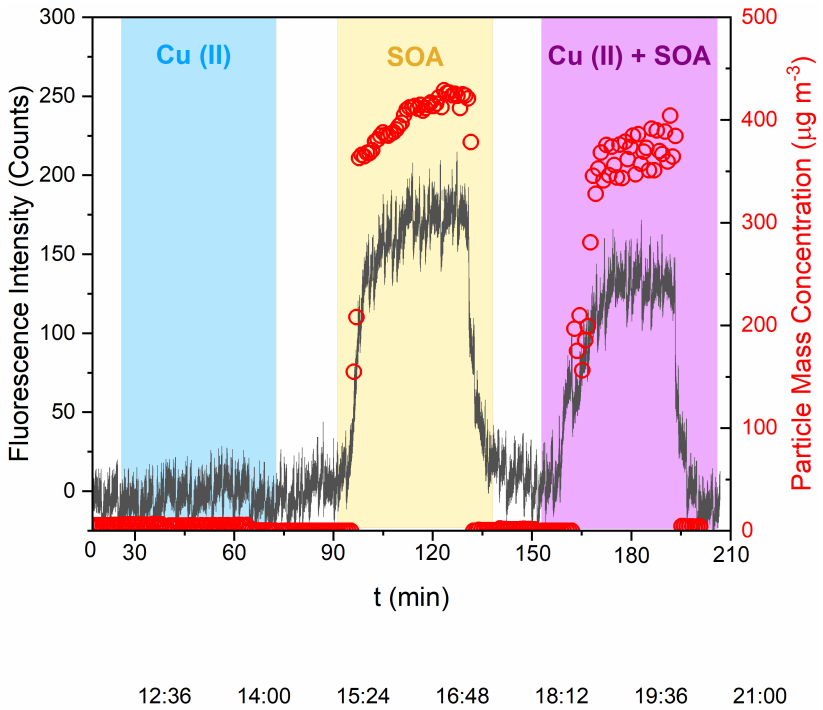

Figure 75: Representative online data illustrating the OPROSI (measuring OPDCFH) response to Cu (II) (blue), ß-pinene SOA (yellow), and a mixture of Cu (II) and ß-pinene SOA (purple) and corresponding total particle mass.

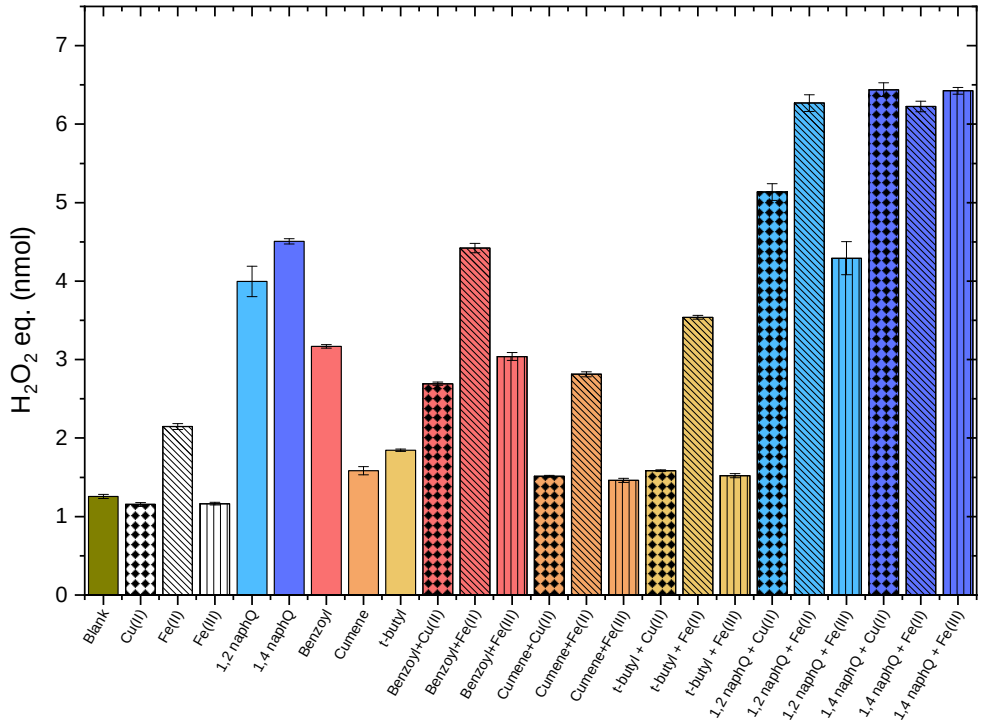

Figure 76: Relative change in OPfrom DCFH when a range of commercially available peroxides and quinones are mixed with Fe(II) and Cu (II).

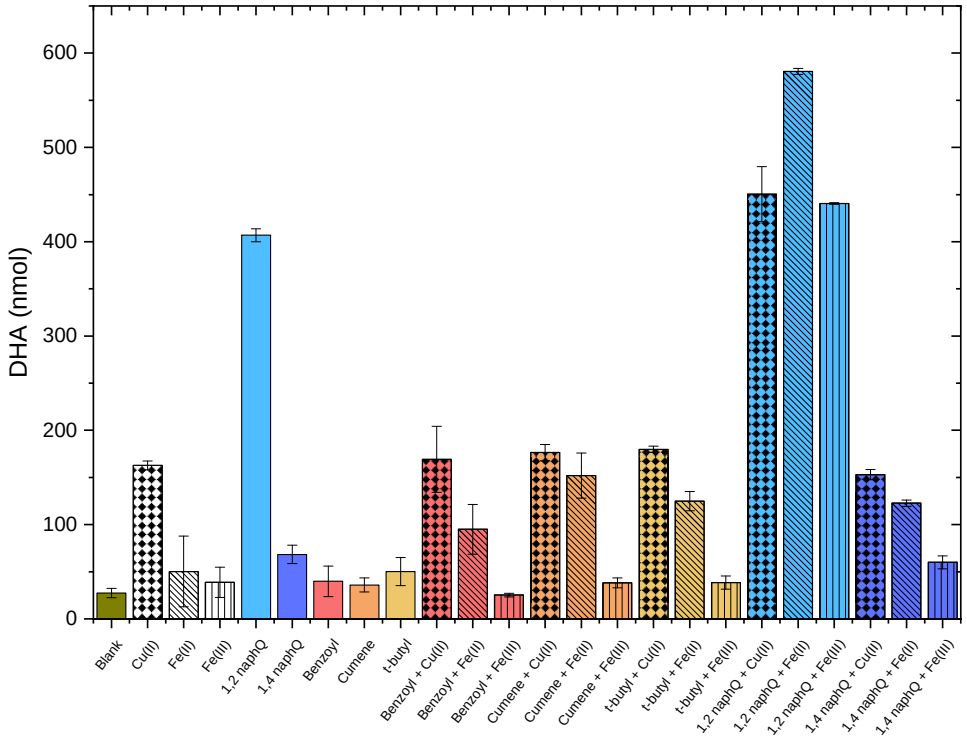

Figure 77: Relative change in OP from AA when a range of commercially available peroxides and quinones are mixed with Fe(II) and Cu (II).

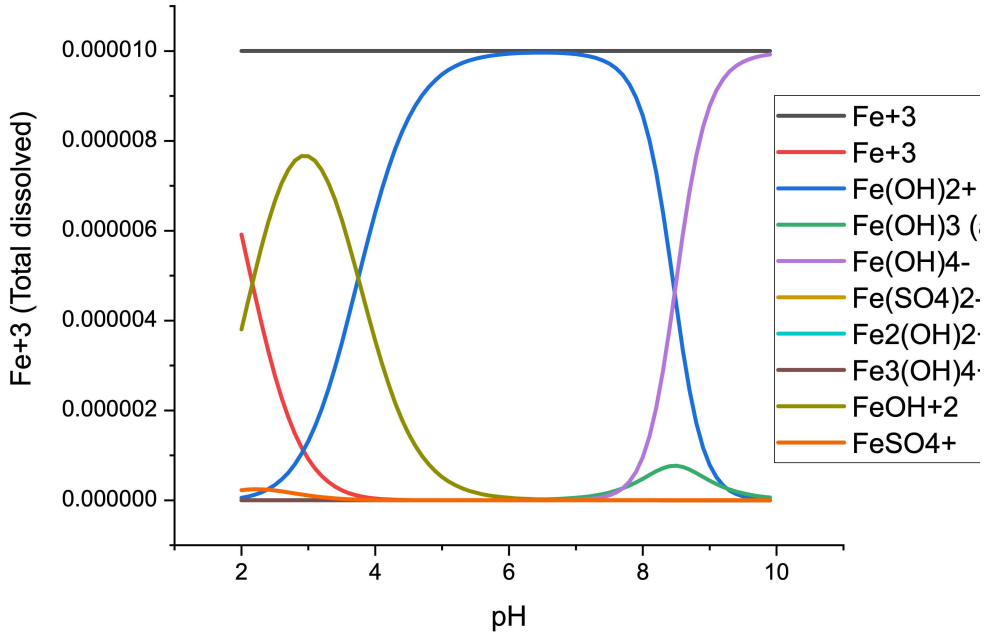

Figure 78: MINTEQ model describing Fe(III) speciation as a function of pH.

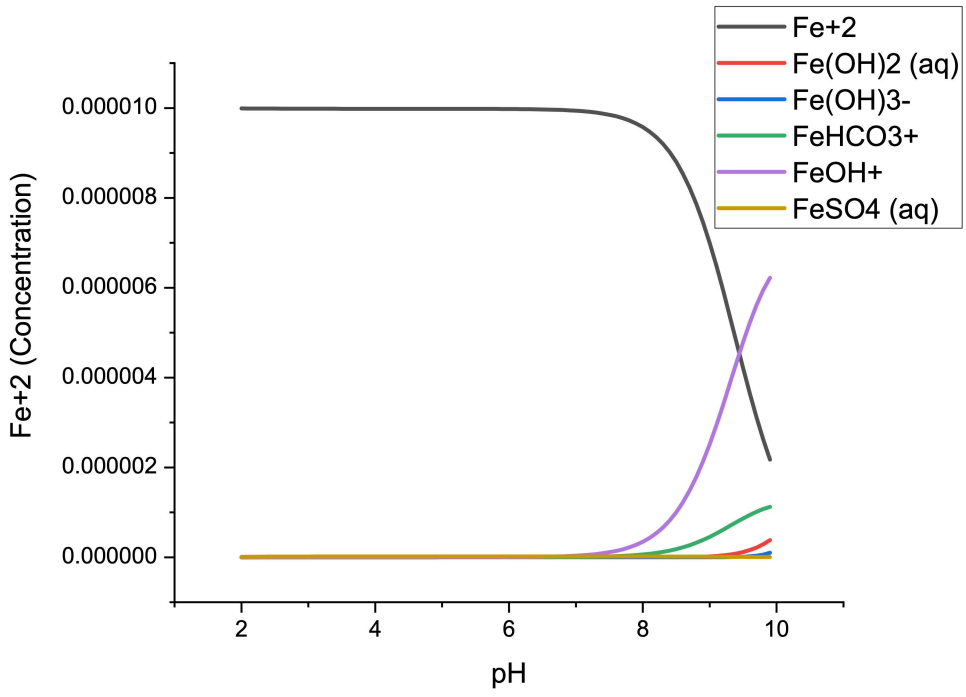

Figure 79: MINTEQ model describing Fe(II) speciation as a function of pH.

Table 4: Kinetic

No.	Reaction	k_f (M^{-1} s^{-1}, s^{-1})	k_b (M^{-1} s^{-1}, s^{-1})	K_{eq} (M^{-1} s^{-1}, s^{-1})	ref	
Ascorbate Reactions						
1	$AH_2 \rightleftharpoons AH^- + H^+$			7.94E-5	8	
2	$AH^- \rightleftharpoons A^{2-} + H^+$			1.58E-12	8	
3	$AH \rightleftharpoons A^{\cdot -} + H^+$			7.24	8	
4	$AH_2 + OH^{\cdot} \rightarrow A^{\cdot -} + H_2O + H^+$	7.9E9			9	
5	$AH_2 + HO_2^{\cdot} \rightarrow A^{\cdot -} + H_2O_2 + H^+$	1.6E4			10	
6	$AH_2 + O_2^{\cdot -} \rightarrow A^{\cdot -} + H_2O_2$	5.48E7			11	
7	$AH^- + OH^{\cdot} \rightarrow A^{\cdot -} + H_2O$	1.1E10			8	
8	$AH^- + HO_2^{\cdot} \rightarrow A^{\cdot -} + H_2O_2$	1.25E6			10	
9	$AH^- + O_2^{\cdot -} \rightarrow A^{\cdot -} + HO_2^-$	5E4			10	
10	$A^{\cdot -} + HO_2^{\cdot} \rightarrow DHA + HO_2^-$	5E9			11	
11	$A^{\cdot -} + O_2^{\cdot -} \rightarrow DHA + HO_2^- - H^+$	2.6E8			11	
12	$2A^{\cdot -} \rightleftharpoons AH^- + DHA - H^+$	5E4	3E-12	1.67E16	12	
13	$2A^{\cdot -} \rightleftharpoons AH_2 + DHA - 2H^+$	8E7	3.8E-13	2.1E20	12	
14	$Fe(III)^{++} + AH_2 + O_2 \rightarrow Fe(III)^{++} + DHA + H_2O_2$	5.7E4			13	
15	$Fe(III)^{++} + AH^- + O_2 \rightarrow Fe(III)^{++} + DHA + H_2O_2 - H^+$	4.7E4			13	
16	$Cu(II)^{++} + AH_2 + O_2 \rightarrow Cu(II)^{++} + DHA + H_2O_2$	1.0E5			13	
17	$Cu(II)^{++} + AH^- + O_2 \rightarrow Cu(II)^{++} + DHA + H_2O_2 - H^+$	2.5E6			13	
DHA Reactions						
18	oPDA + DHA → DHA − oPDA	4.6			14	
19	$DHA + OH^{\cdot} \rightarrow$ product	1E10				
20	$DHA + H_2O \rightarrow DKG$	5.8E-4			15	
21	$DKG + OH^{\cdot} \rightarrow$ product	1E10				
22	$DHA + H_2O_2 \rightarrow$ products	3.4E-2			16	
Fenton Reactions						
23	$H_2O_2 + Fe(II) \rightarrow {}^{\cdot}OH + {}^{\bullet}OH$	63-76			17	
24	$H_2O_2 + Fe(II) \rightarrow Fe(IV)O^{2+} + H_2O$	63-76			18	
25	$H_2O_2 + Fe(III) \rightarrow HO_2{}^{\bullet} + Fe(II) + H^+$	0.01-0.001			19,20	
26	$H_2O_2 + {}^{\bullet}OH \rightarrow HO_2{}^{\bullet} + H_2O$	3.3×10^7			17,21,22	
27	$H_2O_2 + 2\ Fe(IV)O_2^+ \rightarrow HO_2{}^{\bullet} + Fe^{3+} + {}^{\cdot}OH$	1×10^4			23	
ROS Reactions						
28	$OH^{\cdot} + OH^{\cdot} \rightarrow H_2O_2$	5.5×10^9			24	
29	$H_2O_2 + OH^{\cdot} \rightarrow HO_2^{\cdot} + H_2O$	3.2×10^7			25	
30	$O_2^{\cdot -} + OH^{\cdot} \rightarrow OH^- + O_2$	1.01×10^{10}			24	
31	$HO_2^{\cdot} + OH^{\cdot} \rightarrow H_2O + O_2$	7.1×10^9			24	
32	$O_2^{\cdot -} + H_2O_2 \rightarrow OH^- + OH^{\cdot} + O_2$	0.13			24	
33	$O_2^{\cdot -} + O_2^{\cdot -} \rightarrow O_2 + H_2O_2 - 2H^+$	6.0×10^5			26	
34	$HO_2^{\cdot} + O_2^{\cdot -} \rightarrow HO_2^- + O_2$	9.7×10^7			24	
35	$H_2O_2 + HO_2^{\cdot} \rightarrow H_2O + O_2 + OH^{\cdot}$	0.5			27	
36	$HO_2^{\cdot} + HO_2^{\cdot} \rightarrow O_2 + H_2O_2$	8.3×10^5			24	
37	$O_2^{2-} + H^+ \rightarrow HO_2^-$	1×10^{10}			24	
38	$HSO_4^- + OH^{\cdot} \rightarrow SO_4^- + H_2O$	3.5×10^5			28	
General Equilibria						
39	$H_2O \rightleftharpoons H^+ + OH^-$	1.3E-3	1.3E11	1E-14	27	
40	$H_2O_2 \rightleftharpoons H^+ + HO_2^-$	1.26E-2	1E10	1.26E-12	27	
41	$HO_2 \rightleftharpoons H^+ + O_2^{\cdot -}$	1.14E6	7.2E10	1.58E-5	25	
42	$H^+ + SO_4^{2-} \rightleftharpoons HSO_4^-$			9.77E1	27	

Inorganic Fe (II)/Fe (III) Reactions						
43	$Fe^{3+} + H_2O \rightleftharpoons FeOH^{2+} + H^+$			6.11E-3	[28]	
44	$FeOH^{2+} + H_2O \rightleftharpoons Fe(OH)_2^{+} + H^+$			7.78E-6	[28]	
45	$Fe^{2+} + H_2O \rightleftharpoons FeOH^{+} + H^+$			3.16E-10	[27]	
46	$Fe^{3+} + SO_4^{2-} \rightleftharpoons FeSO_4^{+}$			8.32E3	[27]	
47	$Fe^{3+} + 2SO_4^{2-} \rightleftharpoons Fe(SO_4)_2^{-}$			2.63E5	[27]	
48	$Fe^{2+} + SO_4^{2-} \rightleftharpoons FeSO_4$			1.78E2	[27]	
49	$Cl^- + Fe^{3+} \rightleftharpoons FeCl^{2+}$	3E3	2.16E3	1.39	[27]	
50	$Fe^{2+} + O_2 \rightarrow Fe^{3+} + O_2^{\cdot-}$	3.9			[26]	
51	$Fe(III)^* + O_2^{\cdot-} \rightarrow Fe^{2+} + O_2$	5E7			[27]	
52	$FeSO_4^{+} + O_2^{\cdot-} \rightarrow Fe^{2+} + SO_4^{2-} + O_2$	<1E3[Δ]			[27]	
53	$Fe(SO_4)_2^{-} + O_2^{\cdot-} \rightarrow Fe^{2+} + 2SO_4^{2-} + O_2$	<1E3[Δ]			[27]	
54	$Fe(III)^* + HO_2^{\cdot} =\rightarrow +O_2 + H^+$	2E4			[27]	
55	$FeSO_4^{+} + HO_2^{\cdot} \rightarrow Fe^{2+} + SO_4^{2-} + O_2 + H^+$	<1E3[Δ]			[27]	
56	$Fe(SO_4)_2^{-} + HO_2^{\cdot} \rightarrow Fe^{2+} + 2SO_4^{2-} + O_2 + H^+$	<1E3[Δ]			[27]	
57	$Fe^{3+} + H_2O_2 \rightarrow Fe(HO_2)^{2+} + H^+$	3.1E7	1E10	3.1E-3	[27]	
58	$FeOH^{2+} + H_2O_2 \rightarrow Fe(OH)(HO_2)^{+} + H^+$	2E6	1E10	2E-4	[27]	
59	$Fe(II)^* + OH^{\cdot} \rightarrow Fe^{3+} + OH^-$	2.7E8			[27]	
60	$FeSO_4 + OH^{\cdot} \rightarrow Fe^{3+} + SO_4^{2-} + OH^-$	2.7E8			[27]	
61	$Fe(II)^* + O_2^{\cdot-} \rightarrow +O_2^{2-}$	1E7			[27]	
62	$FeSO_4 + O_2^{\cdot-} \rightarrow Fe^{3+} + SO_4^{2-} + O_2^{2-}$	5E8			[27]	
63	$Fe(II)^* + HO_2^{\cdot} \rightarrow Fe^{3+} + HO_2^-$	1.2E6			[27]	
64	$FeSO_4 + HO_2^{\cdot} \rightarrow Fe^{3+} + SO_4^{2-} + HO_2^-$	1.2E6			[27]	
65	$Fe^{2+} + H_2O_2 \rightarrow Fe^{3+} + OH^{\cdot} + OH^-$	55			[27]	
66	$FeOH^{+} + H_2O_2 \rightarrow Fe^{3+} + OH^{\cdot} + 2OH^-$	55			[27]	
67	$FeSO_4 + H_2O_2 \rightarrow Fe^{3+} + SO_4^{2-} + OH^{\cdot} + OH^-$	78			[27]	
68	$Fe(HO_2)^{2+} \rightarrow HO_2^{\cdot} + Fe^{2+}$	2.3E-3			[27]	
69	$Fe(OH)(HO_2)^{+} \rightarrow Fe^{2+} + HO_2^{\cdot} + OH^-$	2.3E-3			[27]	
Inorganic Cu(I)/Cu(II) Reactions						
70	$Cu^{2+} + H_2O \rightleftharpoons CuOH^{+} + H^+$			1.12E-8	[29]	
71	$Cu^{2+} + 2H_2O \rightleftharpoons Cu(OH)_2 + 2H^+$			6.31E-17	[29]	
72	$Cu^{2+} + 3H_2O \rightleftharpoons Cu(OH)_3^{-} + 3H^+$			2.51E-27	[29]	
73	$Cu^{2+} + 4H_2O \rightleftharpoons Cu(OH)_4^{2-} + 4H^+$			1.82E-40	[29]	
74	$2Cu^{2+} + H_2O \rightleftharpoons Cu_2OH^{3+} + H^+$			3.98E-7	[29]	
75	$2Cu^{2+} + 2H_2O \rightleftharpoons Cu_2(OH)_2^{2+} + 2H^+$			3.72E-11	[29]	
76	$3Cu^{2+} + 4H_2O \rightleftharpoons Cu_3(OH)_4^{2+} + 4H^+$			7.94E-22	[29]	
77	$Cu^{2+} + SO_4^{2-} \rightleftharpoons CuSO_4$			223.9	[29]	
78	$Cu^{2+} + Cl^- \rightleftharpoons CuCl^{+}$			6.76	[29]	
79	$Cu^{2+} + 2Cl^- \rightleftharpoons CuCl_2$			3.98	[30]	
80	$Cu(II)^* + OH^{\cdot} \rightleftharpoons CuOH^{2+}$	1.17E4	3E4		[30]	
81	$Cu(II)^* + HO_2^{\cdot} \rightarrow Cu^{+} + O_2 + H^+$	1E8			[31,32]	
82	$Cu(II)^* + H_2O_2 \rightarrow Cu^{+} + O_2^{\cdot-} + 2H^+$	<1, 70			[32]	
83	$Cu^{+} + O_2 \rightleftharpoons Cu^{2+} + O_2^{\cdot-}$	4.6E5	8E9		[30]	
84	$Cu^{+} + OH^{\cdot} \rightarrow Cu^{2+} + OH^-$	3E9			[30]	
85	$Cu^{+} + H_2O_2 \rightarrow Cu^{2+} + OH^{\cdot} + OH^-$	<100			[33]	
86	$Cu^{+} + H_2O_2 \rightarrow Cu^{3+} + 2OH^-$	61			[34]	
87	$Cu^{+} + Cu^{3+} \rightarrow 2Cu^{2+}$	3.5E9			[34]	
88	$Cu^{+} + HO_2^{\cdot} \rightarrow Cu^{2+} + H_2O_2 - H^+$	2.3E9			[30]	
89	$Cu^{+} + O_2^{\cdot-} \rightarrow +H_2O_2 - 2H^+$	1E10			[30]	
Naphthoquinone Chemistry						
90	$AH_2 + 12NQN \rightarrow A^{\cdot-} + 12NQN^{\cdot-}$	9.03E+01			[35]	
91	$12NQN^{\cdot-} + O_2 \rightarrow + O_2^{\cdot-} + 12NQN$	2.77E+08			[36]	
92	$12NQN^{\cdot-} + O_2^{\cdot-} + 2H^+ \rightarrow 12NQN + H_2O_2$	1.99E+09			[36]	
93	$AH_2 + 14NQN \rightarrow A^{\cdot-} + 14NQN^{\cdot-}$	3.79E			[35]	
94	$12NQN^{\cdot-} + O_2 \rightarrow + O_2^{\cdot-} + 14NQN$	2.77E+08			[36]	

95	$14NQN^{\cdot-} + + O_2^{\cdot-} + 2H^+ \rightarrow 14NQN + H_2O_2$	1.99E+09			36	
96	$14NQN + 14OHNQN \rightarrow 14NQN^{\cdot-} + 14NQN^{\cdot-}$	1700			37	
97	$14NQN^{\cdot-} + 14NQN^{\cdot-} \rightarrow 14NQN + 14OHNQN$	1E5			37	
98	$14NQN + AH^- \rightarrow A^{\cdot-} + 14NQN^{\cdot-} + H^+$	45			38	
99	$12NQN + AH^- \rightarrow A^{\cdot-} + 12NQN^{\cdot-} + H^+$	5500			38	
100	$14NQN^{\cdot-} + O_2 \rightarrow 14NQN + + O_2^{\cdot-}$	1.1E8	2.0E8		39	
101	$14OHNQN + + O_2^{\cdot-} \rightarrow 14NQN^{\cdot-} + H_2O_2$	8E4			39	
102	$14NQN^{\cdot-} + + O_2^{\cdot-} \rightarrow 14NQN + H_2O_2$	2E9			39	
103	Fe(III) + 14OHNQN → Fe (II) + $14NQN^{\cdot-}$	6E2			39	
104	Fe (III) + $14NQN^{\cdot-}$ → Fe (II) + 14NQN	5E4			39	
105	Cu (II) + 14OHNQN → Cu (I) + $14NQN^{\cdot-}$	4E4			39	
106	Cu (II) + 14ONQN → Cu (I) + $14NQN^{\cdot-}$	1.2E7			39	
Organic Peroxide Reactions						
107	ROOH → RO +$OH^{\cdot}$	0.0015			40	
108	$OH^{\cdot}$ + ROOH → ROOH + HO_2	3.3E5			40	
109	RO → R	5E5			41	
110	$R + O_2 \rightarrow \rightarrow RO$	4.8E9			41	
111	$AH^{\cdot} + RO \rightarrow A^{\cdot-} + ROH$	1E4			40	
112	Fe (II) + ROOH → RO + $OH^{\cdot}$	4E4			42	
113	Fe (II) + ROOH → $RO^{\cdot}$ + OH	4.4E3			42	
114	RH + OH → R + H_2O	1E8			42	
Fe-HULIS Reactions						
115	Fepp + HULIS → Fepp-HULIS	10E10	2.9E4	3.5E10	25	
116	Feppp + HULIS → Feppp-HULIS	1.3E6			25	
117	Fepp + HULIS → FeppHULIS1	6.3E-3			25	
118	Fepp-HULIS + $O_2 \rightarrow + O_2^{\cdot-}$ + Feppp-HULIS	5.1			24	
119	Fepp-HULIS + + $O_2^{\cdot-}$ + 2Hp → Feppp-HULIS + H2O2	2E7			25	
120	Fepp-HULIS + H_2O_2 → Feppp-HULIS + OH + $OH^{\cdot}$	4.3E3			24	
121	Fepp-HULIS + OH → Feppp-HULIS + $OH^{\cdot}$	10E10			25	
122	FeppHulis1 → Feppp-HULIS	3E-3			24	
123	Feppp-HULIS + $O_2^{\cdot-}$ →FeppHULIS + O2	2.8E5			25	
124	FepppHULIS + Hascm → FepppHULIS + Hp + $A^{\cdot-}$	10E2			8	
125	HULIS + OH → HULISox + + $O_2^{\cdot-}$	5E9			25	
126	HULIS + + $O_2^{\cdot-}$ → HULISox + H_2O_2	9E3			25	
Terepthalate Probe						
127	TA + OH → (Y) TAOH + (1-Y) X	4.4E9			44	
128	X + OH → z	1E9			24	
129	TAOH + OH → $TAOH_{OX}$	6.3E9			44	
Buffer Chemistry						
130	$HEPES \rightleftharpoons H^+ + HEPES^-$			1E-3	45	
131	$HEPES^- \rightleftharpoons H^+ + HEPES^{2-}$			2.73E-8	45	
132	$H_3PO_4 \rightleftharpoons H^+ + H_2PO_4^-$			7.08E-3	46	
133	$H_2PO_4^- \rightleftharpoons H^+ + HPO_4^{2-}$			6.31E-8	46	
134	$HPO_4^{2-} \rightleftharpoons H^+ + PO_4^{3-}$			4.79E-13	46	
135	$H_2PO_4^- + OH^{\cdot} \rightarrow H_2PO_4^{\cdot} + OH^-$	2E4			47	
136	$HPO_4^{2-} + OH^{\cdot} \rightarrow HPO_4^{\cdot-} + OH^-$	1.5E5			47	
137	$PO_4^{3-} + OH^{\cdot} \rightarrow PO_4^{\cdot2-} + OH^-$	7E6			48	

Atmos. Meas. Tech., 16, 2641–2654, 2023
https://doi.org/10.5194/amt-16-2641-2023

Atmospheric Measurement Techniques
Open Access
EGU

An automated online field instrument to quantify the oxidative potential of aerosol particles via ascorbic acid oxidation

Battist Utinger[1], Steven John Campbell[1,2], Nicolas Bukowiecki[1], Alexandre Barth[1], Benjamin Gfeller[1], Ray Freshwater[3], Hans-Rudolf Rüegg[1], and Markus Kalberer[1]

[1]Department of Environmental Sciences, University of Basel, 4056 Basel, Switzerland
[2]Department of Atmospheric and Oceanic Sciences, University of California at Los Angeles, Los Angeles, CA 90095-1565, USA
[3]Department of Chemistry, Centre for Atmospheric Science, University of Cambridge, Cambridge, CB2 1EW, UK

Correspondence: Markus Kalberer (markus.kalberer@unibas.ch)

Received: 31 January 2023 – Discussion started: 14 February 2023
Revised: 17 April 2023 – Accepted: 23 April 2023 – Published: 30 May 2023

Abstract. Large-scale epidemiological studies have consistently shown that exposure to ambient particulate matter (PM) is responsible for a variety of adverse health effects. However, the specific physical and chemical properties of particles that are responsible for the observed health effects, as well as the underlying mechanisms of particle toxicity upon exposure, remain largely uncertain. Studies have widely suggested that the oxidative potential (OP) of aerosol particles is a key metric to quantify particle toxicity. OP is defined as the ability of aerosol particle components to produce reactive oxidative species (ROSs) and deplete antioxidants in vivo. Traditional methods for measuring OP using acellular assays largely rely on analyzing PM collected in filters offline. This is labor intensive and involves a substantial time delay between particle collection and OP analysis. It therefore likely underestimates particle OP because many reactive chemical components which contribute to OP are short-lived and therefore degrade prior to offline analysis. Thus, new techniques are required to provide a robust and rapid quantification of particle OP, capturing the chemistry of oxidizing and short-lived, highly reactive aerosol components and their concentration dynamics in the atmosphere. To address these measurement shortcomings, we developed a portable online instrument that directly samples particles into an ascorbic acid-based assay under physiologically relevant conditions of pH 6.8 and 37 °C, providing continuous, accurate OP measurements with a high time resolution (5 min). The instrument runs autonomously for up to 3 d and has a detection limit of about 5 $\mu g\,m^{-3}$ in an urban environment, which allows the characterization of particle OP even in low-pollution areas.

1 Introduction

Numerous epidemiological studies have linked anthropogenic air pollution to adverse health effects (Laden et al., 2006; Lepeule et al., 2012; Hart et al., 2015). They demonstrate that exposure to elevated levels of ambient aerosol particles is linked to increased hospital admissions and premature death from various diseases such as cancer and respiratory and cardiovascular diseases (Brunekreef and Holgate, 2002; Künzi et al., 2013). The World Health Organization estimates in a recent report (World Health Organization, 2016) that one in eight deaths worldwide are related to air pollution. Despite compelling epidemiological evidence, the chemical and physical properties of aerosol particles and the detailed pathways of particle toxicity that cause these negative health effects are largely unknown (Bates et al., 2019).

Many countries adopted limit values for the total particle mass as an indicator of particle toxicity. However, several studies have shown that composition, for example, elemental black carbon or transition metal levels, is a better proxy for particle toxicity than particle mass concentrations alone (Oberdörster et al., 2005; Koike and Kobayashi, 2006; Godri et al., 2010). Moreover, studies have demonstrated that the oxidative stress resulting from exposure to $PM_{2.5}$ could be

Published by Copernicus Publications on behalf of the European Geosciences Union.

a key mechanism to explain the health effects observed upon exposure to particles. Oxidative stress occurs when an imbalance develops in cells and tissues between reactive oxygen species (ROSs) and natural antioxidant defense mechanisms. This imbalance could lead to oxidative stress and therefore trigger various biological effects, such as inflammation, alteration of DNA and/or proteins, cell damage, and death (Prahalad et al., 2001; Baulig et al., 2003; Donaldson et al., 2001; Li et al., 2003; Offer et al., 2022).

ROSs (i.e., inorganic and organic radicals and peroxides such as hydroxyl radical ($^{\bullet}OH$), superoxide ($O_2^{\bullet-}$) and hydrogen peroxides (H_2O_2), in some cases including organic peroxides) can be delivered exogenously by inhalation of PM into the lung. ROSs can also be generated in vivo through redox chemistry initiated by aerosol components such as redox-active transition metals and quinones. This ability of PM components to produce ROSs, possibly catalytically, through redox chemistry and subsequent antioxidant depletion in biological cells or tissue is defined as oxidative potential (OP) (Bates et al., 2019). Measurement methods have been developed to quantify OP using cellular assays (Lehman et al., 2016) or acellular assays (Campbell et al., 2021). In epidemiological studies, cellular and acellular assays have shown a correlation between the overall oxidative capacity of PM and its negative effects on human health (Steenhof et al., 2011; GBD 2013 Risk Factors Collaborators, 2015; Yang et al., 2016; Bates et al., 2019; Zhang et al., 2021). In recent years, several acellular assays have been developed. The advantages of acellular assays are that they are usually cheaper and less time-consuming. The most commonly used assays are the dithiothreitol (DTT), ascorbic acid (AA), glutathione (GHS) and 2,7-dichlorofluorescin–horseradish peroxidase (DCFH) assays.

Traditionally, acellular ROS and OP measurement methods are based on the collection of PM filters, with quantification of OP taking place days, weeks or even months later (Venkatachari et al., 2005; Godri et al., 2011; Salana et al., 2021; Zhang et al., 2021). This most likely results in an underestimation of PM OP because many highly reactive aerosol components, including particle-bound ROSs (e.g., ROOH, R$\bullet$ and RO$\bullet_x$ species in particular) are short-lived and unstable (Fuller et al., 2014; Zhang et al., 2021). In a recent study, we showed that only a very small fraction ($< 10\,\%$) of particle-bound ROSs in organic aerosol collected on filters is stable when compared to in situ online DCFH measurements (Zhang et al., 2021), emphasizing the need for the rapid collection of particles to capture the chemistry of highly reactive aerosol components. Other studies, which measured the decay rate of organic radicals (Campbell et al., 2019b), peroxy pinic acid (Steimer et al., 2018) or hydrolysis of organic hydroperoxides in particles (Zhao et al., 2018), also show the half-life times of these unstable compounds, ranging from minutes to hours.

Therefore, new direct online measurement methods are required with direct-to-assay particle collection and rapid OP quantification to accurately assess the influence of highly reactive components on total OP. Providing robust OP measurements is a key step in achieving a more realistic assessment of the link between particle OP and particle toxicity (Fuller et al., 2014). Thus, various attempts have been made to build online methods and instruments to obtain faster measurements with a higher temporal resolution (Wang et al., 2011; Fang et al., 2015; Wragg et al., 2016; Gao et al., 2017).

The OP measurement depends on not only the aerosol composition but also the assay used. The human lung-lining layer contains, in addition to AA, other components such as glutathione, uric acid and many more anti-oxidants. Calas et al. (2017) showed that a simulated, epithelium lung lining to mimic the lung conditions might be favorable. However, Pietrogrande et al. (2019) demonstrated that, when assessing the OP with a mixture of antioxidants, the absolute signal of each antioxidant is lower because the OP is reduced by different antioxidants, which results in higher detection limits.

In this study, we present the development, characterization and first field deployment of a new online instrument that continuously quantifies OP in aerosol particles based on AA oxidation with a high time resolution (ca. 5 min). The online oxidative potential ascorbic acid instrument (OOPAAI) is the first instrument that provides rapid, highly-time-resolved OP quantification based on the oxidation of ascorbic acid. We run the OOPAAI using an AA-only-based assay to achieve as low a detection limit as possible, allowing quantification of OP in a range of polluted and moderate-pollution environments. The OOPAAI is an instrument with vastly improved performance, e.g., a better detection limit and functionality, compared to the method presented by Campbell et al. (2019a), now running at physiologically relevant conditions and including improved hardware components compared to the instrument developed by Wragg et al. (2016).

2 Methods

2.1 Reagents

All chemicals were obtained from Sigma-Aldrich, and all gases were obtained from Carbagas and were used without further purification unless otherwise indicated; these chemicals and gases include ascorbic acid (AA, 99.0 %), dehydroascorbic acid (DHA, 99.0 %), 0.1 M HCl solution, 0.1 M NaOH solution, Chelex 100 sodium form, $CuSO_4$ (99.0 %), FeSO4 (99 %), $Fe_2(SO_4)_3$ (98 %), *o*-phenylenediamine (OPDA, $\geq$ 99.5 %), HEPES (4-(2-hydroxyethyl)-1-piperazineethanesulfonic acid, $\geq$ 99 %), α-pinene ($\geq$ 98 %), β-pinene ($\geq$ 98 %), naphthalene ($\geq$ 99 %), zero-grade air (Medipac 2000 Superplus, Donaldson Company) and N_2 gas (purity 99.999 %). The H_2O used to prepare the solutions was purified with an ultrapure water (resistivity $\geq 18.2\,M\Omega\,cm^{-1}$; Synergy, Merck).

2.2 Chemical preparation

All solutions were made fresh every day, unless otherwise specified. Ultrapure water was additionally purified using a fritted column filled with 100 g of Chelex 100. An amount of 500 mL of ultrapure water was added, and the valve was adjusted to a flow of one drop per minute. The Chelex resin treatment was used to remove trace metals (e.g., copper and iron) from ultrapure water and to ensure a stable, low transition-metal-free background, which would otherwise interfere with AA oxidation from the sample. The AA solution (200 µM) was prepared at least 1 h before the experiment so that the background drift could stabilize with a 20 mM HEPES buffer at pH 6.8. The HEPES buffer working solution was prepared using 1 : 10 dilution with Chelexed ultrapure water from a stock solution, which is stored in the refrigerator. OPDA solutions were prepared by dissolving 0.432 g of OPDA in 250 mL of 0.1 hydrochloric acid (20 mM OPDA) immediately before the experiment to reduce OPDA oxidation. AA solutions were stored in opaque plastic bottles (250 mL; Nalgene, Merck) which were rinsed with hydrochloric acid to remove trace amounts of metals.

2.3 Ascorbic acid chemistry

An AA assay was used to quantify the OP of a given sample by measuring the oxidized form of AA, dehydroascorbic acid (DHA), as shown in Fig. 1. The pKa of AA is around 4.1; therefore, at pH 6.8 in an aqueous environment, AA is present mostly as the ascorbate anion (AH^-). AA and AH^- can be directly oxidized by metals such as Fe(III) or Cu(II) to form DHA, or they can be oxidized over the intermediate monodehydroascorbate radical ($A^{\bullet-}$). In Fig. 1, only the most important pathways that occur at a physiologically relevant pH 6.8 are shown. In the oxidation of AA, DHA is the first stable reaction product, and therefore DHA was chosen here as a direct measure of AA oxidation. DHA was then further reacted in a condensation reaction with *o*-phenylenediamine (OPDA) under acidic conditions at pH 2 to form the fluorophore (1,2-dihydroxyethyl)-fluoro[3,4-b]quinoxaline-1-one (DFQ) that is quantified in this assay. The chemistry of the AA assay and the mechanism of AA oxidation are described in more detail by Campbell et al. (2019a) and Shen et al. (2021).

The fluorescence detection approach (i.e., reaction of DHA with OPDA) was selected over a direct UV–VIS absorbance measurement of AA because fluorescence spectra are often more specific for an individual compound than UV–VIS absorbance, although the fluoresce detection approach needs an additional condensation step (see Fig. S1 in the Supplement). AA has a broad UV absorption peak at a wavelength of 265 nm. Many other organic compounds present in aerosol extracts also have strong absorbance in near-UV (see Fig. S2) (Birdwell and Engel, 2010; Huang et al., 2018). Therefore, it is not feasible to devise an instrument for continuous online operation using absorbance detection where a decrease in AA would need to be quantified in the presence of a larger background that potentially varies substantially with changes in the organic aerosol composition.

2.4 Offline measurements

Secondary organic aerosol (SOA) particles (using α-pinene as the precursor) were collected on filters for offline AA analysis to determine particle OP decay. SOA produced from OH-initiated photooxidation of α-pinene is commonly used as an atmospherically representative SOA (Campbell et al., 2019b). High-mass-concentration SOA (approximately 80 mg m^{-3}) was produced using the Organic Coating Unit (OCU) (Keller et al., 2022) collected on quartz filters for 100 s. These very high aerosol concentrations were necessary to minimize the time between particle generation and analysis and therefore reduce the decay of short-lived OP-active aerosol components. Keller et al. (2022) showed that the OCU produces SOA, even at high masses, with an atmospherically relevant, realistic chemical composition when compared to conditions in the particle mass range of low microgram values per cubic meter (Keller et al., 2022). In the OCU, an organic precursor is oxidized in a small flow chamber by OH and ozone under controlled relative humidity (65 %) and temperature conditions (fully described by Keller et al., 2022). After the OCU, an additional flow tube with additional ozone flow was added to oxidize the VOC that was not oxidized in the OCU and to increase the particle mass. Furthermore, the aerosol passed through a charcoal denuder to remove unreacted ozone and VOCs with an efficiency of 99.9 % (Campbell et al., 2019b).

The filters were then collected and extracted after different time intervals and analyzed with an offline AA assay using the same chemical conditions as the OOPAAI AA-based assay. A 47 mm quartz filter was extracted directly in 3 mL of 200 µM AA, buffered with 20 mM HEPES and then vortexed for 3 min. The slurry is then filtered with a syringe filter (PTFE, pore size 0.45 µm, Agilent). An amount of 900 µL of the extract was then incubated for 20 min in a 37 °C heating bath, which corresponds to the reaction time between aerosol extract and AA in the online instrument (see below). Subsequently, 100 µL OPDA dissolved in 0.1 M HCl was added and reacted for an additional 3 min at room temperature, and then the fluorescent signal was measured immediately with a spectrometer (QePro-UV-VIS, Ocean Insight). The fluorescent product DFQ was excited at $\lambda_{ex} = 365$ nm, with peak fluorescence emission monitored at $\lambda_{em} = 430$ nm.

2.5 The online oxidative potential ascorbic acid instrument (OOPAAI)

Figure 2 shows a schematic overview of the OOPAAI. The key components of the instrument are as follows: (1) the PILS (PILS, model 4001, Brechtel), where the aerosol par-

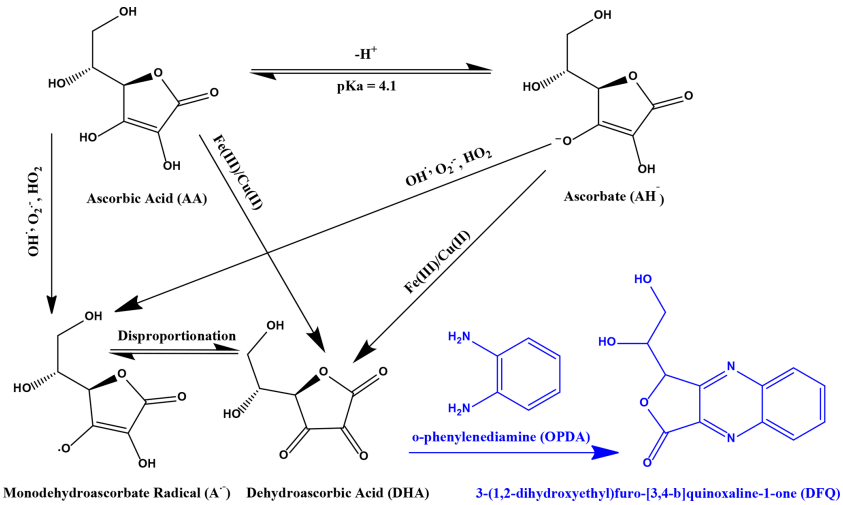

Figure 1. Simplified reaction scheme describing AA and AH oxidation by ROSs and redox-active transition metals (black) and the condensation reaction with *o*-phenylendiamine (OPDA) to the fluorophore (1,2-dihydroxyethyl)-fluoro[3,4-b]quinoxaline-1-one (DFQ) (purple).

ticles are collected into the liquid phase; (2) the heating bath, where ROS and the other OP-active particle components react with AA to form DHA under physiological conditions (pH 6.8 and 37 °C) and where the condensation reaction occurs between DHA and OPDA to form the fluorescent product DFQ; (3) the detection cell, where the fluorophore DFQ is quantified using a spectrometer.

The aerosol is pumped into the instrument using a vacuum pump (N035.1.2AN.18, KNF) at a flow rate of 16 L min^{-1} through a sample inlet (Fig. 2, black lines), where a solenoid valve allows switching between a HEPA filter (HEPA-CAP 75, Whatman), which removes 99.9 % of particles (to allow for blank measurements with particle-free air), and no HEPA filter. The aerosol then passes through four activated-charcoal honeycomb denuders (charcoal honeycomb denuders, Ionicon) with a total length of 14 cm to remove all gaseous oxidizing volatile compounds that can result in an increased OP signal. After the charcoal denuder, particles > 2.5 µm are removed with a round jet impactor. The impactor is part of the PILS, which was modified for our purposes. The wash flow in the PILS is not operated by the internal peristaltic pump but with an external peristaltic pump (Ismatec_REGLO Peristaltic Pump, Fisher Scientific) that can adjust flows for each channel independently. Furthermore, the internal bubble trap was removed from the PILS and replaced with two external ones. External bubble traps are placed after mixing with the OPDA, contributing to better mixing. To maximize and stabilize the air flow rate to 16 L min^{-1}, the internal orifice was enlarged, and an additional needle valve was added after the pump. In the condensation chamber of the PILS, the particles are activated by supersaturated water vapor before they reach the impaction plate. Although steam is generated around 100 °C, the measured temperature in the condensation chamber, even close (1 cm) to the tip of the heat generator, is only between 35 and 40 °C. Therefore, it is unlikely that this moderate temperature increase will significantly affect the concentrations of OP-active aerosol components within the PILS. The extraction efficiency of the PILS was determined by comparing the AA oxidation of aerosol measured directly with the PILS (normal setup, as described in Fig. 2) and aerosol simultaneously collected on a filter (assuming 100 % particle collection efficiency on the filter), which was then extracted and the AA oxidation quantified using the fluorescence detection setup in the OOPAAI. Taking the differences of these two analyses, the collection efficiency of the PILS operated under conditions described here (i.e., very low liquid flow rates and further modifications) was calculated to be 20 %–25 %. The online measurements in Fig. 3 are corrected for the lower particle collection efficiency to ensure inter-comparison between online and offline measurements, but the other measurements are not corrected because we want to show the actual capability of the instrument at its current development stage.

Activated aerosol particles are collected on the quartz impaction plate at the end of the condensation chamber of the PILS (Weber et al., 2010). This quartz impaction plate is washed with a continuous flow of 60 µL min^{-1} of AA (200 µM) buffered at pH 6.8 with a 10 mM HEPES buffer. HEPES is considered to be a buffer that generally does not form strong complexes with metals, which is advantageous because the AA assay is very sensitive to redox-active transition metals (see Fig. S3 in the Supplement) (Ferreira et al., 2015). For several highly OP-active metals such as iron or

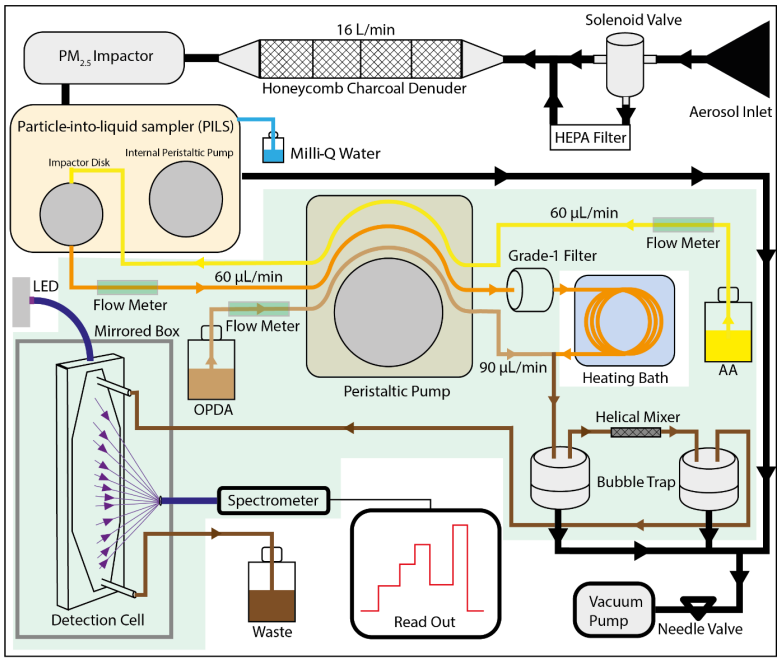

Figure 2. Schematic overview of the OOPAAI. Black lines illustrate air flows where air gets pulled into the PILS via a denuder and an impactor. In the PILS, the aerosol is collected with a wash flow containing ascorbic acid (yellow line) and pumped into a heating bath via a grade-1 filter (orange line). OPDA (light-brown line) is then added, and the condensation reaction of DHA with OPDA to form DFQ takes place (dark-brown line). After a mixing piece and two bubble traps, the liquid is pumped into the detection cell, where DFQ is excited by an LED and the fluorescent emission is quantified by a spectrometer. All components are mounted in an aluminum box, and the components with a light-green background are in the thermos-controlled compartment of the OOPAAI.

copper, the speciation of soluble complexes and the distribution between their soluble form and precipitates are strongly pH dependent. Therefore, maintaining a physiologically relevant pH is crucial to avoid changing the soluble fraction of metals and their speciation because the reactivity of AA (or any anti-oxidant) with metals will change significantly depending on the metal speciation and soluble or insoluble fractions.

The buffered AA–aerosol mixture is then pumped from the PILS in a polyether ether ketone (PEEK) tube through a peristaltic pump operated with polyvinyl chloride (PVC) peristaltic tubing (AHF, inner diameter 1.02 mm, white-white) at a flow rate of 60 µL min^{-1} flow through a cellulose filter (grade-1 filter, pore size 11 µm, Whatman) to remove any insoluble particles. Then, the reaction mixture flows through a heating bath filled with ethylene glycol at 37 °C, with a residence time of 20 min. This ensures that fast-reacting particle components contributing to OP, for example, organic radicals, as well as radicals formed by metals catalytically, are captured. A different residence time might change the sensitivity of the instrument towards specific OP components, where a longer residence time might enhance the contribution of catalytically active or slowly reacting components to the overall measured OP signal, and a shorter reaction time might enhance the contribution of short-lived OP components. Additionally, as DHA is not stable over time (Huelin, 1949) under physiological conditions, an extended residence time would lead to enhanced degradation of DHA, reducing the sensitivity of the OOPAAI. This reaction time of 20 min in the heating bath at body temperature and physiologically representative AA concentrations (200 µM) and physiologically relevant pH (pH 6.8) mimics the conditions in the human lung and the initial reactivity of the aerosol components with AA when aerosol particles get deposited on the lung-lining layer.

The liquid flow is then mixed in a *t* piece and two helical mixers (1/16 in. or 1.5875 mm, Stamixco) with a 90 µL min^{-1} flow of OPDA (20 mM in 0.1 M hydrochloric acid) for approximately 2 min before reaching the detector. The short reaction time was optimized to minimize shifting reaction conditions as a result of the low pH (see the Supplement for details). DHA and OPDA react to form the fluorescent product DFQ with a 1 : 1 stoichiometry, which is then detected by fluorescence spectroscopy. To reduce oxidation

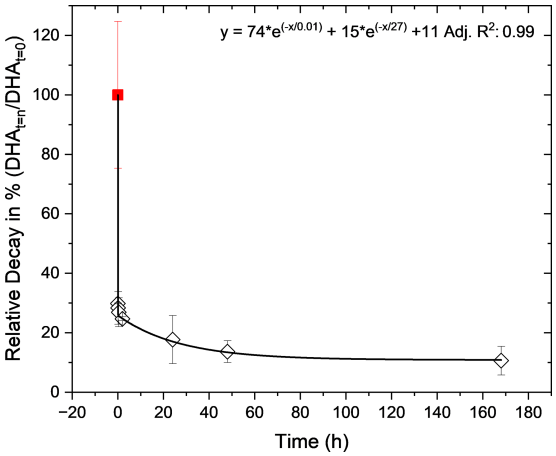

Figure 3. Offline decay of AA oxidation by α-pinene aerosol (black diamonds) and comparison with online quantification using the OOPAAI (red square). For the offline decay of OP-active compounds in SOA, DHA concentrations were quantified between 2 min and 7 d after sampling. A two-phase exponential decay function is used for the fit and gives an adjusted R square of 0.998. The relative decay values are normalized to 100 % for the online signal. Error bars represent the standard deviation observed over three experimental repeats.

and keep the solutions fresh over multiple days, the AA and OPDA solutions in the reservoir were continuously degassed with 50 mL min^{-1} of N_2. There was only a minimal increase in the blank signal over time, which was detrended by a linear fit if necessary.

All liquid flows in the system are constantly monitored using liquid flow meters (SLF3S-0600F, Sensirion). For fluorescence measurements, the liquid enters the detection cell before being pumped out of the instrument as waste. The detection cell is a home-built unit that uses a commercial flow through the cell (137-2-40, Hellma Analytics) with a height of 2 mm, a length of 40 mm and a width of 10 mm. At the end of the detection cell, the cuvette narrows where the inlet and outlet are placed perpendicular to the flow direction (see Fig. 2). To enhance light transmission through the cuvette, the narrow sides of the cuvette are polished to make them transparent. The LED (Roithner Lasertechnik, type UVLED-365-330-SMD, peak emission wavelength 365 nm) is soldered on a printed circuit board (PCB), which is screwed to a home-built thermoelectric element to ensure stable temperature conditions and therefore a more stable LED output.

The optical fiber from the LED is in close contact with the polished short side of the detection cell and excites the solute. The emitted light is then collected from the side of the large surface area of the detection cell with a collimating lens (74-UV, Ocean Insight) and focused on a 1500 µm fiber with a numerical aperture of 0.5 (UV–VIS fiber, FP1500RET SMA, Thorlabs). The fluorescence detection cell is enclosed in a light-tight box, which has a mirroring surface (reflecting tape) to maximize the collection efficiency of the fluorescence emission. Right in front of the collimating lens, a bandpass filter (FBH430-10, Thorlabs) from 420 to 440 nm is installed to remove the scattering of the excitation peak. The peak fluorescence emission light at 430 nm is measured using a spectrometer (QePro-UV-VIS, Ocean insight). The fluorescence signal was integrated at a window over 10 nm across the peak emission at 430 nm (425–435 nm). A raw spectrum of DFQ, measured with the QePro from Ocean Insight, is shown in the Supplement (see Fig. S4).

The liquid reservoirs, all tubing, the peristaltic pump, the spectrometer and the flow cell are enclosed in a compartment inside the aluminum box that is insulated and temperature controlled by a thermoelectric cooler (PK 50, ELMEKO) and the corresponding control unit (TPC300, ELMEKO) with two thermistors to measure and regulate the temperature to minimize temperature-related changes in reaction rates (green box in Fig. 2). The control of instrument components, as well as data acquisition, is performed using a LabVIEW (National Instruments) script, which sets the input parameters for the peristaltic pump and monitors the liquid flow rates of the flow meters. A feedback maintains a constant flow at the specified set point. Furthermore, the LabVIEW collects auxiliary data (various temperatures and potential errors).

All these components and devices are integrated into an aluminum box ($60 \times 60 \times 40$ cm) for better thermal stability and for easy transport. A fixed position of the different components ensures improved instrument performance and stability, as movement of key components, such as the optical fibers, has a noticeable effect on the fluorescence signal. The vacuum pump is kept external to minimize vibrations within the instrument. The waste reservoir is also kept external to minimize the amount of liquid inside the OOPAAI.

3 Results and discussion

3.1 OP lifetime of SOA particles

SOA is often a major component of aerosol particles in urban and remote locations (Chen et al., 2022). However, little is known about the OP properties of SOA, particularly how long-lived the components which contribute to OP in SOA are. In the online instrument, the AA solution is brought into contact with the particles inside the PILS, i.e., within seconds after the particles entered the OOPAAI; therefore, very reactive components are also quantified, as described in detail in the method section above. Seven filters were collected and stored at room temperature between 2 min and 7 d and analyzed in triplicates. Figure 3 shows the relative decrease in DHA formation over time, normalized to the online OOPAAI measurement (red square). The offline measurements (black diamonds) and the online measurements are fitted with a two-

phase exponential decay function. The stability of OP-active components in α-pinene SOA can be broadly divided into the following three fractions: a very reactive and short-lived fraction with a half-life of less than 1 min, which is only captured by the online OOPAAI; a second fraction that decays slower and has a half-life time of about 20 h; and a third fraction that is stable for more than a week. The online signal is more than 3 times higher than the immediately measured offline time point, and after a week almost 90 % of the OP-active components are lost. Overall, this will lead to a significant underestimation of the OP signal when using traditional offline analysis, especially if filter samples are not analyzed immediately. In a recent review, Wang et al. (2023) reported lifetimes for peroxide from seconds to days. Therefore, the decomposition of these peroxides may contribute to reduced OP on filter samples, as they may well degrade prior to analysis. A similar decay was also observed for offline measurements for the DCFH assay in several studies (Fuller et al., 2014; Wragg et al., 2016; Zhang et al., 2021). Note that OP decay characteristics could be different for SOA produced from other precursors. In addition, in ambient PM, inorganic particle components such as redox-active transition metals could also contribute to OP. These experiments clearly demonstrate that OP-active components in SOA decay on a timescale (minutes to about 1–2 d) that is much faster than typical offline analysis from particles collected on filters or impactors.

3.2 Response of the OOPAAI: condensation of DHA with OPDA

For the routine calibration of the OOPAAI, we use aqueous solutions of known concentrations of DHA to determine the instrument response and detection limit with respect to DHA detection. The calibration of the OOPAAI was performed at pH 2 to assure stability of the solutions during the calibration procedure. Calibration solutions of known DHA concentrations were pumped directly through the PILS without altering anything else in the instrument. The advantages of this calibration method are that there are minimal changes in the instrument setup, and at the same time, it also offers an easy and robust method to perform calibrations during field deployments of the OOPAAI. Figure 4 shows a calibration of DHA in which nine concentrations of DHA ranging from 0–100 µM were measured for 20 min each.

Figure 4a shows the raw detector signal that illustrates the fast time response after changing the DHA calibration solution. At concentrations < 10 µM, i.e., the concentration range measured in ambient particles (see Fig. 8), the signal equilibrated to a new steady-state DHA concentration within 5 min, which is equal to the instrument's time resolution. This smear-out effect is due to diffusion, wall effects and turbulence in the tubing, bubble traps and the connectors of the instrument. Thus, the instrument is able to resolve changes in the OP concentration under ambient conditions on a timescale of a few minutes. Figure 4b shows the calibration curve for DHA concentrations from 1–100 µM. At DHA concentrations larger than 100 µM, the calibration curve starts to flatten, and such DHA concentrations are therefore considered to be beyond the linear calibration range of the instrument (data not shown). The error bars indicate the standard deviation obtained for each plateau of the corresponding measurement. This demonstrates a strong linear relationship between DHA concentration and fluorescence signal, with a dynamic range of at least 2 orders of magnitude. All subsequent calibration curves are blank subtracted (see first 30 min in Fig. 4a) and converted from fluorescence counts into DHA concentration using data from the calibration curve (Fig. 4), as shown in the first term of Eq. (1).

3.3 AA oxidation by filter extracts from SOA, metals and ambient aerosol

The AA assay is highly sensitive to redox-active transition metals such as Fe and Cu (Shen et al., 2021) but also reacts with organic components present in secondary organic aerosols but less efficiently than with metals (Pietrogrande et al., 2022). To determine the sensitivity of the OOPAAI to both metals and organic aerosols, calibrations were performed as illustrated in Fig. 5. In Fig. 5a, the calibration of α-pinene SOA aqueous extracts is shown with an adjusted R^2 of 0.994, which indicates a good linearity over 2 orders of magnitude. In Fig. 5b, the OOPAAI response for iron(II) sulfate solutions is given with an adjusted R^2 of 0.99 for a sigmoidal fit. The linear range of the response for Fe(II) is between about 0.5–2 µg mL^{-1}; above about 2 µg mL^{-1}, the calibration curve flattens. The reactivity of our AA assay is approximately 2 orders of magnitude higher for iron(II) sulfate than for α-pinene SOA, consistent with Campbell et al. (2019a). However, in ambient aerosol particles, the mass concentration of the organic aerosol is often 1–2 orders of magnitude higher than that of redox-active metals (Kamphus et al., 2010; Calvo et al., 2013; Hama et al., 2018), so despite the lower sensitivity of the AA assay towards organic constituents, they still have a large impact on the overall OP of the particles measured with AA and therefore potentially on the oxidative stress that aerosols might generate in the lung.

To characterize the OOPAAI with a more complex chemical system, we used an aqueous extract of ambient aerosol samples collected on filters. This allowed us to evaluate the instrument performance with solutions of complex chemical composition that include a wide range of organic and inorganic components. For these measurements, the PILS was bypassed, and the AA solution was mixed in the instrument with the filter extract using the peristaltic pump of the OOPAAI. Figure 6 shows a series of dilutions of a filter collected in Beijing in 2016 during the Atmospheric Pollution and Human Health campaign (APHH) (Shi et al., 2019; Campbell et al., 2021). For these measurements, 10 punches (diameter of 1 cm) were extracted in 30 mL of ultrapure Chelexed water by vortexing a 50 mL falcon tube for 3 min.

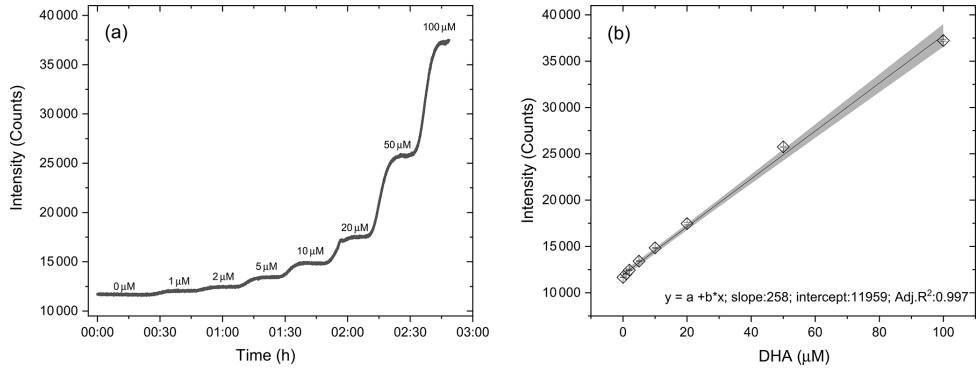

Figure 4. DHA calibration curve. **(a)** Each concentration of DHA solution was measured for 20 min with the setup described in Fig. 1. **(b)** The calibration curve is linear (adj. $R^2 = 0.997$) in the dynamic range of 0–200 µM. The error bars are calculated from the standard deviation of each plateau.

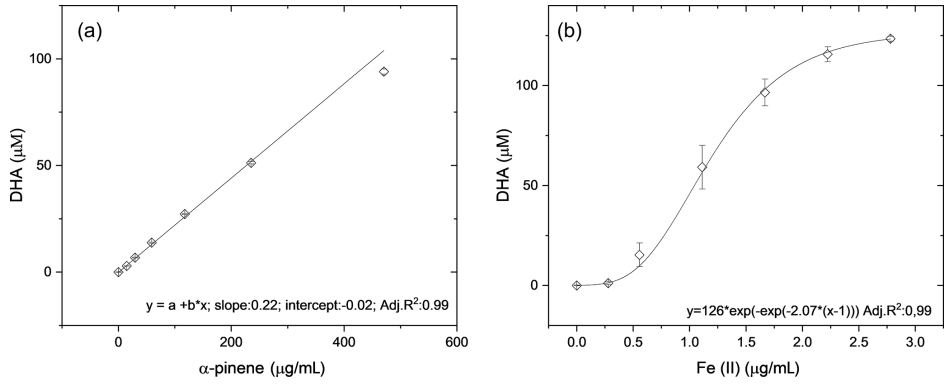

Figure 5. Response curves generated form **(a)** α-pinene SOA from filter extracts and **(b)** from Fe(II)SO_4 solutions. The error bars represent the standard deviation of the spectrometer signal normalized to the DHA concentration during the 30 min measurement. The slope of the linear fits through the data and, therefore, the sensitivity are around 100 times higher for the iron sulfate than for SOA.

Afterwards, the filter slurry was filtrated with a syringe filter (0.45 µM pore size) and collected in another falcon tube (full description of the method in Campbell et al. (2019a). A good linearity (R^2 of 0.99) is obtained, illustrating that complex ambient aerosol extracts can also be quantified with the OOPAAI.

3.4 Calibration with biogenic and anthropogenic aerosol

As a further experiment to show the linearity of the OOPAAI response towards SOA aerosol particles in a wide mass range, the OOPAAI was run in full operational mode (i.e., including the PILS). The aerosol generated by the OCU was diluted to generate particle concentrations in the range of around 50 to 1000 µg m^{-3} and passed through a home-built charcoal denuder, removing ozone and gaseous VOC residues. In parallel, a scanning mobility particle sizer (SMPS (3080), DMA (3081), CPC (3776), TSI) was operated. The SMPS was set to a scan time of 105 s, and a SOA particle density of 1.4 g cm^{-3} was assumed (Kostenidou et al., 2007). SOA from two different precursors of VOC, an anthropogenic precursor (naphthalene) and a biogenic precursor (β-pinene), were generated and quantified with the OOPAAI. In Fig. 7, the OOPAAI response is shown as a function of SOA mass per cubic meter for the two SOA types. It illustrates the linear relationship over more than 1 order of magnitude of particle mass with synthesized, atmospherically relevant aerosol particles; this is in contrast to the filter extract, which was used for the measurements shown in Figs. 5 and 6. The abscissa error in Fig. 7 is the standard deviation of the variability in the production of particle mass. The ordinate error represents the standard deviation of the variability of the OOPAAI signal. Naphthalene

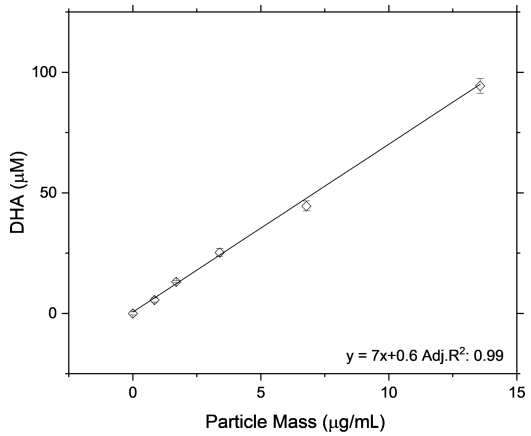

Figure 6. Response of the OOPAAI using particle extracts from a filter collected at an urban location in Beijing, China. A clear linear relationship is obtained between the particle mass in the extracts and the instrument signal. Error bars represent the variability of the OOPAAI signal.

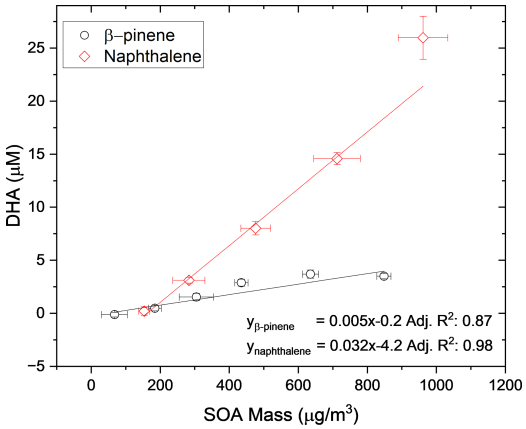

Figure 7. SOA was produced from an anthropogenic and biogenic precursor at different mass concentrations using an Organic Coating Unit (OCU) (Keller et al., 2022). The OOPAAI signal shows a linear response for both SOA types as a function of particle mass, with the anthropogenic SOA being much more reactive towards the AA assay.

SOA particles cause a significantly higher OOPAAI response (i.e., slope) than β-pinene SOA, which has also been seen by others (Tuet et al., 2017; Chowdhury et al., 2018; Zhang et al., 2021; Offer et al., 2022). This could be because AA reacts very efficiently and catalytically with quinones, which are known oxidation products in naphthalene SOA, in comparison to β-pinene SOA, where no quinones are present (Isaacs and Van Eldik, 1997; McWhinney et al., 2013; Roginsky et al., 1999).

3.5 Ambient measurements

To determine the response of the OOPAAI for ambient aerosol, proof-of-concept measurements were performed at an urban background location in the city center of Basel, Switzerland. In Fig. 8a, the raw detector signal from an ambient measurement is shown where OP, in nanomole DHA per cubic meter of air, is plotted over a 4 d period together with $PM_{2.5}$ data for the same time. OP and $PM_{2.5}$ show a clear diurnal cycle, with maxima of around 12 nmol DHA m^{-3} and 17 µg m^{-3}, respectively, in the evening and during the night. $PM_{2.5}$ concentrations were measured with a Fidas 200 (PALAS) at Basel St. Johanns-Platz by Luftqualität Nordwestschweiz with a time resolution of 1 min (Lufthygiene Amt beider Basel, 2023). This station is in close proximity (approximately 500 m) to the measurement location where the OOPAAI was operated. The air-volume-normalized signal of OOPAAI (Fig. 8a) has a very similar diurnal trend compared to the aerosol mass, demonstrating that OOPAAI is capable of quantifying OP in urban particles, even at low PM concentrations of only a few µg m^{-3}, with a high time resolution of approximately 5 min.

Figure 8b shows the OP data mass normalized for $PM_{2.5}$, with OP concentrations varying by more than 1 order of magnitude from about 0.1 to 2 nmol µg^{-1}. The formula used to calculate mass-normalized OP is given in Eq. (1). The first term in Eq. (1) converts the counts of the spectrometer in the OOPAAI into DHA concentrations via the DHA calibration curve. The second term normalizes the OP signal for volume air through the liquid and air flow rates of the OOPAAI, and the third term normalizes for $PM_{2.5}$ mass.

Figure 8b clearly indicates that the OP content in $PM_{2.5}$ is not constant on a diurnal timescale and that, in some cases (e.g., 30 November, 18:00 UTC+1), OP concentrations change by more than a factor of 5 within about an hour. This demonstrates that the composition of $PM_{2.5}$ and sources with very different OP content can vary quickly in an urban environment. Organics and metals, for example, have very different OPs, as illustrated in Fig. 5, and could contribute to the changes in the OP-active aerosol mass fraction. Alternatively, inorganic ions such as nitrate, sulfate and ammonium are OP inactive but may also exhibit a diurnal profile (Timonen et al., 2014) that would affect the total mass fraction of OP. To better understand how such compositional changes drive the OP particle mass fractions and potentially particle toxicity, more ambient measurements are required.

The limit of the detection of the OOPAAI characterized in this study was calculated using the $3_{\sigma bl}$ methods. The detection limit of the OOPAAI for DHA is 0.7 ± 0.1 µM. For the urban ambient aerosol measured in this study, the OOPAAI is sensitive enough to show a significant response down to

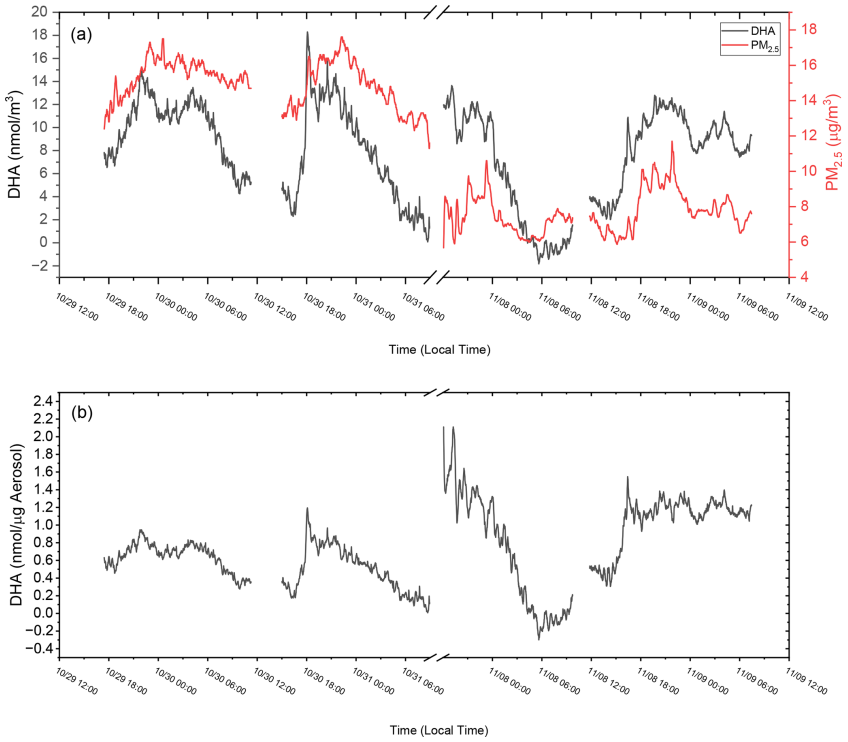

Figure 8. Ambient OOPAAI measurements in Basel (Switzerland) at Klingelbergstrasse 27, an urban background location, in October and November 2022. **(a)** On the left x axis, DHA in nanomole normalized to air volume is plotted versus time; on the right x axis, $PM_{2.5}$ mass over time is plotted versus time. **(b)** DHA concentrations normalized to the mass of $PM_{2.5}$ at the same time. Gaps in the data are due to changing solutions in the OOPAAI or blank measurements. The LOD for ambient measurements is approximately $5\,\mu g\,m^{-3}$.

$PM_{2.5}$ mass concentrations of around $5\,\mu g\,m^{-3}$.

$$\mathrm{OP}\left(\frac{\text{nmol DHA}}{\mu\text{g aerosol}}\right) = \frac{(\text{counts} - \text{intercept})}{\text{slope}}\,\text{DHA}\,(\mu\text{M}) \times \frac{\text{liquid flow rate}\left(\frac{\text{mL}}{\text{min}}\right)}{\text{gas flow rate}\left(\frac{\text{m}^3}{\text{min}}\right)} \times \frac{1}{\text{aerosol mass}\left(\frac{\mu\text{g}}{\text{m}^3}\right)} \quad (1)$$

4 Conclusion

A novel automated, online OP instrument has been designed and thoroughly characterized. The OOPAAI can continuously quantify OP concentrations in different types of aerosols with a physiologically relevant AA assay (i.e., pH 6.8 and 37 °C) with an unparalleled time resolution of about 5 min. The OP-active components in the particles react within seconds after the particles enter the instrument, and thus very short-lived OP components (the majority of the total OP in SOA particles) are quantified, overcoming the limitations of current offline-based measurement methods. A comparison of the OOPAAI instrument with offline filter-based OP quantification shows that about 90 % of OPs in SOA particles have a lifetime of minutes to hours and that only about 10 % of OP can be detected after a couple of days. In particular, the OP components which have the shortest lifetime of less than a minute are likely formed in the particle via photochemical processes. These compounds may be continuously formed while particles are exposed to sunlight or oxidants in the atmosphere (Alpert et al., 2021); thus, this short-lived OP fraction might also be relevant for health aspects. Therefore, to capture the entire OP concentration, an online instrument such as the one presented here, with fast collection and analysis time, is essential for an accurate quantification of aerosol OP, and any offline method is likely to severely underestimate health-relevant OP.

The instrument is portable and capable of running autonomously for about 3 d; thus, it is well suited to field campaigns and laboratory experiments. The OOPAAI is sensitive to a wide range of different compounds and aerosol types and

can measure their OP over a wide range of environments, from ambient to laboratory-generated particles. Its detection limit for urban aerosol is around $5\,\mu g\,m^{-3}$, and a proof-of-principle deployment at an urban background site in Basel, Switzerland, demonstrated the highly dynamic nature of OP-active components in $PM_{2.5}$, which can only be captured with the fast-response, high-time-resolution and robust OP measurement facilitated by the OOPAAI.

This novel online instrument characterizes and accurately quantifies OP for the first time in extended field studies at a high time resolution, which will be essential for an improved understanding of the sources and formation processes of particle OP and to identify the link between particle OP and particle health effects.

Code availability. All LabVIEW VIs can be accessed from the corresponding author upon request.

Data availability. All data can be accessed from the corresponding author upon request.

Supplement. The supplement related to this article is available online at: https://doi.org/10.5194/amt-16-2641-2023-supplement.

Author contributions. BU developed the instrument, conducted all the experiments, analyzed the data and wrote the paper. SJC, AB and BG helped with the various experiments. NB wrote the software, RF designed and built many of the electronic components, and HRR assisted with the hardware. MK conceived the study and oversaw the research.

Competing interests. The contact author has declared that none of the authors has any competing interests.

Disclaimer. Publisher's note: Copernicus Publications remains neutral with regard to jurisdictional claims in published maps and institutional affiliations.

Acknowledgements. The authors gratefully acknowledge Sandra Andris-Ogorka and René Glanzmann from the Lufthygieneamt beider Basel for the FIDAS data and the mechanical workshop of the University of Cambridge and Basel for the construction of the hardware parts.

Financial support. This research has been supported by the Schweizerischer Nationalfonds zur Förderung der Wissenschaftlichen Forschung (grant no. 200021_192192/1).

Review statement. This paper was edited by Pierre Herckes and reviewed by Rodney Weber and two anonymous referees.

References

Alpert, P. A., Dou, J., Corral Arroyo, P., Schneider, F., Xto, J., Luo, B., Peter, T., Huthwelker, T., Borca, C. N., Henzler, K. D., Schaefer, T., Herrmann, H., Raabe, J., Watts, B., Krieger, U. K., and Ammann, M.: Photolytic radical persistence due to anoxia in viscous aerosol particles, Nat. Commun., 12, 1–8, https://doi.org/10.1038/s41467-021-21913-x, 2021.

Bates, J. T., Fang, T., Verma, V., Zeng, L., Weber, R. J., Tolbert, P. E., Abrams, J. Y., Sarnat, S. E., Klein, M., Mulholland, J. A., and Russell, A. G.: Review of Acellular Assays of Ambient Particulate Matter Oxidative Potential: Methods and Relationships with Composition, Sources, and Health Effects, Environ. Sci. Technol., 53, 4003–4019, https://doi.org/10.1021/acs.est.8b03430, 2019.

Baulig, A., Garlatti, M., Bonvallot, V., Marchand, A., Barouki, R., Marano, F., and Baeza-Squiban, A.: Involvement of reactive oxygen species in the metabolic pathways triggered by diesel exhaust particles in human airway epithelial cells, Am. J. Physiol.-Lung C., 285, L671–L679, https://doi.org/10.1152/ajplung.00419.2002, 2003.

Birdwell, J. E. and Engel, A. S.: Characterization of dissolved organic matter in cave and spring waters using UV-Vis absorbance and fluorescence spectroscopy, Org. Geochem., 41, 270–280, https://doi.org/10.1016/J.ORGGEOCHEM.2009.11.002, 2010.

Brunekreef, B. and Holgate, S. T.: Air pollution and health, Lancet (London, England), 360, 1233–1242, https://doi.org/10.1016/S0140-6736(02)11274-8, 2002.

Calas, A., Uzu, G., Martins, J. M. F., Voisin, D., Spadini, L., Lacroix, T., and Jaffrezo, J. L.: The importance of simulated lung fluid (SLF) extractions for a more relevant evaluation of the oxidative potential of particulate matter, Scientific Reports, 7, 1–12, https://doi.org/10.1038/s41598-017-11979-3, 2017.

Calvo, A. I., Alves, C., Castro, A., Pont, V., Vicente, A. M., and Fraile, R.: Research on aerosol sources and chemical composition: Past, current and emerging issues, Atmos. Res., 120–121, 1–28, https://doi.org/10.1016/J.ATMOSRES.2012.09.021, 2013.

Campbell, S. J., Utinger, B., Lienhard, D. M., Paulson, S. E., Shen, J., Griffiths, P. T., Stell, A. C., and Kalberer, M.: Development of a physiologically relevant online chemical assay to quantify aerosol oxidative potential, Anal. Chem., 91, 13088–13095, https://doi.org/10.1021/acs.analchem.9b03282, 2019a.

Campbell, S. J., Stevanovic, S., Miljevic, B., Bottle, S. E., Ristovski, Z., and Kalberer, M.: Quantification of Particle-Bound Organic Radicals in Secondary Organic Aerosol, Environ. Sci. Technol., 53, 6729–6737, https://doi.org/10.1021/acs.est.9b00825, 2019b.

Campbell, S. J., Wolfer, K., Utinger, B., Westwood, J., Zhang, Z.-H., Bukowiecki, N., Steimer, S. S., Vu, T. V., Xu, J., Straw, N., Thomson, S., Elzein, A., Sun, Y., Liu, D., Li, L., Fu, P., Lewis, A. C., Harrison, R. M., Bloss, W. J., Loh, M., Miller, M. R., Shi, Z., and Kalberer, M.: Atmospheric conditions and composition that influence $PM_{2.5}$ oxidative potential in Beijing, China, Atmos. Chem. Phys., 21, 5549–5573, https://doi.org/10.5194/acp-21-5549-2021, 2021.

Chen, G., Canonaco, F., Tobler, A., Aas, W., Alastuey, A., Allan, J., Atabakhsh, S., Aurela, M., Baltensperger, U., Bougiatioti, A., De Brito, J. F., Ceburnis, D., Chazeau, B., Chebaicheb, H., Daellenbach, K. R., Ehn, M., El Haddad, I., Eleftheriadis, K., Favez, O., Flentje, H., Font, A., Fossum, K., Freney, E., Gini, M., Green, D. C., Heikkinen, L., Herrmann, H., Kalogridis, A.-C., Keernik, H., Lhotka, R., Lin, C., Lunder, C., Maasikmets, M., Manousakas, M. I., Marchand, N., Marin, C., Marmureanu, L., Mihalopoulos, N., Močnik, G., Nęcki, J., O'Dowd, C., Ovadnevaite, J., Peter, T., Petit, J.-E., Pikridas, M., Matthew Platt, S., Pokorná, P., Poulain, L., Priestman, M., Riffault, V., Rinaldi, M., Różański, K., Schwarz, J., Sciare, J., Simon, L., Skiba, A., Slowik, J. G., Sosedova, Y., Stavroulas, I., Styszko, K., Teinemaa, E., Timonen, H., Tremper, A., Vasilescu, J., Via, M., Vodička, P., Wiedensohler, A., Zografou, O., Cruz Minguillón, M., and Prévôt, A. S. H.: European aerosol phenomenology – 8: Harmonised source apportionment of organic aerosol using 22 Year-long ACSM/AMS datasets, Environ. Int., 166, 107325, https://doi.org/10.1016/j.envint.2022.107325, 2022.

Chowdhury, P. H., He, Q., Lasitza Male, T., Brune, W. H., Rudich, Y., and Pardo, M.: Exposure of Lung Epithelial Cells to Photochemically Aged Secondary Organic Aerosol Shows Increased Toxic Effects, Environ. Sci. Tech. Let., 5, 424–430, https://doi.org/10.1021/acs.estlett.8b00256, 2018.

Donaldson, K., Stone, V., Seaton, A., and MacNee, W.: Ambient particle inhalation and the cardiovascular system: Potential mechanisms, Environ. Health Persp., 109, 523–527, https://doi.org/10.1289/ehp.01109s4523, 2001.

Fang, T., Verma, V., Guo, H., King, L. E., Edgerton, E. S., and Weber, R. J.: A semi-automated system for quantifying the oxidative potential of ambient particles in aqueous extracts using the dithiothreitol (DTT) assay: results from the Southeastern Center for Air Pollution and Epidemiology (SCAPE), Atmos. Meas. Tech., 8, 471–482, https://doi.org/10.5194/amt-8-471-2015, 2015.

Ferreira, C. M. H., Pinto, I. S. S., Soares, E. V., and Soares, H. M. V. M.: (Un)suitability of the use of pH buffers in biological, biochemical and environmental studies and their interaction with metal ions – a review, RSC Adv., 5, 30989–31003, https://doi.org/10.1039/c4ra15453c, 2015.

Fuller, S. J., Wragg, F. P. H., Nutter, J., and Kalberer, M.: Comparison of on-line and off-line methods to quantify reactive oxygen species (ROS) in atmospheric aerosols, Atmos. Environ., 92, 97–103, https://doi.org/10.1016/j.atmosenv.2014.04.006, 2014.

Gao, D., Fang, T., Verma, V., Zeng, L., and Weber, R. J.: A method for measuring total aerosol oxidative potential (OP) with the dithiothreitol (DTT) assay and comparisons between an urban and roadside site of water-soluble and total OP, Atmos. Meas. Tech., 10, 2821–2835, https://doi.org/10.5194/amt-10-2821-2017, 2017.

GBD 2013 Risk Factors Collaborators: Global, regional, and national comparative risk assessment of 79 behavioural, environmental and occupational, and metabolic risks or clusters of risks in 188 countries, 1990–2013: A systematic analysis for the Global Burden of Disease Study 2013, Lancet, 386, 2287–2323, https://doi.org/10.1016/S0140-6736(15)00128-2, 2015.

Godri, K. J., Duggan, S. T., Fuller, G. W., Baker, T., Green, D., Kelly, F. J., and Mudway, I. S.: Particulate matter oxidative potential from waste transfer station activity, Environ. Health Persp., 118, 493–498, https://doi.org/10.1289/ehp.0901303, 2010.

Godri, K. J., Harrison, R. M., Evans, T., Baker, T., Dunster, C., Mudway, I. S., and Kelly, F. J.: Increased oxidative burden associated with traffic component of ambient particulate matter at roadside and Urban background schools sites in London, PLoS One, 6, e21961, https://doi.org/10.1371/journal.pone.0021961, 2011.

Hama, S. M. L., Cordell, R. L., Staelens, J., Mooibroek, D., and Monks, P. S.: Chemical composition and source identification of PM10 in five North Western European cities, Atmos. Res., 214, 135–149, https://doi.org/10.1016/J.ATMOSRES.2018.07.014, 2018.

Hart, J. E., Liao, X., Hong, B., Puett, R. C., Yanosky, J. D., Suh, H., Kioumourtzoglou, M. A., Spiegelman, D., and Laden, F.: The association of long-term exposure to $PM_{2.5}$ on all-cause mortality in the Nurses' Health Study and the impact of measurement-error correction, Environmental Health, 14, 38, https://doi.org/10.1186/s12940-015-0027-6, 2015.

Huang, S., Gan, W., Yan, M., Zhang, X., Zhong, Y., and Yang, X.: Differential UV–vis absorbance can characterize the reaction of organic matter with ClO_2, Water Res., 139, 442–449, https://doi.org/10.1016/J.WATRES.2018.04.006, 2018.

Huelin, F. E.: Investigations on the stability and determination of dehydroascorbic acid, Aust. J. Biol. Sci., 2, 346–354, https://doi.org/10.1071/BI9490346, 1949.

Isaacs, N. S. and Van Eldik, R.: A mechanistic study of the reduction of quinones by ascorbic acid, J. Chem. Soc. Perk. T. 2, 8, 1465–1467, https://doi.org/10.1039/a701072i, 1997.

Kamphus, M., Ettner-Mahl, M., Klimach, T., Drewnick, F., Keller, L., Cziczo, D. J., Mertes, S., Borrmann, S., and Curtius, J.: Chemical composition of ambient aerosol, ice residues and cloud droplet residues in mixed-phase clouds: single particle analysis during the Cloud and Aerosol Characterization Experiment (CLACE 6), Atmos. Chem. Phys., 10, 8077–8095, https://doi.org/10.5194/acp-10-8077-2010, 2010.

Keller, A., Kalbermatter, D. M., Wolfer, K., Specht, P., Steigmeier, P., Resch, J., Kalberer, M., Hammer, T., and Vasilatou, K.: The organic coating unit, an all-in-one system for reproducible generation of secondary organic matter aerosol, Aerosol Sci. Technol., 56, 947–958, https://doi.org/10.1080/02786826.2022.2110448, 2022.

Koike, E. and Kobayashi, T.: Chemical and biological oxidative effects of carbon black nanoparticles, Chemosphere, 65, 946–951, https://doi.org/10.1016/j.chemosphere.2006.03.078, 2006.

Kostenidou, E., Pandis, S. N., Pathak, R. K., Pandis, S. N., Kostenidou, E., and Pandis, S. N.: An Algorithm for the Calculation of Secondary Organic Aerosol Density Combining AMS and SMPS Data, Aerosol Sci. Tech., 41, 1002–1010, https://doi.org/10.1080/02786820701666270, 2007.

Künzi, L., Mertes, P., Schneider, S., Jeannet, N., Menzi, C., Dommen, J., Baltensperger, U., Prévôt, A. S. H., Salathe, M., Kalberer, M., and Geiser, M.: Responses of lung cells to realistic exposure of primary and aged carbonaceous aerosols, Atmos. Environ., 68, 143–150, https://doi.org/10.1016/j.atmosenv.2012.11.055, 2013.

Laden, F., Schwartz, J., Speizer, F. E., and Dockery, D. W.: Reduction in fine particulate air pollution and mortality: Extended follow-up of the Harvard Six Cities Study, Am. J. Resp.

Crit. Care, 173, 667–672, https://doi.org/10.1164/rccm.200503-443OC, 2006.

Lehman, S. E., Morris, A. S., Mueller, P. S., Salem, A. K., Grassian, V. H., and Larsen, S. C.: Silica nanoparticle-generated ROS as a predictor of cellular toxicity: Mechanistic insights and safety by design, Environ. Sci.-Nano, 3, 56–66, https://doi.org/10.1039/c5en00179j, 2016.

Lepeule, J., Laden, F., Dockery, D., and Schwartz, J.: Chronic exposure to fine particles and mortality: An extended follow-up of the Harvard six cities study from 1974 to 2009, Environ. Health Persp., 120, 965–970, https://doi.org/10.1289/ehp.1104660, 2012.

Li, N., Hao, M., Phalen, R. F., Hinds, W. C., and Nel, A. E.: Particulate air pollutants and asthma: A paradigm for the role of oxidative stress in PM-induced adverse health effects, Clin. Immunol., 109, 250–265, https://doi.org/10.1016/j.clim.2003.08.006, 2003.

Lufthygiene Amt beider Basel: Luftqualität Nordwestschweiz, https://luftqualitaet.ch/messdaten/datenarchiv/abfrage, last access: 7 January 2023.

McWhinney, R. D., Zhou, S., and Abbatt, J. P. D.: Naphthalene SOA: redox activity and naphthoquinone gas–particle partitioning, Atmos. Chem. Phys., 13, 9731–9744, https://doi.org/10.5194/acp-13-9731-2013, 2013.

Oberdörster, G., Oberdörster, E., and Oberdörster, J.: Nanotoxicology: An emerging discipline evolving from studies of ultrafine particles, Environ. Health Persp., 113, 823–839, https://doi.org/10.1289/ehp.7339, 2005.

Offer, S., Hartner, E., Di Bucchianico, S., Bisig, C., Bauer, S., Pantzke, J., Zimmermann, E. J., Cao, X., Binder, S., Kuhn, E., Huber, A., Jeong, S., Käfer, U., Martens, P., Mesceriakovas, A., Bendl, J., Brejcha, R., Buchholz, A., Gat, D., Hohaus, T., Rastak, N., Jakobi, G., Kalberer, M., Kanashova, T., Hu, Y., Ogris, C., Marsico, A., Theis, F., Pardo, M., Gröger, T., Oeder, S., Orasche, J., Paul, A., Ziehm, T., Zhang, Z.-H. H., Adam, T., Sippula, O., Sklorz, M., Schnelle-Kreis, J., Czech, H., Kiendler-Scharr, A., Rudich, Y., and Zimmermann, R.: Effect of Atmospheric Aging on Soot Particle Toxicity in Lung Cell Models at the Air-Liquid Interface: Differential Toxicological Impacts of Biogenic and Anthropogenic Secondary Organic Aerosols (SOAs), Environ. Health Persp., 130, 1–19, https://doi.org/10.1289/EHP9413, 2022.

Pietrogrande, M. C., Bertoli, I., Manarini, F., and Russo, M.: Ascorbate assay as a measure of oxidative potential for ambient particles: Evidence for the importance of cell-free surrogate lung fluid composition, Atmos. Environ., 211, 103–112, https://doi.org/10.1016/j.atmosenv.2019.05.012, 2019.

Pietrogrande, M. C., Romanato, L., and Russo, M.: Synergistic and Antagonistic Effects of Aerosol Components on Its Oxidative Potential as Predictor of Particle Toxicity, Toxics, 10, 196, https://doi.org/10.3390/TOXICS10040196, 2022.

Prahalad, A. K., Inmon, J., Dailey, L. A., Madden, M. C., Ghio, A. J., and Gallagher, J. E.: Air pollution particles mediated oxidative DNA base damage in a cell free system and in human airway epithelial cells in relation to particulate metal content and bioreactivity, Chem. Res. Toxicol., 14, 879–887, https://doi.org/10.1021/tx010022e, 2001.

Roginsky, V. A., Barsukova, T. K., and Stegmann, H. B.: Kinetics of redox interaction between substituted quinones and ascorbate under aerobic conditions, Chem.-Biol. Interact., 121, 177–197, https://doi.org/10.1016/S0009-2797(99)00099-X, 1999.

Salana, S., Wang, Y., Puthussery, J. V., and Verma, V.: A semi-automated instrument for cellular oxidative potential evaluation (SCOPE) of water-soluble extracts of ambient particulate matter, Atmos. Meas. Tech., 14, 7579–7593, https://doi.org/10.5194/amt-14-7579-2021, 2021.

Shen, J., Griffiths, P. T., Campbell, S. J., Utinger, B., Kalberer, M., and Paulson, S. E.: Ascorbate oxidation by iron, copper and reactive oxygen species: review, model development, and derivation of key rate constants, Sci. Rep.-UK, 11, 1–14, https://doi.org/10.1038/s41598-021-86477-8, 2021.

Shi, Z., Vu, T., Kotthaus, S., Harrison, R. M., Grimmond, S., Yue, S., Zhu, T., Lee, J., Han, Y., Demuzere, M., Dunmore, R. E., Ren, L., Liu, D., Wang, Y., Wild, O., Allan, J., Acton, W. J., Barlow, J., Barratt, B., Beddows, D., Bloss, W. J., Calzolai, G., Carruthers, D., Carslaw, D. C., Chan, Q., Chatzidiakou, L., Chen, Y., Crilley, L., Coe, H., Dai, T., Doherty, R., Duan, F., Fu, P., Ge, B., Ge, M., Guan, D., Hamilton, J. F., He, K., Heal, M., Heard, D., Hewitt, C. N., Hollaway, M., Hu, M., Ji, D., Jiang, X., Jones, R., Kalberer, M., Kelly, F. J., Kramer, L., Langford, B., Lin, C., Lewis, A. C., Li, J., Li, W., Liu, H., Liu, J., Loh, M., Lu, K., Lucarelli, F., Mann, G., McFiggans, G., Miller, M. R., Mills, G., Monk, P., Nemitz, E., O'Connor, F., Ouyang, B., Palmer, P. I., Percival, C., Popoola, O., Reeves, C., Rickard, A. R., Shao, L., Shi, G., Spracklen, D., Stevenson, D., Sun, Y., Sun, Z., Tao, S., Tong, S., Wang, Q., Wang, W., Wang, X., Wang, X., Wang, Z., Wei, L., Whalley, L., Wu, X., Wu, Z., Xie, P., Yang, F., Zhang, Q., Zhang, Y., Zhang, Y., and Zheng, M.: Introduction to the special issue "In-depth study of air pollution sources and processes within Beijing and its surrounding region (APHH-Beijing)", Atmos. Chem. Phys., 19, 7519–7546, https://doi.org/10.5194/acp-19-7519-2019, 2019.

Steenhof, M., Gosens, I., Strak, M., Godri, K. J., Hoek, G., Cassee, F. R., Mudway, I. S., Kelly, F. J., Harrison, R. M., Lebret, E., Brunekreef, B., Janssen, N. A. H., and Pieters, R. H. H.: In vitro toxicity of particulate matter (PM) collected at different sites in the Netherlands is associated with PM composition, size fraction and oxidative potential - the RAPTES project, Part. Fibre Toxicol., 8, 26, https://doi.org/10.1186/1743-8977-8-26, 2011.

Steimer, S. S., Delvaux, A., Campbell, S. J., Gallimore, P. J., Grice, P., Howe, D. J., Pitton, D., Claeys, M., Hoffmann, T., and Kalberer, M.: Synthesis and characterisation of peroxypinic acids as proxies for highly oxygenated molecules (HOMs) in secondary organic aerosol, Atmos. Chem. Phys., 18, 10973–10983, https://doi.org/10.5194/acp-18-10973-2018, 2018.

Timonen, H., Aurela, M., Carbone, S., Saarnio, K., Frey, A., Saarikoski, S., Teinilä, K., Kulmala, M., and Hillamo, R.: Seasonal and diurnal changes in inorganic ions, carbonaceous matter and mass in ambient aerosol particles in an urban, background area, Boreal Environ. Res., 19, 71–86, https://helda.helsinki.fi/handle/10138/160095 (last access: 27 December 2022), 2014.

Tuet, W. Y., Chen, Y., Fok, S., Gao, D., Weber, R. J., Champion, J. A., and Ng, N. L.: Chemical and cellular oxidant production induced by naphthalene secondary organic aerosol (SOA): Effect of redox-active metals and photochemical aging, Sci. Rep.-UK, 7, 1–10, https://doi.org/10.1038/s41598-017-15071-8, 2017.

Venkatachari, P., Hopke, P. K., Grover, B. D., and Eatough, D. J.: Measurement of particle-bound reactive oxygen

species in rubidoux aerosols, J. Atmos. Chem., 50, 49–58, https://doi.org/10.1007/s10874-005-1662-z, 2005.

Wang, S., Zhao, Y., Chan, A. W. H., Yao, M., Chen, Z., and Abbatt, J. P. D.: Organic Peroxides in Aerosol: Key Reactive Intermediates for Multiphase Processes in the Atmosphere, Chem. Rev., 123, 1635–1679, https://doi.org/10.1021/acs.chemrev.2c00430, 2023.

Wang, Y., Hopke, P. K., Sun, L., Chalupa, D. C., and Utell, M. J.: Laboratory and Field Testing of an Automated Atmospheric Particle-Bound Reactive Oxygen Species Sampling-Analysis System, Journal of Toxicology, 2011, 419476, https://doi.org/10.1155/2011/419476, 2011.

Weber, R. J., Orsini, D., Daun, Y., Lee, Y. N., Klotz, P. J., and Brechtel, F.: A Particle-into-Liquid Collector for Rapid Measurement of Aerosol Bulk Chemical Composition, Aerosol Sci. Tech., 35, 718–727, https://doi.org/10.1080/02786820152546761, 2010.

World Health Organisation: Ambient Air Pollution: A Global Assessment of Exposure and Burden of Disease, World Health Organization, https://www.who.int/publications/i/item/9789241511353 (last access: 8 February 2021), 2016.

Wragg, F. P. H., Fuller, S. J., Freshwater, R., Green, D. C., Kelly, F. J., and Kalberer, M.: An automated online instrument to quantify aerosol-bound reactive oxygen species (ROS) for ambient measurement and health-relevant aerosol studies, Atmos. Meas. Tech., 9, 4891–4900, https://doi.org/10.5194/amt-9-4891-2016, 2016.

Yang, A., Janssen, N. A. H., Brunekreef, B., Cassee, F. R., Hoek, G., and Gehring, U.: Children's respiratory health and oxidative potential of $PM_{2.5}$: the PIAMA birth cohort study, Occup. Environ. Med., 73, 154–160, https://doi.org/10.1136/oemed-2015-103175, 2016.

Zhang, Z.-H., Hartner, E., Utinger, B., Gfeller, B., Paul, A., Sklorz, M., Czech, H., Yang, B. X., Su, X. Y., Jakobi, G., Orasche, J., Schnelle-Kreis, J., Jeong, S., Gröger, T., Pardo, M., Hohaus, T., Adam, T., Kiendler-Scharr, A., Rudich, Y., Zimmermann, R., and Kalberer, M.: Are reactive oxygen species (ROS) a suitable metric to predict toxicity of carbonaceous aerosol particles?, Atmos. Chem. Phys., 22, 1793–1809, https://doi.org/10.5194/acp-22-1793-2022, 2021.

Zhao, R., Kenseth, C. M., Huang, Y., Dalleska, N. F., Kuang, X. M., Chen, J., Paulson, S. E., and Seinfeld, J. H.: Rapid Aqueous-Phase Hydrolysis of Ester Hydroperoxides Arising from Criegee Intermediates and Organic Acids, J. Phys. Chem. A, 122, 5190–5201, https://doi.org/10.1021/acs.jpca.8b02195, 2018.

Supplement of Atmos. Meas. Tech., 16, 2641–2654, 2023
https://doi.org/10.5194/amt-16-2641-2023-supplement

Atmospheric Measurement Techniques
Open Access
EGU

Supplement of

An automated online field instrument to quantify the oxidative potential of aerosol particles via ascorbic acid oxidation

Battist Utinger et al.

Correspondence to: Markus Kalberer (markus.kalberer@unibas.ch)

1 Supplementary Information

1.1 OPDA and DHA Reaction Time

The reaction kinetics of the condensation reaction between OPDA and DHA to form DFQ was determined. DHA and OPDA were mixed in a vial at concentrations used in the OOPAAI and every 5 min an aliquot was measured with the same setup that was used for all offline measurements. Campbell et al., 2019 (Campbell et al., 2019) and Vislisel et al., 2007 (Vislisel et al., 2007) assumed pseudo first-order kinetics for this reaction and estimated that using conditions of the OOPAAI, the reaction should be completed within minutes. However, the experiments conducted in this study (Figure S1) showed that the reaction is much slower and that it takes about 10min for 50% DHA to react. This agrees with the kinetics described in Deutsch and Weeks 1965 (Deutsch and Weeks, 1965). In the actual design of the OOPAAI a short reaction time was chosen (around 3 min) to minimize potential artefact that could occurs due to the lower pH of the DHA-OPDA condensation reaction (see main text).

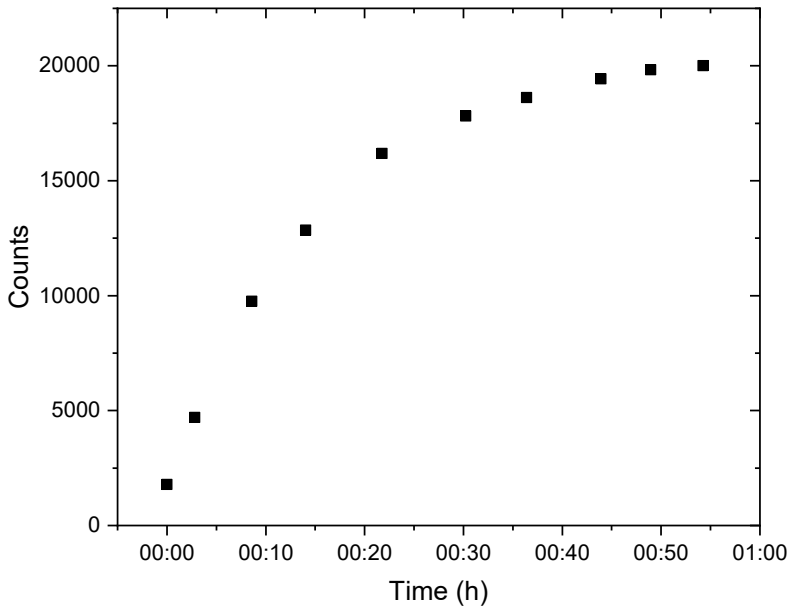

Figure S1 Formation kinetics of DFQ from the condensation reaction of DHA with OPDA.

1.2 Absorbance AA and Filter Extract

For offline measurements of OP with AA, the AA decay is mostly quantified with UV absorbance measurements and not via fluorescence detection (Fang et al., 2015; Perrone et al., 2019; Zhang et al., 2021). We performed some preliminary tests to evaluate if absorption measurement would also be a suitable analysis strategy for an online AA instrument. The potentially biggest issue for an absorbance-based online instrument would be a strong absorbance of aerosol components absorbing at the same or similar wavelength as AA causing high background levels and poor detection limits.

To test the absorbance of ambient aerosol components, an extract from a filter collected during the Atmospheric Pollution and Human Health campaign (APHH) (Shi et al., 2019) was diluted to four concentrations that correspond to realistic outdoor air pollution levels up to 30 $\mu g/m^3$. Filter extracts were then reacted with AA and the absorbance of AA and filter extracts was measured at 265 nm using a 1 m liquid waveguide capillary cells (LWCC, WPI) through which the extracts were pumped continuously. Unfortunately, the shoulder of the absorbance of aerosol components contributes substantially to the overall absorbance at 265 nm as can be seen in Figure S2. As the absorption properties of the aerosol could vary substantially over time, an absorbance measurement would not be a straight forward strategy to quantify the AA reactivity with an online instrument.

For offline measurements (i.e. filter extracts), the AA consumption is usually observed over time, and therefore self-absorbance is not a problem because only the relative change in the absorbance at 265nm are measured. For a true online instrument, however, measuring AA absorbance at different time points would not be feasible and therefore quantifying the AA reactivity using absorbance was not further considered in this study.

A dual channel online instrument might potentially be an option to implement AA absorbance where one channel would measure continuously the aerosol absorbance and the second channel would measure the sum of the aerosol absorbance and of AA.

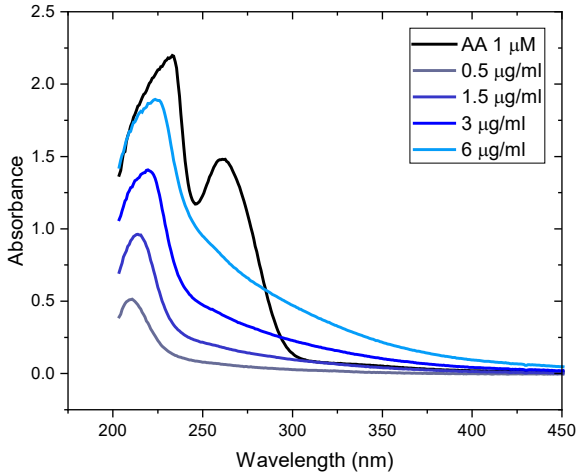

1.3 Figure S2 Absorbance of AA (black line) and ambient filter extract (blue lines) with different particle concentrations. The black line shows the absorbance of pure AA, and all the blue lines are the absorbance of filter extract without AA.The Appropriate Buffer for the AA Assay.

In many assays quantifying ROS or OP in aerosols, phosphate buffer is used (Gao et al., 2017; Pietrogrande et al., 2019; Wragg et al., 2016). Because AA reacts efficiently with metals, phosphate might severely affect OP quantification, because it may chelate metals, influencing their redox chemistry. Figure S3 illustrates the effect of phosphate buffer and HEPES buffer on soluble Fe^{3+} speciation over a pH range of 2-9 modeled with the chemical equilibrium model Visual MINTEQ. In Figure S3A the speciation of Fe^{3+} is shown when the solution is buffered with HEPES where most of the iron is present as $(Fe(OH)_2^+)$ at pH7. On the contrary, when the system is buffered with phosphate, a substantial fraction of Fe^{3+} is present as iron phosphate $(FeHPO_4^{2+})$ under acidic and neutral pH conditions (Figure S3B, light green line), which might significantly affect the redox chemistry of Fe^{3+}. In the model, only species that are important for the reaction and present at a sufficient concentration are displayed. Depending on the chosen buffer, the metal speciation can be very different. Other metals might form other complexes, but HEPES is considered to be a buffer that generally does not form strong metal complexes (Shipman, 1969; Yoshimura et al., 1992). These findings indicate that phosphate buffer is not a suitable buffer to quantify metal-initiated OP because of the chelation of phosphate with metals.

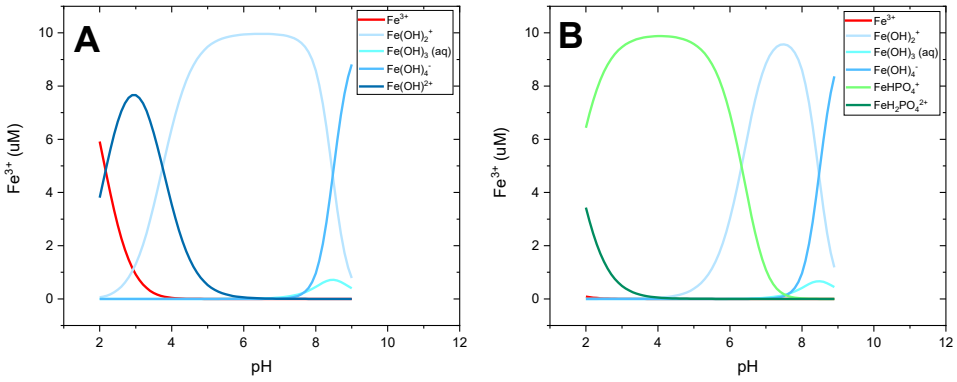

55

Figure S3 Modeling Fe^{3+} speciation with different buffers using Visual MINTEQ. (A) HEPES buffer does not chelate metals and at pH 7 iron is almost entirely present as $Fe(OH)_2^+$. When iron is buffered with phosphate (B), a substantial fraction of the total Fe^{3+} at pH 7 is present as iron phosphate ($FeHPO_4^{2+}$).

1.4 DFQ Spectrum

In Figure S4 a spectrum of 200 µM DHA with 20 mM OPDA is shown. The spectrum was taken with the QePro spectrometer as described in the main text. The main peak at 430 nm is the fluorescence peak of DFQ and the small peak at 365 nm is scatter light from the LED. DFQ gets photolyzed over time to a product, which we have not characterized and which is absorbing at around 500 nm where the shoulder of a second small peak can be seen. Note that this is a relative spectrum measured with the settings used in this experiment, and that the absolute peak shape could slightly change depending on the exact spectrometer type and settings.

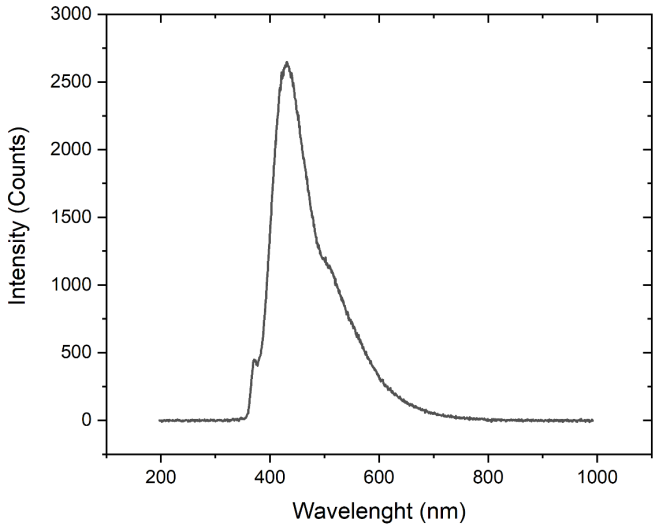

Figure S4 DFQ Spectrum. The small peak at 365 nm is the scattering of the LED, and the large peak at 430 nm is the emission of the DFQ. The shoulder at around 500 nm is due to an unidentified decomposition product of DFQ.

References

Campbell, S. J., Utinger, B., Lienhard, D. M., Paulson, S. E., Shen, J., Griffiths, P. T., Stell, A. C. and Kalberer, M.: Development of a physiologically relevant online chemical assay to quantify aerosol oxidative potential, Anal. Chem., doi:10.1021/acs.analchem.9b03282, 2019.

Deutsch, M. J. and Weeks, C. E.: Microfluorometry Assay for Vitamin C, J. AOAC Int., 48(6), 1248–1256, doi:10.1093/JAOAC/48.6.1248, 1965.

Fang, T., Verma, V., Guo, H., King, L. E., Edgerton, E. S. and Weber, R. J.: A semi-automated system for quantifying the oxidative potential of ambient particles in aqueous extracts using the dithiothreitol (DTT) assay: Results from the Southeastern Center for Air Pollution and Epidemiology (SCAPE), Atmos. Meas. Tech., 8(1), 471–482, doi:10.5194/amt-8-471-2015, 2015.

Gao, D., Fang, T., Verma, V., Zeng, L. and Weber, R. J.: A method for measuring total aerosol oxidative potential (OP) with the dithiothreitol (DTT) assay and comparisons between an urban and roadside site of water-soluble and total OP, Atmos. Meas. Tech., 10(8), 2821–2835, doi:10.5194/amt-10-2821-2017, 2017.

Perrone, M. R., Bertoli, I., Romano, S., Russo, M., Rispoli, G. and Pietrogrande, M. C.: PM2.5 and PM10 oxidative potential at a Central Mediterranean Site: Contrasts between dithiothreitol- and ascorbic acid-measured values in relation with particle size and chemical composition, Atmos. Environ., 210, 143–155, doi:10.1016/J.ATMOSENV.2019.04.047, 2019.

Pietrogrande, M. C., Bertoli, I., Manarini, F. and Russo, M.: Ascorbate assay as a measure of oxidative potential for ambient particles: Evidence for the importance of cell-free surrogate lung fluid composition, Atmos. Environ., 211(May), 103–112, doi:10.1016/j.atmosenv.2019.05.012, 2019.

Shi, Z., Vu, T., Kotthaus, S., Harrison, R. M., Grimmond, S., Yue, S., Zhu, T., Lee, J., Han, Y., Demuzere, M., Dunmore, R. E., Ren, L., Liu, D., Wang, Y., Wild, O., Allan, J., Acton, W. J., Barlow, J., Barratt, B., Beddows, D., Bloss, W. J., Calzolai, G., Carruthers, D., Carslaw, D. C., Chan, Q., Chatzidiakou, L., Chen, Y., Crilley, L., Coe, H., Dai, T., Doherty, R., Duan, F., Fu, P., Ge, B., Ge, M., Guan, D., Hamilton, J. F., He, K., Heal, M., Heard, D., Hewitt, C. N., Hollaway, M., Hu, M., Ji, D., Jiang, X., Jones, R., Kalberer, M., Kelly, F. J., Kramer, L., Langford, B., Lin, C., Lewis, A. C., Li, J., Li, W., Liu, H., Liu, J., Loh, M., Lu, K., Lucarelli, F., Mann, G., McFiggans, G., Miller, M. R., Mills, G., Monk, P., Nemitz, E., O'Connor, F., Ouyang, B., Palmer, P. I., Percival, C., Popoola, O., Reeves, C., Rickard, A. R., Shao, L., Shi, G., Spracklen, D., Stevenson, D., Sun, Y., Sun, Z., Tao, S., Tong, S., Wang, Q., Wang, W., Wang, X., Wang, X., Wang, Z., Wei, L., Whalley, L., Wu, X., Wu, Z., Xie, P., Yang, F., Zhang, Q., Zhang, Y., Zhang, Y. and Zheng, M.: Introduction to the special issue "In-depth study of air pollution sources and processes within Beijing and its surrounding region (APHH-Beijing)," Atmos. Chem. Phys., 19(11), 7519–7546, doi:10.5194/acp-19-7519-2019, 2019.

Shipman, C.: Evaluation of 4-(2-hydroxyethyl)-1-piperazineëthanesulfonic acid (HEPES) as a tissue culture buffer, Proc. Soc. Exp. Biol. Med., 130(1), 305–310, doi:10.3181/00379727-130-33543, 1969.

Vislisel, J. M., Schafer, F. Q. and Buettner, G. R.: A simple and sensitive assay for ascorbate using a plate reader, Anal. Biochem., 365(1), 31–39, doi:10.1016/j.ab.2007.03.002, 2007.

Wragg, F. P. H., Fuller, S. J., Freshwater, R., Green, D. C., Kelly, F. J. and Kalberer, M.: An automated online instrument to quantify aerosol-bound reactive oxygen species (ROS) for ambient measurement and health-relevant aerosol studies, Atmos. Meas. Tech., 9(10), 4891–4900, doi:10.5194/amt-9-4891-2016, 2016.

Yoshimura, Y., Matsuzaki, Y., Watanabe, T., Uchiyama, K., Ohsawa, K. and Imaeda, K.: Effects of Buffer Solutions and Chelators on the Generation of Hydroxyl Radical and the Lipid Peroxidation in the Fenton Reaction

System, J. Clin. Biochem. Nutr, 13, 147–154, 1992.

Zhang, Z.-H. H., Hartner, E., Utinger, B., Gfeller, B., Paul, A., Sklorz, M., Czech, H., Yang, B. X., Su, X. Y., Jakobi, G., Orasche, J., Schnelle-Kreis, J., Jeong, S., Gröger, T., Pardo, M., Hohaus, T., Adam, T., Kiendler-Scharr, A., Rudich, Y., Zimmermann, R. and Kalberer, M.: Are reactive oxygen species (ROS) a suitable metric to predict toxicity of carbonaceous aerosol particles?, Atmos. Chem. Phys. Discuss., 22(August), 1–29, doi:10.5194/acp-2021-666, 2021.

List of Abbreviations and Acronyms

AA	Ascorbic Acid
BSOA	β-pinene Secondary Organic Aerosol
BVOC	Biogenic Volatile Organic Compound
cDNA	Complementary Deoxyribonucleic Acid
COPD	Chronic Obstructive Pulmonary Disease
DAP	2,3-Diaminophenazine
DCFH	Dichlorofluorescin
DFQ	(1,2-dihydroxyethyl)-fluoro[3,4-b]quinoxaline-1-one
DHA	Dehydroascorbic Acid
DMA	Differential Mobility Analyser
DMSO	Dimethyl Sulfoxide
DTT	Dithiothreitol
EPR	Electron Paramagnetic Resonance
GHS	Glutathion
HCl	Hydrochloric Acid
HEPA	High Efficiency Particle Arresting
HEPES	(4-(2-hydroxyethyl)-1-piperazineethanesulfonic acid

HO_2	Hydroperoxyl Radical
HRP	Horseradish Peroxidase
HULIS	Humic-Like Substances
IR	Infrared
LDH	Lactate Dehydrogenase
LLF	Lung Lining Fluid
LOD	Limit of Detection
NA	Nummerical Aperture
NSOA	Naphthalene Secondary Organic Aerosol
NMR	Nuclear Magnetic Resonance
NVOC	Non-volatile Organic Compound
O_2.-	Superoxide
O_3	Ozone
OC	Organic Carbon
OCU	Organic Coating Unit
OH	Hydroxyl Radical
OP	Oxidative Potential
OPDA	Ortho-Phenylenediamine
OOPAAI	Online Oxidativ Potential Ascorbic Acid Instrument

OPROSI	Online Particle-bound ROS Instrument
PA	Primary Aerosol
PCA	Principle Component Analysis
PEEK	Polyether Ether Ketone
PILS	Particle-into-Liquid Sampler
PM	Particulate Matter
PM_{10}	PM <10 µm diameter
$PM_{2.5}$	PM <2.5 µm diameter
POA	Primary Organic Aerosol
ppb	Parts per Billion
ppb	Parts per Million
PTFE	Polytetrafluoroethylene
RNA	Ribonucleic Acid
RO_2	Peroxy Radicals
ROS	Reactive Oxygen Species
(RT-PCR)	Real-time Polymerase Chain Reaction
RTLF	Respiratory Tract Lining Fluid
RWC	Residential Wood Combustion
SA	Secondary Aerosol

SLF	Surrogate Lung Fluid
SMA	SubMiniature Version A
SMPS	Scanning Mobility Particle Sizer
WSOC	Water-Soluble Organic Carbon
SOA	Secondary Organic Aerosol
SVOC	Semi-Volatile Organic Compound
TECooler	Thermoelectric Cooler
TMB	3,3‘,5,5‘-Tetramethylbenzidine
VOC	Volatile Organic Compound

List of Figures

List of Tables